
Barium cycling in Antarctic waters:
interactions with oceanic and coastal processes



Kimberley M. Pyle

Supervisors: Katharine R. Hendry, Michael P. Meredith, Robert M. Sherrell, Ian R. Hall

A thesis submitted to Cardiff University
in accordance with the requirements for the award of the degree of Doctor of
Philosophy in the School of Earth and Ocean Sciences

8th July 2016

Abstract

Oceanic barium has many potential proxy applications, from the quantification of export productivity using sedimentary barite, to the tracing of freshwater inputs or the circulation of deep water masses. Using these proxies to reconstruct past oceanic conditions is of particular importance in the Southern Ocean, where the ventilation of deep water masses and the biological drawdown of CO₂ are thought to play a significant role in climate regulation. However, the distribution of particulate and dissolved barium in this region is not solely controlled large scale water mass circulation and predictable biological associations, but by an additional combination of spatially and temporally variable local and coastal processes.

In this thesis I have found that stronger near-surface gradients are observed in Antarctic waters than in other ocean basins, with a significant association between Ba_d and silicic acid in surface waters at the WAP. As no direct link was observed between Ba_d and biological productivity, these observations can be explained by an association between Ba_d and siliceous detrital material, either by adsorption mechanisms or through barite precipitation in surface waters. Greater levels of Ba_d release and inferred barite precipitation production are observed from the decay of diatom-dominated detrital material.

The accumulation of particulate barium phases in WAP shelf sediments appears to produce a benthic Ba_d flux that acts as a significant source of Ba_d to coastal waters. Sea ice is found to be a further, little studied, control on Antarctic coastal Ba_d distributions, with non-conservative distributions of Ba_d observed in sea ice cores that may be due to abiotic barite precipitation, and large fluxes of sea ice melt associated with unusually low surface Ba_d concentrations.

Acknowledgments

I would like to thank my primary supervisor, Kate Hendry, for all of her help and patience throughout the past few years, and for encouraging and supporting me in a huge range of scientific experiences. I am also very grateful to my secondary supervisors, Mike Meredith, Rob Sherrell, and Ian Hall, for all of the time and effort they have given both remotely and in person.

I am very grateful to Rob and Kate for giving me the opportunity to work at Rutgers University for a short time and learn the ID ICP-MS method. I am particularly grateful to Maria Lagerström (now at Stockholm University) for patiently teaching me the ID ICP-MS method and introducing me to the Element ICP-MS. I am also very much indebted to Anabel Morte-Ródenas, at Cardiff University, for helping me to set up and develop this method at the Cardiff University School of Earth and Ocean Sciences, providing dedicated assistance with the Element ICP-MS and invaluable moral support. Thanks are also due to all the members of the Bristol Isotope Group, particularly Chris Coath, for their assistance in setting up and developing this method at the University of Bristol, and for frequently needed technical assistance with the element ICP-MS.

From Cardiff University, I am grateful to Caroline Lear for insightful discussions during my Annual Review meetings, and to all members of the 'Changing: Earth' Research Group for their support, with particular thanks to Anna Mikis for useful conversations and excellent baking.

From Bristol University, I would like to thank the members of the 'Bristol Oceans Past and Present' Research Group for many useful and challenging discussions of the work presented in this thesis. Particular thanks to Laura Robinson, Peter Spooner, Hong Chin Ng, Lucie Cassarino, Tianyu Chen, George Rowland, Stephanie Bates, Vanessa Fairbank, and Elaine Mawbey.

The work presented in this thesis would not have been possible without the input of a range of complimentary datasets, accessed through open data platforms or provided directly by collaborators.

- I would like to thank Hugh Ducklow and all other contributors to the Palmer, Antarctica Long Term Ecological Research Project, funded by NSF Awards-ANT 0823101 and PLR 1440435. I am particularly grateful to Oscar Schofield, Hugh Ducklow, and Mike Meredith, for providing me with ancillary datasets for dissolved inorganic nutrients, primary productivity, and oxygen isotopes (Chapter 4). Thanks also to the captain and crew of the ARSV *Lawrence M. Gould*, and Marie Seguret for collecting seawater samples for barium analysis during the PaLLTER annual cruises in 2011 and 2012.

-
- I would like to thank the personnel at Rothera Station, particularly the marine assistants during 2014 to 2015 who collected seawater samples for barium analysis during RaTS sampling events. I am also very grateful for the wealth of other data collected as part of this time series, and to the British Antarctic Survey personnel who collect, analyse, process and curate it. Particular thanks are due to Hugh Venables and Mike Meredith (Chapter 5).
 - Similarly, I would like to thank the captain and crew of the RRV James Clark Ross, and the scientific team, led by Andrew Meijers, who tirelessly collected hundreds of samples for barium analysis during BAS cruise JR299. I am particularly grateful to Hugh Venables and Heather Regan for processing the CTD data, to all of the scientific crew members who processed salinity samples on board, and to Oliver Legge for performing Winkler titrations whilst at sea to calibrate the oxygen sensors (Chapter 3).
 - Further thanks are due to Oliver Legge and to Andy Hind at the University of East Anglia, for analysing JR299 samples for dissolved inorganic nutrients and sharing the data with me (Chapter 3).
 - I am grateful both to my supervisor, Kate Hendry, and to Paul Dodd at the Norwegian Polar Institute, for providing me with sea ice samples for barium analysis from Rothera and from the Arctic N-ICE 2014 and 2015 cruises (Chapter 6).
 - I am indebted to Barney Butler (MSci), who worked tirelessly to analyse N-ICE sea ice samples as part of his Masters project at the University of Bristol, and allowed me to use this data in my thesis (Chapter 6).

I would also like to acknowledge that none of this work would have been possible without the studentship I was awarded from the National Environment Research Council (NERC studentship 126577).

Finally, I would like to thank all those who have supported me throughout the past four years, in Bristol, Cardiff, Exeter, Cambridge, London, and Newcastle. The invaluable pep talks, cups of tea, and general awesomeness have been greatly appreciated, from all the ex-residents of James Street (and co.), Vanessa, Steph, Jen, and George. I would also like to thank all those who took part in the JR299 Antarctic cruise, particularly Siobhán Moran and Heather Regan, for taking a once in a lifetime experience to a whole new level.

Table of contents

CHAPTER 1	1
INTRODUCTION	1
1. STUDYING ANTARCTIC WATERS	2
2. CONTROLS ON THE DISTRIBUTION OF BARIUM IN THE OCEAN	3
2.1. <i>Inputs of Ba_d to the ocean</i>	6
2.1.i Riverine inputs	6
2.1.ii Hydrothermal vents	7
2.1.iii Recycling from sediments	7
2.2. <i>Export and burial</i>	8
2.3. <i>Biogeochemical cycling in the water column</i>	11
2.3.i Biogenically mediated precipitation of marine barite	11
2.3.ii Abiotic precipitation of marine barite	14
2.4. <i>Large scale ocean circulation and mixing</i>	15
2.4.i Distinctive continental signatures	16
2.4.ii Lateral shelf transport	16
3. PROXY POTENTIAL IN THE MODERN OCEAN AND THE GEOLOGICAL RECORD	17
3.1. <i>Biogenic Ba in sediments</i>	17
3.2. <i>Ba_{excess} enrichment in the water column</i>	19
3.3. <i>Ba/Ca in skeletal carbonate</i>	19
3.4. <i>Ba/Ca and $Ba_{totclay}$ as records of freshwaters fluxes</i>	21
3.5. <i>Sr/Ba in marine barite</i>	22
3.6. <i>Barium isotopes in seawater and particulate barium</i>	22
4. UNDERSTANDING BARIUM CYCLING IN ANTARCTIC WATERS	23
CHAPTER 2	25
METHODOLOGY	25
1. MEASURING Ba_o IN SEAWATER AND SEA ICE	25
1.1. <i>Capturing small dynamic ranges: the need for precision</i>	25
1.2. <i>Isotope dilution (ID) ICP-MS</i>	26
2. SAMPLE COLLECTION	28
2.1. <i>Seawater collection from ship-board CTD and towfish</i>	34
2.1.i Palmer LTER annual cruises (West Antarctic Peninsula)	34
2.1.ii BAS JR299 cruise (Scotia and Weddell Seas, Antarctica)	34
2.2. <i>Seawater collection at Rothera Oceanographic and Biological Times Series (RaTS)</i>	36
2.3. <i>Collection of sea ice brine samples at Rothera Point, Adelaide Island</i>	36

2.4. Collection of sea ice melt from Arctic drill cores (<i>N-ICE</i> cruise and <i>Test</i> cruise).....	36
3. SAMPLE STORAGE	36
3.1. Evaporation checks.....	37
4. DETAIL OF THE ID-ICP-MS METHOD	40
4.1. Sample preparation and spiking.....	40
4.1.i Cleaning of equipment.....	42
4.1.ii Spike calibration.....	42
4.1.iii Determining ratio of spike to sample: preventing error magnification	46
4.1.iv Gravimetric determination of solution quantities	46
4.2. Contamination checks: blanks	47
4.2.i Sample collection blanks and procedural blanks	47
4.2.ii Acid blanks	49
4.3. Determination of barium counts through ICP-MS.....	50
4.3.i Typical sequence set-up (Method, differences between various Element machines).....	51
4.3.ii Mass calibration.....	52
4.3.iii Accounting for matrix effects and interferences from seawater analyte	52
4.3.iv Calculating K: monitoring and accounting for mass bias.....	53
5. QUANTIFYING UNCERTAINTY.....	54
5.1. Procedural uncertainty	54
5.1.i Weighing errors	54
5.1.ii Internal precision of mass spectrometry	55
5.1.iii Counting statistics.....	55
5.1.iv Duplicate averaging	55
5.1.v Full error propagation through ID calculation	55
5.2. Consistency checks.....	56
5.2.i Sampling consistency: sample duplicates	56
5.2.ii Procedural consistency: sample preparation duplicates	56
5.2.iii Internal consistency: running duplicates	58
5.2.iv External consistency: measurement of standard solutions over time	60
5.3. Accuracy: comparison of standard solution measurements across labs	63
CHAPTER 3	65
CONTROLS ON THE OCEANIC DISTRIBUTION OF DISSOLVED BARIUM IN THE SCOTIA AND	
WEDDELL SEAS (ANTARCTICA)	65
1. INTRODUCTION	65
1.1. The Scotia Sea.....	66
1.2. The Weddell Sea	71
2. MATERIALS AND METHODS.....	72
2.1. Dissolved barium	72
2.2. Dissolved inorganic nutrients.....	74

2.2.i Oxidised nitrogen (NO _x).....	74
2.2.ii Phosphate (PO ₄).....	74
2.2.iii Silicate/silicic acid (Si(OH) ₄).....	75
2.3. <i>Temperature, salinity, and oxygen concentrations</i>	75
2.4. <i>Quantifying deviation from Ba_d/Si(OH)₄ trends</i>	75
3. RESULTS.....	77
3.1. <i>Identifying polar frontal zones and major water masses</i>	77
3.2. <i>Antarctic continental waters</i>	79
3.3. <i>The Antarctic Zone (AAZ)</i>	81
3.4. <i>North of the PF (PFZ-SAZ)</i>	86
3.5. <i>The North Scotia Ridge</i>	89
3.6. <i>The Weddell Sea</i>	89
4. DISCUSSION	91
4.1. <i>Linking the distributions of Ba_d and macronutrients</i>	92
4.1.i Non-linear global relationship between Ba _d and NO _x or PO ₄	93
4.1.ii Linear global relationship between Ba _d and silicic acid.....	94
4.2. <i>De-coupling Ba_d and silicic acid in the Scotia Sea</i>	100
4.2.i Near-surface behaviour and the biogeochemical divide	100
4.2.ii Barium signals in intermediate waters (200 to 2000 m): large scale circulation and the overprinting of barite cycling.....	102
4.2.iii Invariance of Ba _d in deep waters (below 2000m) of the Scotia Sea.....	105
5. CONCLUSIONS	105
CHAPTER 4	107
THE INFLUENCE OF COASTAL PROCESSES ON DISSOLVED BARIUM CYCLING AT THE WEST ANTARCTIC PENINSULA – SPATIAL ANALYSIS	107
1. INTRODUCTION	107
2. REGIONAL SETTING OF THE WEST ANTARCTIC PENINSULA	108
3. MATERIALS AND METHODS.....	108
3.1. <i>Dissolved barium</i>	110
3.2. <i>Dissolved inorganic nutrients and primary productivity</i>	111
3.3. <i>Water mass fractions</i>	111
4. RESULTS	112
4.1. <i>Distribution of dissolved barium</i>	112
4.2. <i>Inter-year variability in surface distribution</i>	115
4.3. <i>Dissolved barium and silicic acid</i>	116
4.4. <i>Productivity indicators</i>	118
4.4.i Primary productivity and Chl-a	118
4.4.ii Utilised silicic acid	118

4.5.	<i>Dissolved barium and water mass fractions</i>	121
4.6.	<i>Vertical mixing</i>	124
5.	DISCUSSION	124
5.1.	<i>Biological cycling as a primary control on the surface Ba_d distribution</i>	124
5.2.	<i>Identifying a coastal source of dissolved barium</i>	127
5.3.	<i>Sea ice formation as a secondary control on the surface Ba_d distribution</i>	129
6.	CONCLUSIONS.....	132
CHAPTER 5		133
THE INFLUENCE OF COASTAL PROCESSES ON DISSOLVED BARIUM CYCLING AT THE WEST		
ANTARCTIC PENINSULA – TEMPORAL ANALYSIS		133
1.	INTRODUCTION	133
2.	MATERIALS AND METHODS.....	136
2.1	<i>Physical oceanography</i>	136
2.2	<i>Biological oceanography</i>	137
2.3	<i>Dissolved barium</i>	138
2.4	<i>Oxygen isotopes and water mass fractions</i>	140
3.	RESULTS.....	140
3.1	<i>Seasonal variation</i>	141
3.1.i	<i>Autumn-Winter (2013-2014)</i>	146
3.1.ii	<i>Spring (2013-2014)</i>	147
3.1.iii	<i>Summer (2013-2015)</i>	147
3.2	<i>Interannual variation</i>	148
4.	DISCUSSION	149
4.1	<i>Behaviour of Ba_d in relation to biology</i>	149
4.2	<i>Vertical mixing and the enrichment of Ba_d in the water column below 15m</i>	150
4.3	<i>Dilution of surface Ba_d by high levels of sea ice melt</i>	153
5.	CONCLUSIONS	154
CHAPTER 6		157
THE BEHAVIOUR OF DISSOLVED BARIUM IN ARCTIC AND ANTARCTIC SEA ICE.....		157
1.	INTRODUCTION	157
1.1.	<i>Introduction to sea ice</i>	158
2.	MATERIALS AND METHODS.....	159
2.1.	<i>Dissolved barium</i>	160
2.1.i	<i>Ba_d estimates and isotope dilution spiking</i>	161
2.1.ii	<i>Correcting for matrix effects and assessing uncertainty</i>	162
3.	RESULTS	164
3.1.	<i>Rothera sea ice brines (Antarctic)</i>	164

3.2. N-ICE seawater (Arctic).....	165
3.3. N-ICE sea ice cores (Arctic)	166
3.3.i Core 2 (29 th January 2015).....	169
3.3.ii Core 6 (6 th February 2015)	169
3.3.iii Test Core 0 (23 rd February 2014)	169
3.3.iv Test Core 1 (25 th February 2014).....	169
3.3.v Test Core 2 (25 th February 2014)	170
3.3.vi Core 49 (22 nd April 2015).....	170
3.3.vii Core 61 (21 st May 2015).....	170
4. DISCUSSION	173
4.1. Conservative versus non-conservative behaviour of Ba_d in brine and sea ice	173
4.2. Potential non-conservative processes acting within sea ice.....	176
4.3. Meltwater flushing	177
5. CONCLUSIONS	177
CHAPTER 7	179
SYNTHESIS.....	179
1. SUMMARY OF MAJOR FINDINGS	179
1.1. Chapter 3 – Ba_d cycling in the Scotia and Weddell Seas.....	179
1.2. Chapter 4 – Spatial variations in Ba_d at the WAP.....	179
1.3. Chapter 5 – Seasonal variations in Ba_d at the WAP.....	181
1.4. Chapter 6 – Behaviour of Ba_d in sea ice.....	182
2. REFINING THE PICTURE OF THE SOUTHERN OCEAN Ba_d CYCLE	183
2.1. Interactions with biological cycling	183
2.2. The role of sea ice	186
2.3. Benthic sediment fluxes.....	186
REFERENCE LIST.....	189

Chapter 1

Introduction

Over the past several decades, great effort has been directed at finding reliable indicators of past oceanic conditions, particularly for parameters involved in the carbon cycle. Barium was first recognised as a potential proxy for productivity in the 1950s (Goldeberg and Arrhenius 1958; Arrhenius 1959), and as knowledge of its oceanic distribution grew through the GEOSECS expeditions of the 1970s, its links with biological cycling and other oceanic processes became increasingly established (Wolgemuth & Broecker 1970; Chan et al. 1976; Dehairs et al. 1980). However, despite a large body of work that has significantly increased our understanding of how barium is imported to, exported from, and utilised within the oceans, many aspects of the barium cycle remain unknown or poorly quantified. A greater understanding of these processes may allow us to consider barium as a reliable proxy for several key oceanographic parameters, such as ocean export productivity, de-glacial meltwater inputs, and ocean alkalinity.

Barium has the potential to be utilised in various forms as a proxy for organic and inorganic carbon storage within the ocean, providing insight into the role the Southern Ocean has played in climate regulation and biological feedbacks. However, there are complex interactions in this region between the influences of biological activity and the sea ice regime, and the lateral and vertical transport of water masses. The combined effects of these processes

on the distribution of particulate and dissolved barium (Ba_d) in polar waters are not fully understood.

In this thesis, I investigate the distribution of Ba_d in Antarctic waters over several spatial and temporal scales (Figure 1-1), in order to establish the relative controls of coastal and oceanic processes. I aim to investigate the association observed between Ba_d and silicic acid throughout the global ocean, and whether this is significantly altered in Antarctic waters by biological activity, or by the formation and melting of sea ice. I will also assess the role of local interactions vs. large scale ocean circulations on Ba_d distributions, and how this may impact the use of dissolved and particulate barium phases as proxies for certain oceanic processes.

In Section 1 I will briefly discuss the motivation for studying the Southern Ocean, and in Section 2 I will summarise the current scientific consensus on oceanic barium cycling, followed by an outline of the proxy uses of barium in Section 3.

1. Studying Antarctic waters

The need for reliable proxies for past oceanic conditions is particularly important in the Southern Ocean, which is thought to play a key role in the exchange of heat and carbon dioxide between the atmosphere and the ocean.

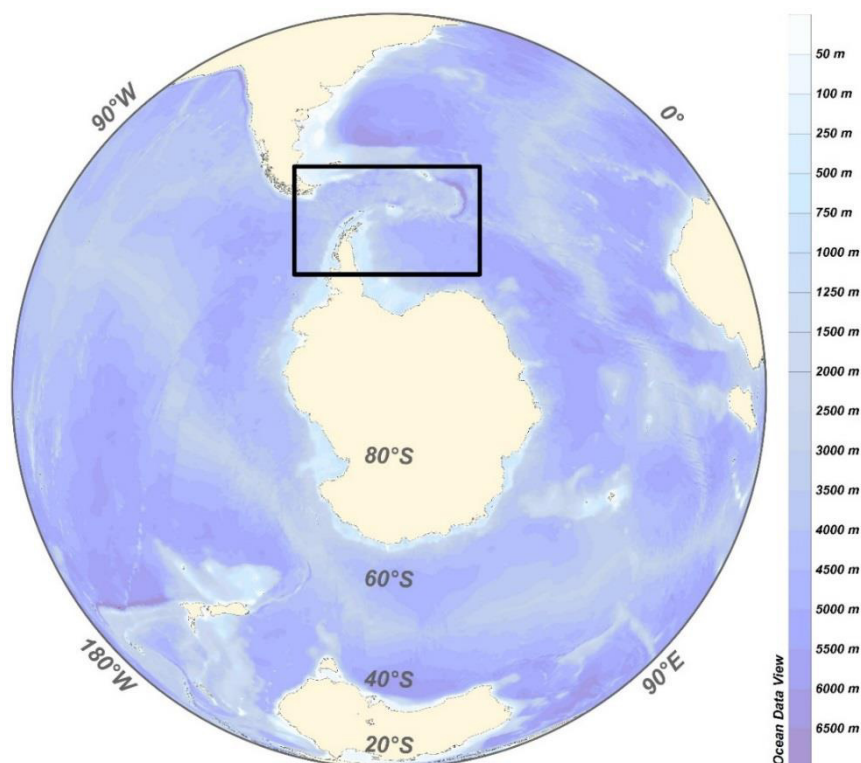


Figure 1-1: The southern hemisphere, with the sampling area that is the main focus of this thesis highlighted by the black rectangle. Sampling is focussed on the Antarctic waters of the Scotia and Weddell Seas, and the waters adjacent to the West Antarctic Peninsula. Colour bar and scale represent ocean bathymetry.

The Southern Ocean is thought to be involved in the regulation of atmospheric carbon dioxide (CO₂) over glacial/interglacial timescales, with the potential to act as a critical net CO₂ source or sink depending on changing circulation and productivity (Skinner et al. 2010; Anderson et al. 2009; Watson & Naveira Garabato 2006; Marinov et al. 2006). As a region of upwelling, the Southern Ocean sees the ventilation of deep water masses that brings nutrients and heat to the upper layers of the ocean, degassing CO₂ into the atmosphere. Despite the high level of macronutrients (nitrate, phosphate, and silicic acid) that this upwelling brings to surface waters, the Southern Ocean is largely a High Nutrient Low Chlorophyll (HNLC) area, with under-utilisation of macronutrients thought to result from micronutrient limitation (specifically iron limitation) (Martin 1990). As biological activity sequesters CO₂ from the atmosphere and transfers it to the deep ocean, the stimulation or suppression of productivity in the Southern Ocean through changes in upwelling or the relief of iron limitation, could significantly alter the net exchange of CO₂ between the atmosphere and the ocean (Lovenduski & Gruber 2005; Anderson et al. 2009). As well as impacting on Southern Ocean CO₂ exchange, changes in productivity and water mass circulation in Antarctic waters may also have further-reaching impacts, disrupting the delivery of nutrients to low latitude waters (Sarmiento et al. 2004).

With such a potentially crucial role to play in the regulation of the global climate, it is particularly important to develop our understanding of the physical and biogeochemical cycles at work in Antarctic waters, and to be able to reconstruct the changes that this system has undergone through geological time. Barium, in various forms, offers insights into this system as a potential proxy for export productivity (Paytan & Griffith 2007), changing freshwater influences (Kasten et al. 2001; Hall & Chan 2004), and deep water circulation (Lea & Boyle 1990), therefore there is a need to ensure that our understanding of the oceanic barium cycle in this region is more clearly understood.

2. Controls on the distribution of barium in the ocean

In the modern global ocean dissolved barium has a generally predictable “nutrient-like” vertical distribution, being partially depleted in surface waters and enriched at depth. This bio-intermediate profile is echoed by its distribution between ocean basins, with higher concentrations of dissolved barium found in the deep Pacific Ocean than in the deep Atlantic (see Chapter 3 for further details), and by the linear correlations often displayed with silicic acid and alkalinity (Dehairs et al. 1980). Such patterns are usually indicative of some biologically mediated uptake in surface waters followed by sinking and regeneration at depth. The processes involved in this uptake of dissolved barium in surface waters is not fully understood, nor is the exact role of biology in the observed downward flux of barium. Traditionally it has been

associated with the formation of barite (barium sulphate, BaSO₄) in the water column, which subsequently sinks and is regenerated either at depth or within the sediment (Dehairs et al. 1980; Bishop 1988; Paytan & Griffith 2007). Although the mechanisms involved in marine barite formation are still unclear, and the various hypotheses proposed will be discussed in detail below, it is accepted that biological organisms play an important part in this synthesis (Stroobants et al. 1991; Bernstein et al. 1998; Dymond et al. 1992) and that the cycling of barium in the oceans is intrinsically linked to the barite and biological cycles.

Due to the assumed nature of its precipitation marine barite is often referred to as 'biogenic barium' and makes up a large proportion of the particulate barium in the water column in the form of aggregated or discrete microcrystals (Bertram & Cowen 1997). The ubiquitous occurrence of microcrystalline barite throughout the world's oceans is a long-standing paradox in ocean geochemistry, as thermodynamic estimates consistently predict that the global ocean is undersaturated with regards to pure solid phase BaSO₄ in all but a few key areas where equilibrium and slight supersaturation are reached (Monnin et al. 1999). Even accounting for realistic levels of strontium impurities, the global oceans are still undersaturated with regards to this mineral (Rushdi et al. 2000; Monnin & Cividini 2006). These findings bolster proposals first suggested by Goldberg and Arrhenius 1958 that the thermodynamic conditions required for barite precipitation may be provided within microenvironments found in aggregates of sinking organic matter. Resolving the nature of these microenvironments and the processes which lead to the formation of the necessary thermodynamic conditions is a major focus of current research into the barite cycle.

Particulate barium in the water column does not only take the form of marine barite. Barium is associated with various other particulate phases, including carbonates, opal, ferromanganese hydroxides, organic matter, and terrestrial silicates (Plewa et al. 2012; Gonnee & Paytan 2006). Analysis of sediments traps and results from leaching experiments suggest that terrigenous barium and barite are the dominant forms (Gonnee & Paytan 2006; Dehairs et al. 1980; McManus et al. 1998), and the terrigenous signal can be removed by normalising particulate barium to aluminium (Al) or titanium (Ti) (Dymond et al. 1992). The remaining barium content of suspended matter is referred to as the 'barium excess' (Ba_{excess}) and is occasionally erroneously equated with marine barite. However it is important to note that although barite crystals are found throughout the oceanic water column, including surface waters (Jacquet et al. 2004; Sternberg et al. 2005, 2008), it is mainly reported as the principal carrier of barium only in mesopelagic depths (200 to 2000 m depth). Previous studies have commonly found that barium excess in the upper mixed layer is dominated by barium associated with phytoplankton or

enriched in the celestite (SrSO_4) tests of acantharians (Hoppema et al. 2010), and the content of these fractions in other levels of the water column and in sediments is variable and should not be neglected (Gonneea & Paytan 2006; Schenau et al. 2001).

Observations of increased particulate barium fluxes associated with high levels of biological activity in the surface oceans are a common theme within the literature on this topic (for example Dymond et al. 1992; Dymond & Collier 1996; Jacquet et al. 2011) and formed the basis of many initial theories linking the barium and biological cycles. Similarly, several studies have recorded decreased concentrations of dissolved barium in surface waters associated with distinct biological events such as phytoplankton blooms (Nozaki et al. 2001; Jacquet et al. 2007; Hoppema et al. 2010). It appears that either by direct biological uptake or adsorption onto cell surfaces, phytoplankton concentrate and remove dissolved barium from surface waters. Therefore sinking phytoplankton debris create a downward flux of barium out of the upper mixed layer. During phytoplankton decay this labile particulate barium appears to be released back into the water column, with a small fraction becoming concentrated in supersaturated microenvironments and precipitating as barite (Bishop 1988). However, directly equating increased particulate barium fluxes with decreases in Ba_d concentrations is not necessarily straightforward; barium removed from solution may not be directly transferred to local barite stocks (Jacquet et al. 2007). Difficulties are also encountered due to the difference in magnitude between the two reservoirs; in the open ocean Ba_d concentrations range from approximately 20 nM (surface waters) to 200 nM (deep Pacific) whilst particulate phase concentrations vary around several hundreds of pM (Griffith & Paytan 2012; Jacquet et al. 2007, 2011).

The distribution of dissolved barium in any region of the global ocean will be the cumulative result of several different processes, including the provenance of the water mass in question, the proximity to local inputs of dissolved barium, and the effect of any in-situ processes leading to removal or addition. It is important to understand all of the contributing factors to this overall distribution, particularly when seeking to interpret data in terms of one process in particular. The different mechanisms concerned in the barium cycle may often have conflicting effects on the observed distribution, for example, surface measurements of Ba_d in the Canadian Arctic Archipelago show little seasonal variation, possibly because major fluvial input events occur concurrently with large pulses of biological activity that export barium from the surface layer (Thomas et al. 2011). It is therefore essential to have a thorough awareness of all the potential controlling factors at work in the barium cycle, including the magnitude of their effects and their spatial and temporal variation.

2.1. Inputs of Ba_d to the ocean

2.1.i Riverine inputs

Rivers are the main source of barium to the oceans, transporting fluxes of approximately 1×10^{10} moles/year (Chan et al. 1976) from regions of continental weathering. It is carried in both dissolved and suspended phases, taking the form of ions or complexes in aqueous solution, ions adsorbed onto particulate matter, or as atoms within the structural lattice of mineral grains (Hanor & Chan 1977). The solute phase constitutes the bulk of the fluvially transported barium, and enhanced concentrations of dissolved barium (Ba_d) are routinely recorded in surface waters around river mouths (Martin & Meybeck 1979; Savenko et al. 2006; Viers et al. 2009). However, these fluvial fluxes of Ba_d are often significantly enhanced in estuaries and other river-ocean mixing zones due to desorption of barium from river-borne sediments. This phenomenon can be observed in plots of dissolved barium concentration vs. salinity, with an initial increase in Ba_d with increasing salinity reflecting a rapid desorption of barium in the low salinity region (Li and Chan 1979; Guay & Falkner 1998; Nozaki et al. 2001). This desorption is most easily explained by the ion exchange model put forward by Hanor and Chan 1977, which postulated that whilst clay minerals preferentially adsorb barium from aqueous solution in fluvial waters, a sufficient increase in the dissolved concentration of other cations will displace some of this barium through simple mass-action. As the system is in chemical equilibrium, the addition of reactive ions such as Mg^{2+} will drive the substitution reaction forward, causing an increase in the displacement of Ba^{2+} . As the ratio of dissolved major cations such as Na^+ , K^+ , and Mg^{2+} to Ba^{2+} increases significantly in river-ocean mixing zones a progressive removal of barium from adsorption sites is therefore to be expected, leading to an increase in Ba_d . This mechanism has been supported by laboratory experiments (Li and Chan 1979), and predictive models of such a scenario closely match observations (Hanor & Chan 1977; Hall & Chan 2004).

Natural variation in the barium content of river loads exists between different river systems due to differences in weathering regimes and continental terranes (Hanor and Chan 1977 and references therein). Temporal variation throughout the year is also to be expected, particularly in high latitudes where melt water run-off in spring and summer creates a distinct seasonality to river discharge levels (Thomas et al. 2011; Mitchell et al. 2001; Guay & Falkner 1998) Variation in the magnitude and location of estuarine desorption has also been observed, both between river systems and within individual localities (Coffey et al. 1997). This variability has been linked to hydrodynamic conditions such as flow rate within the estuary environment (Coffey et al. 1997), and raises the possibility of secondary inputs of barium to the estuary system that are as yet unconstrained, such as groundwater discharge and desorption from

intertidal sediments (Carroll et al. 1993; Moore 1997; Nozaki et al. 2001). There may also be additional inputs of Ba_d from glacial meltwater and icebergs, as these meltwaters can often act as sources of macronutrients, trace metals, and rare earth elements to the coastal system (Raiswell et al. 2008; Sherrell et al. 2015; Kim et al. 2015). Although isolated measurements of alpine glaciers indicate that meltwaters contain low levels of Ba_d (5 nM - Mitchell et al. 2001; Fortner et al. 2009), the Ba_d concentrations of coastal glacial systems has not been well defined, and therefore represent an unconstrained input.

As the dominant external source of barium to the oceans is from riverine discharge, and its uptake at the surface and regeneration at depth are linked to biological cycles, links have been drawn between it and the behaviour of other dissolved constituents such as alkalinity (Lea & Boyle 1989). Although not directly linked by the processes that control their behaviour, the similarity in their sites of uptake and regeneration produces a clear co-variation in the modern ocean (Lea & Boyle 1990; Lea & Spero 1992). This similarity in distribution has formed the basis for the use of palaeo- barium distributions as a proxy for alkalinity, and will be discussed in further detail in Section 3.3.

2.1.ii Hydrothermal vents

Another input of barium to the oceans is through hydrothermal vent systems, demonstrable by the massive concretionary and layered barite deposits near hydrothermal vents of along faults associated with spreading ridge environments (Feely et al. 1990). This hydrothermal barite precipitates inorganically when barium-rich fluids expelled from vents come into contact with sulphate-rich seawater. Attempts to estimate the flux of barium from hydrothermal sources has revealed large variations between different vent fields, with values ranging from $1.1\text{-}6.1 \times 10^9$ moles/year (Edmond et al. 1979; Von Damm et al. 1985). These inputs are clearly not insignificant, and vent environments are consistently enriched in barium compared to average seawater, but the extent of local precipitation makes it difficult to accurately constrain the fluxes involved.

The habit of inorganically precipitated hydrothermal barite crystals differs recognisably from that of biologically mediated marine barite and is not thought likely to survive transport over more than a few hundreds of metres (Feely et al. 1987; Bertram and Cowen 1997). It is therefore reasonably assumed by many authors that hydrothermally associated barite is only a locally important feature (Dehairs et al. 1980).

2.1.iii Recycling from sediments

Another consideration in the broad barium budget of the oceans is the level of recycling that occurs in pelagic sediments. Several investigations into marine barium distributions record

significant barium enrichment in bottom waters and a decoupling between barium and silicic acid trends that suggest a deep water input of barium (Jacquet et al. 2004; Hoppema et al. 2010), whilst benthic incubation experiments have directly recorded barium fluxes from sediments (McManus et al. 1998; McManus et al. 1994). Due to the concentration gradient that exists across the sediment-water interface, with bottom waters invariably undersaturated with regards to barite and pore waters usually at or above the level of saturation, a diffusive flux out of the sediment is to be expected. Detailed pore water profiles from the Arabian Sea and the Equatorial Pacific support the idea of these epibenthic fluxes, with Ba_d concentrations in the pore waters increasing sharply within the first few millimetres of sediment, creating a steep pore water gradient capable of sustaining a diffusive flux of Ba^{2+} to the overlying water column (Schenau et al. 2001; Paytan & Kastner 1996). Such a flux could result in up to 70% of the solid phase barium delivered to the sediments being recycled, with reactive barium released from skeletal and organic material (Li et al. 1973; Paytan & Kastner 1996; Schenau et al. 2001). Attempts to estimate these epibenthic fluxes from pore water concentration gradients have utilised Fick's first law of diffusion modified for sediments, and suggest that the input from this regeneration can range from 15 to over 50 $nmol\ cm^{-2}\ year^{-1}$ (Paytan & Kastner 1996; McManus et al. 1998).

2.2. Export and burial

The major output of dissolved barium from the ocean is the formation of particulate barium, most commonly via the precipitation of barite, and its subsequent sedimentation and burial. Despite the undersaturation of much of the global ocean with respect to barite, it is thought that high sinking speeds allow a relatively large fraction of the barite formed within the water column to reach the sediments without dissolution (Paytan et al. 2007). This marine barite accumulates at the sediment-water interface along with other barium-bearing particulate matter from the water column, including terrigenous barium, barium associated with biogenic opal and carbonate, and adsorbed onto iron and manganese hydroxides (Plewa et al. 2006; McManus et al. 1998). The preservation potential of these various barium phases, particularly marine barite, is of great importance when considering the use of barite (or barium concentrations in sediments) as a palaeoproxy for export production/productivity (Dymond et al. 1992; Francois et al. 1995; Fagel et al. 2002). In order to reliably interpret the barium/barite concentration within sediment cores, the relationship between barite delivered to the sediment and that preserved must either be consistent or predictable from knowledge of other parameters.

Generally barite is thought to be highly refractory in oxic conditions, with a preservation potential much greater than that of organic carbon or biogenic silica; an estimated preservation potential of 30 % compared to <1 % for organic carbon and around 5 % for biogenic silica (Dymond et al. 1992; Paytan & Kastner 1996). This low solubility is one of the reasons for its great potential as a proxy for export productivity. Nevertheless there is a distinct heterogeneity observed in the burial efficiency of barium over different oceanic areas (McManus et al. 1999) therefore it is equally likely that the efficiency in any one area will have varied over time. Several factors have been proposed as the major controls on the degree of barium preservation within the sediment, but the relationships involved have not all been well established or quantified.

The three most important factors that have been proposed are mass accumulation rate, the saturation state of deep waters, and diagenetic reactions due to redox conditions, although there are other factors such as sediment provenance, reworking, and bioturbation whose effects are largely unknown (Fagel et al. 2002). The importance of mass accumulation rates, both of the sediment generally and the level of barite within the sediment, lies in its control over the length of time accumulating sediments are exposed to the undersaturated bottom waters. Rapid rates of accumulation should allow a greater degree of preservation, as deposited sediments will be in contact with the bottom waters for a shorter period of time (Dymond et al. 1992; McManus et al. 2002). Although theoretically sound, surveys do not always record predictable co-variation between preservation potential and mass accumulation rates (Schenau et al. 2001). Moreover, regions with very high sedimentation rates, specifically continental margin settings, usually exhibit poor levels of preservation (Von Breyman et al. 1992; Hendy 2010). This indicates that other factors such as the redox state of the sediment may be of greater importance when considering levels of preservation, although accounting for changes to sedimentation rates should not necessarily be neglected.

Having considered the impact of how long sediments are in contact with undersaturated bottom waters, it is logical to also consider the degree of undersaturation of the waters themselves. As discussed above, early diagenetic dissolution is thought to be controlled by concentration gradients across the sediment-water interface. These gradients, and therefore the magnitude of dissolution, can be altered by variations in the saturation state of the bottom waters. It is predicted that barite saturation states vary both laterally and vertically throughout the ocean (Monnin et al. 1999; Rushdi et al. 2000; Monnin & Cividini 2006). Therefore, the preservation potential of barite in sediments will be to some degree dependent on its geographic location and the depth of the sediment-water interface. Good correlations have been shown between barite saturation index and barium accumulation rates in the upper

2000m of the Arabian Sea, and is thought to account for the increased barite preservation with depth observed in this region (Schenau et al. 2001).

During very early diagenesis barium is thought to be released from reactive phases and concentrated in the pore waters of the upper few millimeters of sediment (Paytan & Kastner 1996). The nature of these reactive phases is not well constrained, but is most likely to be barium adsorbed onto or incorporated into biogenic material such as opal and carbonates (Paytan & Kastner 1996). Under these oxic conditions, barite remains highly refractory (Henkel et al. 2012). However, if the flux of organic matter to the sediment is such that aerobic respiration consumes all of the available oxygen within the sediments, then the oxidation process will progress through a series of subsequent oxidants of decreasing efficiency. In order of use and decreasing energy production per mole of organic carbon consumed these oxidants are: nitrate, manganese oxides, iron oxides, sulphate, and methane (Froelich et al. 1979). As this progression takes place the pore waters within the sediments undergo equivalent shifts in redox conditions, accompanied by the release of ions from the reaction of the new oxidant. When sediments reach sufficiently anoxic conditions for sulphate reduction to occur one of the reactant phases is barium sulphate, and Ba^{2+} ions are released into pore waters (Van Santvoort et al. 1996; Henkel et al. 2012). These ions can then diffuse through the pore spaces of the sediments according to Fick's second law of diffusion and may re-precipitate when sufficient sulphate concentrations are encountered (Van Santvoort et al. 1996; Torres et al. 1996).

The occurrence of such sulphate reduction conditions within the sediments obviously compromises the preservation of solid phase barite, and raises the possibility of extreme diagenetic remobilisation of barium. This remobilisation, migration, and re-precipitation of authigenic barite is thought to be responsible for layered and concretionary 'barite front' deposits within sediments, often marking the redox boundary between sulphate and methane consumption (the sulphate-methane transition or SMT) (Nürnberg et al. 1994; Tribouillard et al. 2006; Hendy 2010; Henkel et al. 2012). Due to the potential misinterpretation of authigenic barite fronts, and the potential diagenetic removal of barium from its original site of deposition, areas that have undergone sulphate reduction are unlikely to be useful in reconstructing patterns of barium accumulation. It is also likely that this kind of diagenetic overprinting caused by high fluxes of organic matter to the sediments is responsible for the low levels of barite preservation observed in near shore continental settings (McManus et al. 1998).

It has been suggested that sulphate reduction may occur not just in fully anoxic sediments, but in anoxic microenvironments within sub-oxic or oxic sediments (McManus et al. 1994, 1998). These microenvironments would most likely form around aggregates of organic

matter; however, the association of barite with such aggregates is not routinely observed below the subsurface (about 200 m), where bacterial decay is thought to break down the aggregates and disperse the discrete barite crystals into the water column (Stroobants et al. 1991). This makes it unlikely that barite crystals would be regularly associated with such bio-aggregates within the sediment. Such a scenario would also be expected to produce a negative correlation between levels of organic carbon and barite concentrations within the sediment. As this is not commonly observed, it is unlikely that anoxic microenvironments play an important role in barite diagenesis (Schenau et al. 2001).

2.3. Biogeochemical cycling in the water column

Numerous observations regarding the distribution of dissolved and particulate barium throughout the global oceans suggest that there is a significant relationship between barium geochemistry in the oceans and biological cycling. The link between barite and productivity was first suggested by Goldberg and Arrhenius 1958, who recorded high rates of barium accumulation in sediments beneath highly productive areas of the Pacific Ocean, and in the 1970s surveys from the GEOSECS expeditions (Wolgemuth & Broecker 1970; Bainbridge 1982; Weiss et al. 1983; Ostlund et al. 1987) established the nutrient-like profile of barium in the oceans. Filtration studies have since shown that areas of high biomass and productivity typically coincide with higher concentrations of barium in suspended matter, and mesopelagic particulate barium correlates with the rate of oxygen consumption in the water column as well as vertical patterns of bacterial activity (Dehairs et al. 1980; Bishop 1988; Jacquet et al. 2007, 2011). Sediment data show a strong positive correlation between fluxes of organic carbon and barium (Dymond et al. 1992; Dymond & Collier 1996), and high barite saturation states often correspond with the depth of maximum respiratory activity (Thomas et al. 2011). More recently, improvements in detection precision have allowed the correlation between biological events and concentrations of dissolved barium in surface waters to be reliably reported: non-conservative mixing behaviour at river mouths has been associated with uptake by phytoplankton blooms (Nozaki et al. 2001), and Ba_d depletions in surface waters in the North Pacific and Southern Oceans have been linked to high productivity events (Esser & Volpe 2002; Hoppema et al. 2010).

2.3.i Biogenically mediated precipitation of marine barite

Whilst it is accepted that biology plays a key role in the barium cycle, the exact nature of its role has been the cause of some controversy. One process that has attracted a great deal of attention, and is still not fully resolved, is the formation of barite in the water column. As discussed above, barite in both its pure and impure forms is almost globally undersaturated in

the oceans (Monnin & Cividini 2006), yet barite microcrystals are found throughout the water column, particularly at mesopelagic depths (200 to 2000 m) (Dehairs et al. 1980, 1991). It is commonly held that this scenario is possible because the precipitation of barite is biologically mediated, either directly or indirectly.

It is thought that some protozoans and algae do precipitate barite directly, although its biological function is not always clear (Finlay et al. 1983). For example, discrete intracellular granules of barite are found in *Loxodes*, an abundant planktonic freshwater protozoan, and in some species of green algae (Finlay et al. 1983; Wilcock et al. 1989). In some of these organisms barite inclusions appear to be an integral biological feature, perhaps acting as statoliths involved in gravitropic responses, and it is thought that they may play a significant role in the freshwater barium cycle (Finlay et al. 1983). However, in marine waters no equivalent planktonic organisms have yet been described that actively precipitate barite (Griffith & Paytan 2012). Bertram & Cowen (1997) described rare occurrences of barite crystals precipitated by benthic foraminifera, and discrete intracellular crystals of barite are found in fairly high concentrations within *Xenophyophores*, benthic protozoans that live mainly in the deep sea (Fresnel et al. 1979; Gooday & Nott 1982; Levin 1994). There is no formal estimate of the contribution of these benthic organisms to the barite budget of the ocean, but it is not thought to be significant (Griffith & Paytan 2012), and it has been suggested that crystals precipitated in this way are morphologically distinct from those that make up the majority of sedimentary barite (Bertram & Cowen 1997).

In the absence of the necessary evidence to support direct biological precipitation, hypotheses involving biologically mediated passive precipitation have been put forward. The most popular and supported of these is the idea that aggregates of decaying organic matter provide the necessary thermodynamic conditions for barite precipitation within contained microenvironments (Dehairs et al. 1980; Bishop 1988; Francois et al. 1995). Referred to as the 'organic aggregate model', it proposes that the decay of phytoplankton and other organic material releases the necessary barium and/or sulphate to create conditions within the aggregates that are supersaturated with respect to barite (Figure 1-2).

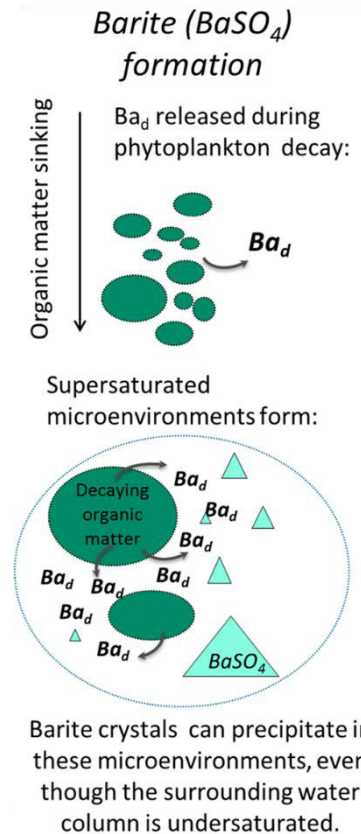


Figure 1-2: Schematic representation of the aggregate model of barite formation: microcrystals of barite precipitate inside microenvironments that become enriched in barium and/or sulphate as biogenic material decays.

As the decay process continues the sinking aggregates are thought to eventually break up, and release the discrete barite microcrystals into the water column. This theory has been supported by detailed scanning electron microscopy- electron microprobe work by Stroobants et al. (1991) on samples from the Scotia-Weddell Sea Confluence (Southern Ocean). They identified barite crystals mainly contained within large bio-aggregates in the upper 200 m of the water column, and below this as free discrete particles. The link between barite precipitation and organic matter decay also tallies with the commonly reported increase in particulate barium at mesopelagic depths, often directly coincident with sites of floc-accumulation (Jacquet et al. 2007), and correlations between maximum particulate barium fluxes and maximum oxygen consumption (Dehairs et al. 1997). The role of bacterial degradation is also supported by observations that vertical barite fluxes co-vary with bacterial activity, that barite fluxes are reduced when efficient remineralisation in surface waters reduces bacterial activity at depth, and that direct bacterial involvement in barite precipitation has been demonstrated under laboratory conditions (Jacquet et al. 2011; Gonzalez-Muñoz et al. 2003, 2012).

Variations on this model have arisen due to disagreements over the source of the released barium and sulphate required to bring the microenvironments to supersaturation with

respect to barite. It has been argued that additional sources of both components are needed, and that these could be provided by dissolution within the aggregates of acantharian tests (Bernstein et al. 1992; Dymond & Collier 1996; Bernstein et al. 1998; Bernstein & Byrne 2004). Acantharians are protists that secrete celestite tests (SrSO_4) which are often enriched in barium. If this is the case, and acantharian tests are a requirement of marine barite formation, then its use as a palaeoproductivity proxy would be severely limited.

This 'celestite model' also confronts an important issue not initially addressed by proponents of the organic aggregate model – if barite precipitation occurs concurrently with organic matter degradation at mesopelagic depths, a mechanism is still required to create a flux of barium downward from the surface layer. Studies have since shown that phytoplankton do appear to have an active role in the uptake of dissolved barium from surface waters (Stecher & Kogut 1999; Esser & Volpe 2002; Hoppema et al. 2010), and Ganeshram et al. 2003 have shown experimentally that decaying phytoplankton can produce the necessary conditions for passive barite precipitation. Moreover, the surface Ba_d depletions observed by Esser and Volpe 2002 in the North Pacific were associated with biological activity with no commensurate depletion of Sr, suggesting that the drawdown could not be attributed to precipitation of acantharian celestite. From this evidence it appears that the organic aggregate theory is still the most feasible explanation for barite precipitation.

2.3.ii Abiotic precipitation of marine barite

There are also a number of processes not linked directly to productivity that may affect the internal geochemical cycling of barium in the oceans. For example, barium accumulation rates (already corrected for lithogenic input) have been found to correlate with terrigenous accumulation rates and accumulation rates of $\text{Fe}_{\text{excess}}$ (a parameter used to track iron oxides) (Schroeder et al. 1997). It has been suggested that this could be due to adsorption of barium onto, or growth of barite crystals within, organic coatings on aeolian particles. It is equally possible that aeolian dust inputs may introduce iron oxides that scavenge barium independently of biological activity (Schroeder et al. 1997; Sternberg et al. 2005). In the few areas where the surface ocean is saturated or slightly supersaturated with respect to barite, such as some regions of the Southern Ocean, the potential for inorganic barite precipitation must also be given greater consideration. Within sea-ice dominated areas, extreme solute concentration within brines may result in supersaturation and inorganic precipitation, and may be accompanied by barite precipitation associated with organic matter degradation within sea-ice (Carson 2008; Hoppema et al. 2010). Although freezing experiments in laboratory conditions have shown no evidence for barite formation (Taylor et al. 2003), strong Ba_d depletions in surface waters associated with ice-

edges in the Arctic suggest that the influence of sea-ice on local biological activity should be considered when discussing barite formation (Guay and Falkner 1997).

2.4. Large scale ocean circulation and mixing

As well as the influence of internal biogeochemical cycling, barium concentrations in the ocean are also controlled by physical factors such as proximity to sources of Ba_d (continental run-off and hydrothermal vents) and the circulation of water masses (Figure 1-3). Regional circulation features have been found to have a strong influence on the distribution of Ba_d (South Atlantic – Horner et al. 2015; Southern Ocean – Jacquet et al. 2004; Hoppema et al. 2010), and Ba_d variation in deep waters can be broadly explained by conservative mixing of water masses associated with large scale oceanic circulation (Horner et al. 2015). Distinguishing the biogeochemical interplay between the dissolved and particulate barium pools from conservative mixing between water masses of differing Ba_d concentrations is one of the crucial difficulties involved in understanding and interpreting the oceanic Ba_d distribution. New tools such as the study of barium isotopes (see Section 3.6) are being applied to de-convolve these different processes (Horner et al. 2015; Cao et al. 2016).

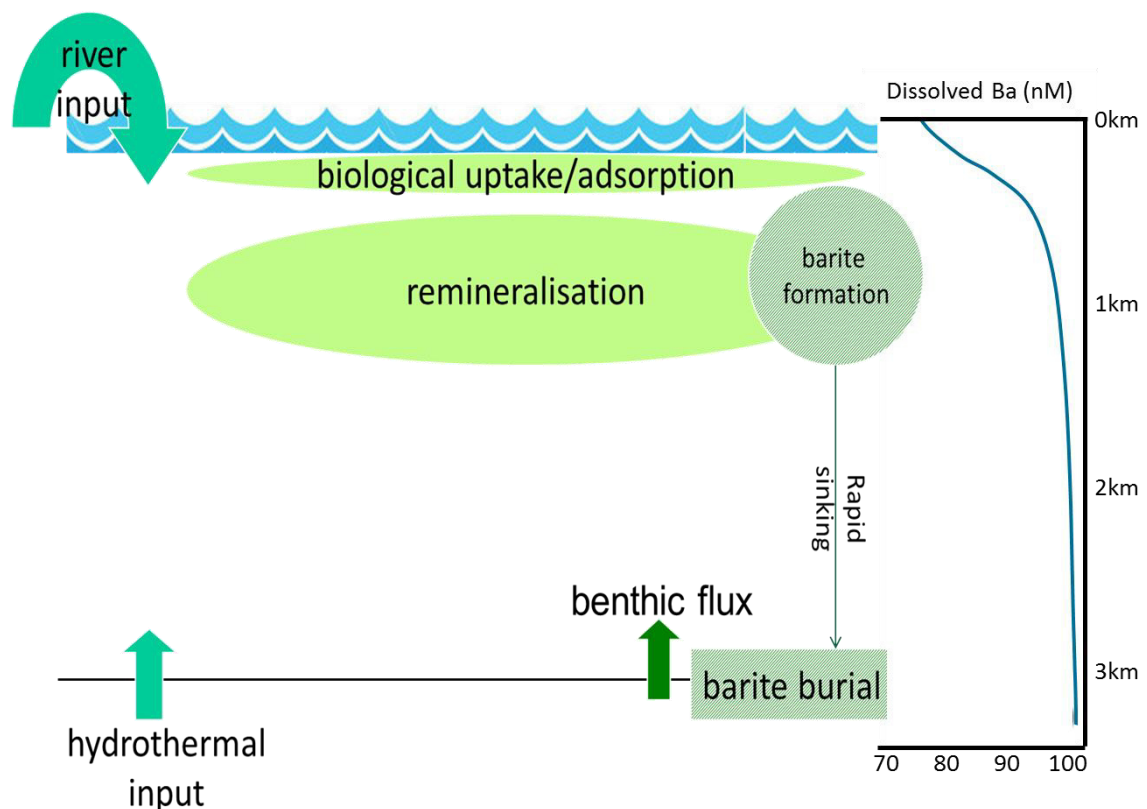


Figure 1-3: Summary schematic of the major inputs (river run-off, hydrothermal vents, and benthic fluxes) outputs (sedimentary burial), and biogeochemical cycles (association with biogenic material, barite formation and dissolution) involving dissolved barium in the oceans.

2.4.i Distinctive continental signatures

As the dominant input of Ba_d to the oceans is through continental run-off via rivers, oceanic water masses with a significant freshwater component may develop distinctive dissolved barium concentration signatures. This elemental abundance can be used in conjunction with more traditional tracers such as salinity, oxygen, nitrate etc. to identify the sources of freshwater inputs (Falkner et al. 1994; Yamamoto-Kawai et al. 2010). This has been demonstrated in the upper Arctic Ocean and its adjacent seas, where $\delta^{18}O$ can be used to distinguish between river run-off and sea-ice melt, and Ba_d concentrations can then be utilised to determine whether the river run-off is of North American or Eurasian origin (Guay & Falkner 1997, 1998; Taylor et al. 2003; Thomas et al. 2011). Barium can be used as an effective tracer in these circumstances because of the natural variability in barium loads between the major Arctic rivers, which persists as a distinctive signal well beyond their estuaries and into the basin itself (Guay & Falkner 1998). Attempts to construct a barium budget for the Arctic basin indicate that on an annual and basin-wide scale barium can be assumed to act as a conservative tracer despite the uncertainties introduced by its biogeochemical cycling (Taylor et al. 2003). Over the scales involved such non-conservative behaviour is thought to be sufficiently suppressed by the ice-field for its effects to be regionally insignificant (Taylor et al. 2003). However, the rapid retreat of Arctic sea-ice may well increase the dominance of these non-conservative processes, making it even more imperative to have a greater understanding of the biological cycling of barium in polar waters.

2.4.ii Lateral shelf transport

As well as a tracer of freshwater inputs, barium has also been utilised as a tracer of shelf waters (Moore & Dymond 1991; Roeske et al. 2012). Due to their similar sources and chemical properties barium is often considered an analogue for radium (van Beek et al. 2009) and Ba and ^{226}Ra generally show a linear correlation with $^{226}Ra / Ba$ ratios fairly constant throughout the ocean (Li et al. 1973; van Beek et al. 2007). However, Moore and Dymond et al. (1991) observed that in sediments traps in the Pacific Ocean this ratio decreased with depth, accompanied by an increase in particulate fluxes of Ba and Al. These observations have been attributed to the introduction of horizontally transported particles (including barite) from continental margins (Moore and Dymond 1991). These 'older' transported particles will have a lower $^{226}Ra / Ba$ ratio due to the decay of ^{226}Ra over time. Therefore the observed relationships between radium, barium, and aluminium can potentially be used to infer the contribution of particulate barium from laterally advected fluxes. It has been proposed that such horizontal transport of resuspended barite and/or refractory organic matter may be one factor responsible for the poorly constrained correlation between particulate barium and organic carbon in nearshore

areas (Fagel et al. 2002; Plewa et al. 2006). Therefore these relationships may be useful not only for tracing shelf waters, but for distinguishing between local and transported particulate barium signals.

3. Proxy potential in the modern ocean and the geological record

Due to its association with organic matter various methods have been established for using barium as a proxy for export productivity, both in the modern ocean (Jacquet et al. 2007; Thomas et al. 2011) and in sediment cores representing past oceanic conditions (Thompson & Schmitz 1997; Nürnberg et al. 1997). Additionally, the inclusion of barium into skeletal carbonate is assumed to represent the ambient barium concentration at the time and location of its growth, enabling Ba/Ca ratios in foraminifera tests and scleractinian corals to be used to reconstruct past oceanic barium concentrations. These barium concentrations are then utilised as proxies for various oceanic conditions and events, from alkalinity to pulses of deglacial meltwater (Lea & Boyle 1989; Lea & Boyle 1990; Hall & Chan 2004; Plewa et al. 2006). It is also possible to use the chemical and isotopic signatures of elements incorporated in to marine barite to reconstruct palaeoceanographic conditions (Griffith and Paytan 2012 and references therein).

These various ways of using barium to develop our understanding of past and present ocean processes are explored below. As well as highlighting the great potential of barium as a proxy, it is also clear that the reliability and application of these methods can be continuously improved via a greater understanding of the barium cycle.

3.1. Biogenic Ba in sediments

The observed association between barium enrichment in sediments and the productivity of overlying waters, particularly in highly fertile regions of upwelling, formed the first basis for utilising barium as a proxy for palaeoproductivity (Goldberg and Arrhenius 1958). Subsequent research aimed at establishing the link between biological cycling and the formation of marine barite (Stroobants et al. 1991; Dymond et al. 1992; Dymond & Collier 1996) has strengthened this hypothesis, although many caveats and unknowns still exist regarding its application. The distribution of barium in deep sea sediment cores has been used by several authors as a qualitative means of assessing changes in palaeoproductivity (Thompson & Schmitz 1997; Schmitz 1987), with increased concentrations of non-terrestrial particulate barium interpreted as the result of increased productivity in overlying waters. This proxy has been applied over a range of timescales, from the Palaeocene-Eocene-Thermal-Maximum (PETM) (Paytan et al. 2007) to the present (Hernandez-Sanchez et al. 2011; Jacquet et al. 2011).

Quantitative approaches to this proxy have also been formulated. Dymond et al. (1992) and Francois et al. (1995) used the ratios of organic carbon/biogenic barium in global sediment trap data to identify a predictable relationship between export production and barite flux to the seafloor. From this relationship a quantitative algorithm can be derived which enables the estimation of new production from biogenic barium accumulation rates. Such an algorithm was proposed by Dymond et al. (1992) which also incorporated a factor related to the dissolved barium concentration of the water column. This was included to account for a spatial trend observed in global $C_{org}/bio\text{-Ba}$ ratios that suggested particulate barium uptake may be influenced by the dissolved barium content of seawater (Dymond et al. 1992). However, after expanding on the initial sediment trap data, Francois et al. (1995) produced a simplified equation which removed the Ba_d term. This larger dataset indicated that particulate barium uptake is not systematically dependant on the dissolved barium content of seawater (Francois et al. 1995). This conclusion has been further supported by laboratory-based studies which suggest that it is the availability of microenvironments, not the diffusion of barium from the surrounding seawater, which is the rate-limiting step in barite formation (Ganeshram et al. 2003).

Although the link between productivity and the biogenic barium content of sediments is well supported in theory (Dymond et al. 1992; Dymond and Collier 1996; Jacquet et al. 2011), there are several practical difficulties involved in using it to derive reliable estimates of palaeoproductivity (e.g. Dymond and Collier 1996; Fagel et al. 2002; Paytan and Griffith 2007). One major problem is the unknowns surrounding the preservation potential of barite in the sediment. As discussed above the general assumption is that barite preservation is reasonably high due to its low solubility in oxic conditions (Dymond et al. 1992; Paytan and Kastner 1996). However, changes to the redox conditions of the sediment over time (sulphate reduction in particular) could lead to variations in the level of barite preservation. Such changes may need to be accounted for in order to derive accurate interpretations from barite records (Hendy et al. 2010). The matter of sediment redox history is of particular importance when considering near shore/margin settings due to the high likelihood of the sediments bearing a diagenetic overprint from anoxic conditions (Von Breyman et al. 1992; Fagel et al. 1999). For this reason, use of biogenic barite as a palaeoproductivity proxy is generally restricted to observing changes in areas of low-moderate productivity (Tribovillard et al. 2006). Even in open ocean settings there are unconstrained factors such as sediment reworking and bioturbation that may affect the preservation of productivity signals in barite deposition (Fagel et al. 2002). However, Ba_{excess} has been found to provide accurate estimates of carbon export (tested against other export proxies), even in complex settings such as the naturally Fe-fertilised Crozet Plateau (Southern Ocean),

provided that appropriate corrections are undertaken for lithogenic inputs, sediment focussing, and barite preservation (Hernandez-Sanchez et al. 2011).

These corrections are a crucial stage in the application of sedimentary Ba_{excess} as a reliable palaeo-proxy, and face two main complications. Firstly, an important challenge when using this correction is that the Ba/Al ratios of lithogenic components are not always well constrained, and the source and composition of this siliciclastic fraction is likely to vary in time and space (McManus et al. 1998; Schenau et al. 2001; Hendy 2010). Despite such uncertainties, Ba_{excess} corrected for in this way is regularly used as a proxy for the biogenic barite content of sediment. Secondly, this correction assumes that any other non-barite phases are either negligible or that they behave similarly to biogenic barium. Sequential leaching studies by Gonnea and Paytan (2006) have shown that this is not the case; non-barite phases can sometimes constitute 20-40% of Ba_{excess} , and do not co-vary predictably with export productivity. Therefore in order to establish a reliable measurement biogenic barite in sediment, it may be necessary to apply extraction methods that can isolate the marine barite fraction (Paytan and Griffith 2007).

3.2. Ba_{excess} enrichment in the water column

As barite formation is thought to be associated with bacterial degradation of organic matter (González-Muñoz et al. 2003; 2012), it has also been suggested that the concentration of discrete barite microcrystals in the water column can be used as an indirect proxy for the mesopelagic mineralisation of organic matter in the modern ocean (Jacquet et al. 2007; Cardinal et al. 2005). Recent attempts to derive carbon export fluxes from mesopelagic Ba_{excess} in the Southern Ocean have not tallied well with estimates produced from other proxies, such as bacterial activity (Jacquet et al. 2011). This may reflect discrepancies in the timescales of the processes involved, and suggests that further work is needed before this proxy can be reliably applied. On the other hand, reasonable estimates of organic carbon export have been derived in the Canadian Arctic using a similar approach (Thomas et al. 2011). In this case, a value for biogenic barium formation (equivalent to Ba_{excess}) was computed using discrepancies between observed concentrations of dissolved barium and projections of the concentrations expected if barium were behaving conservatively (Thomas et al. 2011).

3.3. Ba/Ca in skeletal carbonate

The incorporation of trace metals into marine carbonate is often exploited in attempts to reconstruct past oceanic conditions. Of particular interest to researchers is the ability to reconstruct patterns of past deep ocean circulation through the distribution of refractory nutrients (Lea & Boyle 1991). Dissolved barium is particularly useful in this instance because of

its observed co-variation with alkalinity and dissolved silicate (Figure 1-4), resulting from their shared sites of uptake and regeneration. It has therefore been proposed that past distributions of alkalinity in deep water masses could be reconstructed from past distributions of dissolved barium, providing insights into the upwelling and lateral transport of deep waters (Lea and Boyle 1989). Provided that the incorporation of barium into marine carbonate is representative of the ambient concentration in seawater, it should be possible to reconstruct these past distributions from the Ba/Ca ratio of benthic foraminifera, corals, and other skeletal carbonate material.

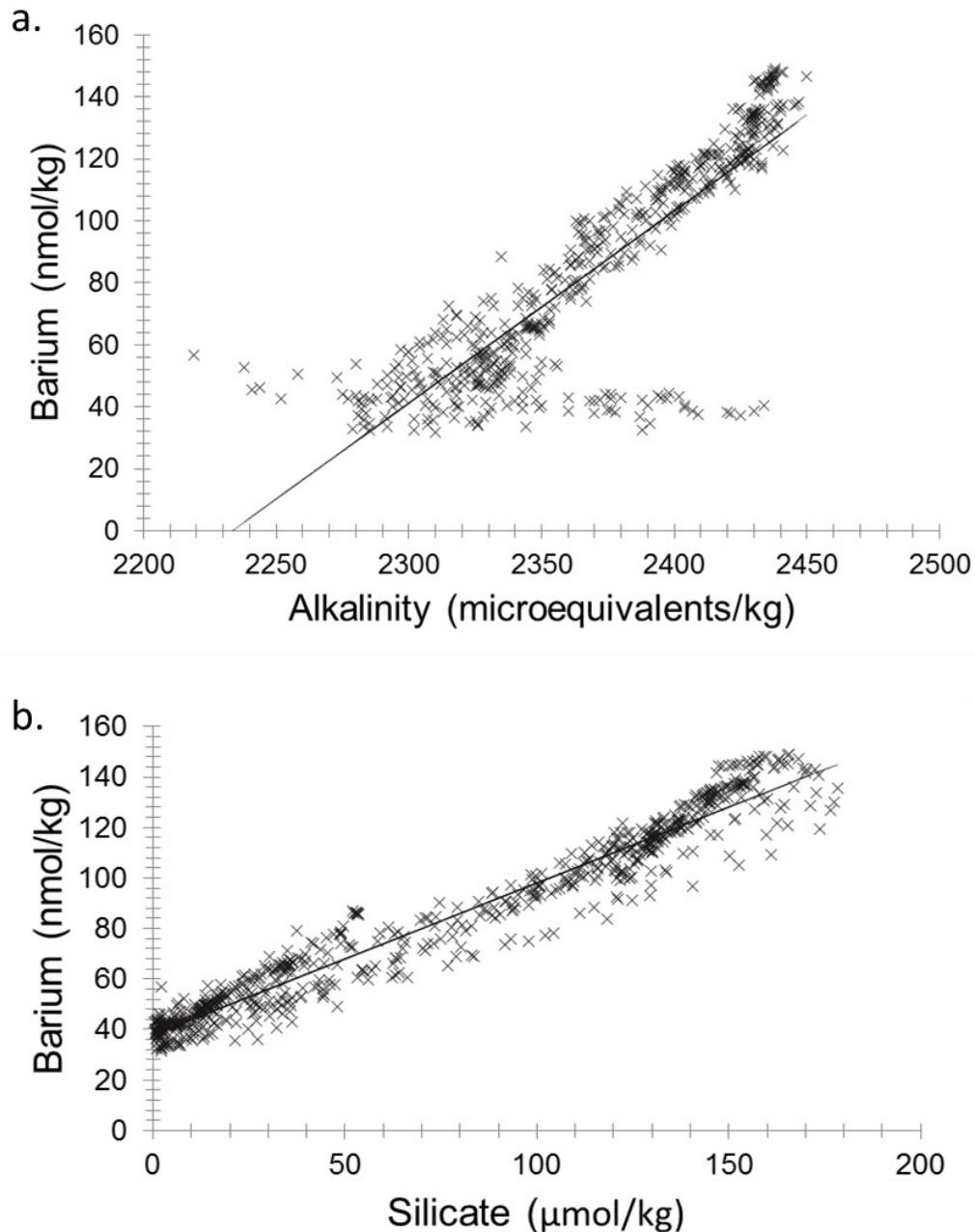


Figure 1-4: Scatter plots showing the relationship between dissolved barium and a. Alkalinity; and b. Silicate from the GEOSECS global database

The size difference between barium and calcium ions (1.35Å vs. 1.00Å) (Shannon 1976) has led to suggestions that the incorporation of barium into calcite should be limited by steric incompatibility (Pingitore 1986). However, Lea and Boyle (1989) found that the Ba/Ca ratios in benthic foraminifera from recent sediment core tops increased linearly with the barium concentrations of bottom waters. Additionally, Lea and Spero (1992) used cultured foraminifera to demonstrate that barium uptake into the calcite lattice responds linearly to increased seawater barium concentrations under laboratory conditions. This suggests that at the low concentrations of barium found in the oceans its uptake is unhindered by steric incompatibility and increases in proportion with ambient concentrations. Records of relative barium variability produced in this way have shown sensitivity to accepted climate cycles that highlight its potential as a palaeoceanographic tracer (Lea & Boyle 1990).

Calibrations of Ba/Ca in skeletal material with contemporaneous seawater Ba_d have opened up the possibility of making quantitative reconstructions of past seawater Ba_d , although observed differences between the incorporation of Ba in different coral taxa have highlighted the need for taxon-specific calibrations if absolute Ba_d reconstructions are to be accurate (LaVigne et al. 2016).

3.4. Ba/Ca and $Ba_{totclay}$ as records of freshwaters fluxes

Whilst past distributions of barium recorded by benthic foraminifera may yield clues about alkalinity and deep water circulation, Ba/Ca in planktonic foraminifera can be used to track past changes in the barium concentration of surface waters (Lea and Spero 1994). Experimental results indicate that barium uptake into foraminiferal calcite can be taken as a reliable indicator of ambient barium concentrations (Lea and Boyle 1991; Lea and Spero 1992; LaVigne et al. 2016). Laboratory cultures also demonstrate that the uptake of Ba into foraminiferal tests is not appreciably affected by variations in temperature and salinity that may be experienced by surface waters (Lea & Spero 1994), and appropriate cleaning methods have been devised to ensure measurement of only lattice-bound barium (Lea and Boyle 1991). Sediment core records of Ba/Ca ratios produced using these methods show elevated barium concentrations coincident with apparent meltwater pulses, corroborated by oxygen isotope data (Hall and Chan 2004). Elevated barium signals can be attributed to enhanced levels of barium in riverine discharge due to increased weathering and erosion during deglaciation, increased export of freshwater due to ice-sheet retreat, or desorption from shelf sediments during sea-level rise (Lea and Boyle 1991; Hall and Chan 2004; Plewa et al. 2006).

In addition to Ba/Ca in planktonic foraminifera, past and present surface ocean freshwater changes have also been reconstructed from other calcifying organisms, including

coralline algae (Hetzinger et al. 2013) and warm-water corals (Sinclair & McCulloch 2004; Allison & Finch 2007). Furthermore, some researchers have suggested that peaks in the total barium content of the clay fraction (Ba_{totclay}) in sediment cores can be equally indicative of freshwater discharge events, as they indicate an increase in terrigenous output (Plewa et al. 2006).

3.5. Sr/Ba in marine barite

Records of cation substitution in marine barite itself can also be explored, with the abundance of elements substituting for barium in the crystal lattice used to reconstruct their distribution in sea water at the time of formation. The most common substitutions for barium (Ba^{2+}) are strontium (Sr^{2+}) and calcium (Ca^{2+}), as well as potassium (K^+), radium (Ra^{2+}), lead (Pb^{2+}), and rare earth elements. Minor substitutions by iron, copper, zinc, silver, mercury and vanadium have also been reported (Griffith and Paytan 2012 and references therein).

As strontium is one of the most common impurities incorporated into marine barite during its formation in the water column, the Sr-isotopic composition of sedimentary barite has been investigated as a means of reconstructing the palaeoceanographic Sr-isotopic ratio of seawater (Paytan et al. 1993). During the course of such studies it has been observed that strontium concentrations in barite crystals from superficial sediments are lower than those sampled from the water column (Bertram and Cowen 1997). Subsequent investigations have revealed that mean Sr/Ba ratios in barite from cores in the Pacific and Southern Oceans appear to decrease with increasing water depth (Van Beek et al. 2003). One explanation for these observations is that Sr-rich barite crystals dissolve preferentially in the water column, so that as barite dissolution increases with depth strontium is disproportionately removed over barium, and thus the Sr/Ba ratio decreases. Van Beek et al. 2003 suggested that this water-depth dependence of the Sr/Ba ratio recorded in sediments could therefore be developed as a proxy for the level of barite dissolution that the sediments have experienced.

3.6. Barium isotopes in seawater and particulate barium

Dissolved barium has been shown to correlate in the global ocean with silicate and alkalinity, displaying a nutrient-like profile with depth (Wolgemuth & Broecker 1970; Dehairs et al. 1980). This apparent biologically-mediated distribution has been attributed to the cycling of marine barite, which is thought to precipitate in specific microenvironments formed around decaying organic matter (Bishop 1988). However, as barite precipitation and dissolution are not thought to be diatom-dependent (Ganeshram et al. 2003) there are many questions still to be answered regarding the strong co-variation of barium and silicate in the ocean.

Measuring the stable isotopes of barium ($\delta^{138/134}Ba_{\text{NIST}}$ – Equation 1-2) in seawater and in particulate barium can provide insights in to mechanisms of barite cycling, as the light isotopes

of barium are preferentially incorporated into barite when it forms (von Allmen et al. 2010), leaving the residual water mass isotopically heavy and depleted in dissolved Ba.

The relationship between Ba and silicate can be investigated using paired concentration measurements and $Ba_d^{residual}$ values (Equation 1-1) to identify areas where these elements decouple.

$$Ba_d^{Residual} = Ba_d^{Measured} - ((Si(OH)_4^{Measured} * \text{slope of correlation}) + \text{intercept})$$

Equation 1-1

If this de-coupling is driven by barite precipitation then this will be shown by variation in barium isotope measurements ($\delta^{138/134}Ba_{NIST}$), whereas if the main driver is silicate remineralisation then barium isotopes should be unaffected. This is because $\delta^{138/134}Ba_{NIST}$ is altered by barite cycling, but should be unaffected by silicate cycling (Sternberg et al. 2005; Horner et al. 2015). If the decoupling is being dominantly driven by water mass mixing then this will be visible in mixing lines plotted in $\delta^{138}Ba$ vs. $1/[Ba]$ space (Horner et al. 2015; Cao et al. 2016).

$$\delta^{138/134}Ba_{NIST} = \left(\frac{^{138}Ba/^{134}Ba_{sample}}{^{138}Ba/^{134}Ba_{NIST\ SRM\ 3104a}} - 1 \right) \times 1000$$

Equation 1-2: Standard delta notation of $\delta^{138/134}Ba$ relative to a standard (NIST SRM 3104a)

4. Understanding barium cycling in Antarctic waters

As discussed in Section 3, there are many proposed uses of dissolved and particulate barium as proxies for past and present oceanic conditions such as export production, alkalinity, and meltwater input (Jacquet et al. 2007; Lea and Boyle 1989, 1990; Hall and Chan 2004). The reliability of these proxies is underpinned by how well we understand the oceanic barium cycle, and its relationship with all of the processes that affect it. Whilst this understanding has increased significantly over the past several decades it is by no means comprehensive. Several unknowns still remain, such as the exact nature of barium's link to the biological cycle, and how this is reflected in the dissolved and particulate pools, the extent of abiogenic barite formation, and factors influencing barite preservation.

One way to address these issues is to further investigate the factors influencing the distribution of dissolved barium in the modern ocean. The responses of this dissolved pool to

external factors such as biological activity, sea-ice formation, dust fluxes, and meltwater input could help to reveal the nature and extent of their involvement in the barium cycle. In the following chapters I investigate these responses using high resolution ID-ICP-MS measurements of dissolved barium in the Scotia Sea, the Weddell Sea, and the waters adjacent to the West Antarctic Peninsula. This investigation will hopefully lead to a greater understanding of what factors affect the barium cycle in this region, and how the application of barite formation as a proxy for palaeoproductivity and/or barium distributions as a proxy for alkalinity or freshwater fluxes can be better constrained.

The aims and objectives of this study are therefore as follows:

- To measure the dissolved barium concentration of seawater in the waters of the Southern Ocean adjacent to the West Antarctic Peninsula, resulting in a dataset that shows the horizontal and vertical distribution of oceanic Ba_d in this region.
- To use this dataset, alongside ancillary parameters, to investigate how Ba_d in this region varies in relation to:
 - Productivity indicators such as macronutrient concentrations, Chl-a concentrations, and estimates of primary production
 - Silica cycling, primarily through the distribution of silicic acid
 - The freshwater regime, including fluxes of meltwater and the forming and melting of sea ice
 - The physical structure of the water column and the movement of different water masses
- To further investigate the role of sea ice formation and melting in barium cycling by comparing measurements of Ba_d in whole ice and interstitial meltwater samples from the WAP and from the Arctic Sea.
- Once investigated, to incorporate these relationships into a more thorough picture of barium cycling in Antarctic waters, and to consider the potential impacts on the use of barium proxies in this area.

Chapter 2

Methodology

This chapter primarily concerns the measurement of dissolved barium (Ba_d) in seawater and sea ice samples from the Southern Ocean and the Arctic Ocean, which were carried out specifically for this thesis. The collection of ancillary data such as macronutrient concentrations, temperature, salinity, and oxygen isotope measurements were all carried out by third parties, and methods will be briefly described in the appropriate data chapters.

1. Measuring Ba_d in seawater and sea ice

In recent decades, investigations throughout the global ocean (the Southern Ocean: Jacquet et al. 2005, 2007; Hoppema et al. 2010. The Arctic: Thomas et al. 2011. The Equatorial Atlantic: Esser & Volpe 2002) have shown that it is possible to form a more comprehensive and quantifiable understanding of the oceanic barium cycle through detailed studies of the distribution of dissolved barium. These detailed studies have been made possible by development of an ID ICP-MS method, which can be used to produce high precision datasets of dissolved barium concentrations using only a few millilitres of seawater, without the need for any separation chemistry.

This chapter will outline the method used and details of how the accuracy and precision of the results have been checked, including repeat measurements, long-term reproducibility of standards, and inter-laboratory calibrations.

1.1. Capturing small dynamic ranges: the need for precision

Concentrations of Ba_d in ocean waters are typically on the order of tens of nM, with the lowest values recorded in the surface waters of the North Atlantic (approximately 40 nM /5 ppb) and the highest in the deep waters of the North Pacific (approximately 150 nM /20 ppb) (see Chapter 3). High Ba_d concentrations are also reported in estuarine environments, as barium is delivered to the oceans via dissolved phases in riverine fluxes and desorption from particulate phases (typically 100 to 400 nM; Coffey et al. 1997). Although this total range throughout the ocean is fairly large, the variations in Ba_d concentration over regional scale horizontal and vertical gradients, and over temporal timescales, are usually much smaller. For example, the variation observed in Ba_d concentrations in WAP surface waters is only 15 nM (70 to 85nM; see Chapter 4). These subtle spatial and temporal variations most likely arise due to interactions between local hydrodynamical and biogeochemical controls (Jacquet et al. 2004). It is the aim of this thesis to investigate and de-convolve the effects of these different controls on the distribution of Ba_d , therefore high precision and high resolution measurements of Ba_d are necessary in order to capture small changes.

Previous methods of measuring barium such as graphite furnace atomic absorption spectrometry (AAS), ICP emission spectrometry, or isotope-dilution thermal ionisation mass spectrometry (IDTIMS), have required large volumes of sample for pre-measurement separation steps. The high sensitivity of inductively coupled plasma mass spectrometry (ICP-MS), coupled with isotope dilution (ID) spiking, negates the need for any preliminary separation steps that may lead to contamination/result in a high procedural blank; the barium isotope ratio of small samples of seawater (100 to 200 μ L) can be measured directly (Klinkhammer & Chan 1990).

1.2. Isotope dilution (ID) ICP-MS

The basic theory of isotope dilution involves a sample with a known isotopic composition of an element, but an unknown elemental concentration. In this case, samples with an unknown concentration of barium are assumed to have a natural isotopic ratio of $^{138}\text{Ba}/^{135}\text{Ba}$. This sample is mixed with a known quantity of a 'spike' solution that is enriched in the naturally rare isotope ^{135}Ba , with a known $^{138}\text{Ba}/^{135}\text{Ba}$ ratio, and a known concentration. Once homogenised, the $^{138}\text{Ba}/^{135}\text{Ba}$ ratio of this 'spiked sample' can be measured using ICP-MS, and its concentration calculated using the known parameters of the original sample and spike (see Figure 2-1, Equation 2-1 and Equation 2-2).

The advantage of using ID-ICP-MS is that only the accurate measurement of the masses involved and determination of the isotope ratio are necessary. Any matrix effects or sensitivity losses may be assumed to affect both isotopes in the same way, and therefore not compromise the accurate determination of the isotope ratio. Also, once the spike-sample mixture has equilibrated, the isotope ratio of the blend is assumed to be constant throughout, therefore the accuracy of the measurements will not be affected by any loss of the analyte. For the seawater measurements performed here, the ability to produce numerous duplicate measurements from a small volume of initial sample has been helpful in establishing robust reproducibility measurements, and increasing confidence in the precision of the data.

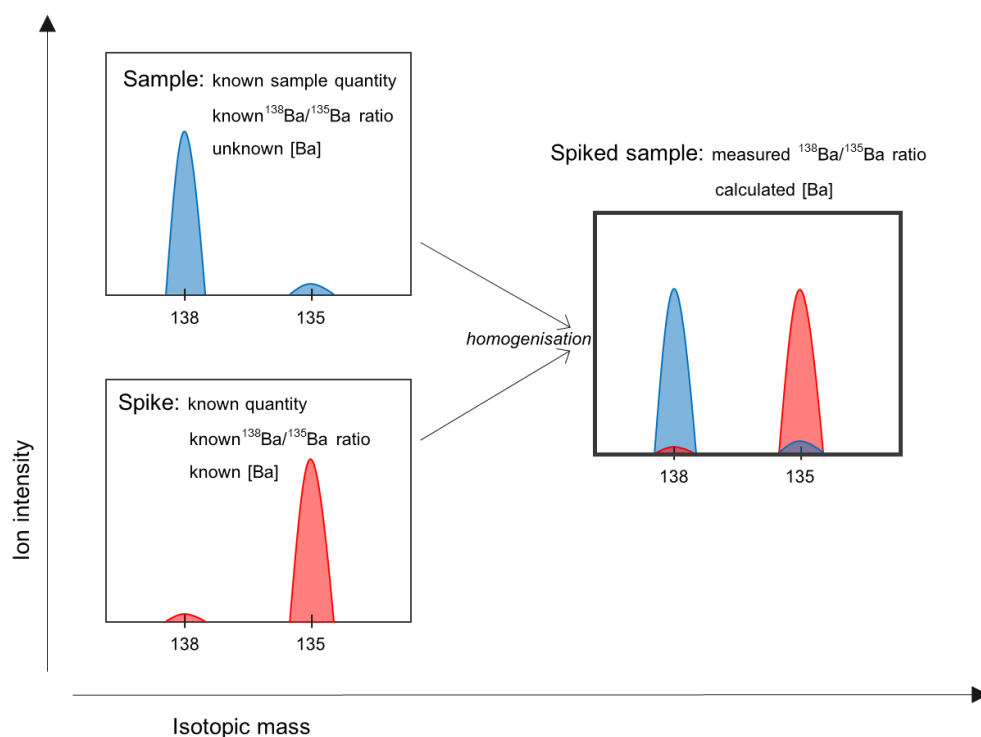


Figure 2-1: Conceptual summary of isotope dilution (after Vogl and Pritzkow 2010), with a known quantity of a spike solution enriched in ^{135}Ba , with a known concentration and a known $^{138}\text{Ba}/^{135}\text{Ba}$ ratio, is mixed with a known quantity of a sample of unknown concentration, assumed to have a natural $^{138}\text{Ba}/^{135}\text{Ba}$ ratio.

$$\left(\frac{^{138}\text{Ba}}{^{135}\text{Ba}}\right)_{\text{measured}} = \frac{\left(^{138}\text{Ba}\right)_{\text{spike}} + \left(^{138}\text{Ba}\right)_{\text{sample}}}{\left(^{135}\text{Ba}\right)_{\text{spike}} + \left(^{135}\text{Ba}\right)_{\text{sample}}}$$

Equation 2-1: Simplified concept of isotope dilution

$$C_{\text{sample}} = C_{\text{spike}} \times \frac{m_{\text{spike}}}{m_{\text{sample}}} \times \left(\frac{R_{\text{spike}} - KR_{\text{sample}}}{KR_{\text{sample}} - R_{\text{natural standard}}} \right) \times \frac{f_{\text{spike}}}{f_{\text{natural standard}}}$$

Equation 2-2: Full isotope dilution equation, where:

C_{sample} = concentration of barium in sample

C_{spike} = concentration of barium in spike

m = mass

R = ratio of $^{138}\text{Ba}/^{135}\text{Ba}$ in sample, spike, or natural standard

f = abundance of ^{135}Ba in spike or natural standard

K = mass bias correction coefficient for dilute seawater

2. Sample Collection

In total, 622 seawater samples and 96 sea ice samples have been analysed across three laboratories (Department of Marine and Coastal Science, Rutgers University, NJ; School of Earth and Ocean Sciences, Cardiff University; and the Bristol Isotope Group, Bristol University). In summary, the following datasets have been produced:

- A. Spatial seawater Ba_d distributions (vertical and horizontal) in the Scotia and Weddell Seas, comprising transects across the Drake Passage (WOCE repeat section A23) and the North Scotia Ridge, and two stations in the Weddell Sea.

Collected during the austral autumn 2014 *RRS James Clark Ross* cruise JR299 (Figure 2-2).

372 seawater samples analysed (Bristol University, 2015)

Ancillary data: temperature, salinity, dissolved inorganic nutrients

Discussed in Chapter 3

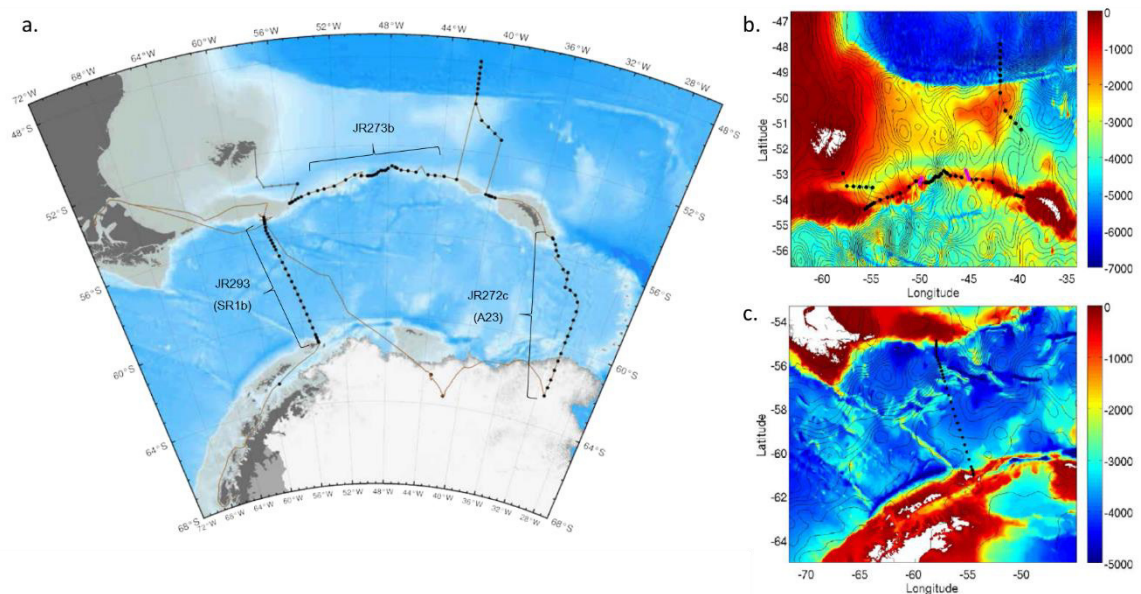


Figure 2-2: a. JR299 cruise track with CTD stations marked by black dots. Extent of Weddell Sea sea ice cover during sampling campaign shown in the south of the image. b. Detailed bathymetry of the North Scotia Ridge transect (JR273b). Colour scale is depth in metres. Contours give sea surface height (SSH) on 21st April 2014 (mauve dots represent locations of drifter deployments). c. Detailed bathymetry of the Drake Passage (JR293, SR1b) (from Meijers 2011)

- B. Spatial surface seawater Ba_d distributions (horizontal only) in waters adjacent to the West Antarctic Peninsula (WAP), comprising surface samples from the Palmer Long Term Ecological Research (PalTER) grid.

Collected during the annual PalTER cruises of the ARSV *Lawrence M. Gould* over two consecutive austral summers: LMG11-01 (2011) and LMG12-01 (2012) (Figure 2-3).

180 seawater samples analysed (Rutgers University, 2014; Cardiff University, 2015)

Ancillary data (*indicates ancillary data not available for every Ba_d sample): temperature, salinity, chlorophyll*, primary production*, dissolved inorganic nutrients*, $\delta^{18}O^*$.

Discussed in Chapter 4

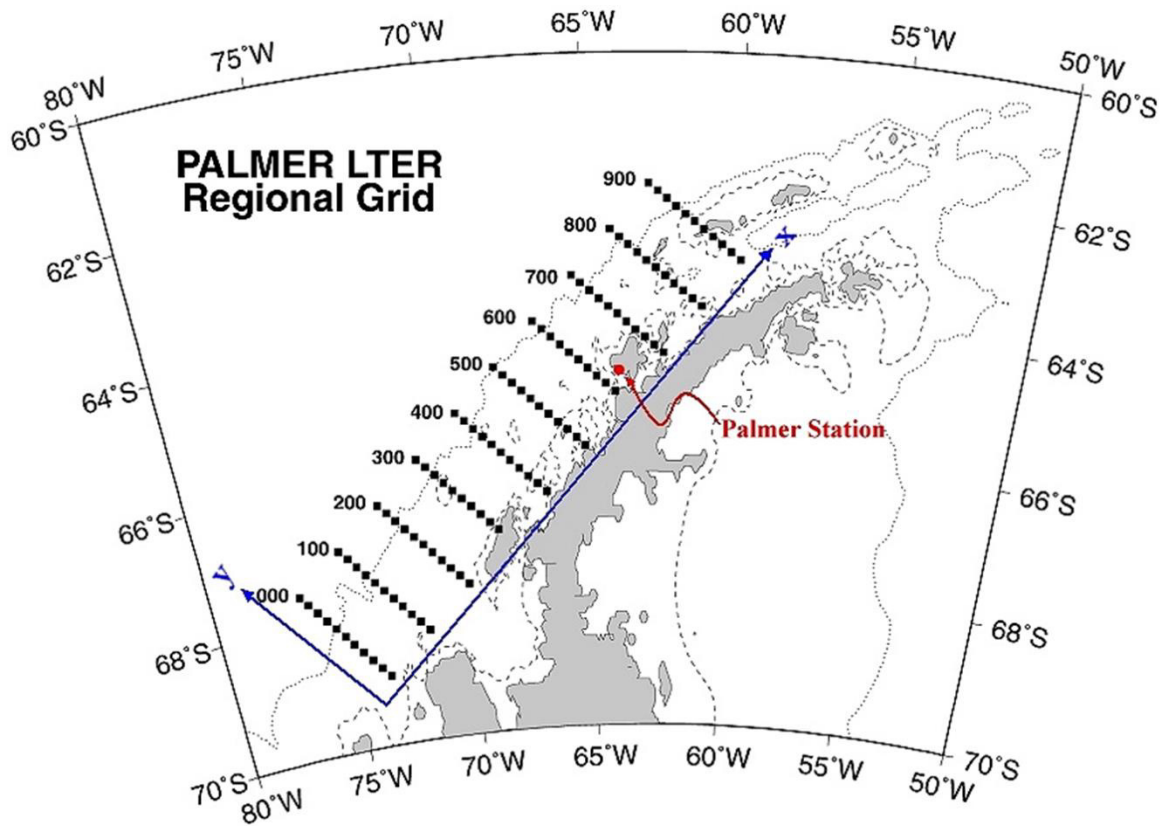


Figure 2-3: Schematic of the Palmer LTER grid of stations adjacent to the WAP. The grid is sampled annually by the R.V. Lawrence J. Gould. (Map view from <http://pal.lternet.edu/research/sampling-grid>)

- C. Temporal seawater Ba_d distributions at the fixed Rothera Oceanographic and Biological Time Series (RaTS) site in Ryder Bay, WAP (Figure 2-4).

Collected over two consecutive years, from March 2013 to January 2015.

70 seawater samples analysed (Bristol University, 2015)

Ancillary data (*indicates ancillary data not available for every Ba_d sample):
 temperature, salinity, size-fractionated chlorophyll, dissolved inorganic nutrients*, $\delta^{18}O^*$.

Discussed in Chapter 5

D. Ba_d concentrations of sackhole sea ice brines from Rothera Point, Adelaide Island, WAP (Figure 2-4).

Collected in 2005 to 2006.

18 sea ice samples analysed (Cardiff University, 2014; Bristol University, 2015)

Discussed in Chapter 6

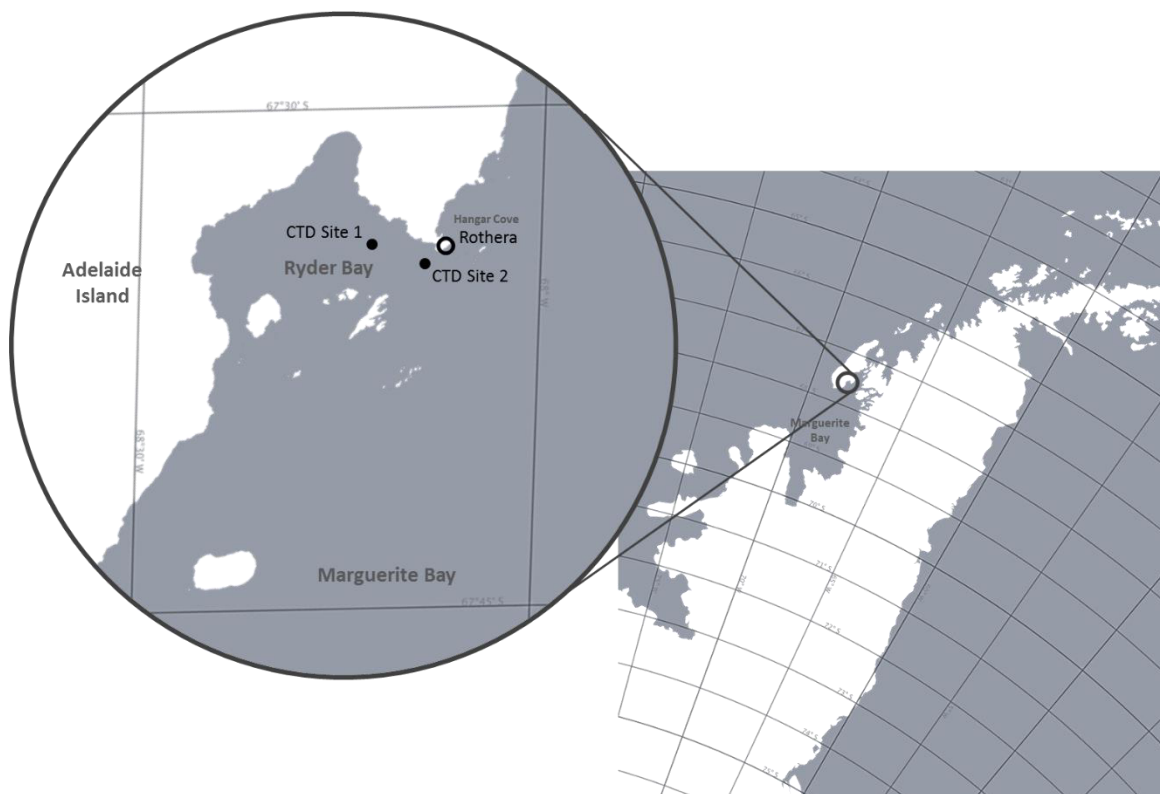


Figure 2-4: Map view of the West Antarctic Peninsula; inset showing a close up of Ryder Bay and the location of Rothera Research Station and the RaTS CTD Sites (maps from SCAR Antarctic Digital Database www.add.scar.org/).

E. Ba_d concentrations of sea ice drill cores from the Arctic Ocean (Figure 2-5)

Collected during the 2014 N-ICE Test Cruise and the 2015 N-ICE *RV Lance* cruise.

78 sea ice samples analysed (Bristol University by B. Butler, 2015/16)

Discussed in Chapter 6

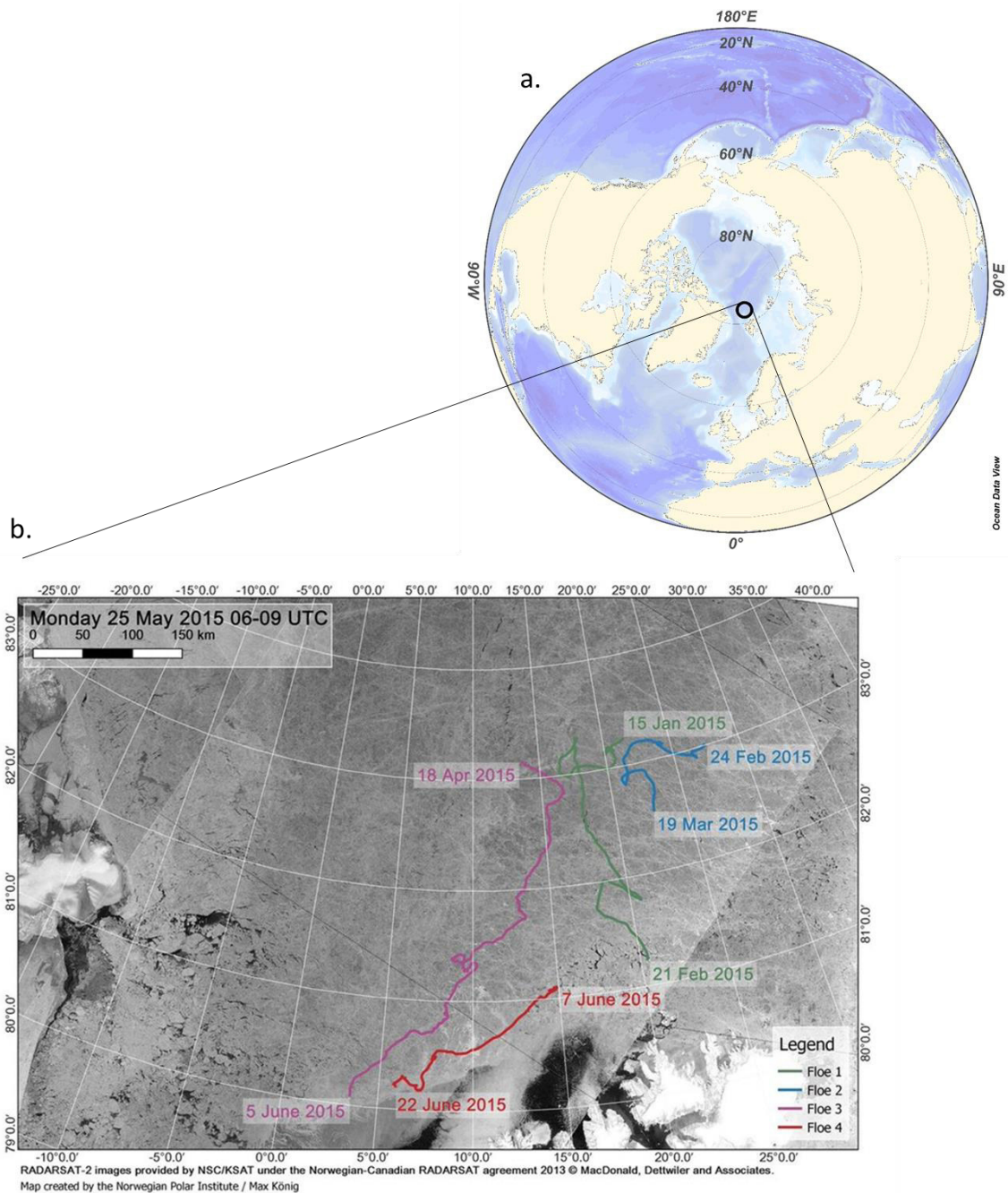


Figure 2-5: a. Northern hemisphere context showing location of N-ICE sampling location north of Svalbard in the Arctic Ocean; b. Detailed view of the N-ICE cruise track, map created by the Norwegian Polar Institute/ Max König.

The following sections detail the collection of the samples for each of these datasets. There were slight discrepancies between the methods of sample collection, with samples for some datasets filtered during collection (Palmer LTER annual cruises, see Section 2.1.i; WAP sea ice interstitial brines, see Section 2.3) and others not filtered (BAS JR299 cruise, RaTS, Arctic sea

ice melt, see Sections 2.1.ii, 2.2, and 2.4 respectively). All samples were acidified within 24 hours of collection and kept in dark conditions to limit any biological activity. Filtration was not undertaken as standard due to the logistical difficulties involved, but this may have introduced uncertainty across the datasets as particulates in unfiltered samples may have dissolved during acidification.

2.1. Seawater collection from ship-board CTD and towfish

2.1.i Palmer LTER annual cruises (West Antarctic Peninsula)

Routine annual cruises are made to sample the PalLTER grid (Figure 2-3), usually by the *ARSV Lawrence M. Gould*. In this thesis samples were analysed from two consecutive annual cruises: LMG11-01 (2nd January 2011 – 6th February 2011) and LMG12-01 (30th December 2011 – 7th February 2012).

A Conductivity-Temperature-Depth (CTD) rosette was deployed at each station, recording the temperature and conductivity of the water column via SeaBird 911+ sensors that were calibrated by SeaBird pre- and post-cruise (Martinson et al. 2008). Water was sampled from 12 L Niskin bottles closed on the upcast of the CTD into clean HDPE bottles, then filtered using 0.2 µm Acropak-200 (Pall) filters and acidified. Two depth profiles collected in this way were analysed in this thesis (Station 200.100 and Station 200.160 collected in 2012).

During ship transit, surface waters were sampled using a trace metal-clean towfish, with samples drawn from this into clean HDPE bottles, filtered using 0.2 µm Acropak-200 (Pall) filters and acidified. The surface samples from 2011 and 2012 analysed in this thesis were all collected in this way by Dr. Marie Seguert, with sub samples for Ba_d analysis aliquoted from 250 mL samples stored at Rutgers University by K. Pyle (samples at Rutgers were kept in the dark at room temperature). Additional samples were collected during the 2012 cruise specifically for Ba_d analysis by Marie Seguret, also from the underway towfish. This has allowed a greater spatial resolution in the 2012 PalLTER dataset than in the 2011 PalLTER dataset.

2.1.ii BAS JR299 cruise (Scotia and Weddell Seas, Antarctica)

I participated in British Antarctic Survey cruise JR299 by the *RRS James Clark Ross* in austral autumn 2014 (9th March to 27th April). The cruise involved two legs: JR293 from Rothera Station on Adelaide Island, WAP, to Punta Arenas, Chile (9th to 24th March) surveying the World Ocean Circulation Experiment (WOCE) repeat transect SR1b; JR272c and JR273b from Punta Arenas to Stanley, the Falkland Islands (via the Weddell Sea and South Georgia) (31st March to 27th April), taking in four SR1b stations abandoned during JR293 due to bad weather and

surveying repeat transect A23 (Weddell Sea to South Georgia), and a transect of the North Scotia Ridge (Figure 2-2).

At each station a CTD rosette was deployed with twenty-four 12 L Niskin bottles and a SBE9Plus unit with dual SBE3Plus temperature and SBE4 conductivity sensors, a Paroscientific pressure sensor, oxygen sensor, fluorometer, altimeter, photosynthetically activate radiation (PAR) sensor and transmissometer. CTD conductivity and salinity were calibrated using regularly collected bottle samples that were analysed on board using a Guildline Autosol 8400B salinometer. Data from the oxygen probe was calibrated using discrete bottle samples from five stations that were analysed on board for dissolved oxygen concentrations using Winkler titration (Full details of calibrations can be found in Meijers 2015).

Samples were collected specifically for Ba_d analysis at 47 stations, with Niskin bottles closed on the CTD upcast at depth chosen to give a representative vertical profile of the water column. Samples for Ba_d were drawn from the 20 L Niskin bottles using specified Tygon tubing into trace-metal clean 60 mL or 125 mL HDPE bottles. The Tygon tubes were reserved for Ba_d sampling, and in between stations were rinsed three times with, and stored in, deionised water. Samplers were required to wear clean nitrile gloves when handling Ba_d bottles and Ba_d sampling equipment, and followed a sampling protocol summarised as follows:

- Attach Tygon tubing to Niskin spigot, and rinse water through tube for several seconds.
- Rinse HDPE bottle three times by filling with approximately 10 mL, capping, shaking, and emptying over the tube and spigot.
- Fill to the neck of the bottle and screw cap on tightly.
- Throughout process, avoid touching the ends of the Tygon tubing, the neck of the bottle, or the thread of the screw caps, to avoid potential contamination from the outer surface of the gloves.

Once samples had been collected they were individually acidified with Optima for Ultra traces analysis 32-35% hydrochloric acid (HCl) (60 μ L of HCl added to 60 mL samples; 125 μ L added to 125 mL samples) in order to prevent biological alteration of the sample during storage. If necessary, the necks of bottles were dried using Kimtech wipes to prevent salt crystal formation at the bottle rim. Bottles were then capped, sealed with Parafilm, and stored in the dark in the cool room at a constant temperature of 2 to 4°C to minimise evaporation effects. Sample acidification was conducted in a fume hood in the Radiation Lab on board the *RRS James Clarke Ross*, which was cleaned thoroughly at the start of the cruise and kept as a 'barium clean' area as much as possible. The length of time that samples were left uncapped was minimised in order to reduce air contamination.

2.2. Seawater collection at Rothera Oceanographic and Biological Times Series (RaTS)

Station personnel at Rothera conduct CTD sampling events for the RaTS time series on a weekly basis, deploying a SeaBird SBE19 and a 5 L Niskin bottle from a rigid inflatable boat at CTD Site 1 in Ryder Bay (Figure 2-4) using a hand-cranked winch. During periods of sufficiently heavy ice-cover, the CTD is instead deployed through a hole cut in the ice. When CTD Site 1 is inaccessible, CTD Site 2 is occupied instead. Conductivity measurements are calibrated post-season using discrete measurements made on an Autosol 8400B salinometer, and by comparison with the SeaBird 911+ instruments carried on the *ARV Laurence M. Gould* and the *RRS James Clarke Ross*. Samples collected by station personnel for Ba_d analysis were acidified but not filtered, and were kept refrigerated and in the dark during storage and transport.

2.3. Collection of sea ice brine samples at Rothera Point, Adelaide Island

Between the 13th October 2005 and 21st November 2006, sea ice interstitial brines were sampled from various sites around Rothera Point (Hangar Cove, CTD Sites 1 and 2, Rothera wharf; see Figure 2-4) by K. R. Hendry via sackhole drilling. Snow was cleared from the sea ice surface using a plastic edge and a hole drilled into the sea ice, which was then cleaned of brash ice and contaminants, and covered for five minutes to one hour. The brine that drained into the hole was collected into clean HDPE containers and taken to Rother Station, where they were filtered using 0.2 micrometer polycarbonate membranes (Whatman), and the filtrate acidified using 1 ml HNO_3 per litre of brine (Hendry et al. 2009, 2010).

2.4. Collection of sea ice melt from Arctic drill cores (N-ICE cruise and Test cruise)

As part of the Norwegian Young sea ICE cruise (N-ICE 2015) project, the *R.V. Lance* was allowed to freeze into sea ice north of Svalbard in the Arctic Ocean and drift passively with the ice throughout the sea ice season (Figure 2-5 b). An initial 'test drift' cruise was carried out in February 2014, whilst the main N-ICE cruise took place from the 7th January to 23rd June 2015. Sea ice drill cores were collected throughout this period, divided into depth sections, and allowed to melt. Sub-samples of this whole-ice melt were drawn into clean HDPE bottles specifically for Ba_d analysis. The water column below the ice was also sampled by deploying a Hydro-Bios Slimline CTD rosette through a 1 m diameter hole cut in the sea ice.

3. Sample Storage

Samples were stored in parafilm clean HDPE bottles (see Section 4.1.i) under refrigerated conditions and in the dark immediately following collection and during transit, in order to prevent alteration of the sample through evaporation or biological activity. Subsequently, samples were typically kept at room temperature in the dark. Efforts were made

to keep the samples at a constant temperature (approximately 21°C). Whilst refrigerated conditions would have been preferable, the large total volume of the samples made this impractical.

Samples were stored double-bagged in batches of 10 to 20, with inner bags and the bottles themselves only exposed within a clean laboratory environment. Standard trace metal laboratory procedures were followed in order to minimise potential contamination of the original samples; aliquots for analysis were poured from sample bottles into clean 15 mL centrifuge tubes (see Section 4.1.i) within a laminar flow hood, and sample bottles were immediately re-sealed with parafilm.

3.1. Evaporation checks

Due to the logistical difficulties of refrigerating the large volume of samples, and the impossibility of guaranteeing constant temperatures during transit of samples (for example, the transport of sample splits between Rutgers University, Cardiff University, and Bristol University), it was necessary to check whether potential evaporation through the HDPE storage bottles could significantly alter the Ba_d concentration of a sample. This was particularly necessary to establish as some samples were kept in storage for several years prior to analysis, whilst others were analysed within a few months of collection (for the period elapsed between collection and analysis, see Section 2 for dates of sample collection and analysis).

Two tests were conducted to assess the potential impact of evaporation effects on measurement reproducibility. The potential effects of evaporation on un-diluted, un-spiked seawater samples were investigated by comparing the measured concentrations of the NASS-5 seawater standard over three years, in three different laboratories. In this case, after the initial analyses at Rutgers University, a 10 mL aliquot of NASS-5 seawater was transported to Cardiff University, and subsequently to Bristol University, and stored at room temperature in a parafilm 15 mL centrifuge tube. At each of these institutions, bulk spiked solutions of NASS-5 were prepared from this aliquot (see Table 2-11) and analysed (Figure 2-6).

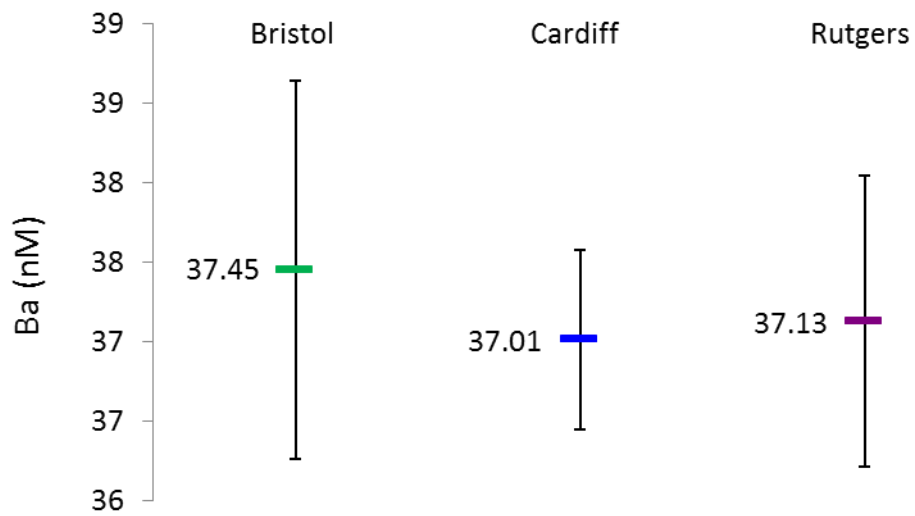


Figure 2-6: Reproducibility of standard seawater solution NASS-5 R (spiked) as a check of potential evaporation effects during storage and transport of samples at room temperature. NASS-5 solution was spiked and analysed at Rutgers University (NASS-5 R). A 10mL aliquot of unspiked, undiluted NASS-5 solution was then transported to Cardiff and Bristol Universities, where spiked solutions were prepared and analysed in February 2014 (Cardiff) and from March-September 2015 (Bristol). Error bars shown are 2*SD on all measurements made in each laboratory. Within this intra-laboratory reproducibility, measurements of Ba_d concentration are identical over the three years that the NASS-5 seawater was stored.

Additionally, standard seawater solutions (In-house standards Amundsen_1 and SO, and certified standard NASS-5) were spiked in bulk (125 mL of final spiked solution) at Rutgers University and analysed on the Element-1 in April 2013. 60 mL sub-samples of these bulk solutions were then transported to Cardiff University and stored at room temperature (approximately 22°C) for eleven months. In February 2014 these solutions were analysed at Cardiff on the Element XR, and the concentrations were found to be within error of the original measurements, with no systematic off-set or alteration (Figure 2-7).

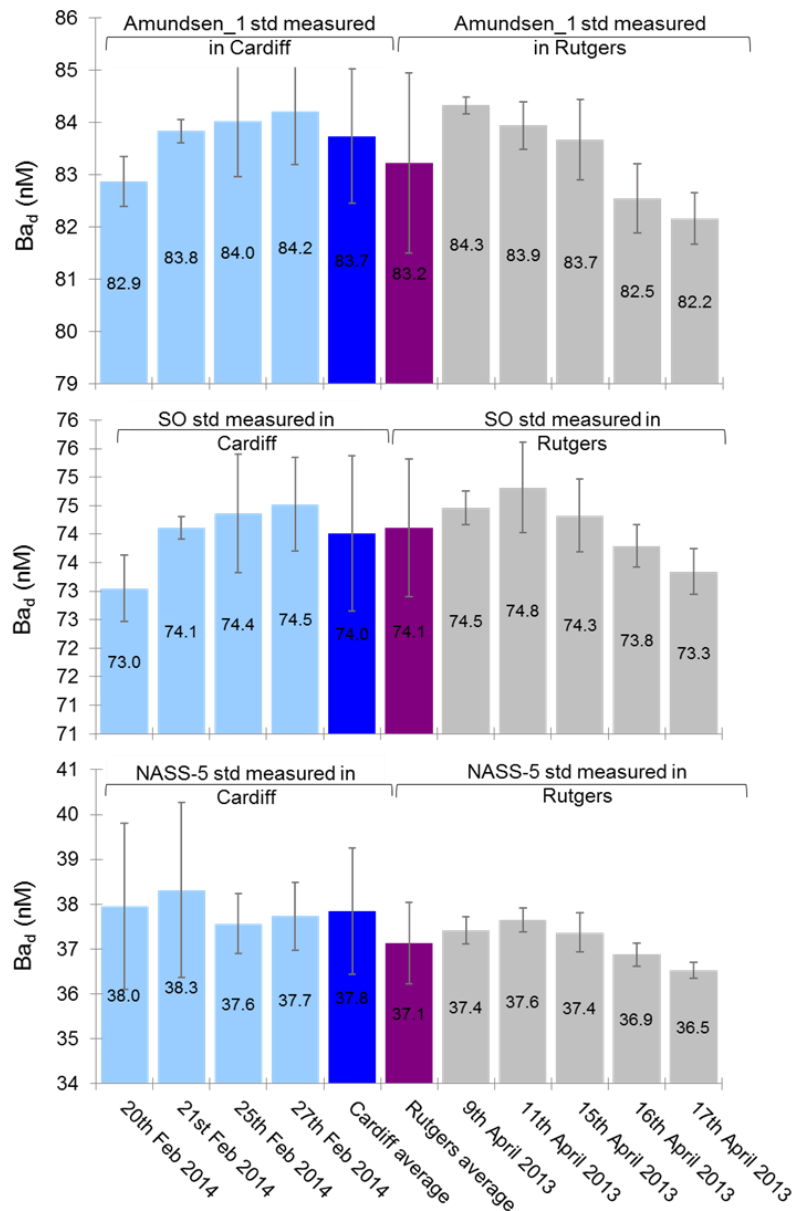


Figure 2-7: reproducibility of standard seawater solutions (Amundsen_1 R, SO R, and NASS-5 R (all spiked in bulk)) as a check of potential evaporation effects during storage and transport of samples at room temperature. The solutions were spiked and analysed at Rutgers University in April 2013 (see Table 2 11), and then transported in parafilm HDPE bottles to Cardiff University where they were re-analysed in February 2014

Both of these tests show that, within analytical error, the Ba_d concentration measured in the same seawater solutions does not vary over the course of one to three years, even when stored at room temperature. This implies that the effect of any evaporation experienced by samples during non-refrigerated storage will have a negligible impact on their Ba_d concentration over this timescale.

4. Detail of the ID-ICP-MS method

4.1. Sample preparation and spiking

Samples were prepared for isotope dilution (ID) under clean laboratory conditions, within laminar flow hoods, typically in batches of 27 (with three duplicates per batch - see Section 5.2.ii). After the method described by Klinkhammer and Chan (1990), aliquots of seawater were spiked gravimetrically with a ^{135}Ba -enriched solution (10 $\mu\text{g}/\text{mL}$ ^{135}Ba , Inorganic Ventures, Christiansburg, VA, USA, gravimetrically diluted to a Working Spike solution with a concentration of approximately 100 nM Ba using high purity 3% HNO_3) to achieve a $^{138}\text{Ba}/^{135}\text{Ba}$ ratio of 0.65 to 1. The volumes of sample and spike solution required varied according to the estimated Ba concentration of the seawater sample, but the majority of seawater samples were analysed using either 250 μL seawater plus 200 μL spike solution, or 200 μL seawater plus 160 μL spike solution (Table 2-1).

A summary of the method protocol used in all laboratories is as follows:

- Weigh run tubes, recording to four decimal places
- Aliquot 2 to 3 mL of sample into sample tubes, recording the tube number of each sample
- Pipette 250 μL /200 μL of each sample into corresponding run tube. Use a new pipette tip for each sample, and discard 250 μL /200 μL into the waste beaker before pipetting the same volume into the run tube.
- Weigh the run tubes (+sample), recording to four decimal places
- Pipette 200 μL /160 μL Working Spike solution (approximately 100 nM) into each run tube. Use the same pipette tip throughout, ensuring that it does not touch the edges of any of the tubes or bottles. Before beginning to pipette the spike, clean the pipette tip by discarding 250 μL /200 μL 2N nitric acid into the waste beaker two times, followed by 250 μL /200 μL Milli-Q water six times.
- Weigh the run tubes (+sample +spike), recording to four decimal places.
- Add an appropriate volume of high purity 3% HNO_3 to dilute the seawater 20 times.
- Invert each tube fifteen times to ensure that the mixture homogenises, and leave to equilibrate for several hours, preferably overnight.

Table 2-1: Typical spiking ratios for a range of potential seawater concentrations, assuming a working spike concentration of 100 nM, with 'Total' referring to solution plus spike ($\text{Total } ^{\text{isotope}}\text{Ba} = (^{\text{isotope}}\text{Ba}_{\text{sample}} * ^{\text{isotope}}f_y) + (^{\text{isotope}}\text{Ba}_{\text{spike}} * ^{\text{isotope}}f_x)$)

Approximate [Ba] (nM)	Sample (mL)	Spike (mL)	[Ba] sample (nmol)	Total [Ba] (nmol)	Total ¹³⁵ Ba	Total ¹³⁸ Ba	¹³⁸ Ba/ ¹³⁵ Ba	Total solution (mL)	HNO ₃ to add (mL)	Seawater dilution
5	1	0.05	0.005	0.005	0.0047	0.0038	0.800	20	18.95	5%
20	0.4	0.09	0.008	0.009	0.0085	0.0061	0.716	8	7.51	5%
30	0.4	0.1	0.012	0.01	0.0094	0.0090	0.951	8	7.5	5%
40	0.21	0.09	0.0084	0.009	0.0085	0.0063	0.750	4	3.7	5%
50	0.2	0.1	0.01	0.01	0.0094	0.0075	0.800	4	3.7	5%
60	0.2	0.13	0.012	0.013	0.0122	0.0091	0.742	4	3.67	5%
70	0.2	0.13	0.014	0.013	0.0122	0.0105	0.858	4	3.67	5%
80	0.2	0.16	0.016	0.016	0.0150	0.0120	0.800	4	3.64	5%
90	0.2	0.16	0.018	0.016	0.0151	0.0135	0.895	4	3.64	5%
100	0.2	0.2	0.02	0.02	0.0188	0.0151	0.800	4	3.6	5%
110	0.2	0.25	0.022	0.025	0.0235	0.0167	0.709	4	3.55	5%
120	0.2	0.25	0.024	0.025	0.0235	0.0181	0.770	4	3.55	5%
130	0.2	0.25	0.026	0.025	0.0235	0.0195	0.831	4	3.55	5%
140	0.2	0.25	0.028	0.025	0.0235	0.0210	0.891	4	3.55	5%
150	0.1	0.15	0.015	0.015	0.0141	0.0113	0.800	2	1.75	5%
200	0.1	0.2	0.02	0.02	0.0188	0.0151	0.800	2	1.7	5%

4.1.i Cleaning of equipment

The HDPE bottles used for storing samples, and the 15 mL sterile PP centrifuge tubes (orange capped Corning Centristar) used for ID-ICP-MS spiking and analysis, were cleaned using 2N nitric acid (analytical reagent grade) and 18 MΩ deionised water. After initial rinsing with deionised water, bottles and tubes were filled approximately 2/3 with 2N nitric acid and stored upright for 24 hours, and upside-down for 24 hours. They were then emptied of acid and rinsed three times with 18 MΩ deionised water before the process was repeated using 18 MΩ deionised water. After a final rinse, bottles and tubes were dried within a laminar flow hood and stored under clean conditions until needed.

4.1.ii Spike calibration

An essential component of the isotope dilution method is establishing the concentration and $^{138}\text{Ba}/^{135}\text{Ba}$ ratio of the ^{135}Ba -enriched spike solution. The manufacturers of the spike solution provide a certification of these properties that is summarised in Table 2-2.

Isotope	Natural abundance (fx)	
^{135}Ba	0.06592	6.6%
^{137}Ba	0.11232	11.2%
^{138}Ba	0.71699	71.7%
	Natural ratio (Rx)	
$^{138}\text{Ba}/^{135}\text{Ba}$	10.87667	
$^{137}\text{Ba}/^{135}\text{Ba}$	1.703883	

Isotope	Certified spike abundance (fy)	
^{135}Ba	0.9273	92.7%
^{137}Ba	0.0091	0.9%
^{138}Ba	0.0404	4.0%
	Certified spike ratio (Ry)	
$^{138}\text{Ba}/^{135}\text{Ba}$	0.043567	
$^{137}\text{Ba}/^{135}\text{Ba}$	0.009813	

Isotope	Certified spike concentration (cy)	
	(ug/mL)	(nM)
^{135}Ba	10.035	73067
^{137}Ba	0.0988	719
^{138}Ba	0.4393	3199

Table 2-2: Certification of Inorganic Ventures ^{135}Ba -enriched spike solution.

Whilst this manufacturer-provided concentration (for Primary spike B – 10 µg/mL) can be taken as a starting estimate, it is important to calculate an accurate concentration for the spike solution, as well as establishing accurate values of the other ID parameters required (R_x = the naturally occurring $^{138}\text{Ba}/^{135}\text{Ba}$ ratio; R_y = the $^{138}\text{Ba}/^{135}\text{Ba}$ ratio in the spike solution; f_y = the abundance of the spike isotope ^{135}Ba in the spike solution. The abundance of the spike isotope ^{135}Ba in nature is assumed to be 6.6%, see Table 2-2). These measurements are determined by calibrating the spike solution via reverse-isotope dilution of blended solutions containing a mixture of the spike solution and a Ba-natural standard from High Purity Standards (Table 2-3). The $^{138}\text{Ba}/^{135}\text{Ba}$ ratio of these blends are measured and used to calculate an accurate concentration of the spike solution using reverse-isotope-dilution. At the same time a 1.5 ppb spike solution is also run to measure f_y and R_y , and a diluted natural standard (1 ppb) is run to measure R_x .

	^{135}Ba (ng/mL)	^{138}Ba (ng/mL)	$^{138}\text{Ba}/^{135}\text{Ba}$
Blend 1	1.0734657	0.7566340	0.7048516
Blend 2	1.0735765	0.7577312	0.7058009

Table 2-3: Isotope quantities and $^{138}\text{Ba}/^{135}\text{Ba}$ ratio in typical solutions prepared for spike calibrations (actual values from Bristol November'15 spike calibration). The blends are a mixture of a 1.5 ppb spike solution to measure for reverse ID spike parameters and diluted natural standard (1 ppb) to measure for reverse ID natural parameters.

Spike calibrations were carried out at regular intervals (every one to two months), so that the ID calculations carried out on samples could be adapted to time-varying sensitivity of the instrument (Figure 2 8 and Table 2 4). The absolute variation in the measured values over time was small, tended to be consistently higher than the values reported by the manufacturer, and did not vary systematically between the different laboratories.

For all measurements made in Cardiff University and Bristol University, the same Primary Spike (B) from Inorganic Ventures was used. Measurements in Rutgers University were made using a Primary Spike solution from a different source (A). The Primary ^{135}Ba -enriched spike solution (B) was diluted in two stages with 3% Romil Super-Pure Acid (SPA) to produce a working spike of approximately 100 nM Ba concentration (Table 2-4). These working spike (WS) solutions were periodically replaced (approximately every six months) to reduce the potential for contamination build-up. The accurate concentration of each new WS was back-calculated using the results of the most recent spike calibration and the gravimetrically measured degree of dilution.

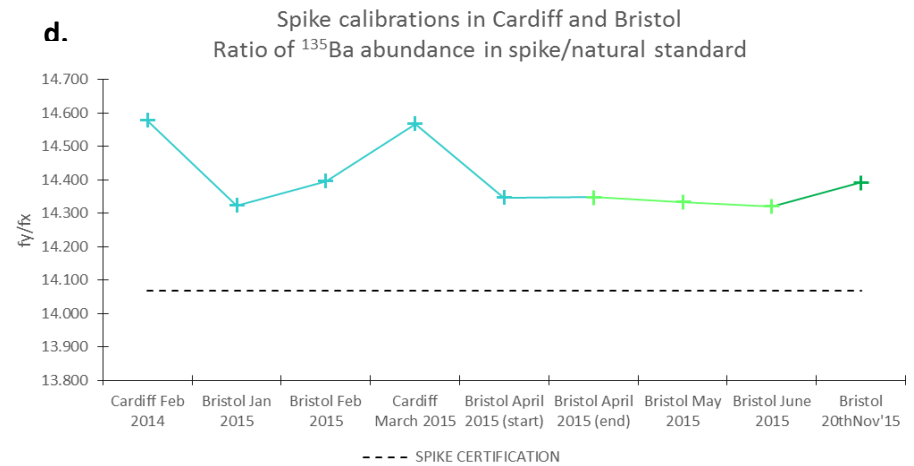
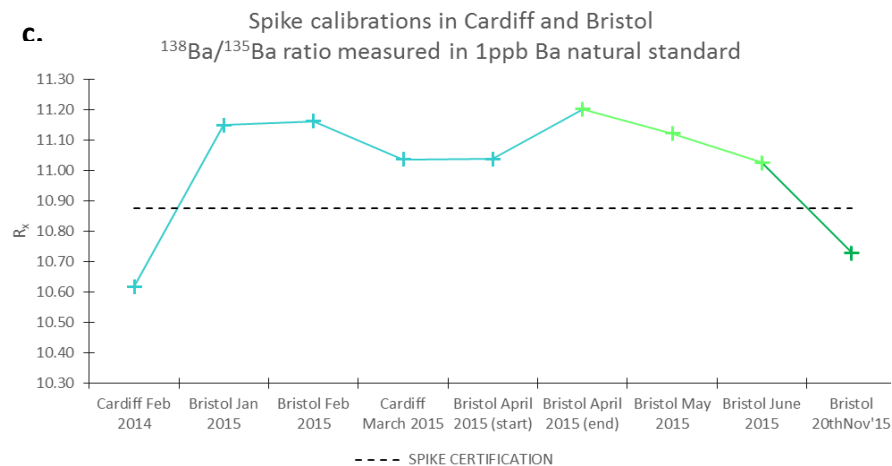
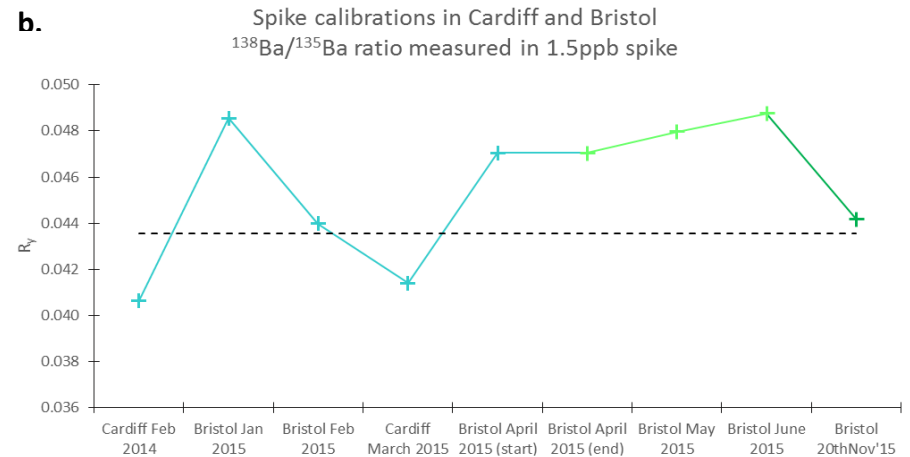
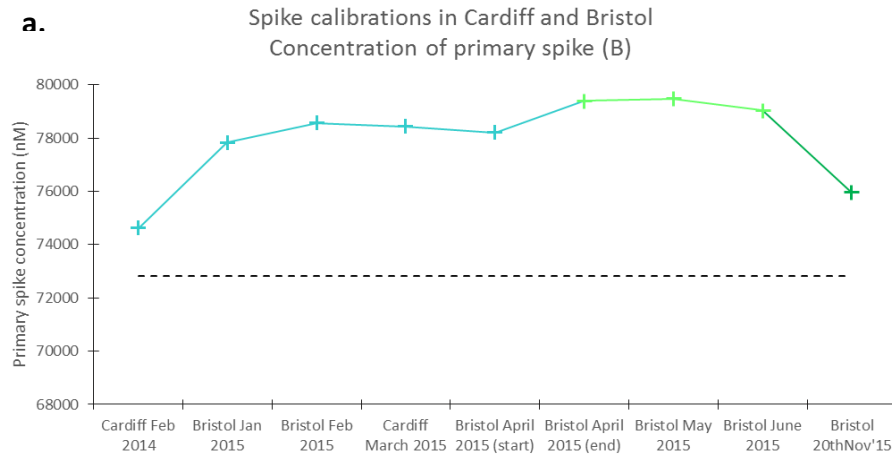


Figure 2-8: Spike calibrations performed in Bristol University and Cardiff University from February 2014 to November 2015 (primary spike B) a. Concentration of primary spike (B) determined by reverse-isotope dilution calculation; b. $^{138}\text{Ba}/^{135}\text{Ba}$ ratio measured in 1.5 ppb spike solution (B); c. $^{138}\text{Ba}/^{135}\text{Ba}$ ratio measured in 1 ppb natural standard; d. f_y/f_x (ratio of the abundance of ^{135}Ba in spike to the abundance of ^{135}Ba in natural standard) measured. Dotted line in all figures represents the value given by the manufacturer (Inorganic Ventures). The colour of markers and lines indicates the values used to calculate concentrations and parameters for different Working Spike solutions (WS_C1 – light blue; WS_B1 – light green; WS_B2 – dark green).

Table 2-4: Details of the concentrations and associated parameters calculated for working spikes from spike calibrations performed at Rutgers University, Cardiff University, and Bristol University. Primary spike concentrations are derived from the spike calibration, with working spike concentrations subsequently calculated using the gravimetrically measured dilution factor. Details of the Primary spike certification from the manufacturer given for reference.

Primary Spike	Working Spike	Spike Calibration	Primary spike concentration		Dilution factor	Working Spike concentration (c _y)		ID parameters from spike calibration				
			(nM)	(µg/mL)		(nM)	(µg/mL)	R _x	R _y	f _y	f _x	f _y /f _x
A	WS_R1	Rutgers pre-2013	223898	30.8	2266	98.8	0.0136	11.05	0.04	96.3%	6.6%	14.60
A	WS_R2	Rutgers April 2013	223898	30.8	2318	96.6	0.0133	11.05	0.04	96.3%	6.6%	14.60
B	WS_C1	Cardiff February 2014	74627	10.2	777	96.0	0.0132	10.62	0.04	96.1%	6.6%	14.58
B	WS_C1	Bristol January 2015	77828	10.7	777	100.1	0.0137	11.15	0.05	94.4%	6.6%	14.32
B	WS_C1	Bristol February 2015	78573	10.8	777	101.1	0.0139	11.16	0.04	94.9%	6.6%	14.40
B	WS_C1	Cardiff March 2015	78434	10.8	777	100.9	0.0139	11.04	0.04	96.0%	6.6%	14.57
B	WS_C1	Bristol April 2015 (start)	78202	10.7	777	100.6	0.0138	11.04	0.05	94.6%	6.6%	14.35
B	WS_B1	Bristol April 2015 (end)	79389	10.9	806	98.5	0.0135	11.20	0.05	94.6%	6.6%	14.35
B	WS_B1	Bristol May 2015	79485	10.9	806	98.6	0.0135	11.12	0.05	94.5%	6.6%	14.33
B	WS_B1	Bristol June 2015	79043	10.9	806	98.1	0.0135	11.03	0.05	94.4%	6.6%	14.32
B	WS_B2	Bristol November 2015	75958	10.4	761	99.8	0.0137	10.73	0.04	94.9%	6.6%	14.39
Primary spike certification (B)			72812	10.0				10.88	0.044	92.7%	6.6%	14.07
Primary spike certification (A)			206000	28.3								

4.1.iii Determining ratio of spike to sample: preventing error magnification

In isotope dilution the uncertainty of the final calculated concentration is largely determined by the precision of the isotopic ratio in the spike-sample mixture. There is an optimum isotopic composition of this mixture which will give the greatest precision (De Bievre and Debus 1965; Hoelzl et al. 1998), which for $^{138}\text{Ba}/^{135}\text{Ba}$ has been found to be between 0.65 and 1.0 (Klinkhammer and Chan 1990).

As the concentration of the Working Spike is constant, a rough estimate of the sample Ba_d concentration is needed in order to calculate the appropriate volumes of sample and spike required to achieve a measured ratio within this 'range of minimum error'. This was a simple matter for most of the samples analysed, as the ranges of Ba_d concentration in seawater change gradually and reasonably predictably zonally and with depth, and it is the subtle variations within these larger ranges that are the subject of this thesis. Samples that were over- or under-spike due to a mistaken estimation of their Ba_d concentration were identified as having a $^{138}\text{Ba}/^{135}\text{Ba}$ ratio less than 0.65 or greater than 1.0, and were prepared again using a re-calculated spike/sample volume and re-analysed. This procedure was particularly common when measuring the sea ice samples, which often had unpredictable Ba_d concentrations.

A summary of the estimated volumes necessary for different concentrations is shown in Table 2-1. For extremes of high and low Ba_d concentrations it was sometimes necessary to alter the total volume of the spike-sample mixture to accommodate the 5 % dilution factor necessary to run seawater samples directly through the ICP-MS. Volumes also had to be adapted to avoid using volumes < 90 μL , as the weighing errors on these small volumes decreased the precision of the calculated concentrations.

4.1.iv Gravimetric determination of solution quantities

The volumes of spike solution and sample used to prepare the spike-sample mixture must be accurately known, therefore I determined them gravimetrically using a four-decimal place balance and an anti-static gate. Tubes were weighed before and after samples were added, and again after the spike solution was added, and the following equations applied:

$$\text{Sample volume} = (\text{Mass}_{\text{tube} + \text{sample}} - \text{Mass}_{\text{tube}}) * \text{Density}_{\text{seawater}}$$

Equation 2-3 (where $\text{Density}_{\text{seawater}}$ is taken as 1.025 kg L^{-1})

$$\text{Spike volume} = (\text{Mass}_{\text{tube} + \text{sample} + \text{spike}} - \text{Mass}_{\text{tube} + \text{sample}}) * \text{Density}_{\text{HNO}_3}$$

Equation 2-4 (where $\text{Density}_{\text{HNO}_3}$ is taken as 1.011 kg L^{-1})

4.2. Contamination checks: blanks

Barium is not abundant in the natural environment, therefore contamination levels are not expected to be high, particularly when work is carried out under clean laboratory conditions. However, it is important to monitor blank levels to ensure that:

- a.) Any variation in blank measurements over time are noted and accounted for;
- b.) There is not a disproportionate blank contribution from one isotope relative to the other, which could lead to inaccuracies in the measured $^{138}\text{Ba}/^{135}\text{Ba}$ ratio.

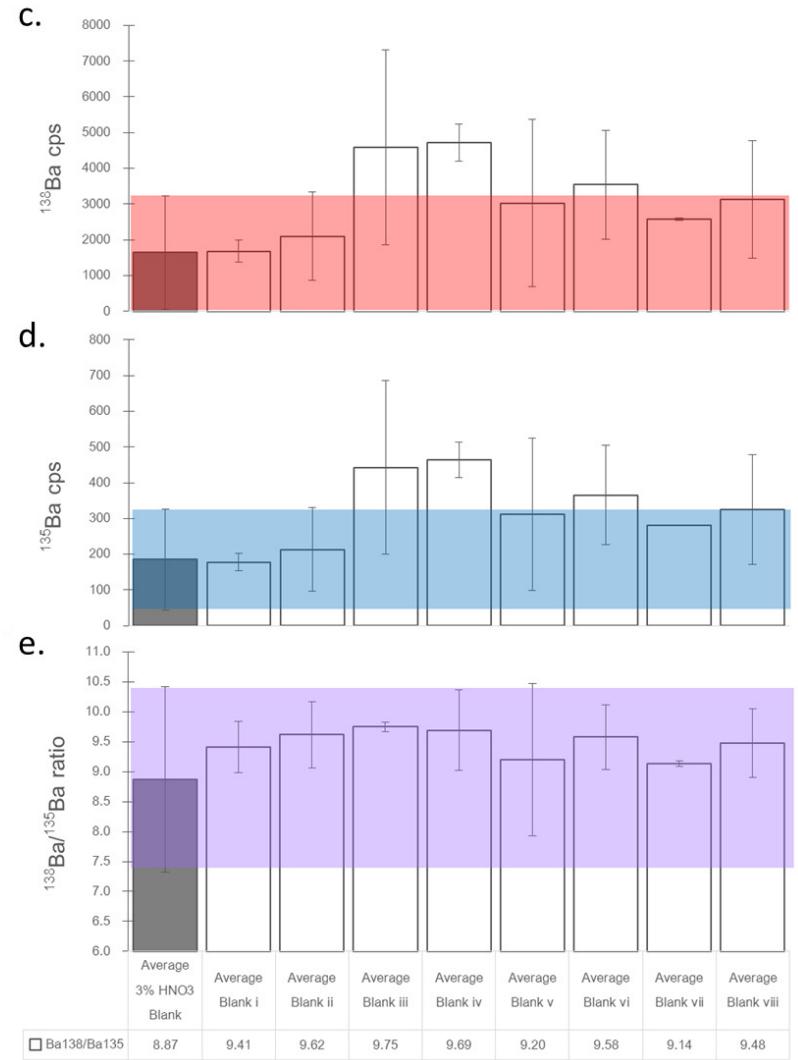
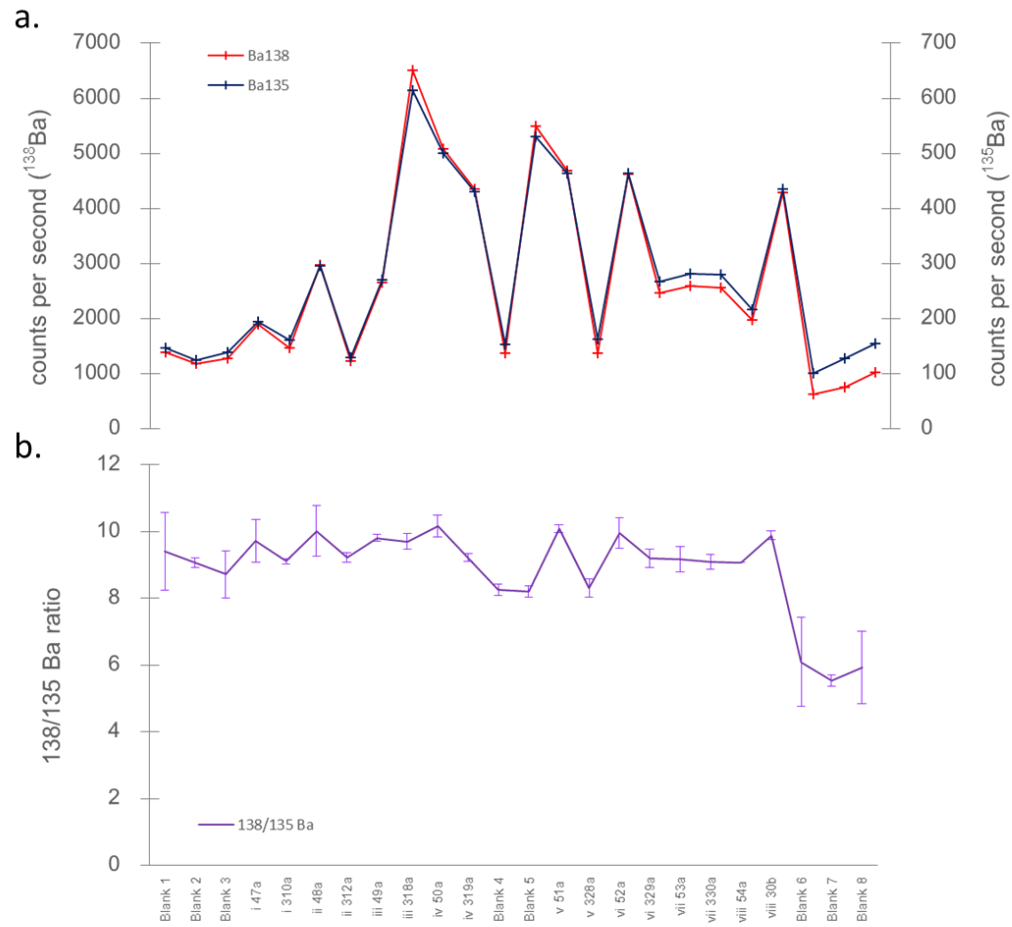
This latter point is particularly pertinent due to the handling of spike solutions with a non-natural $^{138}\text{Ba}/^{135}\text{Ba}$ ratio in the vicinity of samples, which may lead to accidental contamination.

There are three types of blank measurement to be investigated and monitored: sample collection blanks, procedural blanks, and instrument blanks. Each of these, and the steps taken to account for them, are briefly outlined in the sections below.

4.2.i Sample collection blanks and procedural blanks

In order to check for potential contamination during sample collection and preparation, sample collection and procedural blanks are monitored. The sample collection blanks involved collecting eight 'blank samples' in the form of deionised water throughout the BAS JR299 cruise. These 'blank samples' were treated as if they were samples: exposed to the air of the ship for the same length of time, handled similarly around the CTD rosette and in the laboratory, acidified, and stored under the same conditions. The purpose of this was to quantify if these solutions, once diluted with 3% HNO_3 as if they were samples, showed any significant variation in either the absolute amount of Ba_d present, or in the $^{138}\text{Ba}/^{135}\text{Ba}$ ratio measured, from clean HNO_3 blanks considered to have a minimal Ba_d content and a natural $^{138}\text{Ba}/^{135}\text{Ba}$ ratio. The measurement of these eight 'blank samples' via ICP-MS is shown in Figure 2-9; although three of the solutions were found to have slightly elevated absolute Ba compared to clean HNO_3 blanks, they were still below 0.2% and 2.5% of average spiked seawater counts (^{135}Ba and ^{138}Ba respectively). Moreover, the $^{138}\text{Ba}/^{135}\text{Ba}$ ratios measured for each were comfortably within the range measured in standard clean HNO_3 blanks. This indicates that even though there may have been slight sources of Ba contamination on board the RRS James Clarke Ross, the $^{138}\text{Ba}/^{135}\text{Ba}$ ratios of the samples was probably not compromised.

Figure 2-9: (overleaf) Results from JR299 'blank samples' – deionised water collected and stored under the same conditions as samples, then diluted 20 times with 3% HNO_3 and analysed alongside clean HNO_3 acid blanks. Absolute counts per second of ^{135}Ba and ^{138}Ba are elevated in three samples, but all show natural $^{138}\text{Ba}/^{135}\text{Ba}$ ratios comparable to those measured in the clean HNO_3 acid blanks.



Potential contamination during the spiking process was checked by analysing procedural blanks – clean HNO₃ weighed and mixed with spike solution as if it were a sample. Calculation of the Ba_d concentration of blanks prepared in this way were comfortably within error of zero.

4.2.ii Acid blanks

The general background level of Ba contamination that may be present in the laboratory or introduced within the introduction system of the ICP-MS was quantified by analysing clean acid (HNO₃) blanks regularly alongside sample analysis. The average counts per second (cps) measured for each isotope in these blanks were subtracted from sample cps (after correction for matrix effects – see Section 4.3.iii) in order to remove this background signature from the ¹³⁸Ba/¹³⁵Ba ratio measured in samples.

Monitoring blank levels also proved to be a useful tool in diagnosing when there were problems within the workings of the ICP-MS. As can be seen in Figure 2-10, background blank levels were very low, typically constituting < 0.1 % and < 1.0 % of average spiked seawater cps for ¹³⁵Ba and ¹³⁸Ba respectively.

However, there were three periods of time (April/May 2015, June 2015, and September 2015) when the background blank levels measured in Bristol were significantly elevated, with ¹³⁸Ba in particular reaching levels of up to 4 to 9 % of seawater cps. These periods correspond to sample analyses when anomalously low/high concentrations were measured for standard solutions (see Figure 2-17 and Figure 2-18), indicating that the ¹³⁸Ba/¹³⁵Ba ratios measured were not accurate. Given the coincidence of these anomalies with the high blank levels, it was assumed that there was a source of contamination with a non-natural ¹³⁸Ba/¹³⁵Ba ratio. In an effort to isolate this source of contamination, all reagent acids were disposed of and replaced, the ICP-MS introduction system was cleaned with dilute HNO₃ and deionised water, new sample and skimmer cones were introduced, and new spiked standard solutions were prepared and measured. Despite these attempts, the problem persisted intermittently. I therefore carefully monitored the background blank levels and the reproducibility of standard solutions, and did not attempt to analyse samples if the background blanks were above a threshold of 1.5 % ¹³⁸Ba as a percentage of average seawater cps.

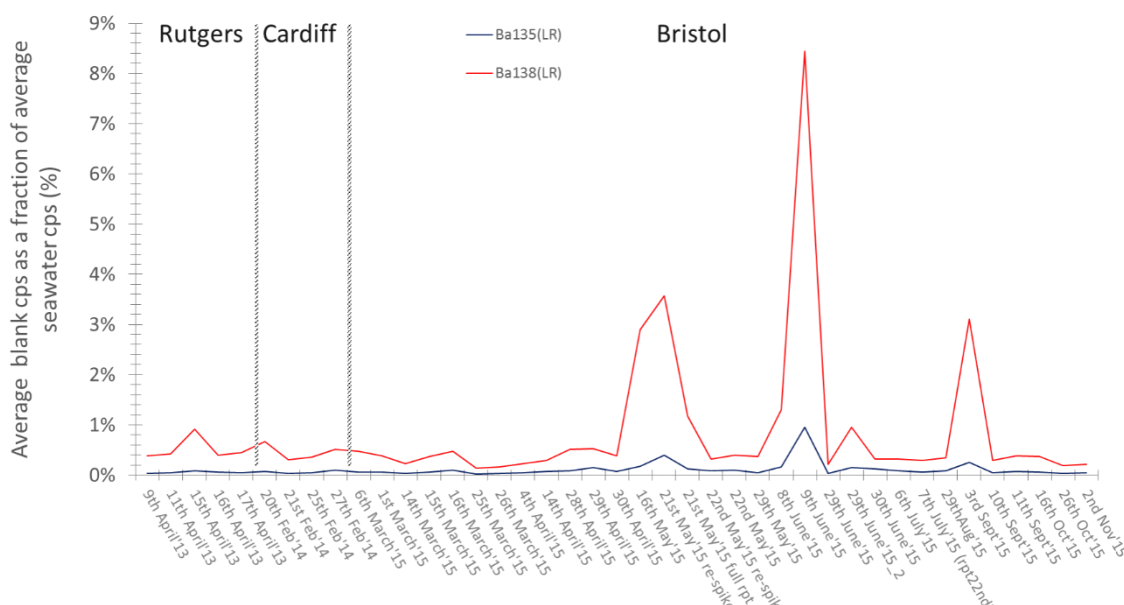


Figure 2-10: A record of background blank levels measured in clean HNO_3 at Rutgers University, Cardiff University, and Bristol University, from April 2013 to November 2015, with hatched lines delineating the measurements made in the different labs. The red line represents the average ^{138}Ba blank cps as a percentage of average seawater cps, whilst the blue line represents the average ^{135}Ba blanks cps as a percentage of average seawater cps. Three periods of elevated background blank levels are observed in April/May 2015, June 2015, and September 2015.

4.3. Determination of barium counts through ICP-MS

4.3.i Typical sequence set-up (Method, differences between various Element machines)

Isotope ratios ($^{138}\text{Ba}/^{135}\text{Ba}$) in spiked samples were analysed in low resolution mode using a Thermo-Finnigan Element-2 ICP-MS (SEM detector only) in Bristol University, an Element XR ICP-MS (dual mode SEM with Faraday detector) in Cardiff University, and an Element-1 ICP-MS (SEM detector only) in Rutgers University. The same counting mode method (Table 2-5) was used on all three instruments, as well as a similar quartz spray chamber and PFA-100 Teflon nebuliser with a flow rate of $125 \mu\text{L min}^{-1}$, an ICPMS Ni 'H' skimmer and ICPMS Ni sample cone.

Isotope	Accurate mass	Method mass offset	Mass window	Mass range	Magnet mass	Sample time	Settling time
135Ba	134.9051	0	10	134.624 - 135.186	134.905	0.002	0.001
138Ba	137.9047	0	10	137.617 - 138.192	134.905	0.002	0.001

Isotope	Samples per peak	Segment duration	Search window	Integration window	Scan type	Detection mode	Integration type
135Ba	100	0.02	80	10	Escan	Counting	Average
138Ba	100	0.02	80	10	Escan	Counting	Average

Table 2-5: Method used to measure barium on Thermo-Finnigan Element 1/2/XR ICP-MS

Samples were analysed alongside regular measurements of spiked standard solutions, blanks, and natural standards, with a typical sequence set-up as shown in Figure 2-11.

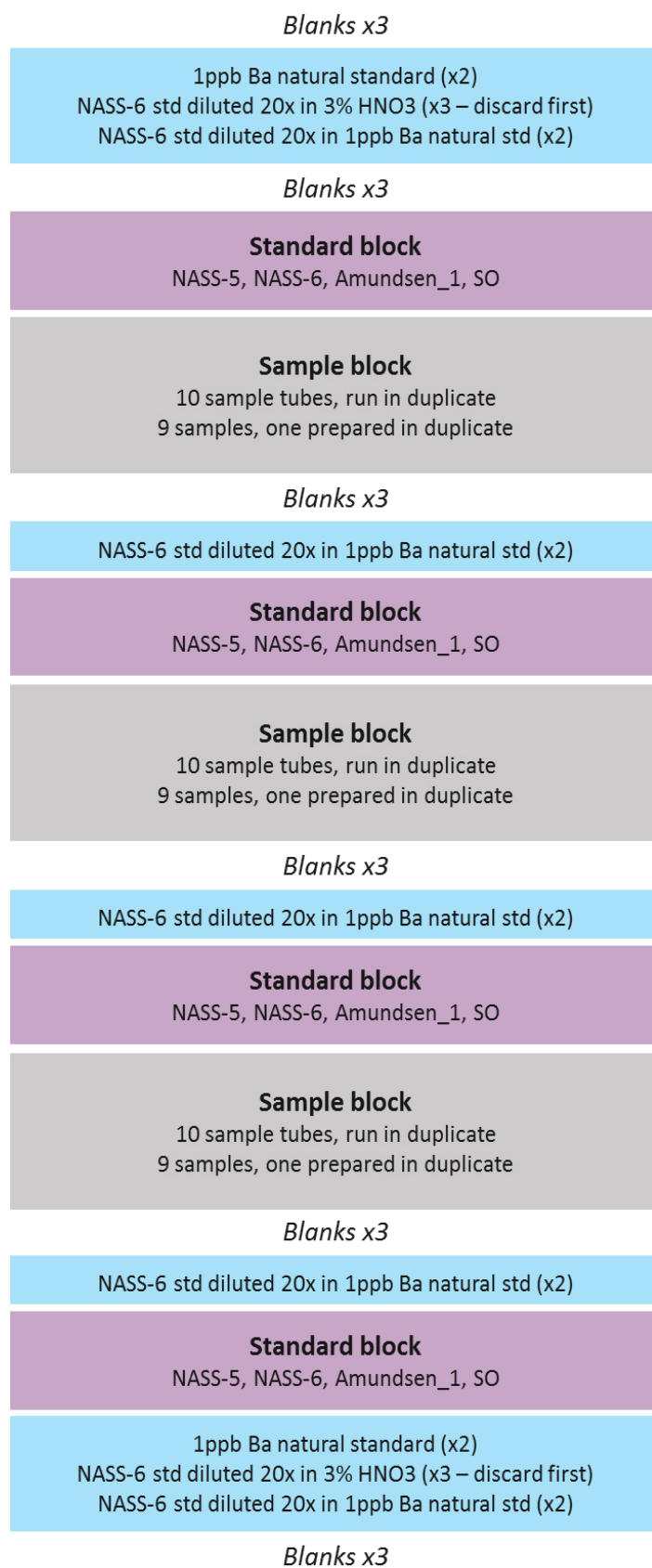


Figure 2-11: Typical sequence set-up to run 27 seawater samples (with three samples prepared in duplicate and all samples run in duplicate). Running this sequence on a Thermo-Finnigan Element ICP-MS using the method outlined in Table 2-5 took approximately 8 to 10 hours.

Samples were typically analysed in duplicate in batches of 27, with three samples prepared in duplicate as well as being analysed in duplicate (see Sections 5.2.i and 5.2.ii). At least two standard solutions were measured in between every nine samples, as well as acid blanks, matrix-correction solutions (see Section 4.3.iii), and a 1 ppb Ba natural standard. The ICP-MS instrument was tuned before every sequence to optimum parameters for high sensitivity, stability, and low oxide production. These parameters included: torch position, sample gas flow, and ancillary gas flow, all of which varied widely during the three years over which samples were analysed. The threshold for uranium oxide production, taken as an indicator of potential barium oxide formation, was set at 5%.

4.3.ii Mass calibration

Prior to every sample sequence a mass calibration was performed in low resolution mode, scanning for 15 elemental peaks in a multi-element 1 ppb Ba standard solution, and using the results to calibrate the programmed search windows for each element.

4.3.iii Accounting for matrix effects and interferences from seawater analyte

Although there were considerable practical advantages to analysing seawater samples directly, without the need for time-consuming separation chemistry, the introduction of a seawater analyte to the ICP-MS instrument introduces its own challenges. Typically, spiked samples were diluted 20 times with 3% Romil SPA HNO₃, although this was altered in cases where samples were known to contain higher/lower salinity (Table 2-1), so that the final solution introduced to the ICP-MS was no more than 5% seawater.

Each sample sequence (see Figure 2-11) took approximately eight to ten hours to complete. Over this time, the sensitivity of the ICP-MS instrument decreased due to the noticeable coating of the sample and skimmer cones with salt precipitates from the dilute seawater analyte. This decrease in sensitivity throughout the course of a run was monitored (Figure 2-12) and was generally observed to constitute a gradual decline of approximately 20% sensitivity over eight hours. Provided that the spiked standard solutions (of comparable Ba_d concentration to the samples being analysed) measured at the start and end of the sequence did not differ beyond analytical uncertainty, this decrease in sensitivity was not deemed to be significant to the accurate measurement of ¹³⁸Ba/¹³⁵Ba ratios.

Even at only 5% of the final analyte, the presence of seawater in the sample solutions analysed could potentially cause unpredictable matrix effects that may alter the sensitivity of the isotope measurements. These matrix effects would not be accounted for in a clean acid blank correction. To overcome this, two solutions of dilute seawater standard NASS-6 were routinely analysed alongside a 1 ppb Ba natural standard solution. The first NASS-6 solution (Solution A)

was diluted 20 times in 3% HNO₃, whilst the other was diluted 20 times in a 1 ppb Ba natural standard solution (Solution B). The contribution of the NASS-6 seawater to the measured isotope content of Solution B was removed by subtracting the measured isotope content of Solution A. The remaining isotope content of Solution B (1 ppb Ba in a 5% seawater matrix) was then compared to the isotope content measured in the pure 1 ppb Ba natural standard solution, to quantify the depression or amplification of the 'true' isotope content of the solution by interference with a dilute seawater matrix. This correction was then applied to the average acid blank contribution which was subtracted from sample counts. The magnitude and sign of this correction varied between individual sets of sample analysis, but generally involved an approximately – 20% modification of the blank for both ¹³⁸Ba and ¹³⁵Ba. This represents an approximately 20% depression of the 'true' content of both isotopes due to the presence of a dilute seawater matrix. However, once again, as this matrix interference appeared to affect both isotopes equally, it does not seem to compromise the measured ¹³⁸Ba/¹³⁵Ba ratio of the samples.

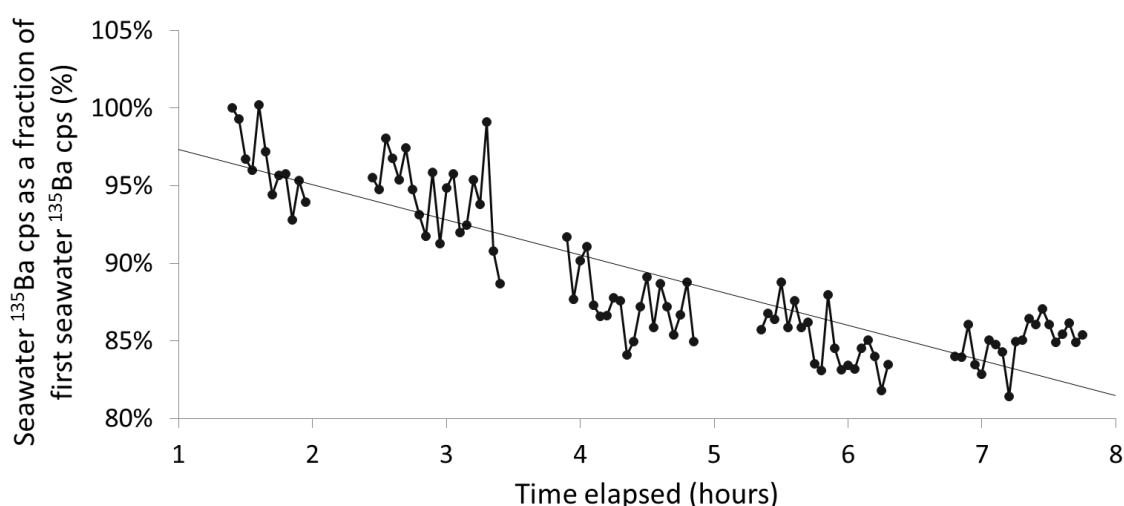


Figure 2-12: Sensitivity loss experienced over a typical run (8 hours). ¹³⁵Ba signal diminished to approximately 80% of initial sensitivity by the end of the sequence. Decrease is fairly gradual. Only seawater sample readings are shown (not standards or blanks). Sequences were set up with the intention of running samples of similar concentrations together. Data show here are from 21st February 2014, analysis performed at University of Cardiff.

4.3.iv Calculating K: monitoring and accounting for mass bias

Within the ICP-MS instrument, artificial isotopic fractionation can occur as a result of variable transmission of the ion beam (variation in the deflection of lighter versus heavier isotopes) that is known as mass bias. This was corrected for by calculating a mass bias correction co-efficient (K) which accounted for the deviation of the ¹³⁸Ba/¹³⁵Ba ratio measured a 1 ppb Ba

natural standard solution prepared in 5% (v/v) seawater (NASS-6 seawater standard of 5 ppb ± 0.15 Ba) ($R_{\text{dilute seawater}}$) from the average natural ratio of $^{138}\text{Ba}/^{135}\text{Ba}$ ($R_{\text{literature}} = 10.88$) (Equation 2-5).

$$K = \left(\frac{R_{\text{literature}}}{R_{\text{dilute seawater}}} \right)$$

Equation 2-5: Equation for the calculation of the mass bias correction coefficient (K) using the natural ratio of $^{138}\text{Ba}/^{135}\text{Ba}$ ($R_{\text{literature}}$) of 10.88, and the measured $^{138}\text{Ba}/^{135}\text{Ba}$ in a solution of NASS-6 seawater diluted 20 times in 1 ppb Ba natural standard ($R_{\text{dilute seawater}}$).

The variation of the isotope ratio determined in this solution ($R_{\text{dilute seawater}}$) is summarised in Table 2-6. The measured uncertainty on this value across each set of samples analysed never exceeded 1.5% (2*RSD). This uncertainty was consistently less than the mass bias determined for each sample run, which was on average a 1.9% deviation from the literature value.

	Bristol	Cardiff	Rutgers
<i>average determined mass bias</i>	2.03%	2.22%	1.48%
<i>minimum determined mass bias</i>	0.47%	1.48%	1.81%
<i>maximum determined mass bias</i>	4.76%	3.21%	1.04%
<i>average precision on $R_{\text{dilute seawater}}$ (2*RSD)</i>	0.50%	0.75%	0.67%
<i>maximum precision on $R_{\text{dilute seawater}}$ (2*RSD)</i>	0.22%	0.31%	0.31%
<i>minimum precision on $R_{\text{dilute seawater}}$ (2*RSD)</i>	1.28%	1.44%	1.14%
<i>range of $R_{\text{dilute seawater}}$ measured</i>	10.67 to 11.40	10.53 to 11.04	10.99 to 11.08

Table 2-1: Summary of mass bias determined during sample analysis at Rutgers University, Cardiff University, and Bristol University. Mass bias is reported here as the proportional deviation of measured $R_{\text{dilute seawater}}$ from $R_{\text{literature}}$.

5. Quantifying uncertainty

5.1. Procedural uncertainty

There are several sources of uncertainty in the calculation of Ba_d concentrations using ID-ICP-MS, which are summarised below:

5.1.i Weighing errors

The mass of sample and spike quantities were determined using a four-decimal place balance, with an implicit uncertainty on final measurements of ± 0.00005 g. Accounting for this error on the two measurements used to calculate each spike or sample volume (Equations 2-3 and 2-4) gives an error of ± 1.41*10⁻⁴ on each final mass (calculated using basic error propagation for addition/subtraction, see Equations 2-6 and 2-7).

5.1.ii Internal precision of mass spectrometry

The isotope content (ions counted per second) reported by the ICP-MS instrument is an average of measurements from 3 passes and 500 runs, with a reported error of 2*RSD (relative standard deviation). Internal RSDs were usually below 1 %. A threshold was set of 3 % RSD, with sample measurements recording internal precision less than this not considered robust.

5.1.iii Counting statistics

The precision of measurements by ICP-MS is limited by counting statistics – the random error encountered in the measurement of ions by the SEM detector. This standard error is proportional to $\frac{1}{\sqrt{N}}$, where N is equal to the number of measurements made. Therefore the standard error decreases as the number of measurements increases. The typical intensity measured for spiked seawater samples was: $^{135}\text{Ba} = 300,000$ cps; $^{138}\text{Ba} = 200,000$ cps. Therefore the standard error contribution from counting statistics was $\pm 0.18\%$ on ^{135}Ba counts, and $\pm 0.22\%$ on ^{138}Ba counts, which can be considered insignificant.

5.1.iv Duplicate averaging

Every spiked seawater sample was analysed in duplicate routinely, with two consecutive measurements made on each solution to ensure internal consistency. The resultant concentrations of duplicate measurements were averaged, and a difference of greater than 1.0% was considered a threshold for samples to be re-prepared and re-analysed.

5.1.v Full error propagation through ID calculation

These individual errors were each considered and propagated through the isotope dilution (ID) equation using basic error propagation relationships for addition, subtraction, multiplication, and division (Equations 2-6 and 2-7).

$$\begin{aligned} \text{Addition/subtraction:} \quad \sigma_x &= \sqrt{\sigma_a^2 + \sigma_b^2 + \sigma_c^2} \\ (x &= a + b - c) \\ \\ \text{Multiplication/division:} \quad \frac{\sigma_x}{x} &= \sqrt{\left(\frac{\sigma_a}{a}\right)^2 + \left(\frac{\sigma_b}{b}\right)^2} \\ (x &= a * b) \end{aligned}$$

Equations 2-6 and 2-7: Error propagation equations for addition/subtraction and multiplication/division, where σ = standard deviation, and subscripts denote the variable concerned.

The full propagation of errors is shown in Equation 2-8:

$$\sigma_{C_x} = \sqrt{\sqrt{\left(\frac{\sigma_{Rb}}{R_b}\right)^2 + \left(\frac{\sigma_K}{K}\right)^2} + \sqrt{\left(\frac{\sigma_{m_y}}{m_y}\right)^2 + \left(\frac{\sigma_{m_x}}{m_x}\right)^2 + \left(\frac{\sigma_{C_y}}{C_y}\right)^2}}$$

Equation 2-8: Propagation of errors through the isotope dilution calculation (Equation 2-2) where: σ = standard deviation;

R_b = $^{138}\text{B}/^{135}\text{Ba}$ ratio measured in spiked seawater solution; K = mass bias correction co-efficient;

m_x = mass of sample;

m_y = mass of working spike;

C_y = concentration of working spike;

C_x = concentration of sample

5.2. Consistency checks

The reliability of the final Ba_d concentration of samples was investigated by assessing the level of uncertainty associated with the sampling procedure, the preparation of samples for ID-ICP-MS analysis, and the analysis itself. Standard seawater solutions were also measured routinely alongside samples to quantify external reproducibility over time.

5.2.i Sampling consistency: sample duplicates

In order to investigate how representative each seawater sample collected was of the larger population it was sampled from, I performed ID-ICP-MS analyses on multiple sets of samples collected from the same location/depth. As can be seen in Figure 2-14 and Figure 2-13, Ba_d concentrations calculated for these sample duplicates were identical within analytical uncertainty.

5.2.ii Procedural consistency: sample preparation duplicates

During sample preparation, even under clean laboratory conditions, there is the potential for error to be introduced through contamination and human error. This was routinely monitored by preparing one sample in every ten twice, resulting in two separately prepared spiked solutions made using one sample. Ideally, if there were no procedural error introduced during sample preparation, these ‘tube duplicates’ would return identical Ba_d concentrations. The same threshold was set for tube duplicates as for the analysis duplicates discussed in Section 5.1.iv – duplicates that did not agree within 1 % would be re-prepared and re-analysed. Nearly all tube duplicates prepared agreed within this error threshold, indicating that the ID preparation procedure was not a significant source of error.

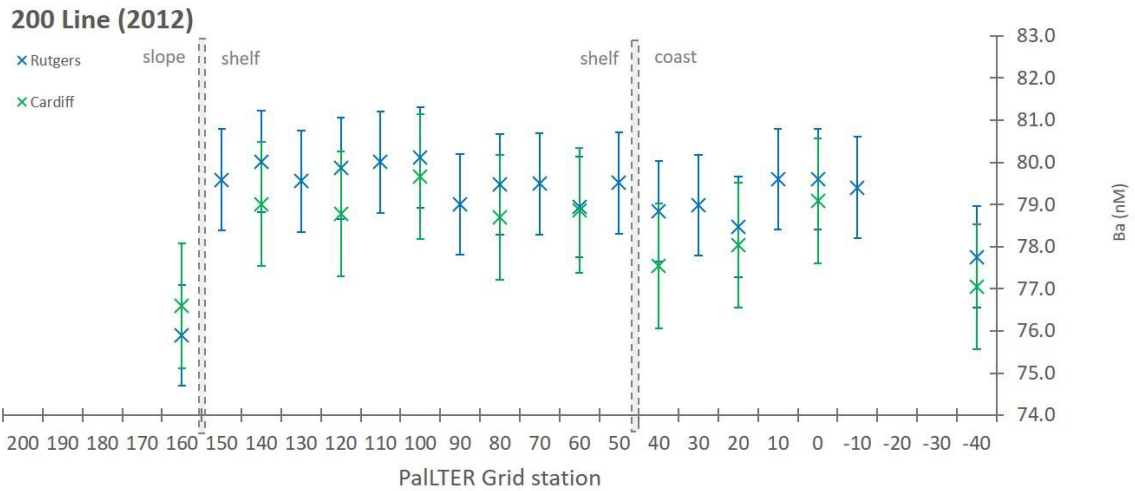


Figure 2-14: Measurements of PalTER sample duplicates. Data shown here from the 200 grid line (2012). Blue crosses represent measurements made at Rutgers University, prepared from samples stored at Rutgers University. Green crosses represent measurements made at Cardiff University, prepared from sample stored at Cardiff University. Error bars are set to 1.2 %, the reproducibility of the SO standard over the duration of the measurements. These two sets of samples were collected simultaneously from the same Niskin bottles during the 2012 PalTER annual cruise, and data from both sample sets have been combined to produce a higher resolution dataset than could be produced from either sample set alone. On occasions when samples were duplicated in both sample sets, both were analysed to check reproducibility. Such duplicate samples typically agreed within 1 %.

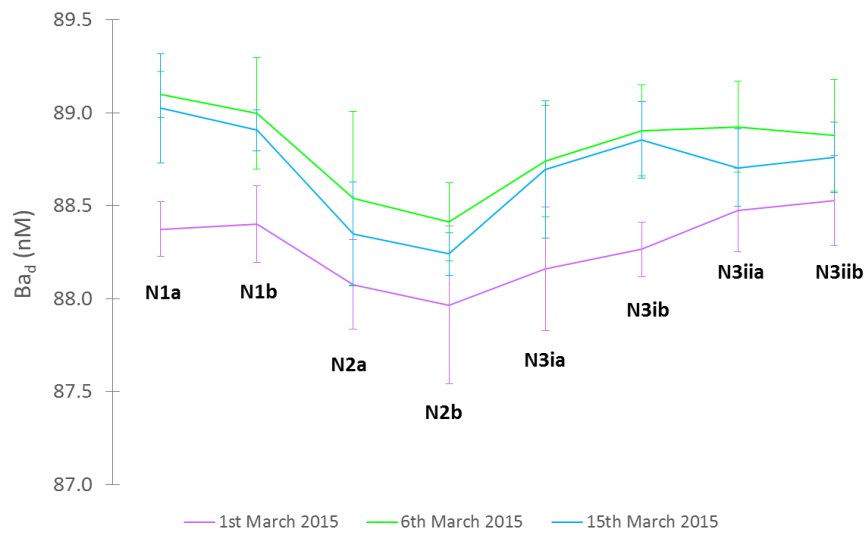


Figure 2-13: Measurements of JR99 Niskin duplicates (samples collected simultaneously from different Niskin bottles closed at the same depth). Samples collected from JR293 Drake Passage transect (SR1b) Station 3, 358 m depth. Samples were collected from three different Niskin bottles (N1, N2, and N3). These samples were spiked and analysed in duplicate (a and b) using the standard barium method, with samples from N3 also prepared in duplicate (Ni and Nii). Analysis was initially performed in Bristol University (1st March 2015) and repeated in Cardiff University (6th March 2015) and again at Bristol University (15th March 2015). Measurements detailed in Table 2-2.

Date of analysis	Laboratory	Average Ba _d (nM)	SD	2*SD	2*RSD
1st March	Bristol	88.3	0.199	0.398	0.45%
6th March	Cardiff	88.8	0.233	0.467	0.53%
15th March	Bristol	88.7	0.270	0.539	0.61%
<i>All measurements</i>		<i>88.6</i>	<i>0.323</i>	<i>0.647</i>	<i>0.73%</i>

Table 2-2: Details of the measurements of JR299 Niskin duplicates represented in Figure 2-13, three samples collected from the same depth (358m) at Station 3, JR293 Drake Passage transect, drawn from three different Niskin bottles, prepared and analysed in duplicate on three separate occasions. The resultant Ba_d concentrations were identical within analytical error.

5.2.iii Internal consistency: running duplicates

As well as routinely analysing sample in duplicate, with the second measurement made directly following the first, checks were performed to ensure that the changing sensitivity of the ICP-MS instrument over time would not significantly alter the Ba_d concentrations measured. Results from sets of samples measured at the beginning and end of a sample sequence (Figure 2-15), and on two consecutive days (Figure 2-16), both show that there is no significant deviation

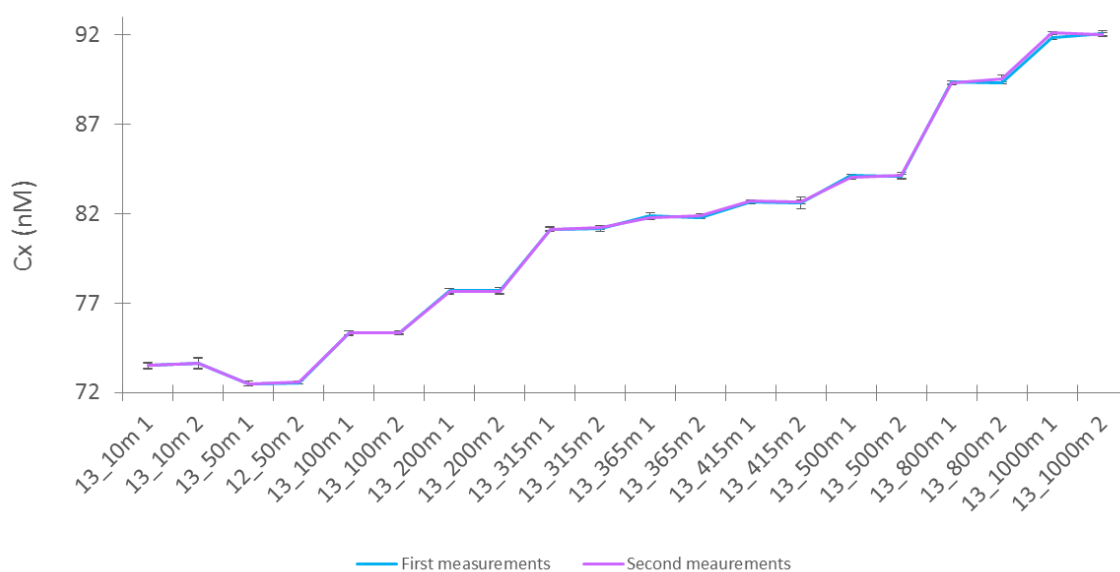


Figure 2-15: Graphical representation of samples run twice in consecutive sample blocks (26th March 2015, Bristol University). Blue line represents the Ba_d concentrations calculated from the first set of measurements, the purple line represents the concentrations calculated from the second set of measurements. Error bars represent the uncertainty on the calculated concentrations. Within this uncertainty, concentrations from the two sample blocks were identical.

in Ba_d concentrations measured over time.

Sample	Average Ba (nM)	SD	duplicate uncertainty (RSD on 4 duplicates)	uncertainty on averaged concentration
13_10m 1	73.6	0.07	0.10%	0.08%
13_50m 1	72.5	0.04	0.05%	0.10%
13_100m 1	75.3	0.01	0.01%	0.07%
13_200m 1	77.7	0.03	0.04%	0.10%
13_315m 1	81.2	0.04	0.05%	0.05%
13_365m 1	81.8	0.06	0.07%	0.09%
13_415m 1	82.6	0.05	0.06%	0.05%
13_500m 1	84.1	0.05	0.06%	0.04%
13_800m 1	89.4	0.09	0.10%	0.05%
13_1000m 1	92.0	0.10	0.11%	0.06%

Table 2-3: Results from samples run twice in consecutive sample blocks (see Figure 2-15) to assess reproducibility of samples within a sequence. Average Ba therefore represents the concentration calculated from four measurements (consecutive duplicate measurements within two sample blocks). Reproducibility of the concentration measurements throughout the sequence was on the same order as uncertainty on the concentration measurements (calculated through propagation of error through isotope dilution equation – see Section 25.1.v). Samples measured on 26th March 2015 in Bristol University.



Figure 2-16: Graphical representation of samples analysed twice on consecutive days (15th March and 16th March 2015, Bristol University). Green line represents the Ba_d concentrations calculated from the analysis on the 15th March, the purple line represents the concentrations calculated from analysis on the 16th March. Error bars represent the uncertainty on the calculated concentrations. Within this uncertainty, concentrations from the analyses were identical.

Sample	15th March'15		16th March'15		Comparison	
	Average Ba (nM)	concentration uncertainty	Average Ba (nM)	concentration uncertainty	Difference in Ba (nM)	Difference of 16th from 15th
9_5m A1	75.2	0.06%	75.4	0.10%	0.12	0.15%
9_10m 1	75.1	0.11%	75.3	0.22%	0.18	0.24%
9_60m 1	75.4	0.16%	75.5	0.18%	0.12	0.16%
9_100m 1	77.0	0.20%	77.1	0.26%	0.15	0.19%
9_254m 1	81.0	0.23%	81.3	0.19%	0.21	0.26%
9_350m 1	83.5	0.10%	83.7	0.06%	0.18	0.21%
7_400m 1	87.0	0.12%	87.2	0.14%	0.23	0.27%
7_600m 1	89.7	0.06%	89.9	0.13%	0.19	0.21%
7_650m 1	89.9	0.11%	90.0	0.05%	0.13	0.14%

Table 2-4: (previous page) Results from samples run twice on the Element ICP-MS over two consecutive days, to assess the reproducibility of samples over separate sequence runs. The samples were prepared and analysed at Bristol University, with the sample solutions stored in 15 mL centrifuge tubes at room temperature (approximately 21 °C) overnight between the analyses (on the 15th March and 16th March 2015). Measurements made on the 16th March were consistently 0.15 to 0.3% higher than measurements on the 15th March. This error is on the same order as uncertainty on the calculated concentrations.

5.2.iv External consistency: measurement of standard solutions over time

Standard seawater solutions, prepared using the same method applied to seawater samples (Table 2-11) were routinely analysed alongside samples to monitor external reproducibility (Table 2-10 and Figure 2-17). The standard most comparable to the bulk of seawater samples measured in this thesis is In-house standard SO, which showed a long-term reproducibility of 1.63 % or better.

Standard:	In – house Std (SO)	NASS-5	NASS-6	
Bristol	2*RSD	1.34%	3.26%	1.73%
	<i>n</i>	72	33	70
	[Ba] (nM)	73.5 ± 1.0	37.4 ± 1.2	49.3 ± 0.9
Cardiff	2*RSD	1.29%	1.53%	1.22%
	<i>n</i>	23	22	23
	[Ba] (nM)	73.7 ± 1.0	37.0 ± 0.6	49.5 ± 0.6
Rutgers	2*RSD	1.63%	2.46%	2.84%
	<i>n</i>	27	27	26
	[Ba] (nM)	74.1 ± 1.2	37.1 ± 0.9	49.7 ± 1.4

Table 2-10: Reproducibility of standards measured in Bristol University (March to November 2016), Cardiff University (February 2014), and Rutgers University (April 2013). Values given are 2*relative standard deviation (2*RSD). In-house Standard 1 SO was collected from the Scotia Sea, at 100 m depth by K. R. Hendry.

	Spiked in:	Spiked with:	Sample weight (g)	Sample volume (mL)	Spike weight (g)	Spike volume (mL)
NASS-5 R	Rutgers	WS_R1	12.679	12.370	5.564	5.502
NASS-5 C	Cardiff	WS_C1	6.4321	6.275	2.8196	2.751
NASS-6 C	Cardiff	WS_C1	6.4006	6.244	2.8211	2.752
SO R	Rutgers	WS_R1	12.769	12.458	10.074	9.961
SO C	Cardiff	WS_C1	6.4251	6.268	5.1103	4.986
Amundsen_1 R	Rutgers	WS_R1	12.835	12.522	10.084	9.971
SO B1	Bristol	WS_C1	6.4368	6.598	5.1387	5.197
NASS-5 B1	Bristol	WS_C1	2.5699	2.634	1.1343	1.147
NASS-6 B1	Bristol	WS_C1	2.5757	2.640	1.1394	1.152
NASS-5 B2	Bristol	WS_C1	3.2127	3.293	1.3766	1.392
NASS-6 B2	Bristol	WS_C1	6.4255	6.586	2.8049	2.837
SO B2	Bristol	WS_B1	6.3862	6.546	5.1065	5.164

Table 2-11: Details of the preparation of standard solutions: certified standards NASS-5 and NASS-6 seawater reference solutions, and in-house standard seawater solutions Southern Ocean (SO) and Amundsen_1. Initials after standard solution denote where the spiked standard solution was made (R – Rutgers University; C – Cardiff University; B – Bristol University); where multiple spiked solutions were made in one location they made been numbered sequentially. WS refers to the working spikes used to prepare the standard solutions (Table 2-4).

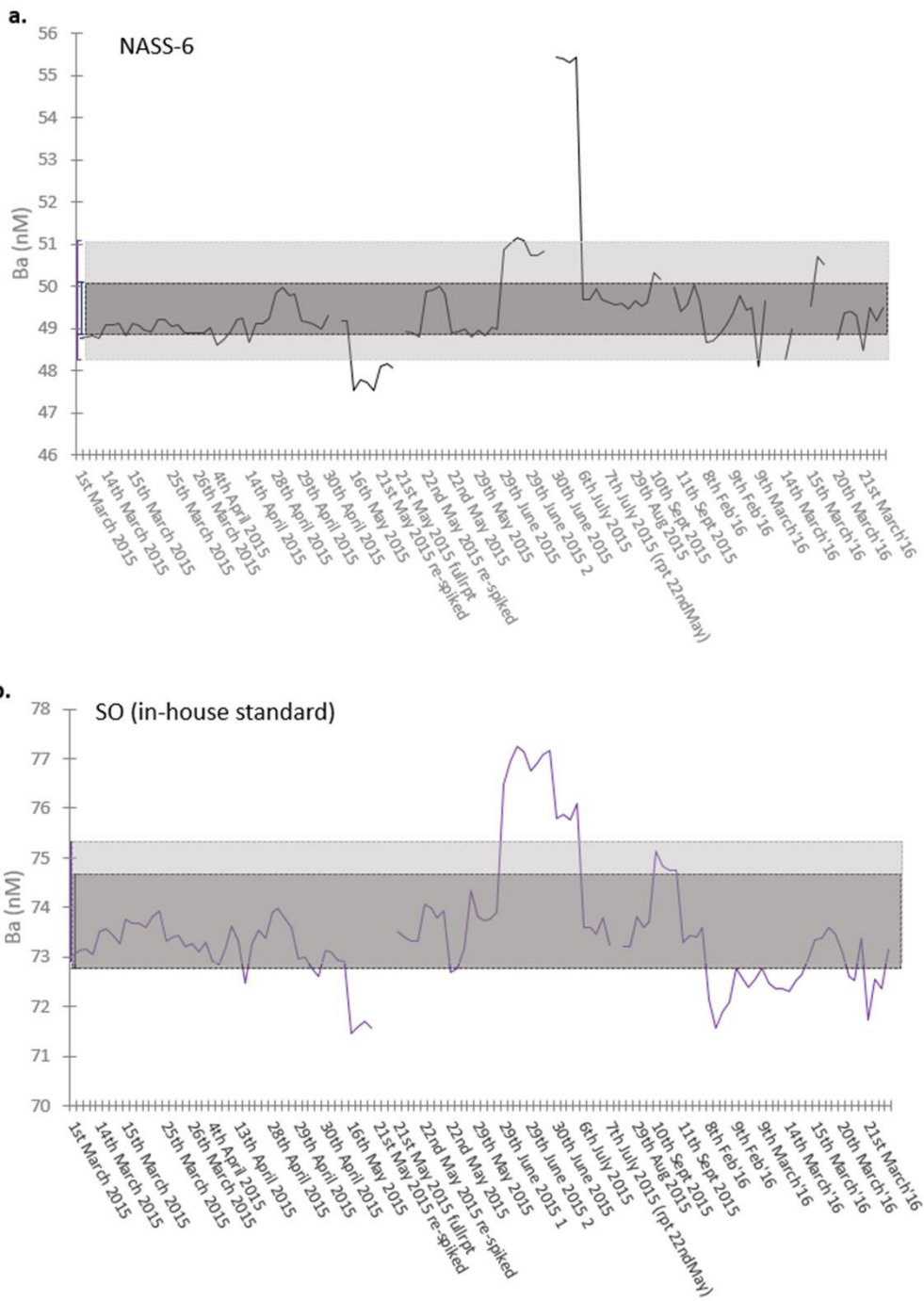


Figure 2-17: Reproducibility of standards measured in Bristol University from March to November 2016. The shaded boxes represent the error bounds of concentrations measured on the same standards at Rutgers University (light grey box) and Cardiff University (dark grey box). a. NASS-6 seawater standard; b. In-house standard SO (from 100 m depth in the Scotia Sea).

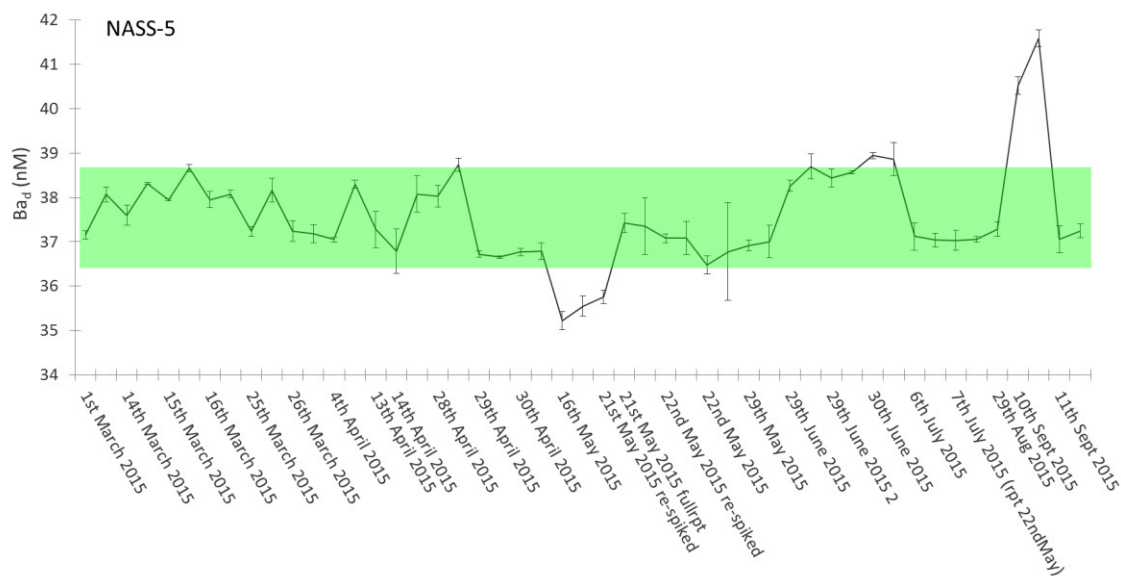


Figure 2-18: Reproducibility of NASS-5 seawater standard, measured in Bristol University between March and September 2015. Error bars show the error on the concentrations calculated (derived from error propagation through the ID equation, see Equation 2-8). The green shaded box represents the error threshold from literature reports of Ba_d measurements of this standard (Figure 2-19).

5.3. Accuracy: comparison of standard solution measurements across labs

Samples were measured in Rutgers University and Cardiff University for several weeks in 2013 and 2014 respectively, whilst samples were analysed in Bristol University over the course of a year (March 2015 to March 2016). The accuracy of the Ba_d concentration of seawater standards were taken to be representative of the accuracy of seawater samples of comparable concentration. However, none of the standard solutions have a certified Ba_d concentration for direct comparison. The Ba_d concentration of the NASS-5 standard has been measured by others, and these reported literature values were used to determine an error threshold envelope for my measurements (Figure 2-18 and Figure 2-19). The Ba_d concentration of the other standards (NASS-6 and SO were the two most commonly measured) were calibrated across the three laboratories in which seawater analyses were carried out, with the error bounds calculated for measurements in Cardiff and Rutgers Universities used to monitor the longer-term analyses in Bristol University. As can be seen in Figure 2-17 (error bounds from Rutgers and Cardiff represented by shaded boxes), there were periods in April/May 2015, June 2015, and September 2015 when concentrations were recorded for one or all of the standard solutions that exceeded the error bounds set from the literature/inter-laboratory calibrations. These anomalous results were potentially linked to the high background blanks recorded during these periods (Figure

2-10), and sample measurements from these periods cannot be considered reliable. All of the samples concerned were re-prepared and re-analysed at a later date.

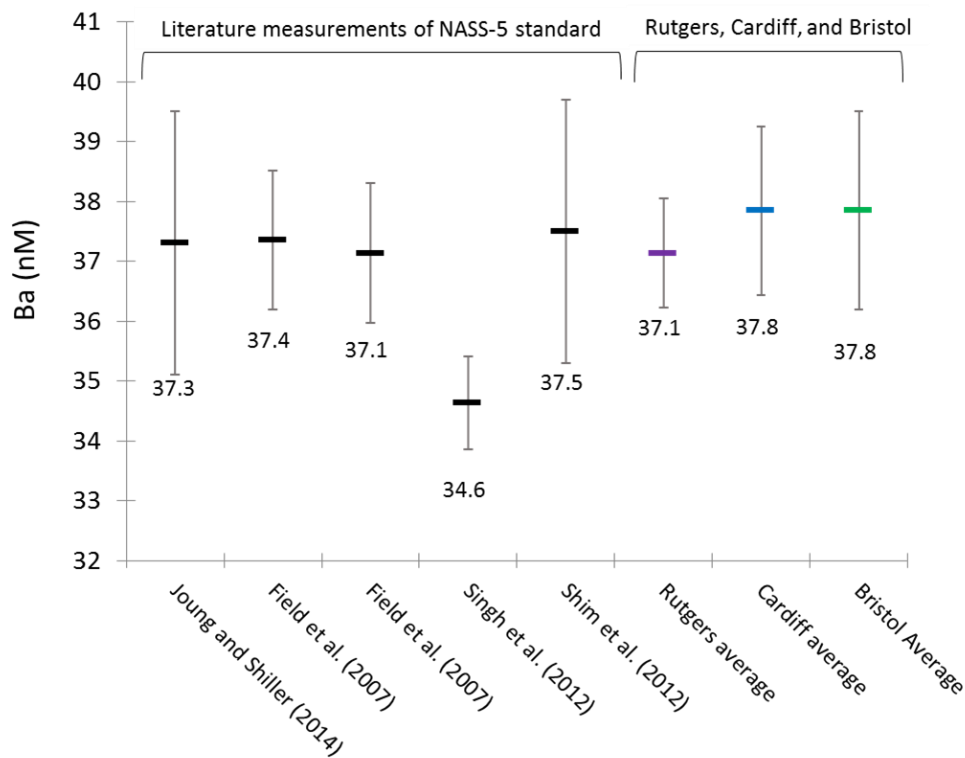


Figure 2-19: A comparison of Ba_d concentrations measured in the NASS-5 seawater standard in Rutgers University, Cardiff University, and Bristol University, with measured concentrations reported in the literature.

This comparison with values of the NASS-5 reported in the literature, as well as the consistent agreement across the three laboratories in which samples were analysed for this study, provides confidence in the accuracy of the Ba_d concentrations measured throughout the thesis. Overall, the external reproducibility (Figure 2-10) measured in comparable standard solutions (Southern Ocean seawater samples are most comparable with In-house standard SO) was better than 1.65%, giving a great enough accuracy to reliably interpret the small variations in Ba_d concentrations observed throughout Antarctic waters.

Chapter 3

Controls on the oceanic distribution of dissolved barium in the Scotia and Weddell Seas (Antarctica)

1. Introduction

Current understanding of the oceanic barium cycle, and its links to the biological activity, freshwater inputs, and ocean circulation for which it is employed as a proxy, has been limited by the relatively sparse datasets available. The Geochemical Ocean Sections Study (GEOSECS) expeditions of the 1970s provided information on the distribution of barium throughout all the major ocean basins (Figure 3-1) and enabled the development of many of the theories of barium biogeochemical cycling that are still being investigated today (Wolegemuth and Broecker 1970; Chan et al. 1976, 1977). However, the wide range of potential controls on barium distribution in the ocean, and the closely associated distribution of marine barite, cannot be thoroughly investigated with data from isolated hydrographic stations. In addition to the more comprehensive ocean surveying undertaken in recent years by programmes such as GEOTRACES, progress in analytical techniques has made it possible to gather more precise measurements of dissolved barium (Ba_d) in seawater, allowing relatively small shifts in spatial distributions to be examined in detail with greater confidence (Jeandel et al. 1996; Volpe & Esser 2002; Jacquet et

al. 2004, 2005, 2007; Hoppema et al. 2010; Thomas et al. 2011). In this chapter I will discuss the additions that can be made to our understanding of the barium biogeochemical cycle by examining a high precision dataset of Ba_d from well-resolved transects of the Scotia and Weddell Seas.

The Southern Ocean is of particular interest in developing our understanding of the oceanic barium biogeochemical cycle, as a climatically important region with a large role in ocean carbon storage. Additionally, the potential applications of marine barite and Ba/Ca as palaeo-proxies for export productivity and deep water circulation (Jacquet et al. 2007; Thompson & Schmitz 1997; Nürnberg et al. 1997; Lea & Boyle 1989; Lea & Boyle 1990) in this region make it crucial that the controls on the barium cycle in these waters are better understood. The heterogeneity of the Southern Ocean, exemplified by the biogeographical zonation caused by the migratory circumpolar frontal zones, also offers an opportunity to investigate the various potential effects on barium distributions of different ecological communities, and the interactions of large and small scale water-mass mixing. In the Scotia Sea, the contraction of the frontal zones by the physical restrictions of the Drake Passage, and the influence of the North and South Scotia Ridges on the movement of water masses and biological activity, offer an ideal region to examine the barium biogeochemical cycle (Figure 3-2). Specifically, variability in the Ba_d distribution and its relationship to biological activity can be investigated across the biogeochemical divide of the Polar Frontal Zone, and this data used to inform interpretations of the global link observed between Ba_d and silicic acid. For example, site-specific decoupling of the well-known $Ba_d/Si(OH)_4$ relationship can be used to trace different water masses, and potentially assess the degree of barite precipitation occurring in different areas.

1.1. *The Scotia Sea*

The Scotia Sea is a large area (approximately $1.5 \times 10^6 \text{ km}^2$) in the southwest Atlantic sector of the Southern Ocean (Figure 3-2) bounded to the west by the Drake Passage, and to the north, east, and south by the Scotia Island Arc system and undersea ridges, which separate the area from the South Atlantic and divides the Scotia Sea from the Weddell Sea to the south. The presence of this surrounding island arc, possible advection of shelf-derived waters from the south, iceberg interactions, upwelling from submarine topography, and the deposition of atmospheric dust, are all possible sources of iron fertilisation, thought to contribute to the Scotia Sea being one of the most productive areas in the Southern Ocean (Murphy et al. 2007; Whitehouse et al. 2012). However, this productivity within the Scotia Sea is spatially highly

variable, with large areas of it also categorised as High Nutrient/Low Chlorophyll (HNLC) (Korb et al. 2005) (Figure 3-3).

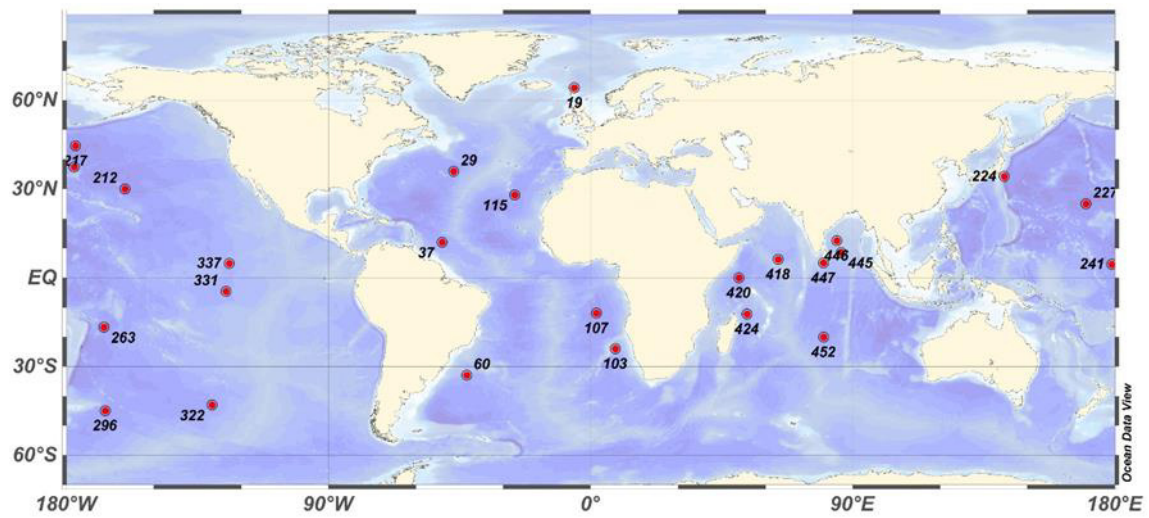


Figure 3-1: Locations of stations sampled for dissolved barium for the GEOSECS programme (KNORR and MELVILLE cruises from 1972-1978) (Ostlund et al. 1987). Data available at <https://odv.awi.de/en/data/ocean/geosecs/>

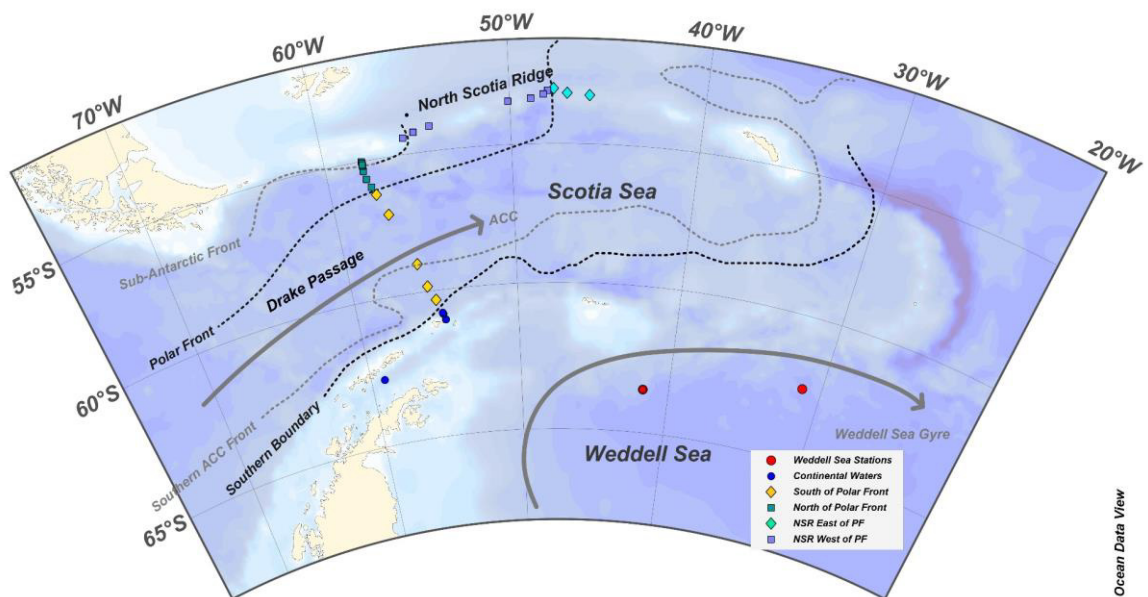


Figure 3-2: Sites of depth profiles collected during cruise JR299 in the Scotia Sea and Weddell Sea. Positions of fronts (after Orsi et al. 1995) marked by dotted lines. Stations north of the Polar Front marked with squares (turquoise in the Drake Passage, purple along the North Scotia Ridge), stations south of the Polar Front marked with diamonds (yellow in the Drake Passage, cyan along the North Scotia Ridge). Stations south of the Southern Boundary are marked by circles (blue in the continental waters adjacent to the Peninsula, red in the Weddell Sea).

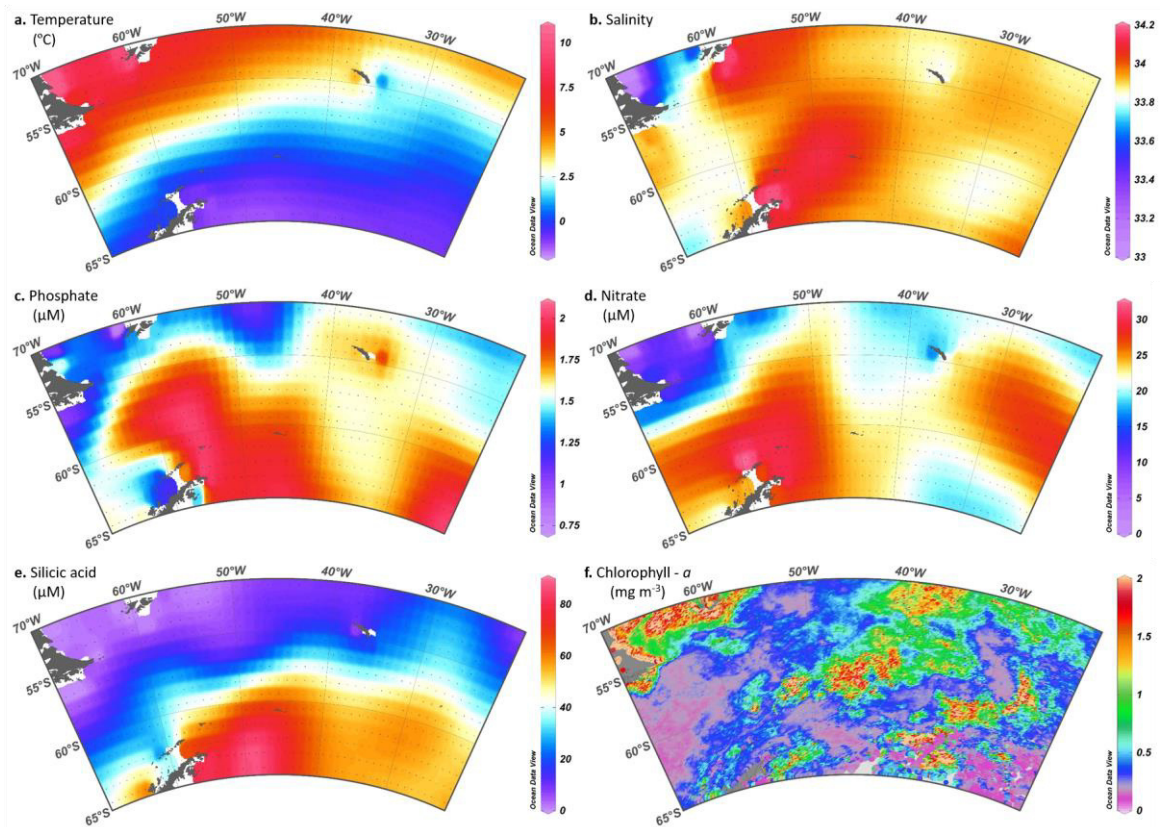


Figure 3-3: a – e. Temperature ($^{\circ}\text{C}$), salinity, phosphate (μM), nitrate (μM) and silicic acid (μM) concentrations from the World Ocean Data Atlas, monthly averages for April, accessed through: https://odv.awi.de/en/data/ocean/world_ocean_atlas_2013/ (Locarnini et al. 2013; Zweng et al. 2013; Garcia et al. 2014); f. Chlorophyll-*a* concentrations (mg m^{-3}) derived from ocean colour data, measured with the NASA Sea-viewing Wide Field-of-view-Sensor (SeaWiFS). The data we use are the 9 km resolution annual mean chlorophyll-*a* concentration in 2010. These data are available from the NASA Ocean Colour website: http://oceandata.sci.gsfc.nasa.gov/SeaWiFS/Mapped/Annual/9km/chlor_a (Werdell et al. 2003);

The circulation of the Scotia Sea is dominated by the Antarctic Circumpolar Current (ACC), a wind-driven current that flows eastwards around the Antarctic continent, transporting approximately 130–140 Sv ($1 \text{ Sv} = 10^6 \text{ m}^3 \text{ s}^{-1}$) (Cunningham et al. 2003). The transport occurring within the ACC is considered to be dominated by several frontal jets identified by large horizontal gradients in oceanic properties. There has been an evolving literature describing the location, causes, and distinguishing features of these fronts (Deacon 1982; Orsi et al. 1995; Belkin & Gordon 1996 and references therein). Current consensus defines four main fronts (from north to south): the Subantarctic Front, the Polar Front, the Southern ACC Front and the Southern Boundary. Whilst these fronts are consistently observed in the narrow constriction of the Drake Passage, at other longitudes there is more complexity, with sub-branches and re-circulations of the fronts observed (Gille 1994; Graham et al. 2012). In the Drake Passage and Scotia Sea these fronts divide the Southern Ocean into three major zones, described by Pollard

et al. (2002) as the Subantarctic zone (SAZ), the Polar Front Zone (PFZ) and Antarctic Zone (AAZ) divided by the Polar Front, and the Antarctic Continental Zone south of the Southern Boundary.

This physical zonation of the Scotia Sea and its control on the distribution of macronutrients in turn creates a biogeochemical zonation, reflected in spatial variations in phytoplankton biomass and community structure (Tréguer & Jacques 1992; Holm-Hansen et al. 2004; Whitehouse et al. 2012). The upward sloping of density surfaces from north to south, geostrophically supporting the ACC, brings nutrient-rich waters closer to the surface, producing positive gradients in seawater nitrate, phosphate, and silicic acid concentrations from north to south. In addition to this, seawater silicic acid concentrations increase southwards along density surfaces, most likely due to diapycnal mixing with deeper waters enriched in silicate due to its deeper remineralisation (Pollard et al. 2002). These high silicic acid concentrations south of the ACC make the region a favourable environment for diatom growth, resulting in high levels of biogenic silica production that are reflected in the deposition of the diatomaceous opal belt, the largest global accumulation of sedimentary opal occurring south of the Polar Front (Franck et al. 2000; Tréguer & De La Rocha 2013). Elevated chlorophyll levels are consistently associated with the Southern Ocean fronts (Moore et al. 1999) (see Figure 3-3 b) most likely due to the relief of iron limitation associated with upwelling waters (Boyd 2002; de Baar et al. 1995).

These zonal features within the Scotia Sea are also accompanied by changes in ocean circulation, with deep (1000 to 2000 m) waters moving southwards across the ACC, balanced by an equatorward flow of lighter and denser layers, including newly formed deep waters from the Weddell Sea (Rintoul et al. 2001). Antarctic Surface Waters (AASW) and remnant Winter Water (WW) flow equatorwards, subducting at the Polar Front and contributing to the formation of Antarctic Intermediate Water (AAIW), marked by a subsurface salinity minimum. Below this, Circumpolar Deep Water (CDW) is transported into the Scotia Sea by the ACC, comprising Lower CDW (LCDW) derived from North Atlantic Deep Water (NADW) and the less dense, older Upper CDW (UCDW) (Figure 3-4) sourced from the Indian and Pacific Oceans (Naveira Garabato et al. 2002). A colder, slightly less saline variety of LCDW referred to as Southeast Pacific Deep Water (SPDW) has also been observed in the Scotia Sea, with a distinctive silicate maximum resulting from mixing with Ross Sea deep waters (Sievers & Nowlin 1984; Naveira Garabato et al. 2002; Peterson & Whitworth 1989). Weddell Sea Deep Water (WSDW) is able to exit from the Weddell Sea into the Scotia Sea by overflowing the South Scotia Ridge (especially in the vicinity of Orkney Passage), flowing westwards and northwards and mixing vigorously with CDW, resulting in a cooling and freshening of CDW waters as they flow eastwards through the Scotia Sea (Naveira Garabato et al. 2002; Meredith et al. 2013).

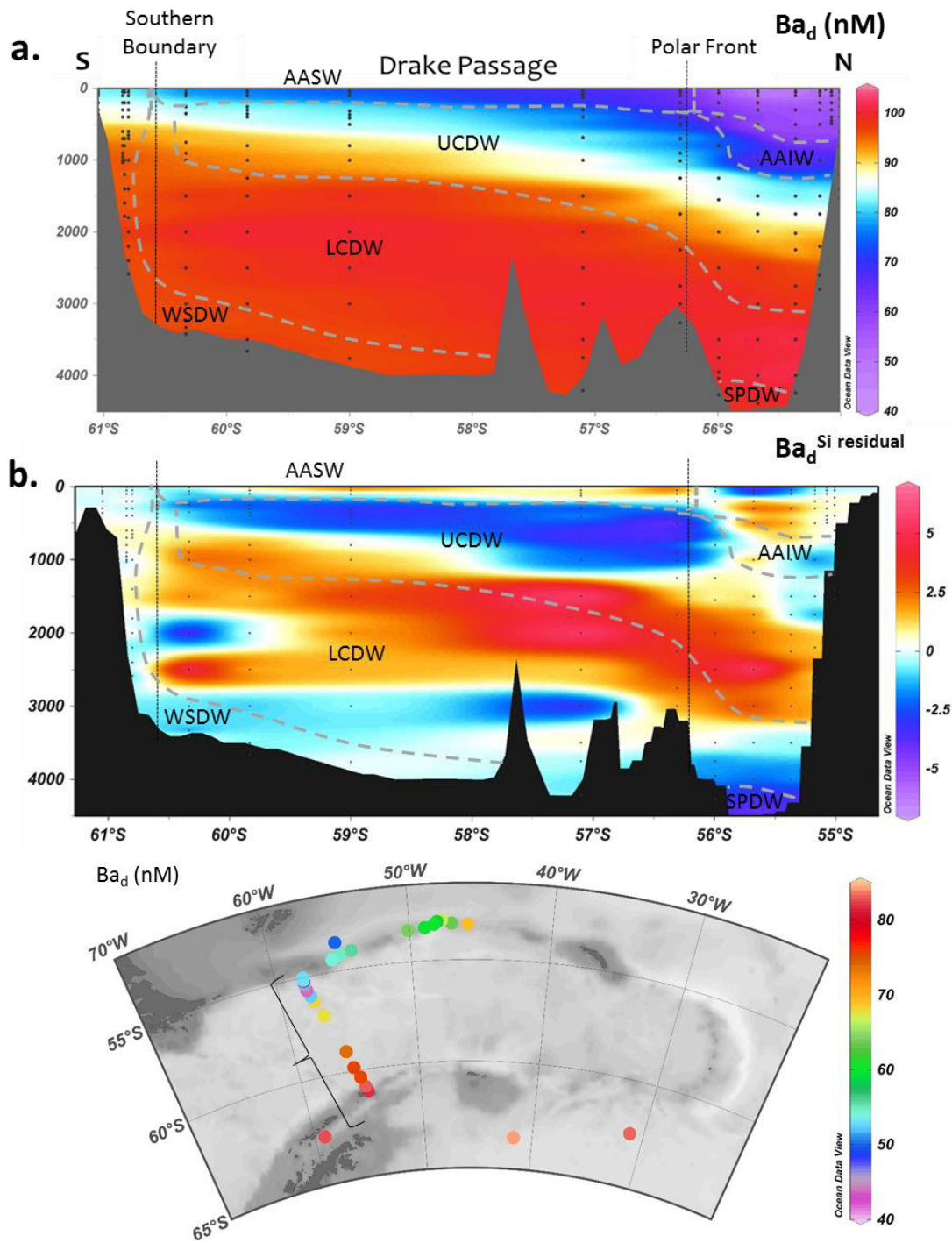
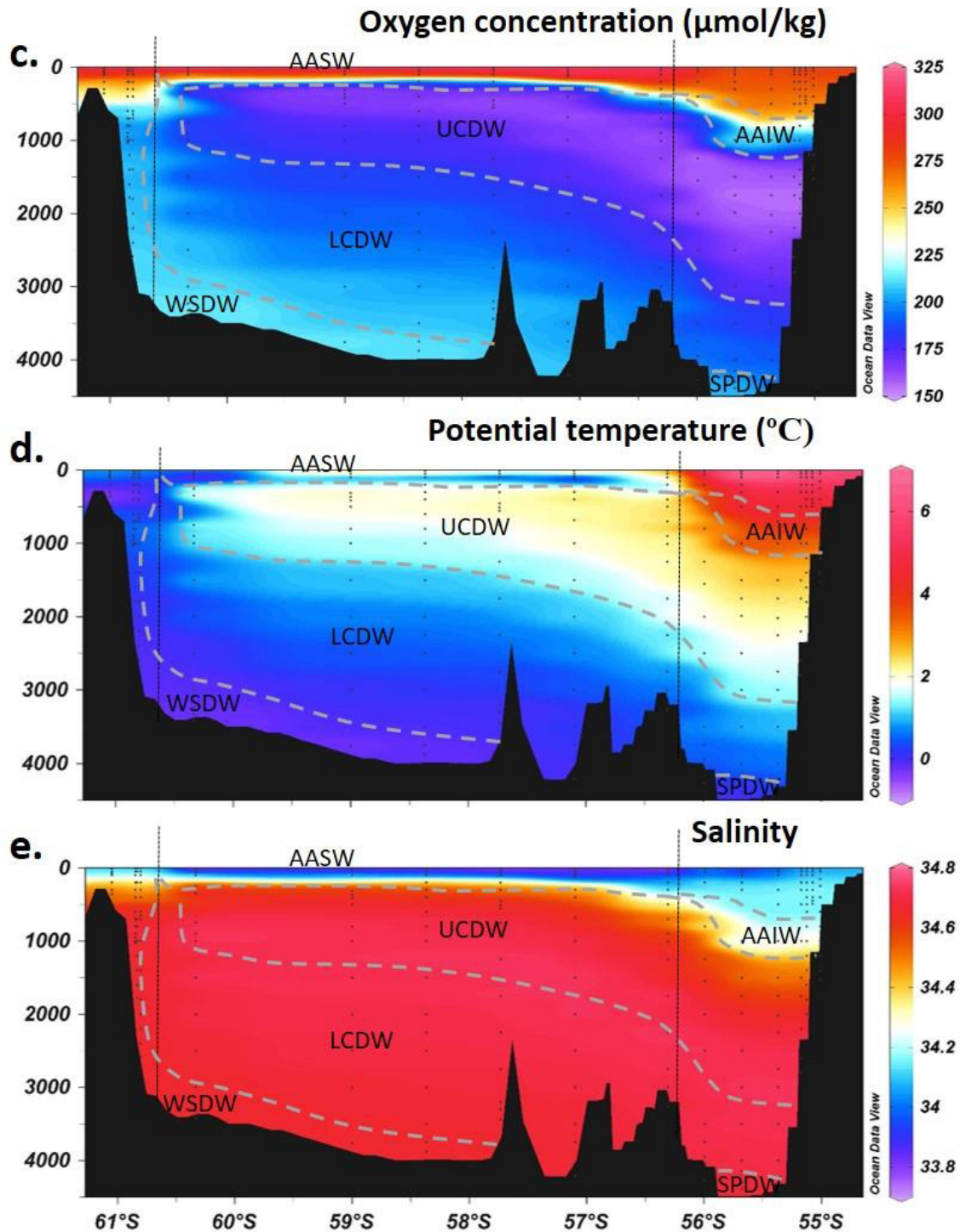


Figure 3-4: Main figures show Drake Passage sections from the tip of the West Antarctic Peninsula (left) to Burdwood Bank (right). Colour scale represents labelled parameters in each panel; locations of Southern Boundary and Polar Front marked by vertical dotted black lines in each panel. Delineation of water masses schematically marked for reference: Weddell Sea Deep Water (WSDW), South Pacific Deep Water (SPDW), Lower and Upper Circumpolar Deep Water (LCDW and UCDW), Antarctic Intermediate Water (AAIW), and Antarctic Surface Water (AASW).
 a. Ba_d concentrations (nM); b. $Ba_d^{Si\ residual}$ values; (inset below shows the surface distribution) (overleaf) c. dissolved oxygen concentrations ($\mu\text{mol kg}^{-1}$); d. potential temperature ($^{\circ}\text{C}$); e. salinity. Inset map (bottom panel, above) shows the distribution of Ba_d measured in surface waters, with colour scale showing Ba_d (nM).



1.2. The Weddell Sea

The Weddell Sea is an important site of deep water formation, with Weddell Sea Bottom Water (WSBW) forming from the mixture of comparatively saline CDW and low temperature shelf waters at the southern and western continental margins of the cyclonic Weddell Gyre (Orsi et al. 1993). As it circulates around the gyre the cold, saline WSBW mixes upwards with warmer CDW to form Weddell Sea Deep Water (WSDW), added to by lateral advection of recently

ventilated waters from outside the Weddell Sea (Meredith et al. 2000; Ohshima et al. 2013). WSDW also forms directly from the descent and mixing of shelf waters in the Weddell Sea (Meredith et al. 2000). WSDW is then able to exit into the Scotia Sea as discussed above, as well as flowing around the South Sandwich Islands and into the Atlantic through the Georgia Basin. This outflow represents the densest contribution to the equatorward-flowing Antarctic Bottom Waters (AABW) (Meredith et al. 2000).

2. Materials and Methods

The Scotia Sea and Weddell Sea data discussed in this chapter were collected during the *RRS James Clark Ross* cruise JR299 in the austral autumn (March to April) 2014. Three sections were sampled (see Figure 2-2), the first being the World Ocean Circulation Experiment (WOCE) SR1b transect from Elephant Island to Burdwood Bank (Cunningham et al. 2003) (JR293), designed to capture the vertical profiles and horizontal gradients of the different water masses across the Drake Passage, and the time-evolving transport of the ACC. Data were also gathered from an additional transect (JR273b) along the North Scotia Ridge, concentrating on collecting depth profiles through Shag Rocks Passage, a 3100 m gap in the ridge through which the Polar Front, and its associated transport, crosses into the Atlantic (Smith et al. 2010). One depth profile (Station 44) was collected in the Weddell Sea amongst rapidly developing pack ice, whilst a second Weddell Sea profile (Station 45) has been analysed from the start of the A23 transect between the edge of the Weddell Sea and South Georgia (JR272c) (for further details of the sections sampled see Chapter 2 Section 2.1.ii).

A total of 609 seawater samples were collected at corresponding stations and depths for dissolved barium, silicic acid, and nitrate and phosphate analysis using Niskin bottles deployed on a CTD (Conductivity-Temperature-Depth) rosette. 372 of these samples were subsequently analysed for dissolved barium concentrations. For further detail of stations and sampling protocols see Chapter 2 Section 2.1.ii.

2.1. Dissolved barium

The dissolved barium concentrations of unfiltered seawater samples were analysed using isotope dilution inductively coupled plasma mass spectrometry (ID ICP-MS) as outlined in Chapter 2 Section 4. Sample preparation and measurements of the JR299 data set were made at the Bristol Isotope Group, Earth Sciences Department, at Bristol University, using a Thermo-Finnigan Element-2 (SEM detector only) for the ICP-MS analysis.

A mass bias correction coefficient (K) was calculated each time samples were analysed by measuring the ratio of $^{138}\text{Ba}/^{135}\text{Ba}$ in a 1 ppb Ba natural standard solution prepared in 5 % (v/v)

seawater (NASS-6 seawater standard of 5 ppb \pm 0.15 Ba), and comparing this to the average natural ratio reported in the literature (10.88) (Chapter 2 Section 4.3.iv). The isotope ratio determined in this solution varied between 10.7 and 11.4, with measured uncertainty across each sample run usually around 0.4 % and never exceeding 1.3 % (2*RSD). Within each run, this uncertainty was always less than the mass bias determined for each sample run, which was on average a 1.2 % deviation from the literature value (minimum deviation 0.47 %; maximum deviation 4.8 %).

Blank solutions of 3 % (v/v of concentrated reagent) HNO₃ in 18.2M Ω ·cm water were analysed to correct for background barium signal from the introduction system of the ICP-MS (¹³⁵Ba blank counts <0.15 % of seawater sample counts; ¹³⁸Ba blank counts <0.5 % of seawater sample counts), and a set of consistency standards were measured at regular intervals to quantify the long-term reproducibility of the measurements (see Table 3-1). A correction for any seawater matrix effects was applied to the blank measurements by monitoring the sensitivity of a natural standard solution in 3% HNO₃ vs. a natural standard solution in 5 % seawater, before the blanks were subtracted from sample counts.

	Standard:	In-house Standard 1	NASS-5	NASS-6
Bristol	<i>2*RSD</i>	1.34%	3.26%	1.73%
	<i>n</i>	72	33	70
	<i>[Ba] (nM)</i>	73.5 \pm 1.0	37.4 \pm 1.2	49.3 \pm 0.9
Cardiff	<i>2*RSD</i>	1.29%	1.53%	1.22%
	<i>n</i>	23	22	23
	<i>[Ba] (nM)</i>	73.7 \pm 1.0	37.0 \pm 0.6	49.5 \pm 0.6

*Table 3-1: Reproducibility of standards measured in Bristol from March to November 2016. Data from Cardiff (measured in 2014) provided for comparison. Values given are 2*relative standard deviation (2*RSD). Errors from In-house Standard 1 (from the Scotia Sea, 100m depth) are considered applicable to the higher range of Scotia and Weddell Sea samples, whilst errors from NASS-6 can be applied to the lower range, as the dissolved barium concentrations are the most comparable. For consistency, the most conservative uncertainty of 1.7 % (from the NASS-6 standard) is applied to all samples.*

Seawater standards of comparable barium concentration to the samples show a long-term external reproducibility of \pm 1.7 % (2*RSD) or better across all analytical runs from March to November 2015 (Table 3-1 and Figure 2-17). Within each analytical run, reproducibility of these seawater standards was \pm 1.1 % (2*RSD) or better. Although none of these seawater standards have a certified barium concentration, accuracy was consistently checked against the average measurements of the same standards, measured using a Thermo-Finnigan Element-XR at the School of Earth and Ocean Sciences, Cardiff University (Chapter 2 Section 5.3). The full range of Ba concentrations in this study varied between 43 nM and 103 nM; high precision

analyses were necessary for the robust identification of relatively subtle Ba gradients within depth profiles and across spatial trends.

2.2. Dissolved inorganic nutrients

Dissolved inorganic nutrients (silicic acid, phosphate, and nitrate + nitrite) were analysed at the University of East Anglia by Oliver Legge and Andy Hind using a San++ Gas Segmented Continuous Flow Analyser (Skalar, Breda, The Netherlands). The accuracy of the measured nutrient concentrations were checked by performing a six point calibration for each analyte, using a mixed standard containing silicate, nitrate, and phosphate (made from reagent grade sodium hexafluorosilicate, sodium nitrate and potassium dihydrogen phosphate respectively). Standards and wash solution were made in a saline solution containing 35 g reagent grade NaCl/L in ultrapure water. Prior to the preparation of the standards and wash solution the NaCl was baked at 400 °C to remove any nitrate contamination.

2.2.i Oxidised nitrogen (NO_x)

Unfiltered seawater samples for NO_x (and PO₄) analysis were frozen within six hours of being sampled, and stored frozen awaiting analysis. As nitrate cannot be measured directly using a segmented flow analyser, the sample was first reduced to nitrite by buffering the solution at pH 8.2 and passing it through a copperised cadmium column. The nitrite was then determined colourmetrically following the method of Skalar (2009a), using N-(1-naphthyl)ethylenediamine dihydrochloride and sulfanilamide; the intensity of the red dye was measured by a photometer using a 540 nm filter (Bendschneider & Robinson 1952). The detection limit for this method was approximately 0.07 µM (3x the standard deviation of repeated blank measurements, as recommended by Taylor (1990)).

Oxidised nitrogen (NO_x) therefore refers to nitrite (NO₂) + nitrate (NO₃). Nitrite occurs in the water column at levels typically 70 times lower than nitrate in the photic zone and approximately 52000 times lower in the aphotic zone (Gruber 2008). The reproducibility of NO_x concentrations was ± 1.70 µM (1*SD), calculated by analysing eighteen sets of duplicate samples.

2.2.ii Phosphate (PO₄)

Unfiltered seawater samples for PO₄ (and NO_x) were frozen within six hours of being sampled, and stored frozen awaiting analysis. Phosphate was measured following the method of Skalar (2009b), based on the principles developed by Murphy and Riley (1962). The sample was introduced to an acidified medium containing ammonium heptamolybdate and potassium antimony (III) oxide tartrate to form an antimony-phosphomolybdate complex. This was then

reduced to a blue coloured complex using ascorbic acid, and the intensity of the colour measured spectrophotometrically using an 810 nm wavelength filter. The detection limit of this method was approximately 0.13 μM , calculated as for the nitrate measurement. The reproducibility of PO_4 concentrations was $\pm 0.18 \mu\text{M}$ (1*SD), calculated by analysing eighteen sets of duplicate samples.

2.2.iii Silicate/silicic acid ($\text{Si}(\text{OH})_4$)

As freezing and defrosting samples can lead to incomplete silicic acid recovery, separate unfiltered seawater samples also were collected and kept refrigerated at 2 to 4 °C awaiting analysis (Aminot et al. 2009). Silicate concentration was analysed using the method of Skalar (2009c), based on that of Brewer and Riley (1966). The sample was acidified with sulfuric acid and mixed with an ammonium heptamolybdate solution. This was then reduced to a blue coloured complex using ascorbic acid, and the intensity of the colour measured spectrophotometrically using an 810 nm wavelength filter. Oxalic acid was added to reduce interference from phosphate. The detection limit of this method was approximately 0.09 μM , calculated as for the nitrate measurement. The reproducibility of $\text{Si}(\text{OH})_4$ concentrations was $\pm 1.64 \mu\text{M}$ (1*SD), calculated by analysing sixteen sets of duplicate samples.

2.3. Temperature, salinity, and oxygen concentrations

Temperature, salinity, and oxygen concentrations were recorded for each CTD cast using a SBE9Plus unit with dual SBE3Plus temperature and SBE4 conductivity sensors and a Paroscientific pressure sensor, and an SBE43 oxygen sensor.

Conductivity measurements were processed and converted to salinity, and calibrated by the regular collection of discrete seawater samples from CTD casts, analysed for salinity using the on board Guildline Autosal 8400B salinometer. Discrete samples were also collected at five CTD stations for on board measurement of dissolved oxygen concentrations via Winkler titration, which were used to calibrate the CTD oxygen probes. Details of these calibrations can be found in the cruise report of the *RRS James Clark Ross* JR299: Scotia Sea circumnavigation and DIMES UK5 (Meijers 2014).

2.4. Quantifying deviation from $\text{Ba}_d/\text{Si}(\text{OH})_4$ trends

Where linear correlations exist between Ba_d and silicic acid, scatter above and below the trendline is quantified by calculating $\text{Ba}_d^{\text{Si residual}}$ values (Equation 3-1). The $\text{Ba}_d^{\text{Si residual}}$ value quantifies the deviation of the Ba_d measurement from the overall $\text{Ba}_d/\text{Si}(\text{OH})_4$ regression of the station profile. Positive $\text{Ba}_d^{\text{Si residual}}$ values indicate that the Ba_d measured is higher than predicted by silicic acid values, whilst negative $\text{Ba}_d^{\text{Si residual}}$ values signify that Ba_d is lower than predicted

(Figure 3-5). This will help to identify decoupling of Ba_d and silicic acid, potentially reflecting processes such as barite formation that only affect one of the parameters.

$$Ba_d^{Residual} = Ba_d^{Measured} - ((Si(OH)_4^{Measured} * \text{slope of correlation}) + \text{intercept})$$

Equation 3-1

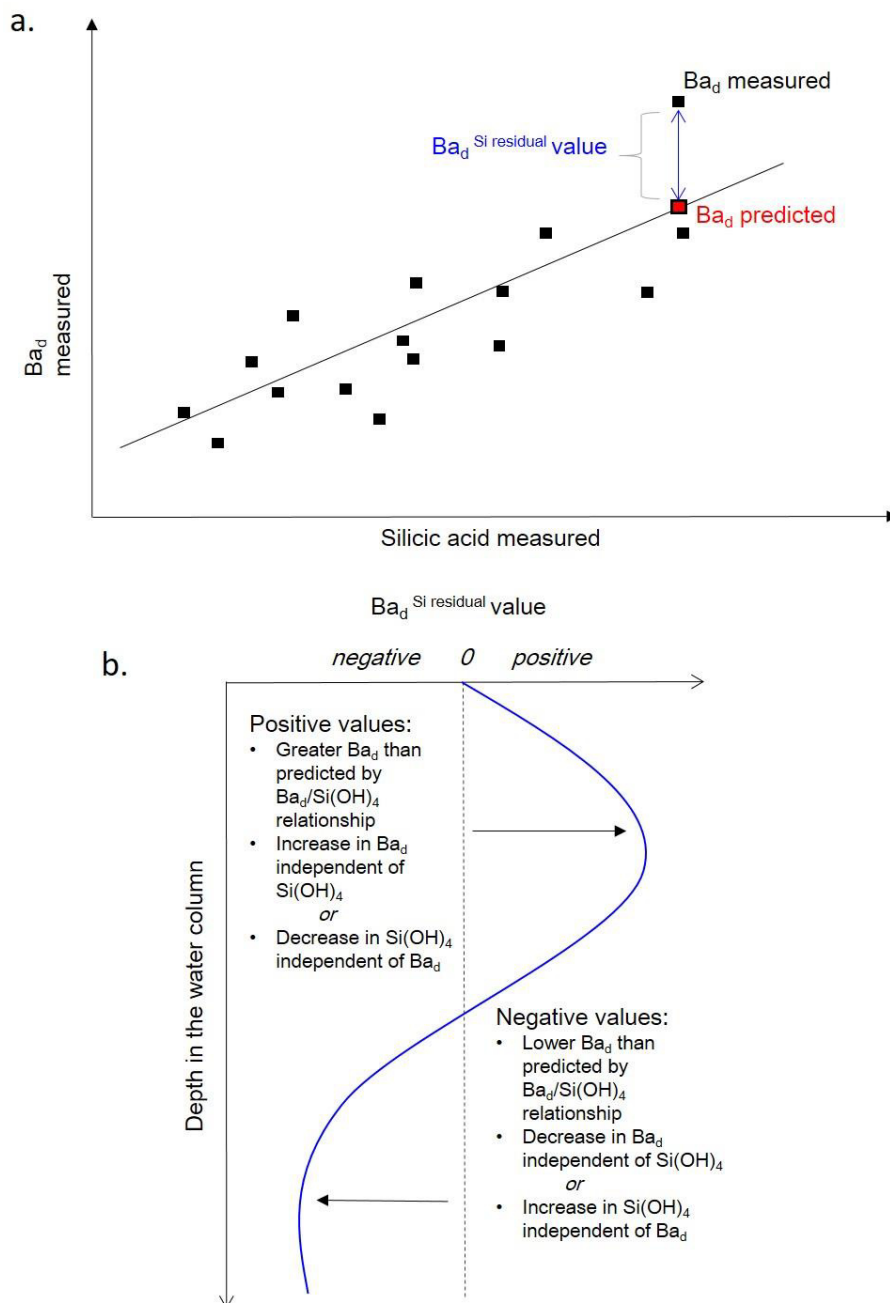


Figure 3-5: Schematic representation of Ba_d^{Si} residual values; a. representation of how Ba_d^{Si} residual values are calculated from $Ba_d/Si(OH)_4$ correlation; b. Indication of how Ba_d^{Si} residual variation through the water column can be interpreted.

3. Results

3.1. *Identifying polar frontal zones and major water masses*

Conservative parameters temperature and salinity were used to establish the location of the ACC fronts across the Drake Passage and North Scotia Ridge transects. The Sub-Antarctic Front, Polar Front, and the Southern ACC Front are dynamic features that can be identified by the location of enhanced horizontal gradients in temperature, salinity, and oxygen concentration, and have traditionally been considered boundaries between distinct water masses (Graham et al. 2012; Orsi et al. 1995). These conservative hydrographic parameters were used to establish the location of the polar frontal zones across the Drake Passage and the North Scotia Ridge transects. Labelled, dashed lines in Figure 3-2 show the approximate locations of these fronts.

Across the Drake Passage transect the Southern Boundary is observed between Stations 7 and 9, marked most clearly in a positive sea surface temperature (SST) gradient (Figure 3-4 d). The location of the Southern ACC Front is indistinct in my data, possibly falling within the less-resolved mid-section of the Drake Passage. The Polar Front is located between Stations 26 and 30, with clear surface gradients in increased SSTs, lower salinity, and lower oxygen concentrations (Figure 3-4 c, d, and e). The Sub-Antarctic Front is also less clearly defined, but is approximated to lie between Stations 35 and 37.

Across the North Scotia Ridge Transect the Sub-Antarctic Front is again less distinct, but can be approximately located between Stations 128 and 125 by an eastward transition to a colder, less saline, less oxygenated water column (Figure 3-6 c, d, and e). The Polar Front is observed between Stations 101 and 100, marked by an eastward increase in surface oxygen concentrations, accompanied by lowered salinity and temperature (Figure 3-6 c, d, and e).

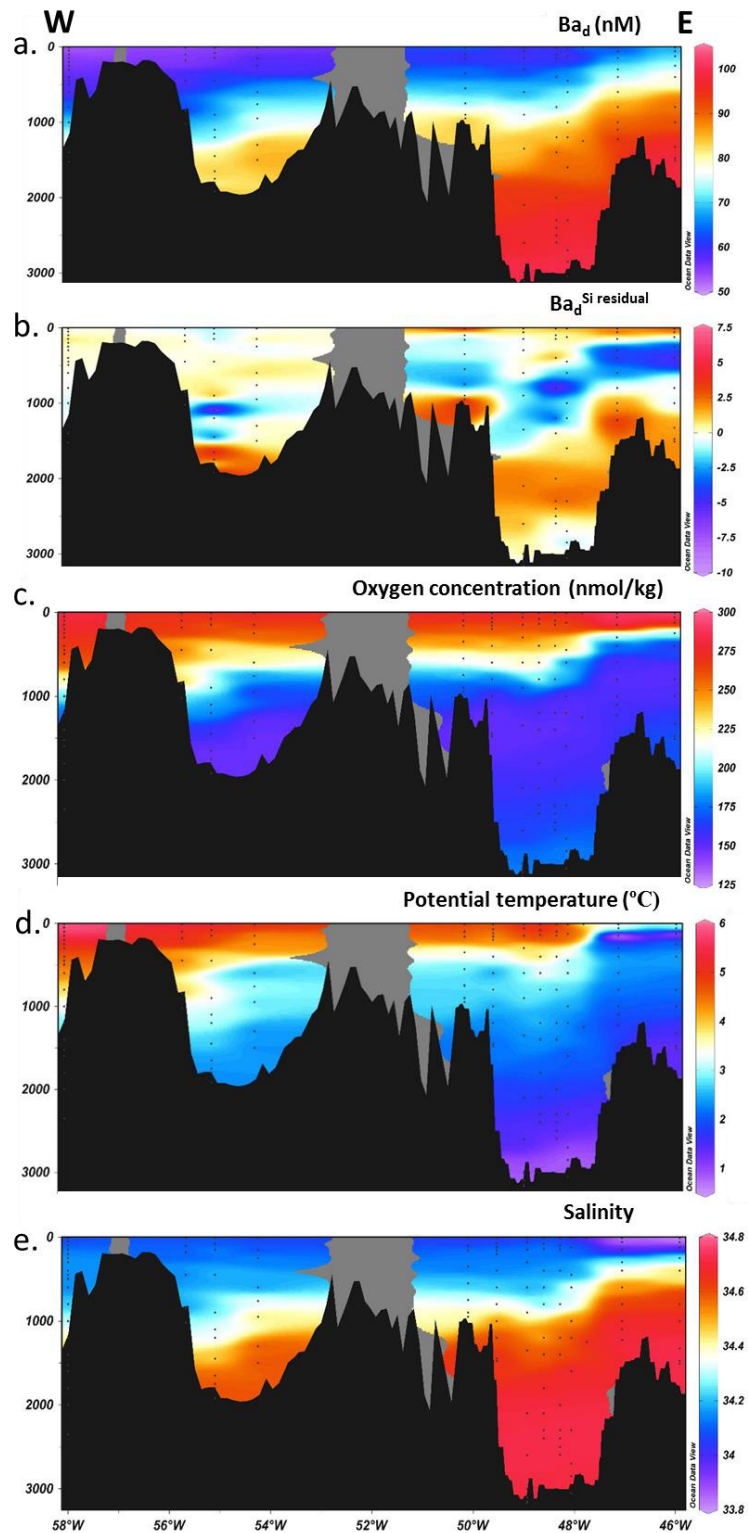


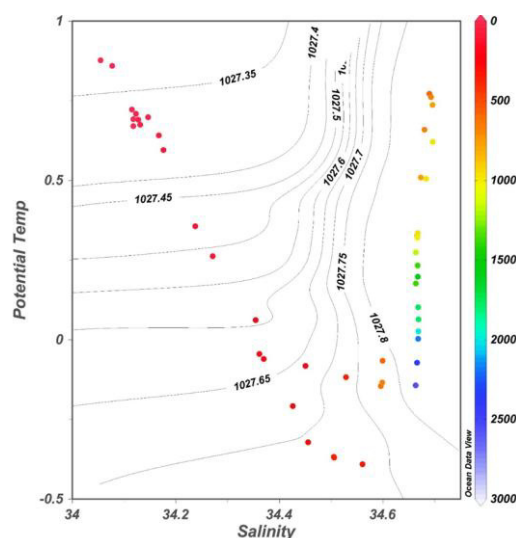
Figure 3-6: (previous page) North Scotia Ridge section from west (left) to east (right). Colour scale represents labelled parameters in each panel; a. Ba_d concentrations (nM); b. Ba_d^{Si} residual values; c. dissolved oxygen concentrations ($\mu\text{mol kg}^{-1}$); d. potential temperature ($^{\circ}\text{C}$); e. salinity.

Within these horizontally bounded frontal zones, the vertical distribution of conservative parameters marks the transition with depth through the cores of key water masses: Antarctic Intermediate Water (AAIW), and Upper and Lower Circumpolar Deep Waters (UCDW and LCDW). These water masses are most distinctly differentiated by their oxygen concentrations (Figure 3-4 and Figure 3-6). In the Drake Passage transect, AAIW can be recognised as a relatively warm, low salinity, well-oxygenated shallow water mass north of the PFZ. This overlies the Circumpolar Deep Waters, divided into the low oxygen UCDW, warmer and more saline than the deep waters of the LCDW (Figure 3-6). At the very base of the water column in the Drake Passage, the colder, slightly fresher SPDW can be distinguished from the bulk of LCDW by increased silicic acid values (Sievers & Nowlin 1984; Peterson & Whitworth 1989; Naveira Garabato et al. 2002).

3.2. Antarctic continental waters

South of the Southern ACC Boundary, Stations 3 to 7 were sited in Antarctic continental waters. The water mass as a whole is 1 to 1.5 $^{\circ}\text{C}$ colder, with less temperature variation than the northward stations of the ACC and PFZ (Figure 3-4 d). Relatively warm sea surface temperatures (SSTs) (0.5 to 0.75 $^{\circ}\text{C}$; salinity 34) overlie a more saline, low temperature layer at the base of the thermocline (approximately 500 m; 0 to -0.5 $^{\circ}\text{C}$; salinity 34.5). Below 500 m the water column is relatively homogeneous with regards to salinity and oxygen concentrations, with potential temperatures ranging from 0.75 $^{\circ}\text{C}$ to just below 0 $^{\circ}\text{C}$ at the base (Figure 3-4 c and Figure 3-7).

Figure 3-7: (right) Potential temperature vs. salinity of Antarctic Continental waters (south of the Southern Boundary), with colour bar representing the depth of samples in the water column (m) and solid lines showing density



Surface water Ba_d concentrations in this near-Antarctic region are relatively high compared to the open Southern Ocean, with the shallow station on the continental slope reaching maximum concentrations (88.5 nM) in the sub-surface by 500 m, and the deeper station 7 reaching maximum values (97.3 nM) at the base of the oxygen minimum zone (Figure 3-8). NO_x and PO_4 concentrations increase with depth throughout the upper 500 m and are

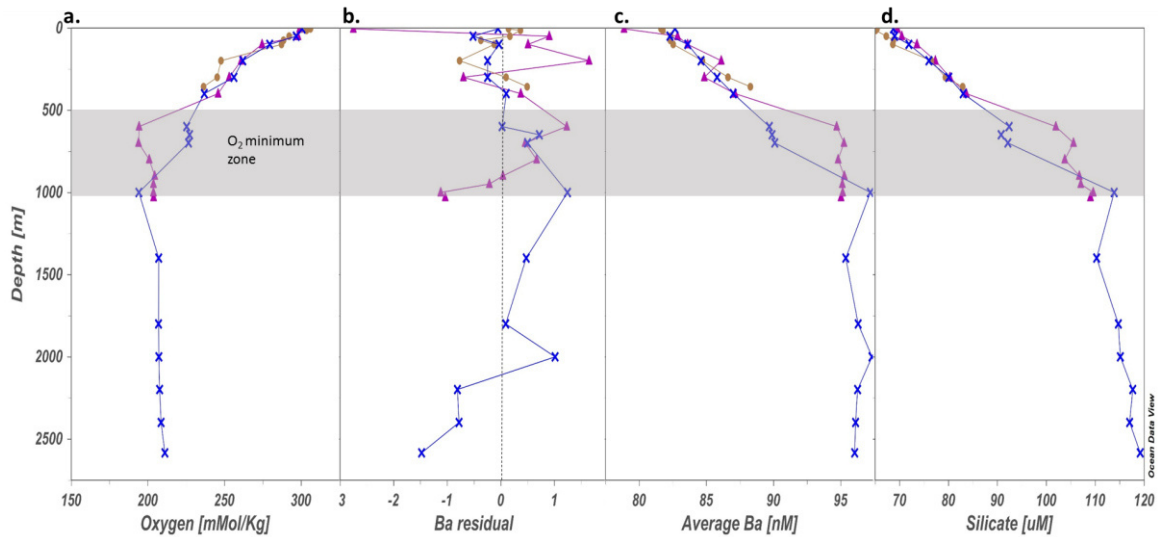


Figure 3-8: Depth profiles of Antarctic continental waters south of the Southern Boundary (Station 3 brown circles; Station 5 purple triangles; Station 7 blue crosses) a. Dissolved oxygen concentrations ($\mu\text{mol} / \text{kg}$); b. $Ba_d^{Si \text{ residual}}$ values, zero line marked by black dotted line for reference; c. Dissolved barium concentrations (nM); d. Silicic acid (μM). Shaded area represents the oxygen minimum zone (approximately 500 to 1000 m).

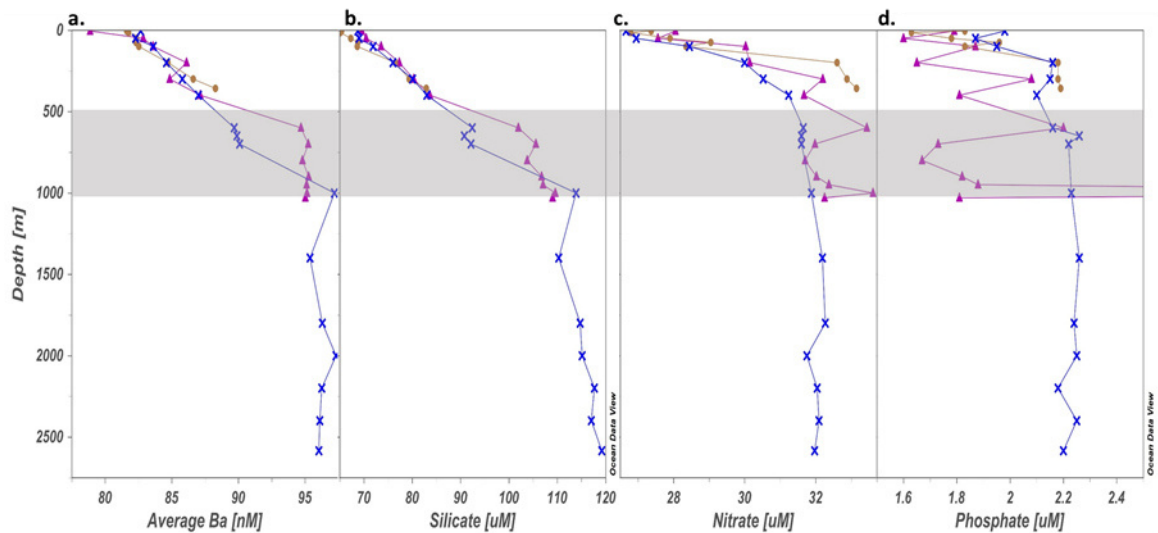


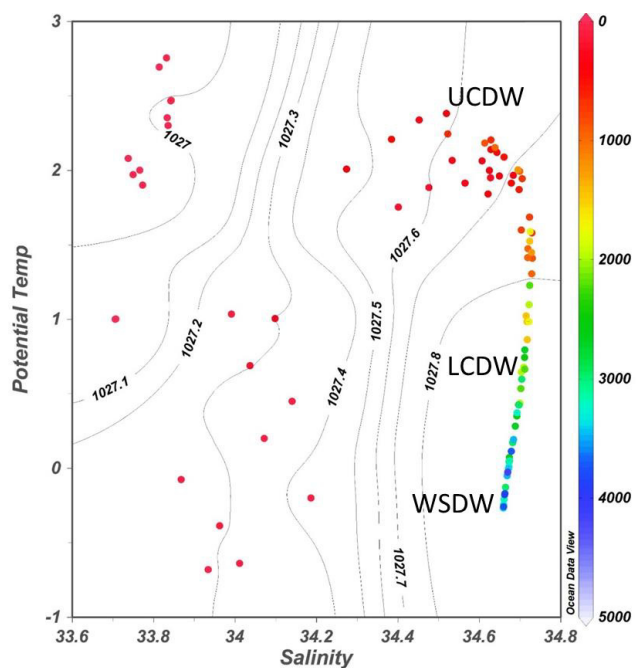
Figure 3-9: Depth profiles of Antarctic continental waters south of the ACC Boundary (Station 3 brown circles; Station 5 purple triangles; Station 7 blue crosses) a. Dissolved barium (nM); b. Silicic acid (μM); c. Nitrate+Nitrite (μM); d. Phosphate (μM). Shaded area represents the oxygen minimum zone (approximately 500 to 1000m).

then largely invariant throughout the rest of the water column, whilst silicic acid largely mimics the behaviour of Ba_d with depth (Figure 3-9). There are significant positive linear correlations between Ba_d and NO_x ($Ba = 2.18 * NO_x + 21.8$; $n = 37$; $R^2 = 0.59$; $p < 0.001$) and Ba_d and silicic acid ($Ba = 0.31 * Si(OH)_4 + 60.1$; $n = 37$; $R^2 = 0.97$; $p < 0.001$), but not between Ba_d and PO_4 ($n = 37$; $R^2 = 0.12$; $p = 0.04$) (Appendix 8). There is very little scatter in the correlation of Ba_d and silicic acid, reflected in little variation from zero in the $Ba_d^{Si\text{ residual}}$ values with depth (Figure 3-8).

3.3. The Antarctic Zone (AAZ)

Stations 9 to 26 lie north of the Southern Boundary and south of the Polar Front, in the core of the eastward flowing ACC. These four stations reach depths of between 3000 to 4000 m and show a well-stratified water column with the stratification dominantly controlled by salinity; relatively warm (2 to 3°C), low salinity (33.7 to 33.8) surface waters (0 to 50 m), a temperature minimum (-1 to 0°C) at approximately 100 m, and a core of relatively warm (2 °C) saline (34.4 to 34.7) UCDW at 250 to 1000 m mixing with colder (0 to 1°C) LCDW and WSDW (-0.7 < T < 0 °C) bottom waters (Figure 3-10).

Figure 3-10: (right) Potential temperature vs. salinity for stations south of the Polar Front and north of the Southern Boundary. Contours show density and colour scale represents depth in the water column. Antarctic Intermediate Water (AAIW), Upper and Lower Circumpolar Deep Waters (UCDW and LCDW), Weddell Sea Deep Water (WSDW) end-members labelled.



Depth profiles of macronutrients (Figure 3-12) show that NO_x and PO₄ are low in surface waters but do not reach zero, and remineralise at relatively shallow depths, reaching maximum

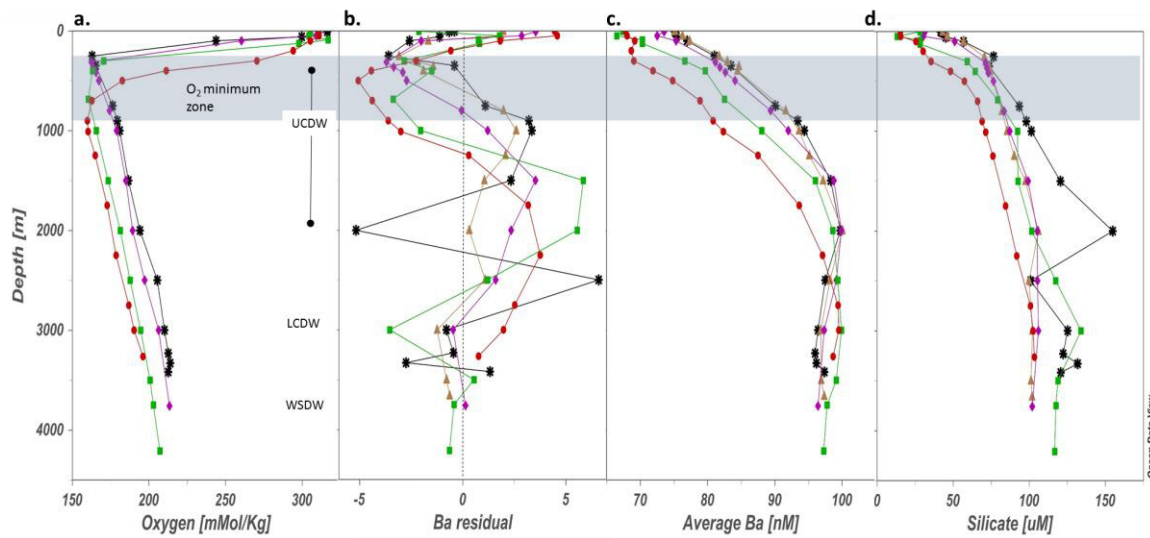


Figure 3-11: Depth profiles of ACC waters south of the Polar Front (Station 9 black asterix; Station 11 brown triangles; Station 13 purple diamonds; Station 19 green squares; Station 26 red circles) **a.** Dissolved oxygen concentrations ($\mu\text{mol/kg}$); **b.** $\text{Ba}_d^{\text{Si residual}}$ values; **c.** Dissolved barium concentrations (nM); **d.** Silicic acid (μM). Shaded area represents the oxygen minimum zone.

values by 500 m. However, silicic acid concentrations show two stages of regeneration, with an initially rapid increase from low surface values down to approximately 500 m. Below 500 m, silicic acid concentrations continue to rise, but at a slower rate, reaching maximum levels at 2000 to 3000 m.

Ba_d concentrations, on the other hand, display a steady rate of increase from lower surface values (70 to 75 nM) to maximum concentrations of 95 to 100 nM at approximately 2000 m. Despite differences in behaviour with depth, there is a strong positive linear correlation between Ba_d and silicic acid ($Ba = 0.32 * Si(OH)_4 + 61.0$; $n = 77$; $R^2 = 0.90$; $p < 0.001$) (Figure 3-13 a), although this trend differs from the linear model fitted to the global GEOSECS data ($Ba = 0.58 * Si(OH)_4 + 39.33$; $n = 322$; $R^2 = 0.94$; $p < 0.01$). Whilst most AAZ samples between depths of 150 m and 1000 m lie centrally at values of $Si(OH)_4 = 60$ to $100 \mu M$ and $Ba_d = 80$ to $100 nM$, consistent with the global trend line, there are deviations from this amongst shallow and deep samples. AAZ samples below 1000 m are invariant with regards to Ba_d yet show a wide variation in silicic acid. Shallow sites within the ACC (top 150 m) record higher Ba_d values relative to silicic acid than the global linear relationship would predict, and these samples record a shallower $Ba_d/Si(OH)_4$ trend, indicating that Ba_d varies less with respect to silicic acid at these shallow ACC sites than it does globally and in the intermediate depth ACC waters (Figure 3-13 a). The relationship exhibited between Ba_d and the other macronutrients, NO_x and PO_4 , is non-linear, with a general positive trend encompassing three broad populations: highly variable NO_x and PO_4 vs less variable Ba_d in surface waters, less variable NO_x and PO_4 vs. highly variable Ba_d in

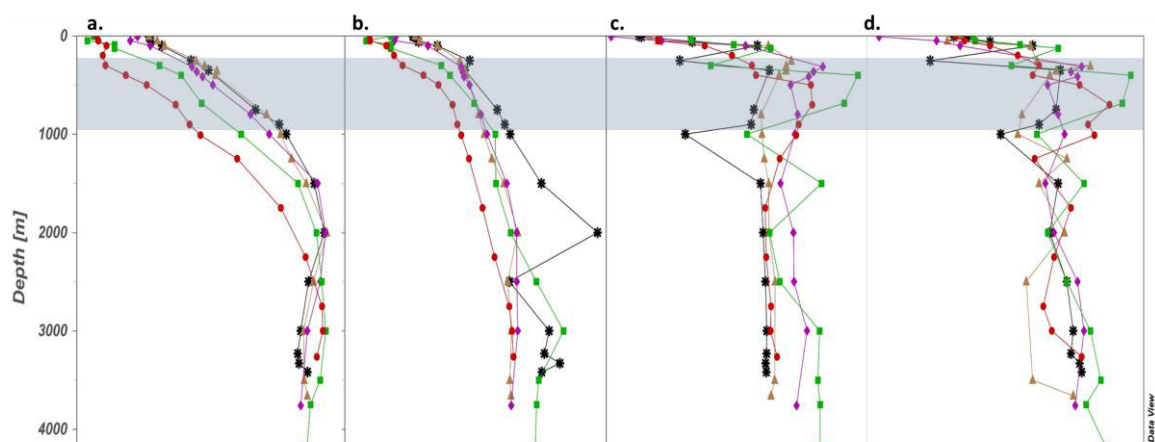


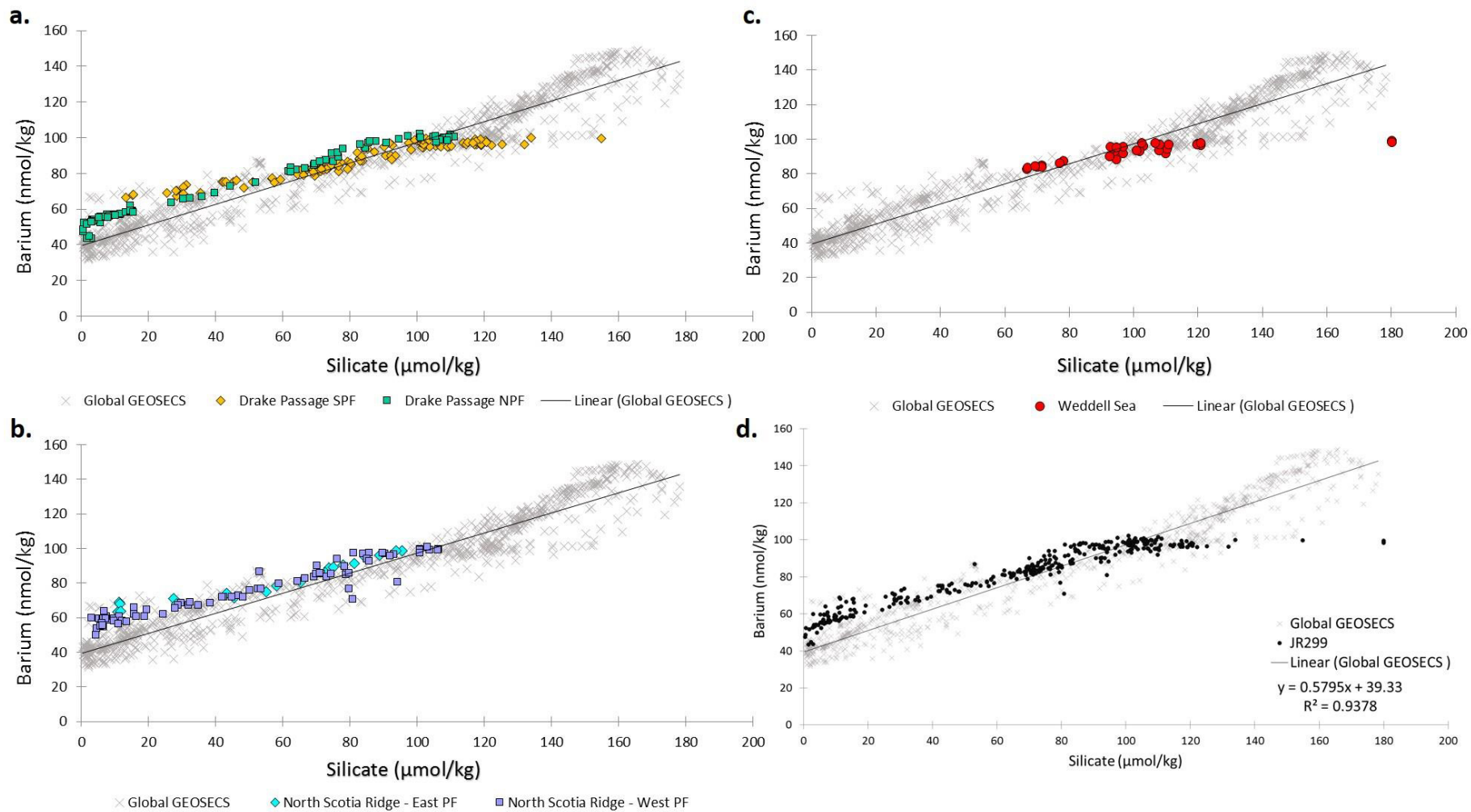
Figure 3-12: Depth profiles of ACC waters south of the Polar Front (Station 9 black asterisk; Station 11 brown triangles; Station 13 purple diamonds; Station 19 green squares; Station 26 red circles) a. Dissolved barium (nM); b. Silicic acid (μM); c. Nitrate + Nitrite (μM); d. Phosphate (μM). Shaded area represents the oxygen minimum zone.

intermediate waters and deeper waters (see Figures in Appendix 8).

Variations in the behaviour of silicic acid and Ba_d with depth are observed in more detail in the $Ba_d^{Si \text{ residual}}$ values calculated from the individual $Ba_d/Si(OH)_4$ relationship at each station, which are positive in surface waters before decreasing to a subsurface minimum between 200 and 800 m, returning to positive values below 1000 m, and decreasing to values of zero by the bottom of the water column (Figure 3-11). The sub-surface minimum of $Ba_d^{Si \text{ residual}}$ values

corresponds with the oxygen minimum zone, denoting both a transition into the UCDW and the depth range of maximum NO_x and PO₄ remineralisation (Figure 3-12). A transition to a subsurface maximum deeper in the water column but within the UCDW water mass occurs in all profiles, with the depth of that maximum increasing northwards (800 m in the south to 2200 m in the north).

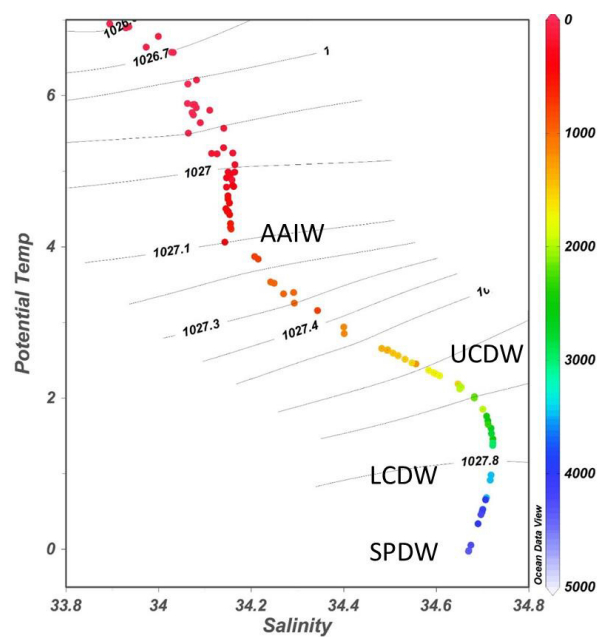
Figure 3-13: (overleaf) Scatter plots of dissolved barium vs. silicic acid for biogeographical divisions of the dataset, superimposed upon the global GEOSECS dataset (Ostlund et al. 1987), plotted in grey crosses. a. Data from the Drake Passage Transect (Stations south of the PF as yellow diamonds, Stations north of the PF as green squares); b. Data from the NSR Transect (Stations east of the PF as blue diamonds, stations west of the PF as purple squares) c. Data from the Weddell Sea as red circles; d. All JR299 data shown together as black dots.



3.4. North of the PF (PFZ-SAZ)

Stations 30 to 41 lie north of the Polar Front, in ACC waters flowing eastwards in the PFZ and SAZ. Three of these stations reach depths below 4000 m whilst Stations 37 and 40 are shallower, reaching bottom depths of 2800 m and 1525 m respectively on the continental rise/slope. The Polar Front is marked at approximately 56 °S by a notable change in the water column; the disappearance of the temperature minimum layer, and the decreased dominance of salinity on stratification (Figure 3-4 d and e). Sea surface temperatures increase to 6 to 7 °C, with warmer temperatures and lower salinities extending down to 1000m, where subducted AAIW (4 °C; salinity 34.2) overlies low oxygen UCDW (2 °C; salinity 34.7) (Figure 3-14).

Figure 3-14: (right) Potential temperature vs. salinity for stations north of the Polar Front. Contours show density and colour scale represents depth in the water column. Main water masses labelled: Antarctic Intermediate Water (AAIW), Upper and Lower Circumpolar Deep Waters (UCDW and LCDW), South Pacific Deep Water (SPDW).



In the top 200 m Ba_d increases rapidly with water depth, more closely following the behaviour of NO_x and PO_4 than silicic acid, which remains fairly constant (Figure 3-6). NO_x and PO_4 concentrations continue to increase below 200 m at a slower rate until reaching maximum levels at approximately 1500 m, which are maintained throughout deeper waters. In contrast, both silicic acid and Ba_d are broadly invariant between 200 and 500 m, before increasing at a similar pace until 1500 m. Ba_d concentrations reach maximum levels at approximately 2500 m,

and silicic acid concentrations continue to rise at the deeper stations until close to bottom depths of 4000 m.

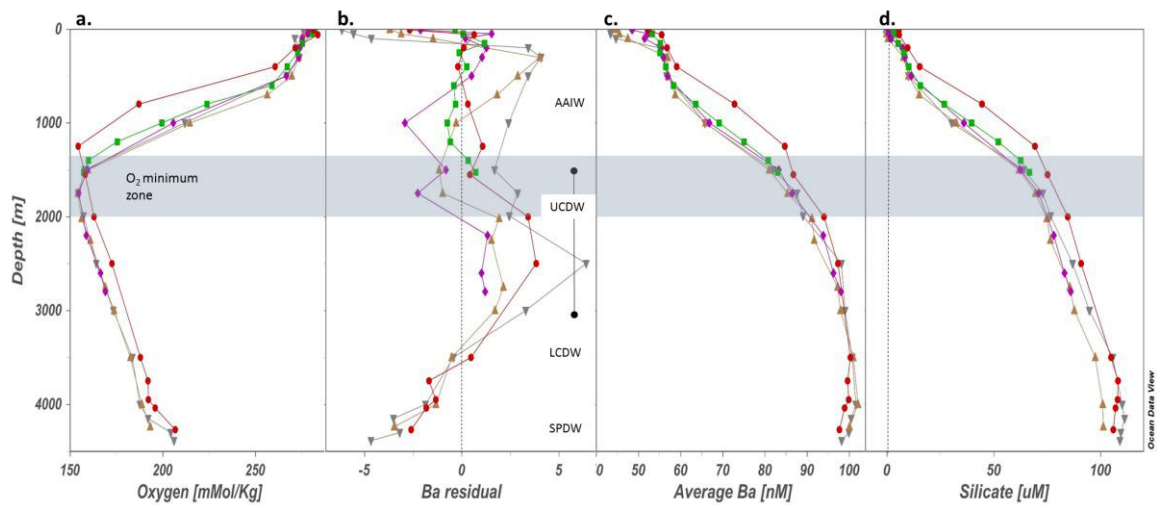


Figure 3-15: Depth profiles of Drake Passage waters north of the Polar Front (Station 30 red circle; Station 33 grey upsidedown triangles; Station 35 brown triangles; Station 41 purple diamonds; Station 40 green squares) a. Dissolved oxygen concentrations ($\mu\text{mol} / \text{kg}$); b. Ba_d^{Si} residual values; c. Dissolved barium concentrations (nM); d. Silicic acid (μM). Shaded area represents the oxygen minimum zone.

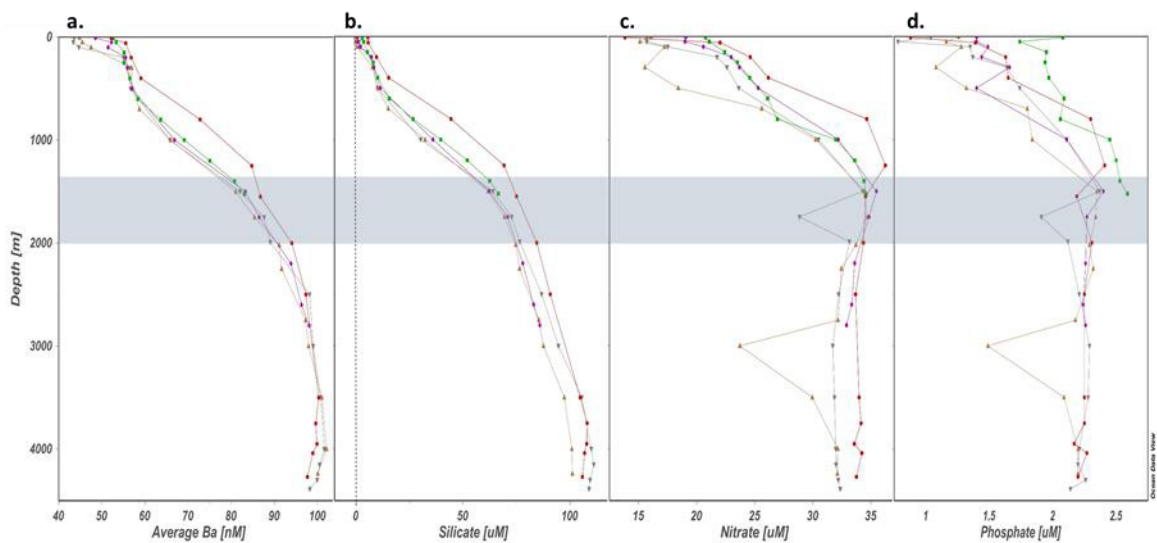


Figure 3-16: Depth profiles of Drake Passage waters north of the Polar Front (Station 30 red circle; Station 33 grey upsidedown triangles; Station 35 brown triangles; Station 41 purple diamonds; Station 40 green squares) a. Dissolved barium (nM); b. Silicic acid (μM); c. Nitrate + Nitrite (μM); d. Phosphate (μM). Shaded area represents the oxygen minimum zone.

Whilst south of the Polar Front there is a strong covariance in the behaviour of Ba_d and silicic acid with depth suggesting a close biogeochemical coupling, that is quite distinct from the behaviour of the other two macronutrients (NO_x and PO_4), such a relationship is less apparent in

these waters north of the Polar Front. Nonetheless, at these PFZ and SAZ stations there is a similarity of behaviour between Ba_d , NO_x , and PO_4 in surface waters (0 to 200 m), which is replaced in intermediate waters by a more dominant similarity between Ba_d and silicic acid (Figure 3-15). Despite the marked similarity in their surface water behaviour, the overall relationships between Ba_d and NO_x/PO_4 are distinctly non-linear, as described in Section 3.3 Appendix 8), whilst a significant overall positive linear correlation between Ba_d and silicic acid is identified ($Ba = 0.32 * Si(OH)_4 + 61.1$; $n = 76$; $R^2 = 0.9$; $p < 0.001$).

These offsets from the linear relationship between Ba_d and silicic acid are shown in the $Ba_d^{Si\ residual}$ values, which are negative in surface waters rising to values around zero over the top 200 m (Figure 3-15 and Figure 3-4 b). At two stations (Stations 33 and 35) that exhibit the most depleted surface Ba_d concentrations, $Ba_d^{Si\ residual}$ values overshoot zero and record positive values. These values then decrease to/remain close to zero until they begin to increase again at the transitions to the oxygen minimum zone/UCDW at approximately 1500 m, reaching peak values at the same depth as maximum Ba_d concentrations.

3.5. The North Scotia Ridge

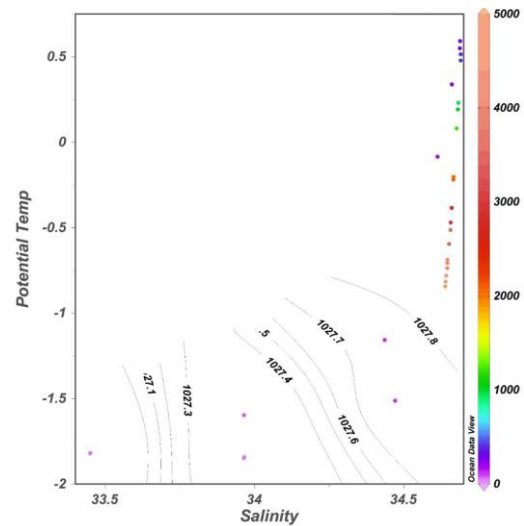
Stations to the west of the Polar Front, as its path curves north through Shag Rocks Passage in the North Scotia Ridge, follow a similar distribution of parameters to the PFZ and SAZ stations across the Drake Passage (Figure 3-4 and Figure 3-6). Positive $Ba_d^{Si\ residual}$ values are associated with the deeper UCDW whilst intermediate waters exhibit less scatter around the strong positive $Ba_d/Si(OH)_4$ correlation, displaced above the global trend line (Figure 3-13 b). East of the Polar Front, the shallowing of UCDW and re-establishing a strong salinity gradient is accompanied by stronger $Ba_d^{Si\ residual}$ gradients, with positive values in surface waters, negative values from the transition to UCDW/oxygen minimum zone at 200 to 300 m, underlain by a return to positive values in the lower part of the UCDW at 1000 m.

3.6. The Weddell Sea

Stations 44 and 45 lie on the edge of the Weddell Gyre, where Ba_d concentrations are consistently higher than at the Scotia Sea stations, with even the surface minima at 85 nM (Figure 3-19). The majority of macronutrient variation is seen in the low temperature (-2 to -1 °C) waters of the top 200 m, with both NO_x and PO_4 increasing from low surface values to sub-surface maxima across a sharp salinity gradient (33.5 salinity at the surface, 35 salinity at 200 m) (Figure 3-17), below which they decrease slightly throughout the bulk of the water column (Figure 3-19 c and d). Silicic acid and Ba_d concentrations do not reach sub-surface maxima until approximately 1000 m, with these values sustained over the next 2000 m until a slight decline in concentrations below depths of 3000 m (Figure 3-18). At Station 44 $Ba_d^{Si\ residual}$ values are

negative at the surface, then maintain slightly positive values from 500 to 4500 m, with silicic acid concentrations elevated relative to Ba_d . Station 45 exhibits more variable $Ba_d^{Si\ residual}$ values, with zero values at the surface, negative values by 200 m that steadily rise with depth until 3500 m, remaining at consistent positive values until 4500 m. The $Ba_d^{Si\ residual}$ values at both stations show sharp variations at the very base of the water column (4500 to 4750 m) (Figure 3-18 b).

Figure 3-17: (right) Potential temperature vs. salinity plot for stations in the Weddell Sea. Contours show density and colour scale represents depth in the water column.



Measurements of dissolved barium concentrations, macronutrient concentrations, and the distribution of dissolved oxygen concentrations have been examined here across the different zones of the Scotia and Weddell Seas. Applying a multivariate linear regression analyses of the whole dataset (Scotia and Weddell Seas and all available parameters) the best model fit to the data (p value <0.01) suggests that Ba_d concentrations could be significantly controlled by potential temperature ($p < 0.01$; intercept -1.78), salinity ($p < 0.01$; intercept 7.59), and silicic acid concentrations ($p < 0.01$; intercept 0.27) (Table 3-2).

	Coefficients	Standard Error	t Stat	P-value
Intercept	-193.528	60.799	-3.183	0.002
Nitrate (uM)	0.043	0.090	0.477	0.634
Phosphate (uM)	-0.048	0.093	-0.518	0.605
Silicate (uM)	0.266	0.016	16.604	0.000
Oxygen (mMol/Kg)	-0.008	0.009	-0.881	0.379
Potential Temp	-1.782	0.234	-7.624	0.000
Salinity	7.590	1.752	4.331	0.000

Table 3-2: Table of results from multivariate linear regression model applied to the whole dataset. Model statistics: $R^2 = 0.94$; $p < 0.001$

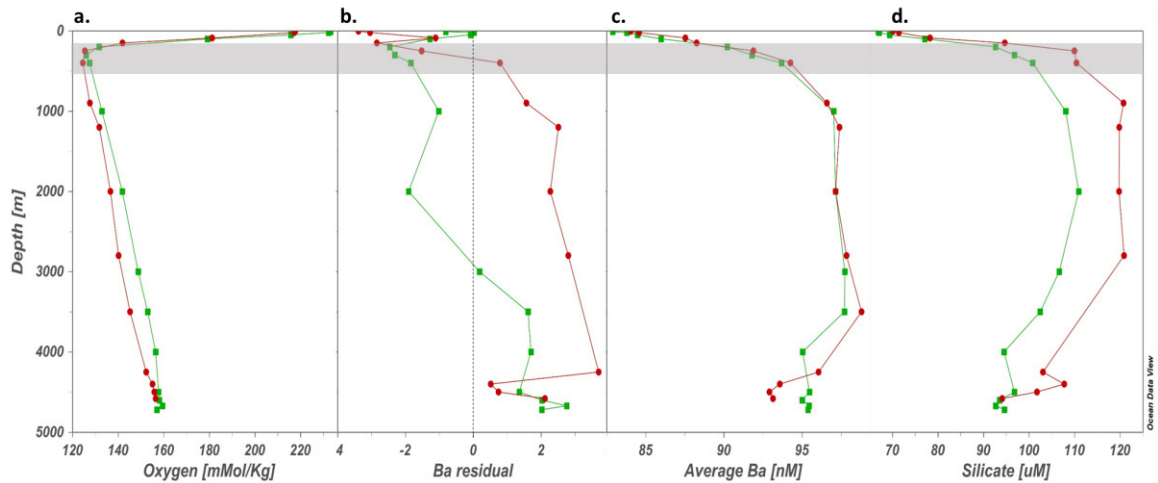


Figure 3-18: Depth profiles of Weddell Sea stations (Station 44 red circles; Station 45 green squares) a. Dissolved oxygen concentrations ($\mu\text{mol/kg}$); b. $\text{Ba}_d^{\text{Si residual}}$ values; c. Dissolved barium concentrations (nM); d. Silicic acid (μM). Shaded area represents the oxygen minimum zone.

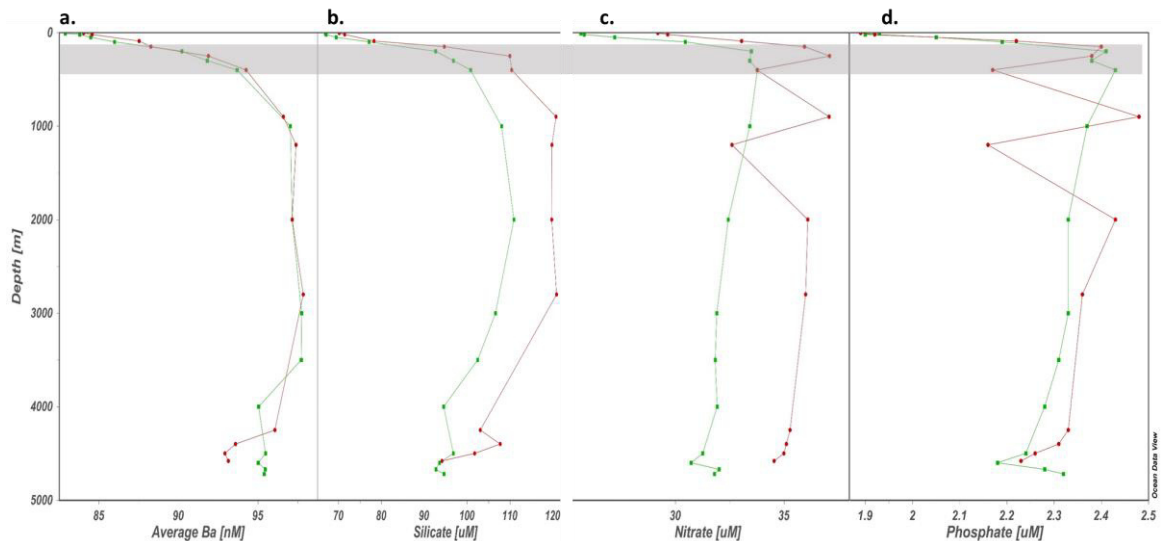


Figure 3-19: (above) Depth profiles of Weddell Sea stations (Station 44 red circles; Station 45 green squares) a. Dissolved barium (nM); b. Silicic acid (μM); c. Nitrate + Nitrite (μM); d. Phosphate (μM). Shaded area represents the oxygen minimum zone.

4. Discussion

Firstly, I will consider the global relationships observed between Ba_d and the macronutrients NO_x , PO_4 , and silicic acid, and how these general distributions compare to the distributions in the Scotia Sea. Whilst the clearest relationship throughout the water column is that between Ba_d and silicic acid, the weakening of this correlation in surface waters, and the co-variation between Ba_d and NO_x/PO_4 north of the Polar Front, implies that the surface cycling of barium varies depending on the dominant phytoplankton ecology. In intermediate and deeper

waters, the coupled and non-coupled behaviour of Ba_d and silicic acid offers insight into the barium and barite cycling, and the transition between characteristic water masses.

4.1. *Linking the distributions of Ba_d and macronutrients*

The first order distribution of barium in the ocean suggests it should be classified it as a 'biointermediate element', with partially depleted concentrations driven by biological processes in surface waters and a steady enrichment with depth, as opposed to 'biolimiting elements' which are reduced to zero at the surface, and are therefore considered limiting to biological activity (Broecker 1974). This biointermediate behaviour of Ba_d can be clearly seen in depth profiles of each ocean basin, for example in the progressive enrichment of Ba_d in the path of deep waters flowing within the global thermohaline circulation, with concentrations in the deep Pacific almost double those in the deep Atlantic (120 to 150 nM in the North Pacific, 65 to 85 nM in the North Atlantic; Figure 3-20). Although this Ba_d pattern is in general agreement with the global distributions of macronutrients, when examined in detail these relationships are more complex. Barium has no known biological function within marine phytoplankton biogeochemistry (Griffith & Paytan 2012), and there are no studies indicating the presence or absence of Ba_d as a limiting factor to biological activity. Yet whilst Ba_d rarely reaches full depletion in surface waters there have been events recorded of lowered surface concentrations associated with high productivity episodes (Nozaki et al. 2001; Esser & Volpe 2002; Hoppema et al. 2010; Stecher & Kogut 1999), and laboratory culture experiments have concluded that living phytoplankton (both diatoms and coccolithophorids) contain a relatively large pool of labile Ba (Ganeshram et al. 2003).

It has been suggested that the biointermediate behaviour of Ba_d is largely a result of its close interaction with the cycling of marine barite ($BaSO_4$), as barite precipitation in the water

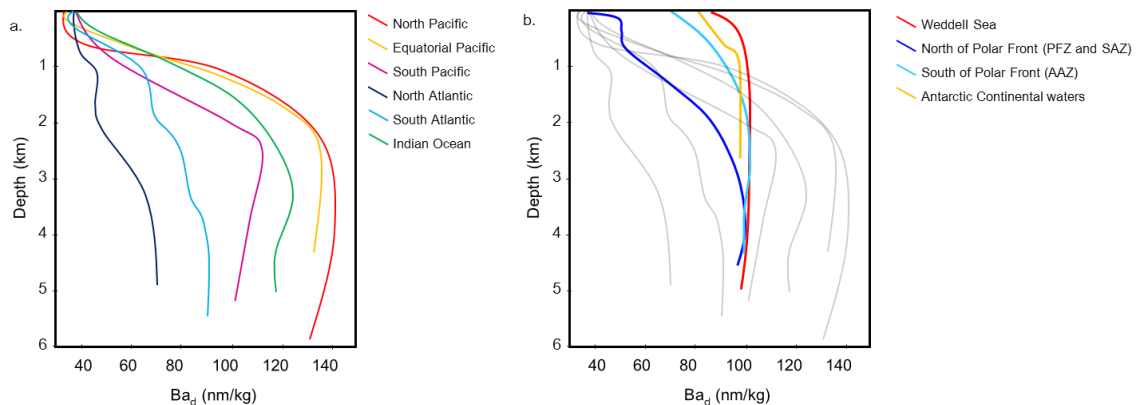


Figure 3-20: a. Schematic summary of the depth profiles of Ba_d concentrations (nM) recorded in different ocean basins by GEOSECS Expeditions (full station profiles in Appendix 7): North Pacific (red line), Equatorial Pacific (yellow line), South Pacific (pink line), North Atlantic (dark blue line), South Atlantic (light blue line), Indian Ocean (green line). b. Schematic summary of Ba_d concentrations (nM) recorded in this study, with GEOSECS summaries greyed out: Weddell Sea (red line), PFZ and SAZ (dark blue line), AAZ (light blue line), Antarctic Continental waters (yellow line).

column is thought to be biologically mediated (Dehairs et al. 1980; Bishop 1988; Collier & Edmond 1984). However, whilst the organic aggregate model of barite precipitation in supersaturated microenvironments associated with decaying organic matter accounts for the distributions of barite microcrystals in mesopelagic waters (Dehairs et al. 1990; Sternberg et al. 2008) and its correlation with organic carbon in underlying sediments (Dymond & Collier 1996), there are still questions to be answered about the initial associations of barium with organic matter in surface waters, and the dominance of the global relationship between Ba_d and silicic acid in comparison to with other macronutrients.

4.1.i Non-linear global relationship between Ba_d and NO_x or PO_4

Throughout the global ocean the relationship between Ba_d and the macronutrients NO_x and PO_4 is similar to that described for AAZ waters above (Section 3.3), with a non-linear positive trend defined by three broad populations: NO_x and PO_4 show consistent drawdown in surface waters, whilst the behaviour of Ba_d in surface waters varies between regions; NO_x and PO_4 quickly reach subsurface maxima which they usually sustain through intermediate depth waters, whilst Ba_d is again highly variable; NO_x and PO_4 concentrations decrease down through deeper waters whilst Ba_d remains constant or continues to increase (Figure 3-9). With the exception of HNLC regions, NO_x and PO_4 are limiting factors for primary productivity, with concentrations depleted to zero in surface waters. Even in HNLC regions such as the large parts of the Southern Ocean, both NO_x and PO_4 still experience surface drawdown, but without reaching fully depleted

levels, with phytoplankton growth instead limited by silicic acid, micronutrients, or the availability of light for photosynthesis. As discussed above, Ba_d never reaches surface concentrations lower than 30 to 40 nM, and in some ocean basins (the North Atlantic and the North Pacific) does not experience any apparent surface drawdown. This Ba_d behaviour is consistent with the concept that although its biogeochemical cycling may be linked to variability in the extent of biological uptake and recycling, there is no regular intracellular uptake of barium into marine organic matter (Ganeshram et al. 2003; Griffith & Paytan 2012). This is again evident in the depth profiles of NO_x and PO_4 , which show relatively shallow remineralisation as particulate organic matter is microbially broken down in the oxygen minimum zone and NO_x and PO_4 are remineralised. Ba_d concentrations, although increasing with depth, do so at a slower rate over a much larger depth range, implying regeneration coupled with the slower dissolution of skeletal material.

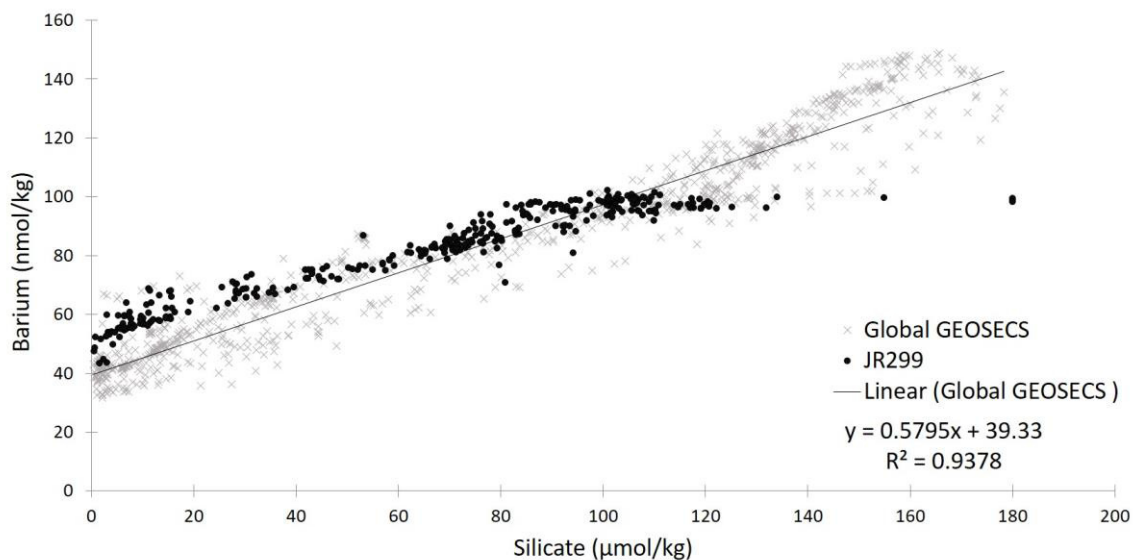


Figure 3-21: Data from the GEOSECS global database of dissolved barium concentrations vs. silicic acid concentrations in seawater (grey crosses). Filled black circles show the entire JR299 Scotia and Weddell Sea datasets from this study.

4.1.ii Linear global relationship between Ba_d and silicic acid

A strong positive correlation between Ba_d and silicic acid is observed throughout the global ocean (Figure 3-21), as is a similar trend between Ba_d and alkalinity that has resulted in the use of Ba/Ca as a palaeoproxy for patterns of past ocean circulation (Lea & Boyle 1989; 1990). Silicic acid and Ba_d appear to follow similar patterns of surface depletion and intermediate water regeneration in every ocean basin (Appendix 7). In the absence of an obvious mechanistic link between the oceanic cycles of the two elements, it has been suggested

that the similarities in distribution are the result of co-location of carrier phases (biogenic silica and barite) and large scale ocean circulation (Lea & Boyle 1993; Jeandel et al. 1996; Jacquet et al. 2005; Horner et al. 2015).

However, the positive linear relationship observed between Ba_d and silicic acid throughout the global ocean is highly significant and overall exhibits very little scatter ($Ba = 0.58 \cdot Si(OH)_4 + 39.33$; $n = 322$; $R^2 = 0.94$; $p < 0.01$). For such a tightly coupled relationship to arise, but without any apparent mechanistic link between the elements seems highly unlikely, and has therefore been the subject of much investigation. Indeed, some studies have shown evidence for a more direct link between the marine barite and silica cycles, finding that high levels of subsurface particulate barium are commonly found in regions where diatoms are a dominant component of the phytoplankton (Stroobants et al. 1991; Dehairs et al. 1991). Investigations in the Southern Ocean have suggested that, although barite does form in non-diatom-dominated regions, its precipitation is favoured where these siliceous organisms make up a significant fraction of the material exported from the surface layer (Bishop 1988).

There are several possible explanations for this observed connection between diatom-rich regions and increased fluxes of particulate barium:

- (i) The remains of diatom frustules may provide a more suitable microenvironment for barite precipitation than the remains of other phytoplankton;
- (ii) The increased ballasting effect of diatom frustules could increase settling rates and reduce recycling in surface waters;
- (iii) The surfaces of diatom tests may offer better adsorption of cations such as Ba^{2+} , thus catalysing barite formation (Stroobants et al. 1991; Dehairs et al. 1990; 1991; Bishop 1988).

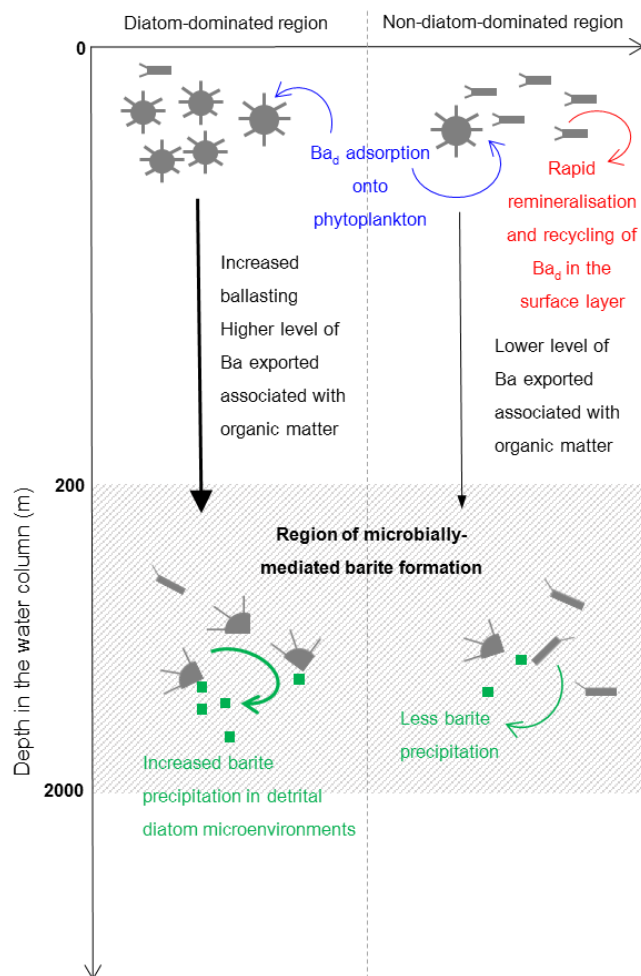
This latter suggestion has been supported by experiments using laboratory cultures of the marine diatom *Thalassiosira weissflogii*, which found that large amounts of Ba can be adsorbed onto the iron oxyhydroxides (FeOx) coatings of the tests (Sternberg et al. 2005).

If the adsorption of Ba onto iron oxyhydroxides observed in *T. weissflogii* were common to other diatom species, then such a process could provide the carrier phase necessary to export Ba_d from surface waters, as well as explaining the increased incidence of particulate barite formation in diatom-dominated waters and the strong relationship observed globally between Ba_d and silicic acid. However, there are difficulties presented by such a model, for example, higher Ba/Fe ratios have been measured in naturally occurring suspended particulates relative to those found in laboratory culture studies (Sternberg et al. 2005), and these culture studies contained high levels of iron, which may not be representative of open ocean conditions. This suggests that there is an excess of Ba relative to Fe in naturally occurring particles that cannot be

accounted for by the FeOx adsorption mechanism (more Ba present than could be adsorbed onto the FeOx present), although this may not be the case in regions of high iron fertilisation.

The FeOx adsorption mechanism discussed above may also apply to non-siliceous organisms, as it is clear from the presence of barite in non-diatom-dominated marine environments that there are ubiquitous processes throughout the global ocean that allow barite to form without the presence of diatoms. The role of non-siliceous organic matter in the cycling of Ba_d from the surface has been confirmed by laboratory production of barite from axenic coccolithophorid cultures, without the presence of opal or fecal pellet packaging (Ganeshram et al. 2003). However, a combination of the possible explanations presented above may explain why the presence of diatoms tends to be associated with enhanced barite precipitation: Ba may associate equally with all phytoplankton (through an FeOx adsorption method or otherwise), but Ba associated with diatom frustules may be more likely to be exported to the typical depths of barite formation (200 to 2000 m), and the detrital diatom material may then form microenvironments that are particularly suited to barite precipitation (Figure 3-22).

Although the data presented here do not directly provide information on particulate barium stocks, the relative distributions of Ba_d and silicic acid with depth can provide insight into the level of interaction between silicate and barite cycling. Of particular use is the measurement of how and where this $Ba_d/Si(OH)_4$ relationship decouples, which is discussed in further detail below in Section 4.2.ii. Also of interest are the variations in the $Ba_d/Si(OH)_4$ relationship between



different ocean basins (Figure 2-23), which suggest that although some regions vary very little from the overall relationship (the South Atlantic, South Pacific, and Indian Oceans), others have

Figure 3-22: Illustration of the proposed variation in interaction between Ba_d , phytoplankton, and barite formation in regions with diatom-dominated and non-diatom-dominated phytoplankton ecology. In both regions, Ba_d is associated with phytoplankton cells in surface waters through some adsorption mechanism. In diatom-dominated regions, a significant fraction of the adsorbed Ba_d is exported from the surface layer within the denser diatom frustules, whilst in non-diatom-dominated waters, much of the adsorbed Ba_d is released back into the water column as the light phytoplankton tests are recycled in the surface layer. In the depth intervals most associated with barite formation (200 to 2000 m), the diatom detritus catalyses barite formation, providing microenvironments well-suited to the organic aggregate model of barite precipitation.

a distinctive regional signal, with the Equatorial Pacific and the North Atlantic exhibiting steeper slopes and lower intercepts, whilst the North Pacific sites display a non-linear relationship similar to that usually seen between Ba_d and NO_x or PO_4 . The Southern Ocean, on the other hand, has been shown by numerous studies (Jeandel et al. 1996; Jacquet et al. 2007; Hoppema et al. 2010; data presented here for the Scotia Sea) to show lower slopes and higher intercepts than those of other regions (Table 3-3).

Location	Slope co-efficient	Intercept at zero $Si(OH)_4$	R^2	P	Reference
<i>North Indian Ocean</i>	0.56	38.2	-	-	Jeandal et al. 1996
<i>South Indian Ocean</i>	0.25	64.5	-	-	Jeandal et al. 1996
<i>Indian Ocean</i>	0.63	34.25	0.98	<0.001	GEOSECS (MELVILLE) 1978
<i>North Pacific</i>	0.66	26.01	0.93	<0.001	GEOSECS (MELVILLE) 1973
<i>Equatorial Pacific</i>	0.74	23.67	0.99	<0.001	GEOSECS (MELVILLE) 1973/4
<i>South Pacific</i>	0.56	42.15	0.96	<0.001	GEOSECS (MELVILLE) 1974
<i>North Atlantic</i>	0.75	38.63	0.95	<0.001	GEOSECS (KNORR) 1972
<i>South Atlantic</i>	0.55	43.83	0.86	<0.001	GEOSECS (KNORR) 1972/3
<i>145°E PFZ-AZ</i>	0.23±0.01	64.1±0.7	0.72	<0.001	Jacquet et al. 2007
<i>145°E SAF-PFZ</i>	0.31±0.01	58.7±0.8	0.91	<0.001	Jacquet et al. 2007
<i>Prime Meridian</i>	0.2645	59.368	0.909	-	Hoppema et al. 2010
<i>Weddell Sea</i>	0.2322	66.227	0.806	-	Hoppema et al. 2010
<i>WAP all</i>	0.21	69.2	0.716	<0.001	PaALTER (2011-12) <i>this study</i>
<i>WAP surface</i>	0.14	72.8	0.266	<0.001	PaALTER (2011-12) <i>this study</i>
<i>JR299 all</i>	0.40	55.1	0.92	<0.001	JR299 (2014) <i>this study</i>
<i>Drake Passage S.PF</i>	0.32	61.1	0.90	<0.001	JR299 (2014) <i>this study</i>
<i>Drake Passage N.PF</i>	0.49	55.6	0.98	<0.001	JR299 (2014) <i>this study</i>
<i>Weddell Sea</i>	0.18	75.0	0.63	<0.001	JR299 (2014) <i>this study</i>

Table 3-3: Summary of studies investigating Ba_d vs. $Si(OH)_4$ in the Southern Ocean

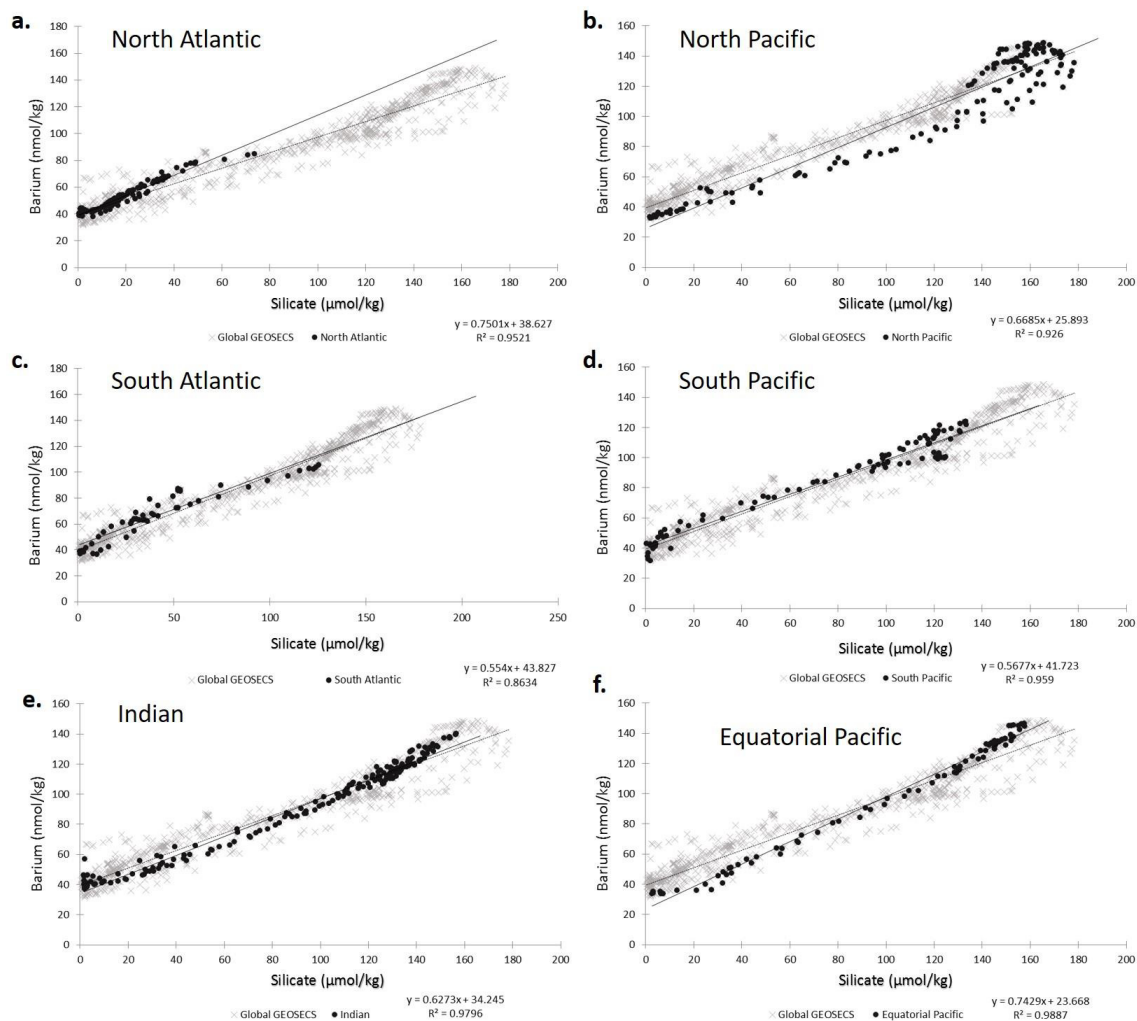


Figure 3-23: Scatter plots of the GEOSECS global database of dissolved barium concentrations vs. silicic acid concentrations in seawater (grey crosses), with datasets specific to each basin highlighted by filled black circles; a. Stations in the North Atlantic; b. Stations in the North Pacific; c. Stations in the South Atlantic; d. Stations in the South Pacific; e. Indian Ocean; f. Equatorial Pacific.

4.2. De-coupling Ba_d and silicic acid in the Scotia Sea

Whilst negative $Ba_d^{Si\text{ residual}}$ values indicate an depletion of Ba_d relative to silicic acid at a particular depth, it is impossible to distinguish solely from these values whether that relative depletion is a result of Ba_d removal or dilution (through barite precipitation or mixing with lower Ba_d waters), or the result of enhanced concentrations of silicic acid (via increased dissolution of biogenic opal, or mixing with higher $Si(OH)_4$ waters). Recent measurements of barium isotopes in the tropical North Atlantic and South Atlantic (Bates et al., in prep; Horner et al. 2015) have established the utility of combining Ba_d and silicic acid concentrations with barium isotope measurements ($\delta^{137/134}Ba$), as the preferential incorporation of light isotopes during barite formation makes the isotopic signature of the remaining water mass sensitive to barite cycling, but unaffected by silicate cycling (Sternberg et al. 2005; Horner et al. 2015; von Allmen et al. 2010; Cao et al. 2016). In the absence of ($\delta^{137/134}Ba$) measurements, useful insights can still be made about barium cycling in this region by investigating the decoupling of Ba_d from silicic acid, and the comparison of these trends to global patterns.

4.2.i Near-surface behaviour and the biogeochemical divide

There is a clear shift in the behaviour of Ba_d in the upper 100 m of the water column as the Drake Passage and North Scotia Ridge transects cross the Polar Front. This is observed not only in the near-surface profiles of Ba_d , but in the changing sign of surface $Ba_d^{Si\text{ residual}}$ values, indicating a change in the relationship between Ba_d and silicic acid across this frontal divide (Figure 3-4 b).

North of the Polar Front there is noticeable drawdown of Ba_d in surface waters, most pronounced at stations 33 and 35 (Figure 3-15, grey and brown triangles respectively) where fluorescence indicates a high level of productivity (Figure 3-24 a). These lowered surface concentrations then follow the pattern of NO_x and PO_4 concentrations, increasing rapidly over the upper 100 m of the water column. This suggests an association at these stations between Ba_d and the rapidly remineralised particulate organic carbon tracked by NO_x and PO_4 . In contrast, in the AAZ waters south of the Polar Front, the enrichment of Ba_d from surface minimum concentrations down through the water column is at a much slower rate than any of the macronutrients, and shows no distinct behaviour in the top 100 m. Where fluorescence data suggest a level of high primary productivity at Station 13, similar to that seen at Stations 33 and 35 (fluorescence of approx. 0.4; Figure 3-24 a), there is no surface drawdown of Ba_d comparable to that seen at the stations to the north (Station 13 represented by purple diamonds in Figure 3-12).

Surveys of the Southern Ocean have established the presence of a clear biogeochemical

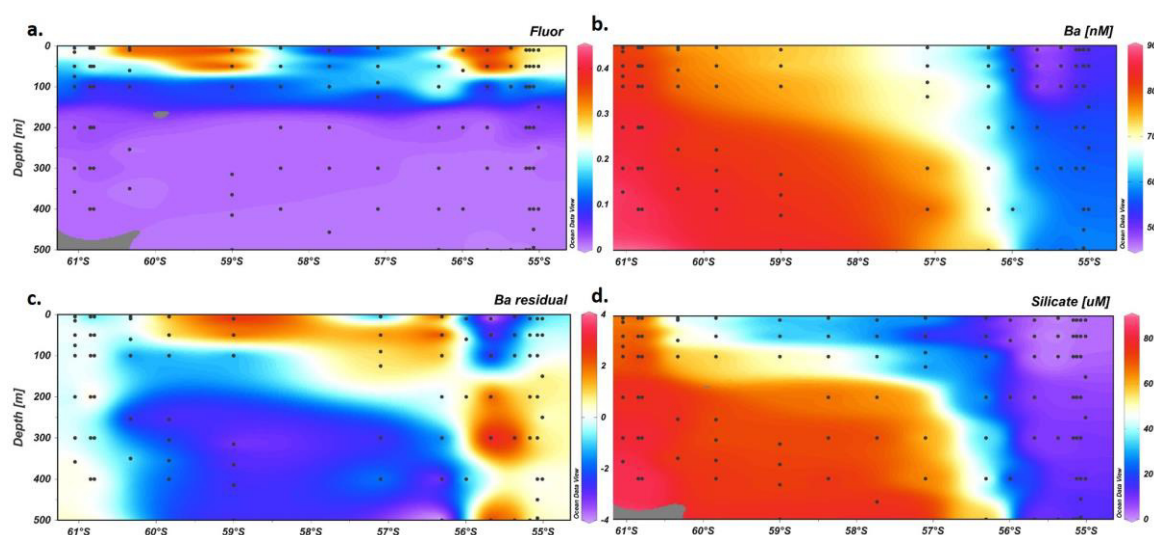


Figure 3-24: Transects of the Drake Passage showing the top 500 m of the water column, with colour bars representing the distribution of the indicated parameters in each panel; **a.** Fluorescence; **b.** Dissolved barium concentrations (nM); **c.** $Ba_d^{Si\text{ residual}}$ values; **d.** Silicic acid concentrations (μM).

divide between AAZ waters and the more northerly waters of the PFZ and SAZ (Boyd 2002; Pollard et al. 2002; Marinov et al. 2006). There is a distinct change in phytoplankton assemblage across the Polar Front, with diatoms dominating to south and nanoflagellates to the north (Mengelt et al. 2001), which coincides with the observed changes in Ba_d . In the nanoflagellate-dominated waters north of the divide there appears to be an association between Ba_d and the organic matter of the organisms that is not observed elsewhere in the Scotia Sea, or indeed in any other stations throughout the global ocean. It is difficult to assess what the nature of this

organic matter association might be, as barium is not known to be taken up intracellularly (Griffith & Paytan 2012). This behaviour parallels NO_x and PO₄ only in the top 100 m, below which the Ba_d distribution resumes its usual more silica-like profile, indicating that the more generally observed association between Ba_d and skeletal material still occurs in this region alongside this unusual surface activity. Although barite precipitation is usually thought to be restricted to mesopelagic depths (Dehairs et al. 1980; Dehairs et al. 1990; Dehairs et al. 1992; Cardinal et al. 2005), it is possible that the increased iron fluxes thought to be responsible for higher levels of primary production in the PFZ (de Baar et al. 1995) could stimulate near-surface inorganic barite precipitation associated with iron oxide particulates (Schroeder et al. 1997; Sternberg et al. 2005). In the relatively warm, barite-understaturated waters north of the Polar Front, these barite microcrystals would be susceptible to rapid re-dissolution, returning the subtracted Ba_d to its usual subsurface pool.

During the spring and summer months diatom blooms are prevalent in the silicic acid and iron limited AAZ waters, consuming silicic acid and causing the silicate front to migrate southwards (Franck et al. 2000; Landry et al. 2002). As these samples were collected during austral autumn, the background levels of productivity in these diatom-dominated waters were relatively low, with silicic acid not reaching depletion in surface waters until reaching the silicic acid front, displaced slightly to the south of the Polar Front (Figure 3-24 d). Nevertheless there is some silicic acid drawdown at the surface, which is not mimicked by similar Ba_d behaviour. The persistence of a slight positive Ba_d^{Si residual} signal in the very surface layer of the AAZ waters (Figure 3-4 b) highlights this decoupling of Ba_d and silicic acid over the depth range of maximum primary production, whilst the sharp transition to negative values at the Polar Front indicates that when non-siliceous organisms dominate the phytoplankton community the Ba_d/Si(OH)₄ relationship in the near-surface can break down even further.

4.2.ii Barium signals in intermediate waters (200 to 2000 m): large scale circulation and the overprinting of barite cycling

Although intermediate waters tend to fall into line with the global linear correlation between Ba_d and Si(OH)₄, there are interesting details observed in the deviation with depth at individual stations. As discussed above, there is a seasonally-variable transition in phytoplankton communities between the diatom-dominated colder AAZ waters and the nanoflagellate-dominated warmer waters of the PFZ and the SAZ (Hinz et al. 2012; Mengelt et al. 2001). However, the Ba_d signals in intermediate waters (between 100 to 200 m and 2000 m) reflect not only the recycling of any biologically related phases of barium sinking down from the surface, but also any mixing between laterally transported water masses. It is also likely that the majority

of biologically-mediated barite precipitation will occur within this depth range. The changing $Ba_d^{Si\ residual}$ values recorded across known water mass transitions is a key tool for de-convolving these different signals.

The multivariate linear regression analysis of the whole dataset suggested that the Ba_d distribution was most significantly linked to the distributions of salinity, temperature, and silicic acid. The predictive power of these parameters can be attributed to the distinct variation in Ba_d distributions between different water masses – not only the horizontal gradient of Ba_d across the frontal zones of the Scotia Sea, but the variation with depth as the cores of vertically layered water masses are sampled.

North of the Polar Front, surface waters transition down into AAIW, with initially invariant silicic acid and Ba_d concentrations that mixes at its base with the higher concentrations of UCDW. South of the Polar Front the oxygen-poor UCDW lies directly below the surface waters, deepening from south to north (Figure 3-4 c), and recording a steady increase in silicic acid and Ba_d concentrations with depth. As well as the in-situ remineralisation of diatom frustules, UCDW carries the signature of deep Pacific waters, with a notable excess of Ba_d relative to silicic acid that is reflected in the shift to positive $Ba_d^{Si\ residual}$ values throughout this water mass (Figure 3-4 b).

However, there appear to be two different types of $Ba_d/Si(OH)_4$ decoupling occurring within the UCDW. This is most distinct south of the Polar Front, where there is a large negative $Ba_d^{Si\ residual}$ signal recorded between 100 and 1000 m (Figure 3-11), denoting a relative depletion in Ba_d as surface waters transition to UCDW. As the surface waters here also have a relative Ba_d excess due to silicic acid uptake by diatoms, this cannot be a feature of the two water masses mixing, but must mark a distinct process. The co-location of this Ba_d event horizon with the oxygen minimum zone, and the subsurface maxima of NO_x and PO_4 (Figure 3-12 c and d) is highly suggestive of this Ba_d depletion relative to silicic acid resulting from microbially-mediated barite precipitation. As discussed above, the current balance of evidence favours the organic aggregate model of marine barite precipitation, with microcrystals forming in oversaturated microenvironments created by bacterial breakdown of organic matter (Dehairs et al. 1997; Jacquet et al. 2007; Jacquet et al. 2011; Gonzalez-Munoz et al. 2003; Gonzalez-Muñoz et al. 2012). This precipitation would transfer barium from the dissolved to the particulate pool, and although the concentrations concerned are likely to be too small to show up as an obvious negative spike in Ba_d (Jacquet et al. 2007), the fact that this process does not involve any change in the silicic acid pool could potentially cause the decoupling suggested by the negative swing in $Ba_d^{Si\ residual}$ values.

Whilst this feature is clear in the AAZ waters, north of the Polar Front the pattern of Ba_d^{Si} residual values is more complex (Figure 3-15). The negative signatures in surface waters (particularly at the highly productive stations 33 and 35) are underlain here by the broadly uniform AAIW, within which Ba_d and silicic acid appear to recouple once the surface drawdown of Ba_d has been returned to the dissolved pool. In the central stations there is then a hint of the profiles being pulled towards negative values at the deeper oxygen minimum zone, but generally the intermediate waters are dominated by the positive UCDW signal.

This could be an indication of much lower levels of barite forming at mesopelagic depths in waters north of the Polar Front relative to south of the Polar Front, which could be directly linked to the shift in overlying phytoplankton assemblages discussed above (see Figure 3-22). Previous studies of barite formation in the Scotia Sea area have suggested that high concentrations of subsurface barite particles are restricted to regions of high diatom abundance, with lower particulate fluxes when productivity is dominated by cyanobacteria or flagellates (Stroobants et al. 1991; Jacquet et al. 2011). The most likely explanation for this is that the larger, slowly dissolving diatom frustules provide a more favourable microenvironment for barite precipitation within sinking bio-aggregates (Bishop 1988; Stroobants et al. 1991). The slight breakdown observed in the $Ba_d/Si(OH)_4$ relationship in surface waters where diatoms are abundant rules out the possibility that diatoms are more efficient than other phytoplankton at removing Ba_d from surface waters. However, it is possible that the association of Ba_d with diatom frustules, possibly in the form of Ba_d adsorption onto iron oxyhydroxides at the cell surfaces (Sternberg et al. 2005), may make the Ba_d more available for barite formation at depth than when it is associated with other biogenic particles. In contrast, the surface water drawdown of Ba_d north of the Polar Front does not seem to translate to a higher formation of barite at depth, with much of the Ba_d instead being initially recycled higher in the water column. It therefore appears that the specific association of Ba_d with siliceous organisms, coupled with the ballasting power of the large diatom frustules, enables the transport of Ba_d to depths and microenvironments that are more favourable for barite formation than those provided by other sinking phytoplankton.

These insights into the effects of surface phytoplankton community structure on the formation of barite in the subsurface could be investigated more thoroughly by measuring barium isotopes in these samples. These isotopic measurements could verify whether or not the $Ba_d/Si(OH)_4$ decoupling events observed in intermediate waters are the result of changes in barite precipitation (for further discussion of this future work see Chapter 7). If levels of biogenic barite precipitation are controlled more by community structure than by net primary

productivity, as indicated here, then this could have important consequences on the use of sedimentary barite as an indicator of palaeo-productivity.

4.2.iii Invariance of Ba_d in deep waters (below 2000m) of the Scotia Sea

In deeper waters (below 2000 to 4000 m) Ba_d concentrations show little variation in any of the regions investigated, maintaining a subsurface maxima down to the base of the water column. Deeper stations in the Drake Passage record a slight decrease in Ba_d values at the base of the water column, with a simultaneous increase in silicic acid concentrations and subsequent negative tick in $Ba_d^{Si\text{ residual}}$ values that marks the presence of Southeast Pacific Deep Water (SPDW) (Figure 3-15). The distinctive silicate maximum associated with this colder, slightly fresher sub-set of LCDW is thought to originate from mixing with Ross Sea deep waters (Sievers & Nowlin 1984; Peterson & Whitworth 1989; Naveira Garabato et al. 2002), and it appears that these waters may also inherit low relative Ba_d concentrations, possibly due to a decoupling of Ba_d and silicic acid cycling in the Ross Sea caused by the rapid dissolution of biogenic silica in surface waters (DeMasters et al. 1992). Both north and south of the Polar Front, the preservation of a consistent Ba maxima indicates that at these depths the exchange between the particulate and dissolved barium pools is at a steady state. This is in contrast to silicic acid concentrations, which generally continue to increase until the base of the water column, and is most likely the result of differing saturation states with regard to biogenic barite and biogenic silicate in this region.

5. Conclusions

There is a positive linear correlation between Ba_d and silicic acid throughout the global ocean water column, a link which is not seen between Ba_d and other macronutrients. An exception to this general rule is observed in the surface waters of the Scotia Sea north of Polar Front, where Ba_d appears more similar to that of NO_x and PO_4 in the top 100 m, suggesting an unusual association between Ba_d and primary production in surface waters in this region. This could be explained by near-surface barite formation, possibly associated with iron oxyhydroxides, which is rapidly re-dissolved as it sinks out of the surface layer.

It has been suggested that the globally observed coupling of silicic acid and Ba_d may be the sole result of co-location in the formation and recycling of separate carrier phases, coupled with the effects of large scale ocean circulation. In support of this, the data presented here suggest that the Ba_d distribution in the Scotia Sea is largely controlled by transition between distinctive water masses, each with slightly differing relationships between Ba_d and silicic acid. However, the signature of barite formation at mesopelagic depths can also be distinguished in

$Ba_d/Si(OH)_4$ decoupling that overprints these larger scale circulation patterns. Variation in the degree of implied biogenic barite formation across the Polar Front supports the idea of a mechanistic link between silicate and barite cycles, as higher levels are observed south of the Polar Front, where the phytoplankton community shifts to one dominated by diatoms. This could be significant consideration when applying the Ba_{excess} palaeo-productivity proxy, as increases in barite concentrations may be related to changes in phytoplankton community structure as well as absolute increases in productivity.

Chapter 4

The influence of coastal processes on dissolved barium cycling at the West Antarctic Peninsula – spatial analysis

1. Introduction

Ba_d is currently used in various forms as a palaeoproxy for components of organic and inorganic carbon storage, and as a quasi-conservative water mass tracer (Jacquet et al. 2007; Lea & Boyle 1989; Hall & Chan 2004; Guay & Falkner 1998). However, as discussed in Chapter 3, the nature of the oceanic barium cycle is not fully understood, particularly in cases where multiple processes may be interacting simultaneously with the dissolved and particulate barium pools. This is particularly the case in coastal polar regions such as the West Antarctic Peninsula, where biological drawdown and remineralisation occur in tandem with sea ice formation and melting, glacial meltwater input, and potential fluxes from shelf sediments.

In this chapter, I will investigate the controls on the distribution of dissolved barium in shelf-slope waters of the West Antarctic Peninsula (WAP), in order to distinguish between the different potential impacts of biological activity, sea ice formation and melting, glacial meltwater discharge, and ocean mixing. The WAP is an ideal natural laboratory in which to study such

relative controls on Ba_d distributions, as coastal and ocean processes occur in close proximity. I will use a high-precision dataset of dissolved barium (Ba_d) from a grid of stations adjacent to the WAP in conjunction with $Si(OH)_4$, the oxygen isotope composition of water, and salinity measurements, to determine the relative control of various coastal processes on the barium cycle throughout the water column.

2. Regional setting of the West Antarctic Peninsula

The Palmer Long Term Ecological (PalTER) Research Grid consists of a grid of stations overlying the western continental margin of the West Antarctic Peninsula (WAP), extending from the northern margin of the Bellinghousen Sea to the tip of the peninsula (Waters & Smith 1992). The grid covers an area of 900 km by 200 km, with grid lines 100 km apart running perpendicular to the coast, with stations spaced 20 km apart along the grid lines (see Figure 2-3). This grid of stations has been sampled annually since its creation in 1991 as part of the LTER network established by the American National Science Foundation (NSF), intended to gather coherent long term ecological datasets spanning many decades and large geographical areas.

In sampling the waters adjacent to the WAP, the PalTER grid provides coverage of an area undergoing the most extreme rapid regional warming anywhere on earth (Smith & Stammerjohn 2001; Vaughan et al. 2003; King et al. 2003). The southern boundary of the Antarctic Circumpolar Current (ACC) passes close to the continental slope of the WAP, with Upper Circumpolar Deep Water (UCDW) flowing onto the shelf through interconnected troughs and channels (Smith et al. 1999; Martinson & McKee 2012). During winter the surface mixed layer comprises Winter Water (WW; Temperature < -1.2 C; 33.85 < Salinity < 34.13), which is preserved through the summer as a remnant temperature minimum layer overlain by a warmer, fresher layer of Antarctic Surface Water (AASW) that develops from the inputs of glacial and sea ice melt (Martinson et al. 2008). The annual and seasonal variability of the sea ice regime and the input of glacial melt water are important factors to consider at the WAP, with 80% of WAP glaciers retreating (Cook et al. 2005), and both the annual sea ice duration and monthly sea ice concentration in the region decreasing (Stammerjohn et al. 2008). The surface waters of the PalTER grid are therefore well placed to investigate the combined influences of circumpolar waters and the changing freshwater regime on the distribution of Ba_d in the area.

3. Materials and Methods

Seawater samples were collected from stations covering the Palmer Long Term Ecological Research (PalTER) grid (Figure 4-1) during annual cruises of the ARSV *Lawrence M. Gould* in two consecutive austral summers: LMG11-01 (2nd January 2011 to 6th February 2011) and LMG12-01

(30th December 2011 to 7th February 2012). Water was sampled either from surface water using a trace metal-clean towfish or at depth using Niskin bottles deployed on a CTD (Conductivity-Temperature-Depth) rosette. Dissolved barium concentration data reported in this chapter are publicly available within the PAL-LTER data system (dataset #266): <http://oceaninformatics.ucsd.edu/datazoo/data/pallter/datasets>.

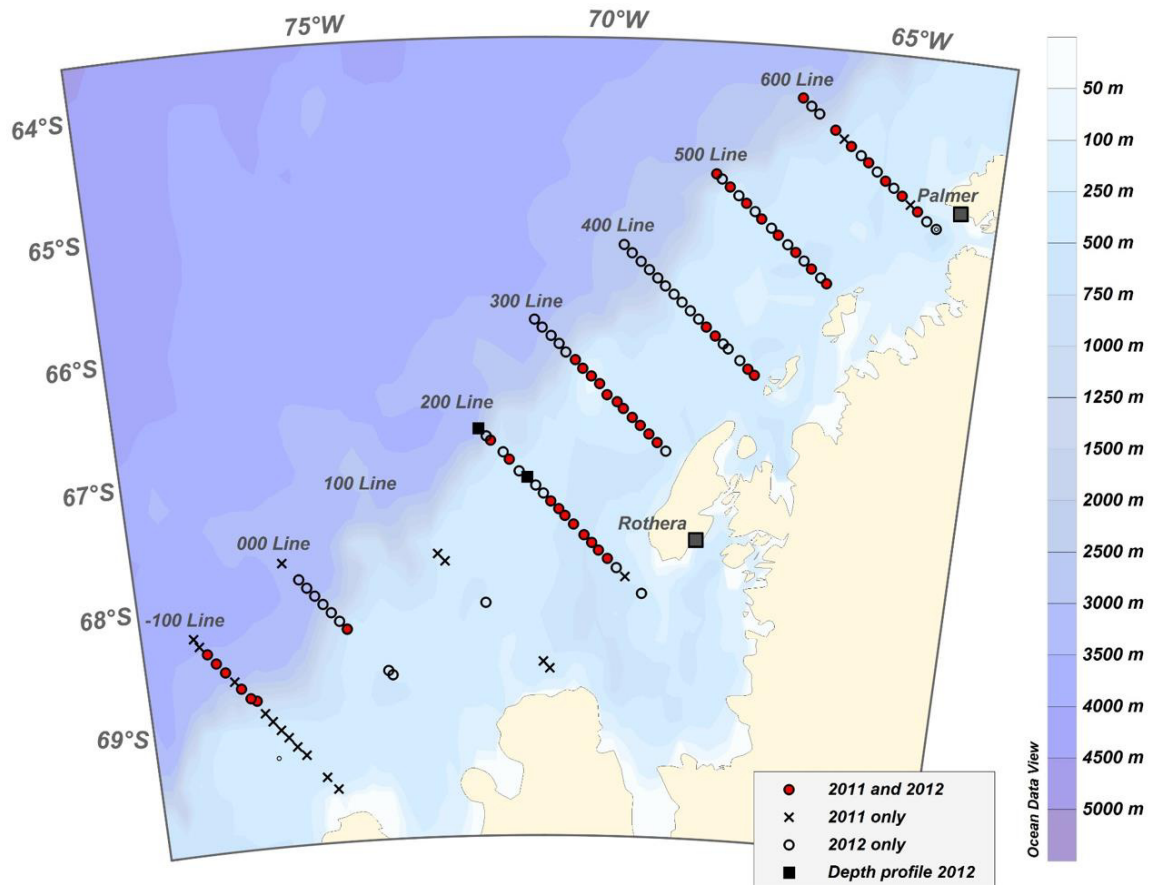


Figure 4-1: Map showing the Palmer Long Term Ecological Grid (PalLTER) covering waters adjacent to the West Antarctic Peninsula. Grid lines are labelled from -100 to 600, stations denoted by grid line plus approximate kilometres from the base tangent of the grid (e.g. 200.100 – station 100km along grid line 200). Black circles and crosses indicate surface sample sites from cruises LMG11-01 (02/01/2011 – 06/02/2011) and LMG12-01 (30/12/2011 – 07/02/2012); red filled circles represent stations occupied in both years, crosses and open circles stations occupied only in 2011 and 2012 respectively. Location of two depth profiles at 200.100 and 200.160 in 2012 shown by large black squares. Grey squares indicate the location of Palmer Station on Anvers Island and the Rothera Station on Adelaide Island.

3.1. Dissolved barium

The dissolved barium concentrations of 0.2 µm filtered (Acropak-200, Pall) seawater samples were analysed using isotope dilution inductively coupled plasma mass spectrometry (ID ICP-MS) as outlined in Chapter 2 Section 4. Sample preparation and measurements of this PalTER dataset were split between Rutgers University and Cardiff University, using a Thermo-Finnigan Element XR (Cardiff University) or Element-1 (Rutgers University) ICP-MS in low resolution mode.

A mass bias correction coefficient (K) was calculated each time samples were analysed by measuring the ratio of $^{138}\text{Ba}/^{135}\text{Ba}$ in a 1ppb Ba natural standard solution prepared in 5% (v/v) seawater (NASS-6 seawater standard of 5 ppb \pm 0.15 Ba), and comparing this to the average natural ratio reported in the literature (10.88) (Chapter 2 Section 4.3.iv). The isotope ratio determined in this solution varied between 10.5 and 11.1, with measured uncertainty across each sample run never exceeding 1.5% (2*RSD). This uncertainty was consistently less than the mass bias determined for each sample run, which was on average a 1.9% deviation from the literature value.

Blank solutions of 3 % (v/v of concentrated reagent) HNO_3 in 18.2 MΩ-cm water were analysed to correct for background barium signal from the introduction system of the ICP-MS (^{135}Ba blank counts < 0.1 % of seawater sample counts; ^{138}Ba blank counts < 1 % of seawater sample counts), and a set of consistency standards were measured at regular intervals (see Table 4-1). A correction for any seawater matrix effects was applied to the blank measurements by monitoring the sensitivity of a natural standard solution in 3 % HNO_3 vs. a natural standard solution in 5 % seawater, before the blanks were subtracted from sample counts.

Sample preparation and measurements were split between the Department of Marine and Coastal Science at Rutgers University, NJ, and the School of Earth and Ocean Sciences at Cardiff University. At Rutgers a Thermo-Finnigan Element-1 (SEM detector only) was used for ICP-MS analysis, whilst at Cardiff an Element XR was used (dual mode SEM with Faraday detector), with the same counting mode method used on both instruments. Seawater standards of comparable barium concentration to the samples show a long term external reproducibility of \pm 2 % or better across all analytical runs at both facilities (2*RSD), and the same solutions measured repeatedly at both institutions show agreement within 1 % despite slight differences in detection methods of the mass spectrometers (Table 4-1). Within each analytical run, reproducibility of these seawater standards was \pm 1.1 % or better. The full range of Ba_d concentrations in this study is 70 to 105 nM, with the majority of data points falling between 78

and 85 nM; high precision analyses were necessary for discerning relatively subtle Ba gradients across surface waters.

	Standard:	In-house Standard 1	In-house Standard 2	NASS-5	NASS-6
Rutgers	<i>2*RSD</i>	1.63%	2.07%	2.46%	2.84%
	<i>n</i>	27	27	27	26
	<i>Average [Ba](nM)</i>	74.1 ± 1.2	83.2 ± 1.7	37.1 ± 0.9	49.7 ± 1.4
Cardiff	<i>2*RSD</i>	1.29%	1.76%	1.53%	1.22%
	<i>n</i>	23	23	22	23
	<i>Average [Ba] (nM)</i>	73.7 ± 1.0	83.8 ± 1.5	37.0 ± 0.6	49.5 ± 0.6

Table 4-1: Reproducibility of standards in the Rutgers and Cardiff labs where samples were measured. Values given are 2*relative standard deviation (2*RSD). Errors from In-house Standard 1 and 2 (from the Southern Ocean and Amundsen Sea respectively) are considered applicable to PaLLTER samples, as the average dissolved barium concentrations are the most comparable.

3.2. Dissolved inorganic nutrients and primary productivity

Dissolved inorganic nutrients (silicic acid, phosphate, and nitrate plus nitrite) were analysed at the Marine Biological Laboratory (Woods Hole, MA) using a Lachat Quickchem 8000 nutrient analyser. The data are available at:

<http://oceaninformatics.ucsd.edu/datazoo/data/pallter/datasets?action=summary&id=27> *

(See Ducklow et al. 2013 and references therein).

Direct quantification of primary productivity was calculated at a small number of sites in ¹⁴C-labelled deck incubation experiments. Data and methodology overview are available at: <http://oceaninformatics.ucsd.edu/datazoo/data/pallter/datasets?action=summary&id=41#overview> † (Oscar Schofield).

3.3. Water mass fractions

Seawater samples were analysed for the ratio of stable oxygen isotopes at the Natural Environment Research Council Isotope Geosciences Laboratory (NIGL) at the British Geological Survey. Samples were equilibrated with CO₂ (Epstein & Mayeda 1953) using a VG Isoprep 18, with ¹⁸O/¹⁶O ratios then measured on a SIRA 10 mass spectrometer. Results were reported in standard δ¹⁸O notation, with reference to (Vienna Standard Mean Ocean Water [VSMOW]). Regular duplicate analyses are used to establish data precision, which is typically better than ± 0.02 ‰ (Meredith et al. 2013).

At sample sites with measured values of salinity and δ¹⁸O, a three-end-member mass balance is used to derive the fractions of sea ice melt, meteoric water, and Circumpolar Deep

* Accessed 22/10/2014

† Accessed 13/10/2014

Water (CDW). This mass balance calculation is based on the de-coupled behaviour of salinity and $\delta^{18}\text{O}$ in the different freshwater sources: sea ice melt, and freshwater of meteoric origin (glacial melt plus precipitation). Developed by Östlund and Hut (Östlund & Hut 1984) for the Arctic, this mass balance (Equation 4-1) is implemented at the West Antarctic Peninsula by Meredith et al. (2008, 2010, 2013).

$$\begin{aligned} f_{\text{SI}} + f_{\text{MW}} + f_{\text{CDW}} &= 1 \\ (S_{\text{SI}} * f_{\text{SI}}) + (S_{\text{MW}} * f_{\text{MW}}) + (S_{\text{CDW}} * f_{\text{CDW}}) &= S \\ (\delta_{\text{SI}} * f_{\text{SI}}) + (\delta_{\text{MW}} * f_{\text{MW}}) + (\delta_{\text{CDW}} * f_{\text{CDW}}) &= \delta \end{aligned}$$

Equation 4-1

where f_{SI} , f_{MW} , and f_{CDW} are the fractions of sea ice melt, meteoric water, and CDW, respectively, that we seek to determine; S_{SI} , S_{MW} , and S_{CDW} are the respective salinities of the end members; and δ_{SI} , δ_{MW} , and δ_{CDW} are their corresponding $\delta^{18}\text{O}$ values. The quantities S and δ are the measured values of salinity and $\delta^{18}\text{O}$ at the sample site. The salinity and $\delta^{18}\text{O}$ values assigned to each end member are: 34.73 and + 0.1 ‰ for CDW; 7 and + 2.1 ‰ for sea ice melt; and 0 and – 16 ‰ for meteoric water, respectively (Meredith et al. 2008; 2010; 2013). The resulting derived freshwater fractions are reported here as percentages: sea ice melt fraction (%SI), and meteoric water fraction (%MW), with typical errors of < 1 % on point values (Meredith et al. 2013). The majority of this 1 % error is due to uncertainty on the values attributed to end-members, and can therefore be considered to be systematic across the dataset.

The meteoric water fraction comprises freshwater input from glacial meltwater and from precipitation. Whilst it would be useful to consider each of these parameters separately, quantitative separation is not possible without an additional conservative freshwater tracer. However, the mean meteoric water budget at the WAP is thought to be dominated by glacial meltwater (Meredith et al. 2013). Whilst changes in direct precipitation could have an impact on the temporal variability of meteoric water, over the relevant periods prior to 2011 and 2012 differences in precipitation are small (Meredith et al. 2016), so the variation observed in meteoric water here can be broadly attributed to changes in glacial melt.

4. Results

4.1. Distribution of dissolved barium

The spatial distribution of dissolved barium (Ba_d) in surface samples across the PaLLTER grid shows similar patterns across the two years studied (Figure 4-2). In both 2011 and 2012 concentrations of dissolved barium are higher on the shelf, dropping to lower levels at the majority of stations over the continental slope (bathymetric division of PaLLTER stations between

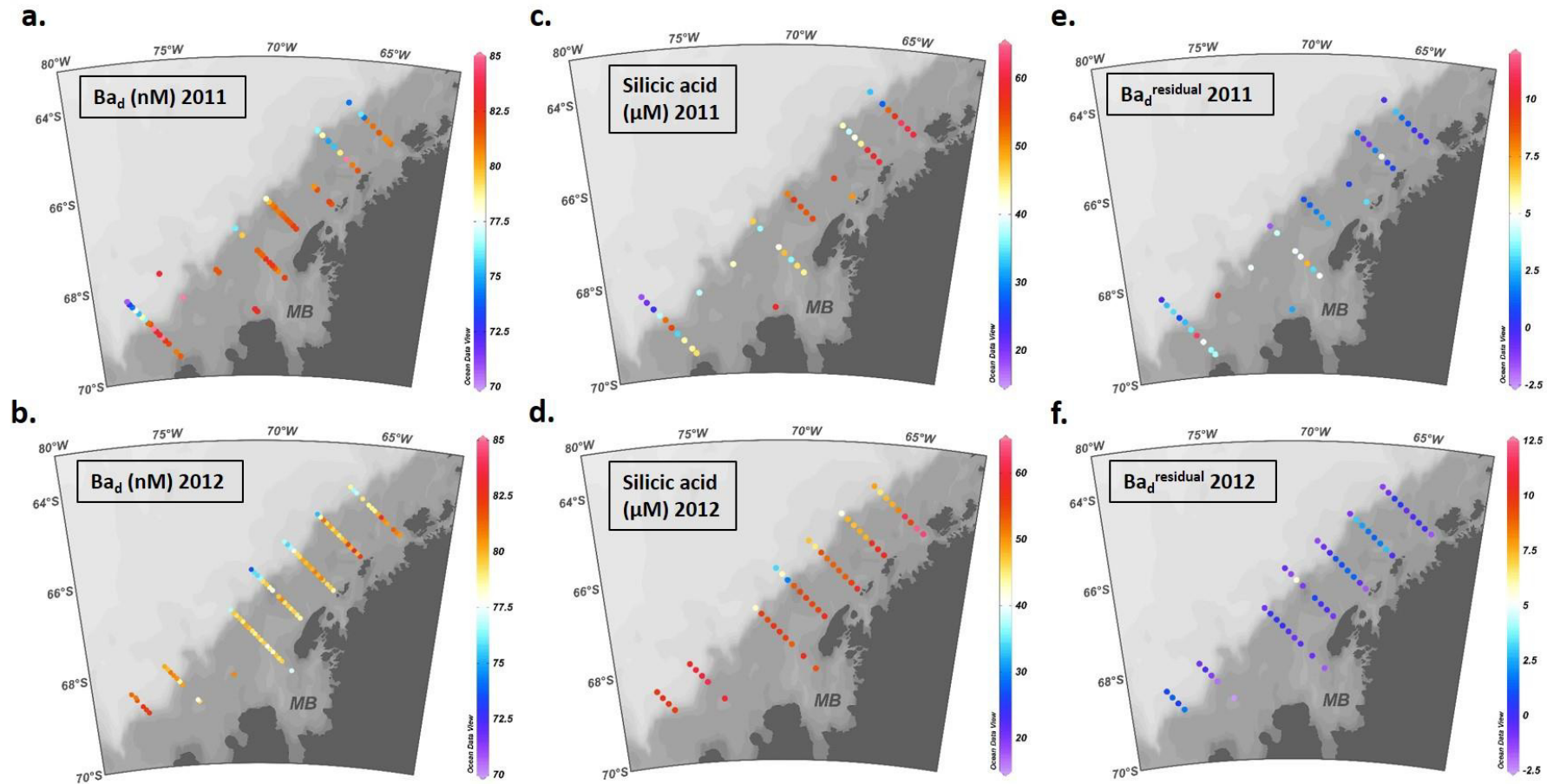


Figure 4-2: Surface distributions across the PalTER: a. Dissolved barium concentrations (Ba_d) (nM) in 2011; b. Dissolved barium concentrations (Ba_d) (nM) in 2012; c. Silicic acid concentrations (μM) in 2011, dotted line shows the division between the continental shelf and slope, after Martinson et al. 2008, MB - Marguerite Bay; d. Silicic acid concentrations (μM) in 2012; e. and f. Barium residual values ($Ba_d^{Residual} = Ba_d^{measured} - ((Si^{measured} * 0.21) + 69.2))$) for 2011 and 2012 respectively.

continental shelf and slope after Martinson et al. 2008 – shelf break delineated in Figure 4-2 c and d). The exceptions to this are stations over the slope in the southern lines of the grid (000 and -100 Lines), which show a continuation of the higher Ba_d concentrations observed on the shelf. This general pattern of distribution in the surface waters can also be observed in the silicic acid data (Figure 4-2).

Despite these general similarities, there are distinct differences between the findings of the two years. Compared with the 2012 measurements, surface values of dissolved barium in 2011 are slightly but consistently elevated across the shelf, with particular highs in the area south-west of Marguerite Bay, and a distinctive low from the outer shelf across the shelf break in the northern peninsula region.

Two depth profiles from 2012 show the vertical distribution expected of a bio-intermediate element, with depleted surface values and enrichment at depth (Figure 4-3). Concentrations of Ba_d are higher in the 500 m water column at the 200.100 site (on the shelf) than corresponding depths at the 200.160 site (over the continental slope), though the profile follows a similar shape. Two samples taken within 70 m of the bottom at 200.100 are distinctly

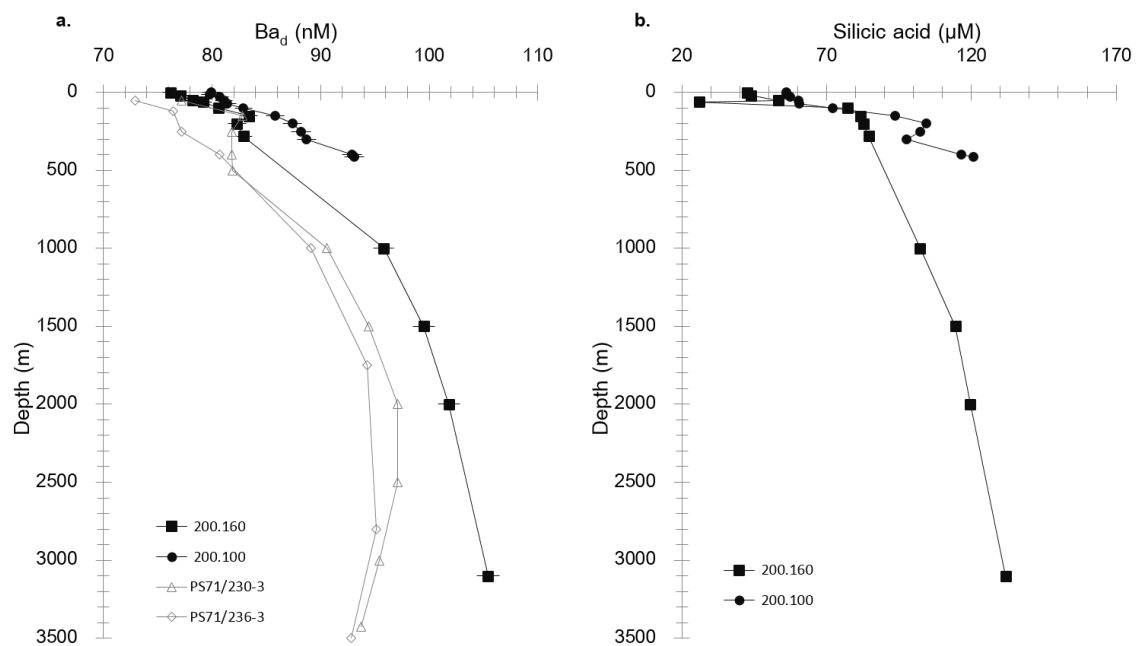


Figure 4-3: a. Depth profiles of dissolved Ba (nM) at PalLTER station 200.100 (filled circles) and station 200.160 (filled squares), horizontal error bars set at 1% to reflect the most conservative reproducibility of comparable seawater standards across these analytical runs. Depth profiles of dissolved barium from the Drake Passage from Roeske and Rutgers van der Loeff (2012), PS71/230-3 (open triangles) [lat -60.1077 °N long -55.2821 °E] and PS71/236-3 (open diamonds) [lat -58.9704 °N, long -58.1388 °E] – see Figure 4-4, error bars within symbol size. b. Depth profiles of silicic acid (μM) at PalLTER station 200.100 (filled circles) and station 200.160 (filled squares).

elevated relative to the rest of the profile. Below 1000m at the continental slope site, the water column is significantly enriched in Ba_d , exhibiting Ba_d concentrations approximately 5 nM higher than equivalent records of Ba_d concentrations measured in the Drake Passage in 2008 (Roeske and Rutgers van der Loeff 2012) (Figure 4-3 a).

The changing Ba_d concentration from the open waters of the Drake Passage to the shelf waters of the PaLLTER is examined by constructing an artificial section from the compilation of depth profiles from the Drake Passage (PS71/236 and PS71/230 from Polarstern cruise ANT-XXIV/3, Roeske and Rutgers van der Loeff, 2012 – see Figure 4-4) and LTER depth profiles (Sites 200.100 and 200.160), with the caveat that these profiles were collected in different years (2008 and 2012 respectively). Following the 34.7 isopycnal along this section, Ba_d increases from approximately 82 nM at one of the open water sites (PS71/230) to approximately 88 nM on the slope (PaLLTER station 200.160) and approximately 91 nM over the shelf (PaLLTER station 200.100).

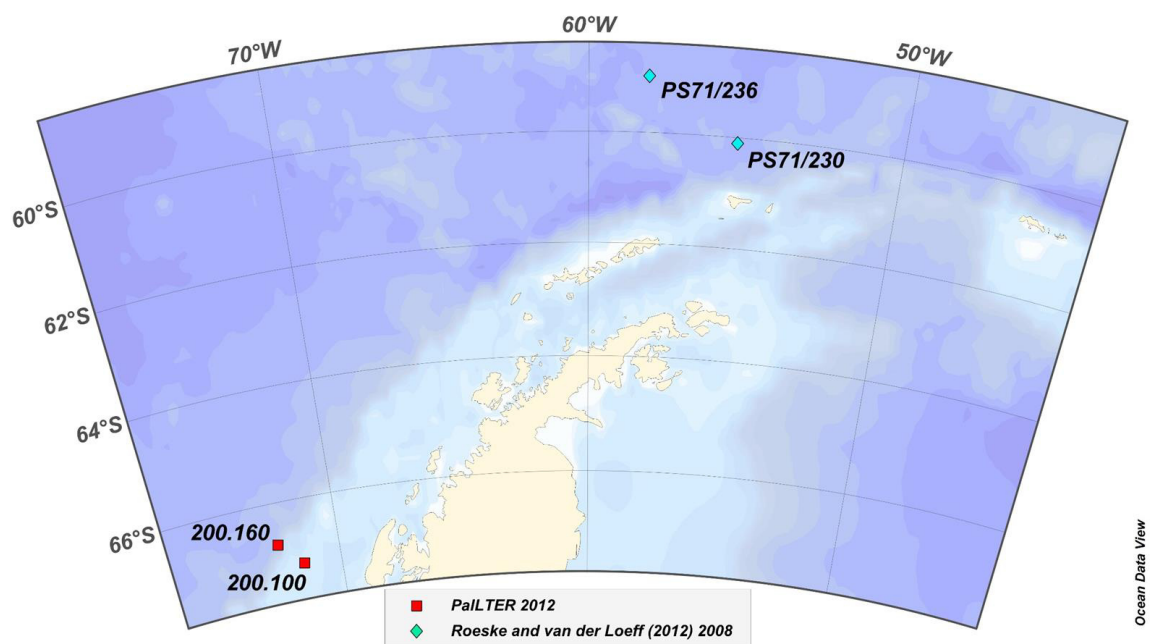


Figure 4-4: Map showing the location of depth profiles used to compare variation in Ba_d concentration with depth on- and off- the continental shelf. Stations 200.100 and 200.160 are part of the PaLLTER dataset analysed for this study, collected in austral summer 2012. PS71/236 and PS71/230 are from Roeske and Rutgers van der Loeff (2012) collected in austral autumn 2008 (PS71/236 collected on 05/04/2008 [lat -58.9704°N long -58.1388°E]; PS71/230 collected on 02/04/2008 [lat -60.1077°N long -55.2821°E]).

4.2. Inter-year variability in surface distribution

The inter-year variability observed is quantified by a simple calculation of the surface ΔBa_d ($Ba_d^{2012} - Ba_d^{2011}$), along with the inter-year variability of other key parameters such as silicic acid and water mass fractions (denoted by Δ). Only stations points that were sampled in both

years were included in this analysis (due to the logistical difficulties involved, the locations of underway stations were not identical between years, but were sufficiently close to warrant inclusion in this analysis).

There is a significant positive correlation between ΔBa_d and $\Delta Si(OH)_4$ ($R^2 = 0.462$; $p < 0.001$; $\Delta Si(OH)_4$ coefficient 0.196 ± 0.04 ; intercept -0.86 ± 0.5 ; $n = 29$), whilst a less distinct negative relationship is observed between ΔBa_d and the fraction of sea ice melt present ($\Delta\%SI$) ($R^2 = 0.316$; $p = 0.0012$; $\Delta\%SI$ coefficient -1.75 ± 0.5 ; intercept 1.22 ± 0.5 ; $n = 30$) (Figure 4-5). No significant relationship is found between ΔBa_d and the inter-year variance of meteoric water input ($\Delta\%MW$) ($R^2 = 0.016$; $p = 0.49$; $n=30$).

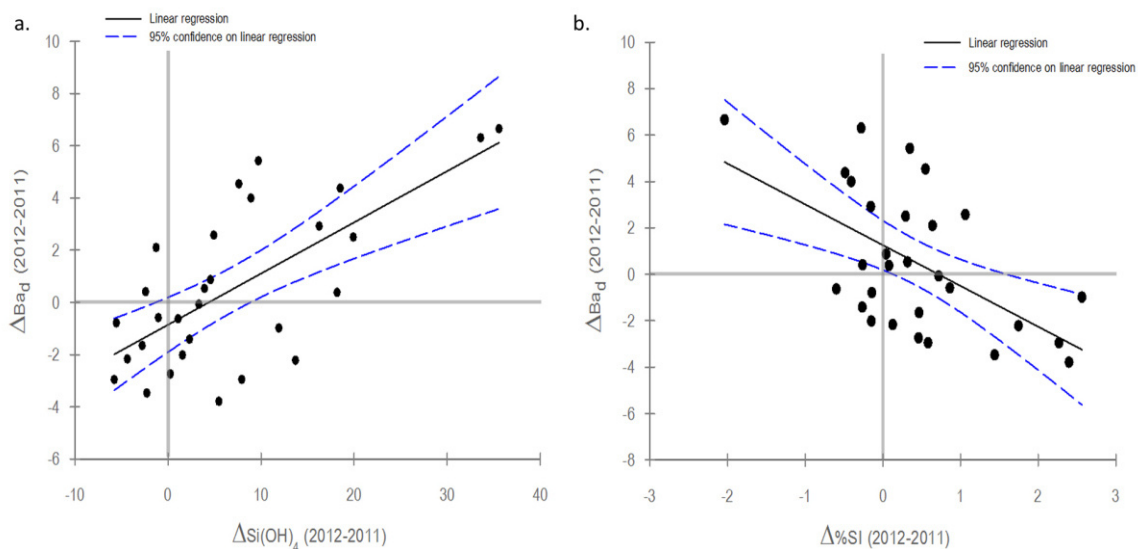


Figure 4-5: a. Scatter plot of ΔBa_d against the $\Delta Si(OH)_4$, indicating change in these parameters between 2011 and 2012. Black line indicates the linear regression model fitted to all data ($R^2 = 0.462$; $p = 4.9 * 10^{-5}$; $\Delta Si(OH)_4$ co-efficient = 0.196; $n = 29$, with 95% confidence limits marked by blue dashed lines; b. Scatter plot of ΔBa_d against the $\Delta\%SI$, indicating change in these parameters between 2011 and 2012. Dotted line indicates the linear regression model fitted to all data ($R^2 = 0.316$; $p = 0.0012$; $\Delta\%SI$ co-efficient = -1.75; $n = 30$), with 95% confidence limits marked by blue dashed lines.

4.3. Dissolved barium and silicic acid

The full data set (2011 surface samples; 2012 depth and surface samples) shows a strong positive correlation between dissolved barium and silicic acid ($Si(OH)_4$) ($R^2 = 0.72$; $p < 0.001$; $Si(OH)_4$ coefficient 0.21 ± 0.01 ; intercept 69.2 ± 0.7 ; $n = 117$; Figure 4-6), following a linear regression model similar to that observed elsewhere in the Southern Ocean and adjoining basins (see Table 3-3), but with a lower slope coefficient and a higher intercept at zero $Si(OH)_4$. In the case of the PalTER dataset this regression is heavily reliant on the relatively few depth values available, although a significant yet more scattered positive relationship still exists when surface samples are considered independently (Figure 4-6). When dissolved barium values are

normalised to an average salinity (33.5) a small component of this coupled variation is removed, but the relationship remains significant.

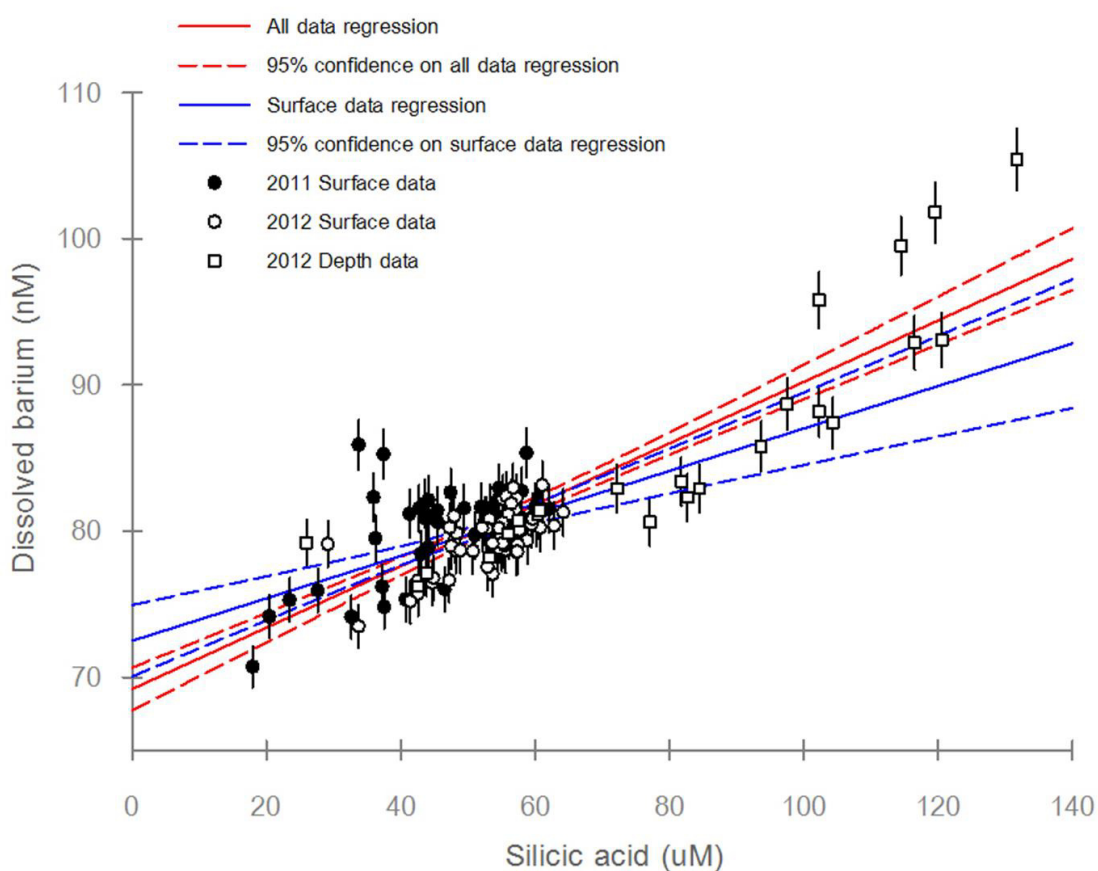


Figure 4-6: Cross plot of dissolved barium (nM) against silicic acid (μM) of seawater samples across the PalTER grid. Filled circles represent surface samples from 2011; open circles represent surface samples from 2012; crosses represent depth samples from 2012. Blue solid line indicates the linear regression model fitted to all of these samples ($R^2 = 0.71$; $p < 0.001$; $\text{Si}(\text{OH})_4$ co-efficient = 0.21; intercept = 69.2; $n = 117$), with 95% confidence bounds indicated by dashed blue lines. Red solid line indicates the linear regression model fitted surface samples only ($R^2 = 0.27$; $p < 0.001$; $\text{Si}(\text{OH})_4$ co-efficient = 0.14; intercept = 72.8), with 95% confidence bounds indicated by dashed red lines. Ba errors shown are set to 2 %, which is the most conservative estimate of uncertainty assessed using the long term external reproducibility of two comparable seawater standards (see Table 4-1).

A large amount of scatter exists around this $Ba_d/Si(OH)_4$ relationship, which is examined through the calculation of a $Ba_d^{Residual}$ value for each data point. The $Ba_d^{Residual}$ value quantifies the deviation of the Ba_d measurement from the overall $Ba_d/Si(OH)_4$ regression of the dataset (Equation 4-2, see Figure 3-4). Positive $Ba_d^{Residual}$ values indicate that the Ba_d measured is higher than predicted by silicic acid values, whilst negative $Ba_d^{Residual}$ values signify that Ba_d is lower than predicted.

$$Ba_d^{Si\ Residual} = Ba_d^{Measured} - ((Si(OH)_4^{Measured} * 0.21) + 69.2))$$

Equation 4-2: Calculation of $Ba_d^{Residual}$ values using the $Ba_d / Si(OH)_4$ linear correlation described by all PallTER data shown in Figure 4-6.

Surface plots of these $Ba_d^{Residual}$ values identify several areas of interest (Figure 4-2). In the 2011 plot the area adjacent to and south-west of Marguerite Bay is highlighted by very high values, corresponding to an anomalous pairing of high Ba_d relative to $Si(OH)_4$ measurements in this region. The 2012 plot reveals lower $Ba_d^{Residual}$ values overall, but with significant lows around Marguerite Bay/the south-west and at certain points along the coast (400 and 600 line transects).

4.4. Productivity indicators

4.4.i Primary productivity and Chl-a

Primary productivity in this region is considered to be dominated by diatoms (Ducklow et al. 2007). As diatoms are siliceous organisms it is common to consider levels of silicic acid in surface waters as representative of the relative abundance of diatom populations across an area. Higher levels of surface silicic acid may result from low uptake, indicating lower levels of diatom productivity, and vice versa. However, in the 2011 and 2012 surface datasets from this area there is no significant correlation between silicic acid and primary productivity ($R^2 = 0.01$; $p = 0.54$; $n = 35$), or silicic acid and Chl- a ($R^2 = 0.01$; $p = 0.52$; $n = 44$). This suggests that surface silicic acid levels may not be a suitable indicator of diatom productivity, or that non-siliceous forms of productivity were dominant at this time. Both measured primary productivity (Figure 4-7) ($R^2 = 0.30/0.27$; $p < 0.01$; $n = 30$) and Chl- a ($R^2 = 0.22/0.46$; $p < 0.01$; $n = 40$) exhibit strong significant negative correlations with other macronutrients (phosphate (PO_4); nitrate plus nitrite (NOx) respectively) (see Figure 4-8 a and b for NOx and PO_4 surface distributions).

4.4.ii Utilised silicic acid

Attempts were made to quantify the level of utilised silicic acid at each station, as a more accurate representation of diatom productivity. Utilised silicic acid was calculated for all stations where full depth profiles were available by subtracting the silicic acid concentration at the

temperature minimum (assumed to represent the remnant stock of silicic acid in the Winter Water, remaining from the previous year) from surface concentrations. However, no relationship was found between these derived values and the more reliable indicators of primary productivity discussed in Section 4.4.i. This suggests that the overprinting of physical mixing and silicic acid recycling in the upper water column make this parameter unreliable as an indicator of diatom productivity, and it was not applied as such.

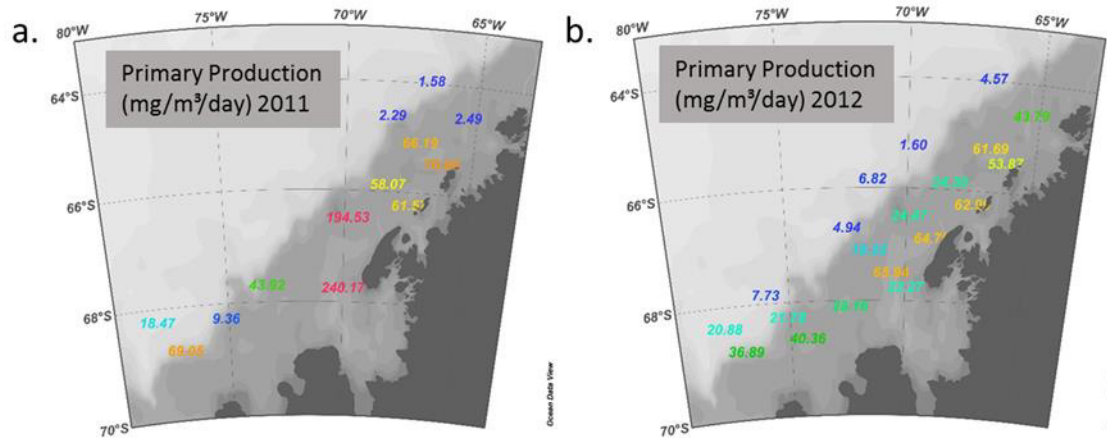


Figure 4-7: Surface plots showing values for primary production (mg/m³/day) at selected stations in the PaLLTER grid. Colour coding – blue indicates lower values, red indicates higher values; a. 2011; b. 2012.

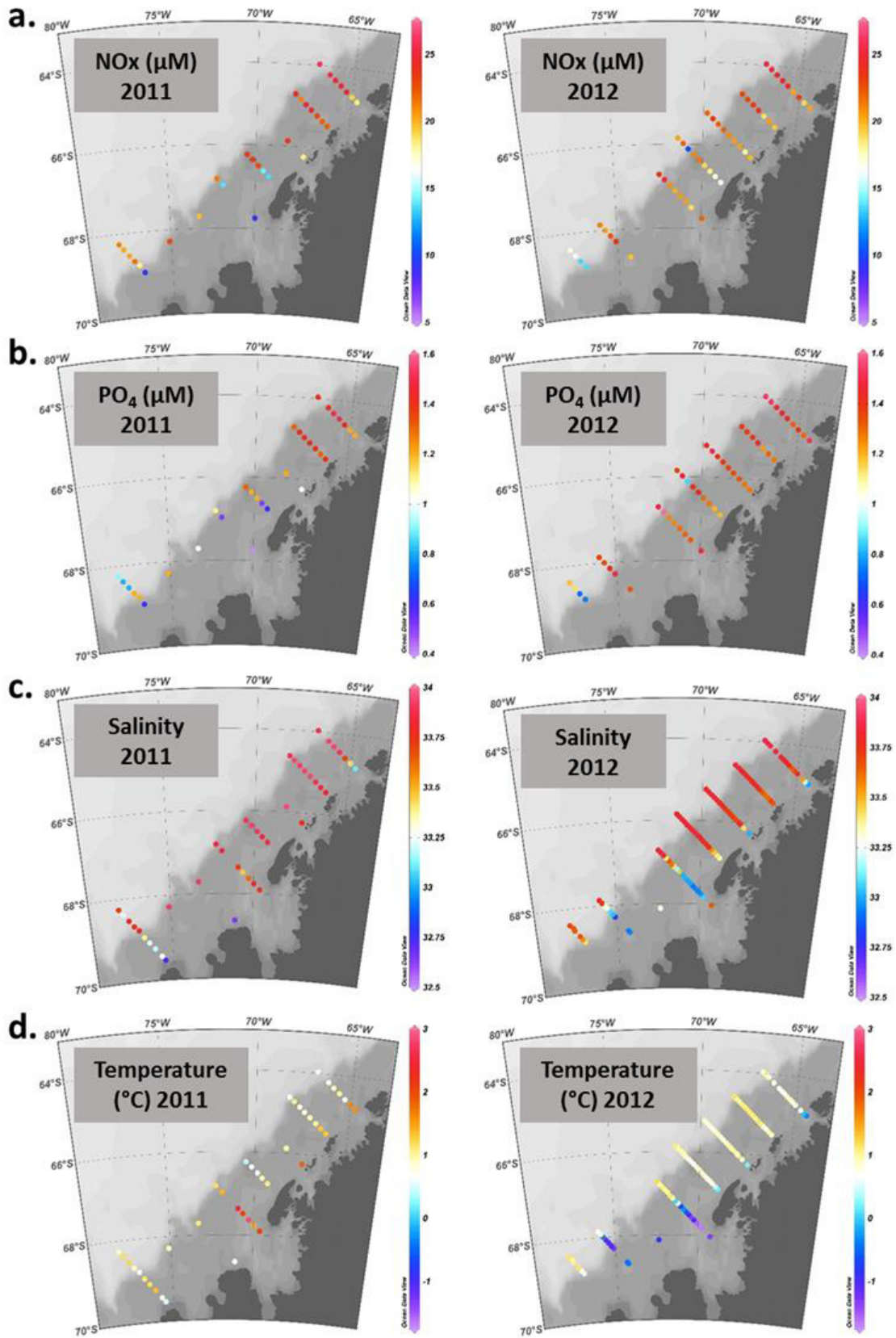


Figure 4-8: Surface distributions across the PaLLTER for 2011 (left hand column) and 2012 (right hand column): a. Nitrate plus nitrite concentrations (NO_x) (μM); b. Phosphate concentrations (PO_4) (μM); c. Salinity; d. Temperature ($^{\circ}\text{C}$).

4.5. Dissolved barium and water mass fractions

As well as significant variation in the dissolved barium distribution, the two years studied exhibit very different regimes of freshwater input (Figure 4-9). The 2012 data is dominated by a higher sea ice melt input, focussed in the region adjacent to and southwest of Marguerite Bay, and at certain sites along the coast to the north east (400 and 600 Lines). Variations in the meteoric water contribution reveal a contrast between gentle gradients perpendicular to the coast in the 2012 data, and localised areas of higher meteoric water concentrations in 2011. Given the general similarity of precipitation inputs preceding the cruises in these two years (Meredith et al. 2016), the differences are inferred to be due most likely to localised changes in glacier discharge, though some impact of precipitation changes cannot be excluded.

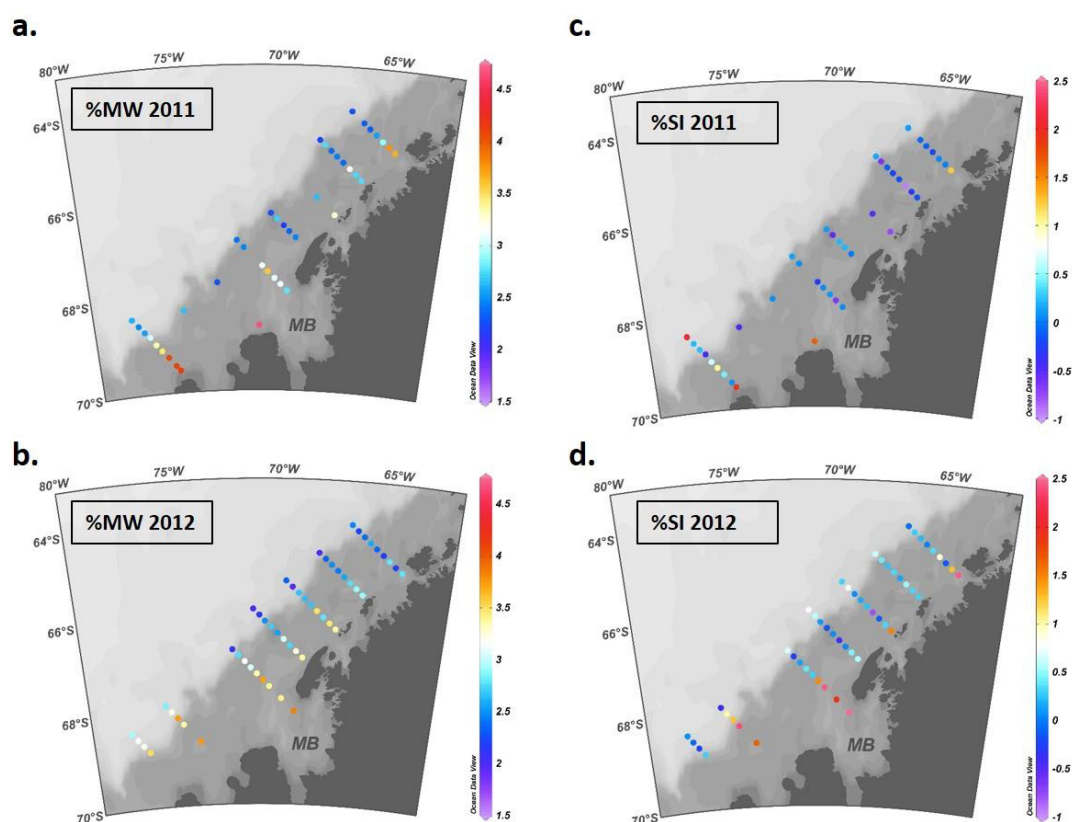


Figure 4-9: Surface distributions of freshwater mass fractions (as calculated in Section 4.3.3) across the PALLTER. Meteoric water and sea ice melt fractions are presented as percentages, with a systematic error of $\pm 1\%$ on all absolute values. a. Fraction of meteoric water (%MW) in 2011; b. Fraction of meteoric water (%MW) in 2012; c. Fraction of sea ice meltwater (%SI) in 2011; d. Fraction of sea ice meltwater (%SI) in 2012.

The behaviour of the Ba_d distribution with regards to salinity also differs between the two years (Figure 4-10), indicating that variation in Ba_d is not merely a feature of ion concentration or dilution (i.e. not a result of conservative processes). A large portion of the data for 2011 and

2012 define a similar trend of varying Ba_d values over a constant, regionally high, salinity. A subset of both datasets then deviate from this main trend; in 2011 sample sites close to the coast record constant Ba_d values as salinity decreases, in 2012 a larger subset (defined by sample sites in Marguerite Bay and the southwest, and those close to the coast) record Ba_d values decreasing slightly with salinity (Figure 4-10).

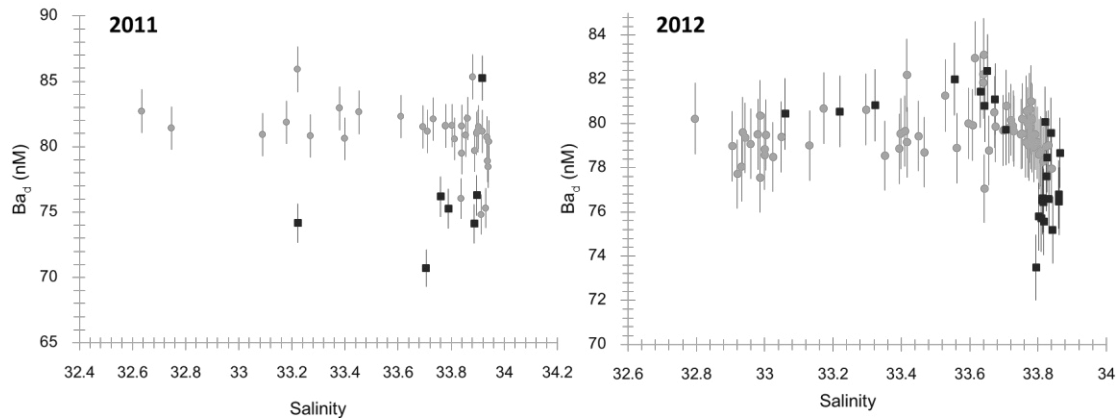


Figure 4-10: Scatter plots of dissolved barium (Ba_d) (nM) against salinity across the PalTER in surface samples. Filled light grey circles represent shelf stations; filled black squares represent off-shelf stations. Ba errors shown are set to 2 %, which is the most conservative estimate of uncertainty assessed using two comparable seawater standards (see Table 4-1).

Linear regression modelling between the derived meteoric water fraction (%MW) and Ba_d indicates that %MW is significantly correlated with Ba_d , particularly for the 2011 sample set (2011 data: $R^2 = 0.23$, $p = 0.0017$, %MW coefficient 2.3 ± 0.7 , intercept 74 ± 2 , $n = 41$; 2012 data: $R^2 = 0.097$; $p = 0.024$; %MW coefficient 1.2 ± 0.5 , intercept 76 ± 1 ; $n = 52$). However, this correlation appears to be an artefact produced by two subsets of data, with most off-shelf sites having consistently low Ba_d and %MW, whilst on-shelf sites exhibit a variation in %MW that is not accompanied by any predictable change in Ba_d (Figure 4-12). Off-shelf sites from the southern lines of the grid (000 and -100 Lines) in 2012 also exhibit this broadly shelf-like behaviour.

In the 2012 data, areas of low $Ba_d^{Residual}$ values (around Marguerite Bay/the south-west and at certain points along the coast) appear to correspond with sites of high sea ice melt input. These observations are corroborated by the appearance of a slight negative correlation between 2012 $Ba_d^{Residual}$ values and the contribution of sea ice melt ($R^2 = 0.24$; $p < 0.01$; %SI coefficient -0.9 ± 0.2 ; intercept 0.5 ± 0.2 ; $n=52$) (Figure 4-11 a).

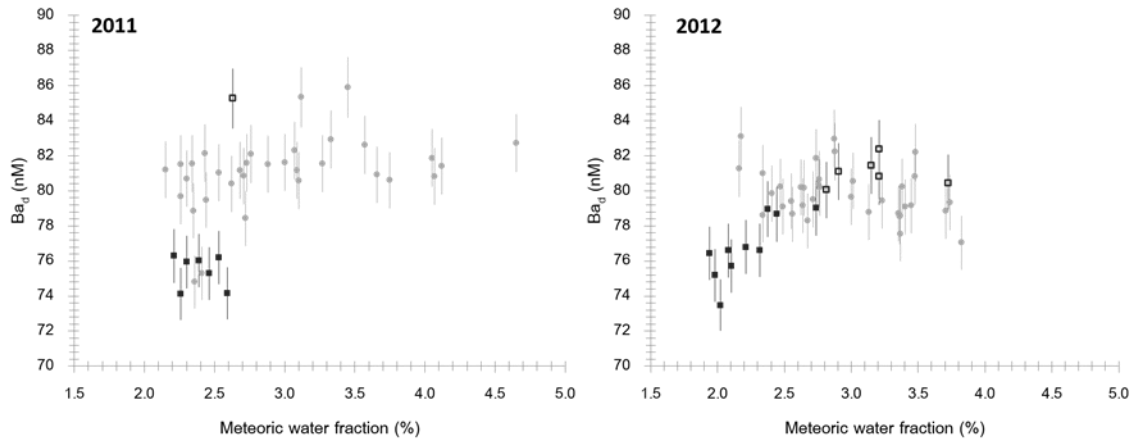


Figure 4-12: Scatter plots of dissolved barium (Ba_d) (nM) against the meteoric water fraction, determined via oxygen isotopes, across the PaLLTER in surface samples. Filled light grey circles represent shelf stations; filled black squares represent off-shelf stations, un-filled squares off-shelf stations from 000 and -100 lines. Ba errors shown are set to 2 %, which is the most conservative estimate of uncertainty assessed using two comparable seawater standards (see Table 4-1). Uncertainty on the meteoric water fraction is ± 1 %, but this is not displayed as the majority of the error can be attributed to uncertainty on end-member values, and is therefore be systematic across the dataset.

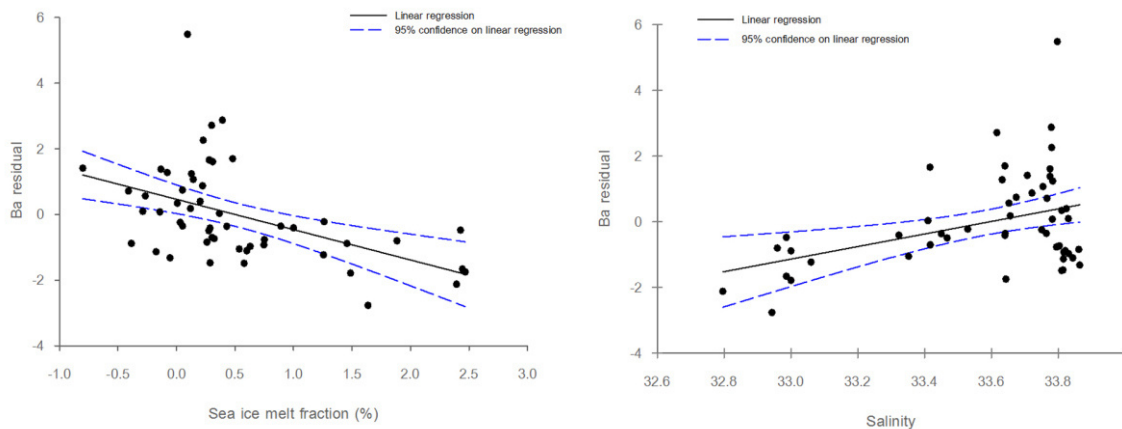


Figure 4-11: a. Scatter plot of $Ba_{Si}^{residual}$ against the fraction of sea ice melt (%) for 2012 surface data. Solid line indicates the linear regression model fitted to all data, dashed lines represent the 95% confidence limit on the model ($R^2 = 0.235$; $p = 0.00026$; SI% co-efficient = -0.92 ; $n = 52$); b. Scatter plot of $Ba_{Si}^{residual}$ against salinity for 2012 surface data. Solid line indicates the linear regression model fitted to all data, dashed lines represent the 95% confidence limit on the model ($R^2 = 0.154$; $p = 0.004$; $n = 52$). Uncertainty on the sea ice melt fraction is ± 1 %, but this is not displayed as the majority of the error can be attributed to uncertainty on end-member values, and is therefore be systematic across the dataset and should not impact on the significance of the linear regression model.

4.6. Vertical mixing

The extent to which upper-ocean vertical mixing has affected the water column at the stations is very difficult to quantify directly, although systematic collection of the necessary measurements has been begun at the WAP (Brearley et al. 2016). In the absence of this mixing data, the impact of mixing on the structure of the water column can be estimated by calculating the mixed layer depth, defined here as the depth at which the potential density anomaly of the water column exceeds 0.05 kg m^{-3} of the surface value (Clarke et al. 2008). An alternative way to quantify the degree of water column stratification is to calculate the density difference between several different depth ranges (Hendry et al. 2010). Whilst the former method provides an upper limit to the current depth to which the ocean is actively mixing, the latter represents the strength of the stratification present in the ocean, which at the WAP is known to be influenced by the level of upper-ocean homogenisation the previous winter (Venables et al. 2013). When both were calculated for the water column at a station, mixed layer depth was found to be a reasonable predictor of stratification estimated from density difference (here taken as the difference in density at 30 m and at 5 m depth), with a significant negative correlation between the two calculated variables ($R^2 = 0.46$, $p = 0.001$, $n=18$). Estimates of stratification from both of these methods were compared to silicic acid and dissolved barium distribution across the LTER grid, and showed no significant correlation (2011 and 2012 respectively, Ba_d / density difference [30 m – 5 m]: $R^2 = 0.09 / 0.04$; $p = 0.22 / 0.4$; $n = 18 / 18$. Si(OH)_4 / density difference [30 m – 5 m]: $R^2 = 0.05 / 0.12$; $p = 0.80 / 0.16$; $n = 15 / 18$. 2012 only, Ba_d / mixed layer depth: $R^2 = 0.008$, $p = 0.70$, $n = 22$. Si(OH)_4 / mixed layer depth: $R^2 = 0.113$, $p = 0.13$, $n = 22$).

5. Discussion

5.1. Biological cycling as a primary control on the surface dissolved barium distribution

Although mainly dominated by diatoms and cryptophytes, the phytoplankton assemblage of the WAP has been shown to display complex spatial and temporal variations, with regional contributions from haptophytes and flagellates (Huang et al. 2012). However, studies of phytoplankton community structure at the LTER have consistently reported high abundances of diatoms and cryptophytes relative to other groups, with diatoms dominating most of the offshore, southern coast and southern shelf areas (Huang et al. 2012; Kozłowski et al. 2011; Moline et al. 2004; Garibotti et al. 2003). It is therefore reasonable to assume that any biologically mediated removal of barium from surface waters in this region would be influenced by diatom productivity, and that silica cycling may play an important role in controlling Ba_d in the water column.

In accord with previous observations, the Ba_d distribution across the PaLTER grid covaries with silicic acid concentrations (Figure 4-2) A strong positive correlation ($R^2 = 0.71$; $p < 0.01$; Figure 4-6) between Ba_d and $Si(OH)_4$ is observed when samples from the whole water column are considered, with much of the relationship defined by a limited number of samples from intermediate and deeper waters. This agrees with previous suggestions that the strong association between barium and silicic acid is sustained by samples at depth. These distributions may result from a similarity in inorganic dissolution behaviour between biogenic opal and barium, coupled with large scale ocean circulation (Jeandel et al. 1996; Jacquet et al. 2007; Horner et al. 2015). However, direct links have been suggested between the marine silicate and barite cycles, with studies in the Southern Ocean reporting higher levels of barite particulates observed in diatom-dominated regions, potentially due to the catalytic effects of sinking diatom frustules on barite precipitation (Bishop et al., 1988; Stroobants et al. 1991; Dehairs et al. 1991).

The overall Ba_d - $Si(OH)_4$ relationship in this region is defined by the depth samples, whilst the surface sites that comprise the majority of the dataset display a lower degree of variability in both Ba_d and $Si(OH)_4$ distribution. However, the relationship between the two parameters does not de-couple entirely in surface waters as has been observed in other regions of the Southern Ocean (Jacquet et al. 2007). Considered independently of the depth profiles, the surface PaLTER dataset still displays a significant, though highly scattered, positive correlation ($R^2 = 0.27$; $p < 0.01$; see Table 3-3) between Ba_d and $Si(OH)_4$. Conversely, surface Ba_d shows no significant correlation with the other macronutrients NO_x and PO_4 . This indicates that the association between Ba_d and $Si(OH)_4$ in surface waters is not related directly to biological uptake or the cycling of organic material. Whilst the high level of inter-annual variability in the surface Ba_d distribution can be largely accounted for by variability in surface concentrations of $Si(OH)_4$ (Figure 4-5 a), this variability does not seem to be linked to estimates of primary productivity, but instead may indicate the varying balance between the removal of $Si(OH)_4$ from surface water via sinking biogenic opal, and recycling between biogenic opal and $Si(OH)_4$ in surface waters. Low concentrations of surface $Si(OH)_4$ may reflect a local dominance of sinking over surface recycling, possibly due to the formation of heavier diatom tests in response to iron limitation (Hutchins & Bruland 1998; Timmermans & van der Wagt 2010).

It is possible that, rather than silicic acid concentrations indicating increased diatom productivity, the covariance of silicic acid and dissolved barium could result instead from a coincident replenishment of surface stocks via upwelling. However, the lack of correlation between the surface variability of these parameters and estimates of water column stratification (mixed layer depths and density differences, see Section 4.6) make such a scenario unlikely in

this case, as any increased vertical mixing in the vicinity of these higher surface concentrations should be detectable using such methods. It is likely that vertical mixing does play a role in Ba_d cycling, but long-term mixing rates are not currently well-constrained by observations except for in a few specific localities (such as the Rothera Oceanographic and Biological Time Series site [RaTS] Brearley et al. 2016).

In addition to the association between Ba_d and $Si(OH)_4$, there is a notable lack of correlation between $Si(OH)_4$ and the other macronutrients in surface waters (PO_4 : $R^2 = 0.25$; $p = 0.023$. NO_x : $R^2 = 0.03$; $p = 0.79$). This could result from relatively shallow remineralisation of phosphate and nitrate, allowing them to be mixed back into the surface layer. Whilst a large proportion of biogenic opal is recycled in surface waters (> 50 % in the Southern Ocean (Tréguer & De La Rocha 2013) the exported fraction dissolves deeper in the water column. Whilst the association between Ba_d and silicic acid at depth is well established, the association observed here in surface waters, albeit weaker, suggests that in this diatom-dominated region, the phase carrying Ba_d from surface waters to the mesopelagic depths of barite precipitation is associated with silicic diatom tests rather than with organic matter. Ba_d has been found to associate with iron oxyhydroxides adsorbed onto diatom cell surfaces in laboratory cultures (Sternberg et al. 2005), which could cause the surface correlation observed if this occurred on a large scale. However, no significant levels of iron have been found on the surfaces of Southern Ocean phytoplankton cells (Twining & Baines 2013), making it unlikely that such a mechanism could have a large impact on Ba_d distributions. It is more likely that Ba_d is associated with biogenic opal-dominated phytodetritus within the euphotic layer through barite precipitation (Horner et al. 2015) that may be catalysed by the presence of diatom frustules (Bishop 1988; Stroobants et al. 1991). This would explain the positive correlation observed between Ba_d and $Si(OH)_4$ in surface waters, with low concentrations of both occurring when the sinking and export of biogenic opal dominates over surface recycling, providing within its phytodetrital microenvironments conditions for the precipitation of barite.

The lower slope and higher intercept value of the surface $Ba_d / Si(OH)_4$ linear regression model implies that in surface waters Ba_d is less variable with regard to silicic acid than it is in deeper waters, with the processes that govern Ba_d distributions differing between surface waters and the deeper water column. There are several mechanisms that could explain this deviation by altering the ratio of Ba:Si in surface waters, such as differences in phytoplankton ecology (varying the extent to which Ba_d and/or silicic acid are removed from the surface), or additional abiotic processes leading to variation in the Ba:Si removal ratio. Processes may also be at work that alter the Ba:Si ratio in deeper waters that are relatively isolated from the surface,

such as differences in the saturation state of the water column with regards to barite (influencing the regeneration ratio of Ba:Si), or variation in epibenthic fluxes. Different combinations of these mechanisms have been employed by previous authors to explain the geographical variation observed in the Ba_d -Si(OH)₄ relationship (Jeandel et al. 1996; Jacquet et al. 2007; Hoppema et al. 2010). The high density spatial coverage and biogeochemical gradients of the PalTER dataset makes it ideal for testing the potential controls on surface uptake.

5.2. Identifying a coastal source of dissolved barium

As well as variation in surface uptake, the distribution of Ba_d will be influenced by any local changes to the sources of barium along the peninsula. Therefore it is necessary to assess through which processes barium is transported into the WAP coastal system. The general distribution of surface Ba_d (Figure 4-2) indicates a coastal source that enriches waters on the shelf, with concentrations decreasing away from the coast as shelf waters mix with the Ba_d -poor waters of the Antarctic Circumpolar Current. In near-continent settings elsewhere this coastal enrichment could be attributed to fluvial input. The bulk of the barium weathered from continental rock is transported fluvially in the dissolved phase, causing the high surface concentrations of Ba_d routinely recorded at river mouths (Martin & Meybeck 1979; Viers et al. 2009). The levels of Ba_d in these regions are increased by estuarine desorption of barium from river-borne sediments in the river/ocean mixing zone (Nozaki et al. 2001; Guay & Falkner 1998; Hanor & Chan 1977).

However, along the coast of the WAP continental freshwater input is restricted to glacial meltwater and precipitation, which plays an important role in the physical and biological dynamics of the water column. As well as releasing low salinity water to the coastal system, meltwater from glaciers may be enriched in terrigenous material acquired through contact with bedrock and dust accumulation (Raiswell et al. 2008; Sherrell et al. 2015). The input of this terrigenous material to marine waters can affect turbidity and light attenuation (Schloss et al. 2002), as well as being a potential source of macro and micronutrients. Differences in the presence of surface meltwater have been linked to variations in phytoplankton biomass both near- and offshore, probably as a result of water column stabilisation (Dierssen et al. 2002). Increased productivity has been observed surrounding free-drifting icebergs in the Weddell Sea in conjunction with evidence for the dispersion of entrained terrigenous particles (Smith et al. 2007) suggesting that glacial ice may also provide a source of trace metals that can stimulate primary production. Studies in Marian Cove (King George Island) have also shown that melting glaciers can be responsible for enriching coastal waters with macronutrients, trace elements, and rare earth elements (Kim et al. 2015).

Specific data regarding the barium content of glacial meltwater is sparse, and studies have shown that the solute and particulate composition of such waters can be highly variable (Mora et al. 1994). Attempts to characterise the trace element export of alpine glaciers have found that in these environments barium is present in significantly lower concentrations than in global stream waters (bulk glacial meltwater in the region of 5 nM Ba_d ; average world stream water in the region of 145 nM Ba_d) (Mitchell et al. 2001; Fortner et al. 2009). This figure is also significantly lower than surface coastal Ba_d values reported from this study (70 to 85 nM), so if the content of WAP glacial meltwater is comparable then it may act to dilute local Ba_d concentrations rather than enriching them. Given the relatively high load of suspended sediment transported in glacial meltwater, it is possible that this could include a high concentration of adsorbed barium. However, this would be expected to desorb into the dissolved pool fairly quickly upon mixing with seawater, as is seen in desorption of barium from riverine sediment loads in estuaries, which is not observed in the Ba_d distribution at the WAP.

The data from the PaALTER show a significant, though highly scattered, positive trend between the derived meteoric water fraction (%MW) and Ba_d for both of the years studied (Figure 4-12). However, these trends appear to be an artefact of two spatial subsets within the data: off-shelf sites with a low meteoric water component and low Ba_d values, and on-shelf sites where Ba_d variation is not linked to %MW. This interpretation is further supported by the lack of a consistent co-variance between Ba_d and salinity (Figure 4-10) indicating that trace element input from glacial meltwater is not responsible for the Ba_d enrichment observed in the WAP shelf waters. There is some indication from surface distributions that areas with pronounced glacial meltwater input in 2011 may be associated with anomalously high Ba_d measurements (Figure 4-2 and Figure 4-9). It is possible that when fluxes of meltwater are sufficiently high, they may lead to localised Ba_d enrichment.

Previous studies into the distribution of marine Ba_d have reported significant barium enrichment in bottom waters, potentially a result of recycling of particulate barium phases from pelagic sediment (Jacquet et al. 2004; Hoppema et al. 2010). Barium is delivered to the sediment in various reactive forms: as particulate barium sulphate (barite), incorporated in celestite or calcite tests, and adsorbed onto Fe-Mn oxyhydroxides and organic matter. The release of Ba^{2+} from these solid phases during early diagenesis can saturate pore waters with respect to barium sulphate, creating a sharp concentration gradient at the sediment/seawater interface. This could lead to a diffusive flux of Ba_d to the overlying water column. There is evidence for such epibenthic Ba_d fluxes in pore water profiles from the Arabian Sea and the Equatorial Pacific (Schenau et al. 2001; Paytan & Kastner 1996), and benthic incubation experiments that have

directly measured barium fluxes from sediments (McManus et al. 1998; McManus et al. 1994). The existence of comparable Ba_d fluxes from the shelf sediments adjacent to the WAP could be responsible for observed enrichment of the overlying shelf waters. However, this hypothesis is difficult to test conclusively without more extensive sampling of shelf bottom waters. The apparent increase of Ba_d concentrations observed along isopycnals from the open waters of the Drake Passage to the slope and shelf waters of the WAP indicates that Ba_d addition is taking place on the shelf. However, as these Ba_d records were not collected in the same year, such a comparison is not conclusive. The dissolution of particulate barium phases within shelf sediments could lead to a flux of barium from the sediment to bottom waters on the shelf. These fluxes are a plausible source of barium to coastal waters, and could be responsible for the observed Ba_d - $Si(OH)_4$ relationship if both silicic acid and barium were diffusing from benthic sources with a relatively low Ba:Si ratio, lowering the regression slope relative to other regions of the ocean whilst still enriching shelf waters with Ba_d .

5.3. Sea ice formation as a secondary control on the surface dissolved barium distribution

As discussed above, the observed correlation between barium and silicic acid is not consistent throughout the water column, breaking down to some degree in surface waters. Additional abiotic factors must exist that influence variation in the uptake ratio of barium to silicate or the saturation state of barite in the water column. It is possible to investigate such abiotic processes, and how they may exert a secondary influence on the surface Ba_d distribution, by using $Ba_d^{Si\text{ residual}}$ values (see Section 4.3). Likely candidates to cause variation in the Ba_d concentration unrelated to biological productivity are the spatial and inter-annual variations in the coastal freshwater regime. As discussed in Section 4.5, the meteoric water fraction (%MW) appears to have little impact on Ba_d distributions spatially in either 2011 or 2012. This is borne out by a lack of any significant co-variance between %MW and $Ba_d^{Si\text{ residual}}$ values (2011 surface dataset: $R^2 = 0.079$; $p = 0.079$; $n = 40$. 2012 surface dataset: $R^2 = 0.028$; $p = 0.233$; $n = 52$).

In contrast, the fraction of sea ice melt (%SI) present at sites in 2012 exhibits a significant negative correlation with $Ba_d^{Si\text{ residual}}$ values ($R^2 = 0.24$; $p < 0.01$; %SI coefficient -0.9 ± 0.2 ; intercept 0.5 ± 0.2 ; $n=52$) (Figure 4-11 a), suggesting that higher fractions of sea ice melt are associated with lower dissolved barium concentrations than predicted by silicic acid levels, and vice versa. The surface plots of %SI and $Ba_d^{Si\text{ residual}}$ values (Figure 4-9 and Figure 4-2) reveal that in this year the high %SI values recorded around Marguerite Bay and the southwest section of the PalTER grid, plus at the coastal sites of the 400 and 600 lines, correspond to similarly distributed low $Ba_d^{Si\text{ residual}}$ values. Although %SI values are not directly correlated with Ba_d or silicic

acid concentrations (Figure 4-13), the correlation of %SI with $Ba_d^{Si\text{ residual}}$ values suggests that fluxes of sea ice melt to surface coastal waters dilute the stock of Ba_d present to a greater degree that they dilute the silicic acid stocks.

The concentrations of Ba_d found in sea ice (10 to 40 nM (Lannuzel et al. 2011)) are significantly lower than the seawater values reported here, so some degree of dilution would be expected from mixing with sea ice meltwater. However, the disproportionate dilution of Ba_d

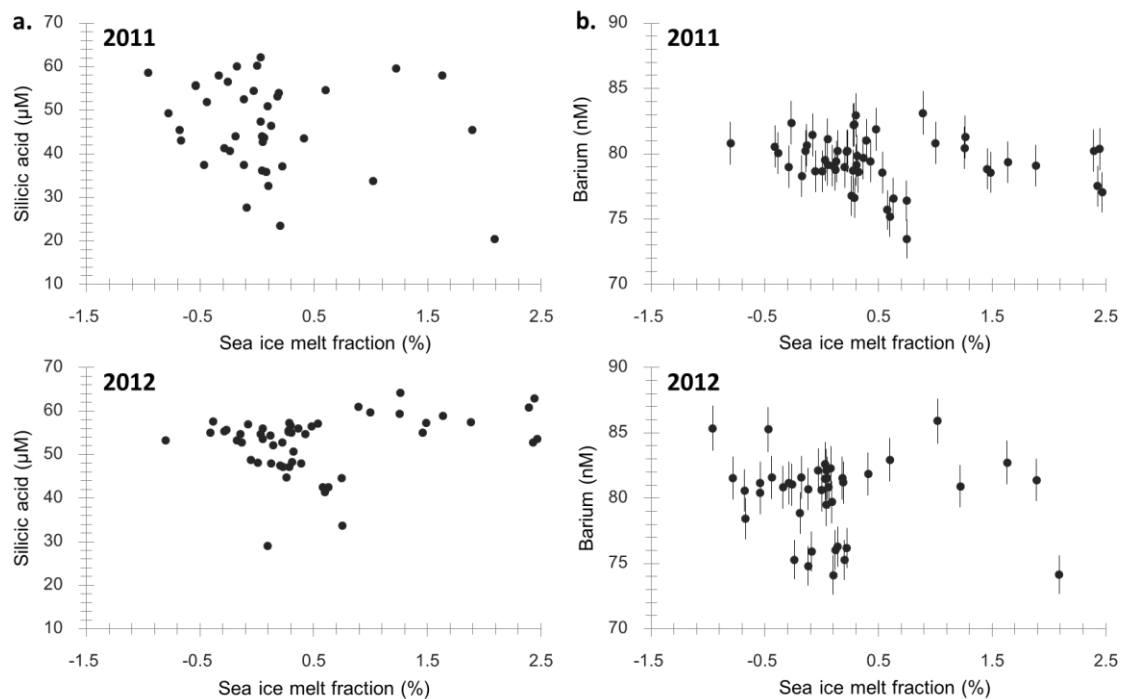


Figure 4-13: a. Scatter plots of sea ice melt fraction (%) vs. silicic acid (μM) for 2011 and 2012, showing no correlation between the parameters (2011: $R^2 = 0.05$, $p = 0.18$, $n = 40$; 2012: $R^2 = 0.07$, $p = 0.064$, $n = 52$) b. Scatter plots of sea ice melt fraction (%) vs. dissolved barium (nM) for 2011 and 2012, showing no correlation between the parameters (2011: $R^2 = 0.01$, $p = 0.57$, $n = 41$; 2012: $R^2 = 0.03$, $p = 0.21$, $n = 52$). Ba errors shown are set to 2 %, which is the most conservative estimate of uncertainty assessed using two comparable seawater standards. Freshwater fraction errors are not displayed, as the majority of the 1 % error on absolute values can be attributed to uncertainty on end-member values, and will therefore be systematic across the dataset.

relative to silicic acid suggests that there may be processes occurring within the sea ice that remove Ba_d , causing resultant meltwater to have a lower Ba:Si ratio than the seawater it formed from.

This dilution signal can be seen in a significant though highly-scattered positive correlation between the 2012 $Ba_{Si}^{\text{residual}}$ values and salinity ($r^2=0.154$; $p=0.004$; Salinity coefficient 1.9 ± 0.6 ; intercept -64 ± 21 ; $n=51$) (Figure 4-12Figure 4-11 b). Assuming that the $Ba_d^{Si\text{ residual}}$ values are solely the result of sea ice melt changing Ba_d concentrations, the slope of the $Ba_d^{Si\text{ residual}}$ /salinity relationship (1.9 ± 0.6) represents a $2.4 \pm 0.8\%$ change in Ba_d for a 3% change in

salinity. This roughly 1:1 relative change indicates that the Ba_d depletion relative to $Si(OH)_4$ is purely a dilution signal, rather than the result of non-siliceous productivity stimulated by the sea ice melt. Mechanisms such as abiotic barite precipitation in supersaturated brine channels, adsorption onto sea-ice algal cells, or biotic precipitation of barite associated with the degradation of algal communities within sea ice, have been proposed as potential pathways linking the presence of sea ice with observed barium depletion in polar surface waters (Hoppema et al. 2010; Falkner et al. 1994). Carson (2009) found that dissolved barium concentrations in sea ice brines from Adelaide Island (WAP) ranged widely from surface water concentrations, and further work on Ba_d in sea ice will be discussed in Chapter 6. Sea ice has been found to contain high levels of particulate barium (up to 3000pM [3nM] in East Antarctic pack and fast ice (Lannuzel et al. 2011) and 7000pM [7nM] in Scotia Sea brown ice (Stroobants et al. 1991)), which supports the possibility that high levels of barite precipitation may be occurring within sea ice, removing barium from solution.

There is no indication of a similar relationship in the 2011 data, possibly because of a lower flux of sea ice melt in this year. The average contribution of sea ice melt to sample sites (%SI) was an order of magnitude lower in 2011 (0.085%) than in 2012 (0.56%), with the difference even more apparent in coastal/shelf sites (0.035% in 2011, 0.56% in 2012). The freshwater regime in 2011 was dominated by meteoric water fluxes, which appear to have a negligible influence on barium distributions. In order to test this idea, multiple regression analysis was performed using the independent variables of inter-year variance in $Si(OH)_4$, %SI and %MW to determine the dependent variable ΔBa_d . As can be seen in Table 4-2, both $\Delta Si(OH)_4$ and $\Delta \%SI$ were shown to be significant predictors, whilst $\Delta \%MW$ has no significant effect.

	Coefficients	Standard Error	t Stat	P-value
Intercept	-0.034	0.503	-0.0675	0.946
$\Delta Si(OH)_4$	0.17	0.0379	4.61	0.0001
$\Delta \%MW$	-0.84	0.716	-1.17	0.252
$\Delta \%SI$	-1.3	0.398	-3.28	0.003

Table 4-2: Multiple regression analysis (R^2 of model 0.631; significance f of model < 0.001) of the inter-year variance (2012-2011), with three independent variables: $\Delta Si(OH)_4$, $\Delta \%MW$, and $\Delta \%SI$, predicting the inter-year variance in the dissolved barium distribution.

6. Conclusions

This high resolution dataset of the distribution of dissolved barium across the PalLTER grid shows that there is a clear relationship between dissolved barium and silicic acid in the water column studied. This relationship is robust not only with depth, but also across the surface waters of the PalLTER grid, and the high level of inter-year variability exhibited by the Ba_d distribution between 2011 and 2012 correlates with the high inter-year variability of silicic acid concentrations. The persistence of the $Ba_d / Si(OH)_4$ relationship in these diatom-dominated surface waters is in contrast to the total breakdown of the relationship observed in other regions. It is possible that the removal of Ba_d from surface waters is facilitated by the presence of diatoms, either by adsorption of Ba_d onto particulates associated with diatoms, or via barite precipitation within diatom-dominated phytodetritus in the euphotic zone. Higher levels of biogenic opal export from surface waters (relative to recycling within the mixed layer) therefore lowers both surface silicic acid concentrations and Ba_d concentrations, adding another dimension to the link between barium and silicic acid cycling.

Our new data also reveal that a coastal source of barium enriches the shelf waters before they mix with barium-depleted ACC waters at the shelf break. This coastal flux of barium is not attributed to glacial meltwater input, which appears to have no consistent impact on the dissolved barium distribution. The enrichment of shelf waters may be due to an epibenthic flux of barium from shelf sediments, but further investigation of sediment pore waters and depth profiles will be necessary to establish this.

Non-conservative processes acting during the formation of sea ice also act as a secondary control on the removal of barium from the surface layer. When high levels of sea ice melt dominate the freshwater regime of the coastal waters of the WAP, local surface concentrations of dissolved barium are significantly lowered.

Chapter 5

The influence of coastal processes on dissolved barium cycling at the West Antarctic Peninsula – temporal analysis

1. Introduction

In previous chapters I have discussed the relationship between dissolved barium (Ba_d) and biological activity in surface waters, particularly the change in the surface behaviour of Ba_d when phytoplankton ecology changes from a diatom-dominated community to a nanoflagellate-dominated community (Chapter 3), and the potential association of Ba_d with silicic diatom frustules in surface waters (Chapter 4). In Chapter 4 I also investigated the role of sea ice in surface Ba_d distributions, and the potentially large impacts of vertical mixing with Ba_d -enriched bottom waters on the shelf. It was particularly challenging to evaluate this latter theory due to the lack of available depth profiles from the LTER at the time of analysis.

In this Chapter, the importance of surface processes such as biological interactions and sea ice formation and melt will be addressed more directly by analysing a time series from 15 m depth at the Rothera Biological and Oceanographic Time Series (RaTS), West Antarctic Peninsula. This temporal sample set, collected from March 2013 to January 2015, allows a direct analysis of

the seasonal changes in Ba_d with relation to the development of phytoplankton blooms and the seasonal cycles of sea ice at a fixed site in Ryder Bay (Figure 5-1). The site sampled is known to be reliably representative of the broader Marguerite Bay environment in terms of stratification and physical properties, and to show variability commensurate with regional and large-scale (hemispheric) forcing (Venables & Meredith 2014; Meredith et al. 2004).

Previous preliminary work on concentrations of dissolved and particulate barium at the RaTS site (Figure 5-2) indicated that particulate barium may exhibit an inverse relationship with biological activity, potentially due to the biogenically-mediated precipitation of barite during phytoplankton decay. By measuring dissolved barium concentrations at a higher precision than was available at the time of this previous study and in a more complete record, the timing and magnitude of this potential relationship can be investigated more robustly.

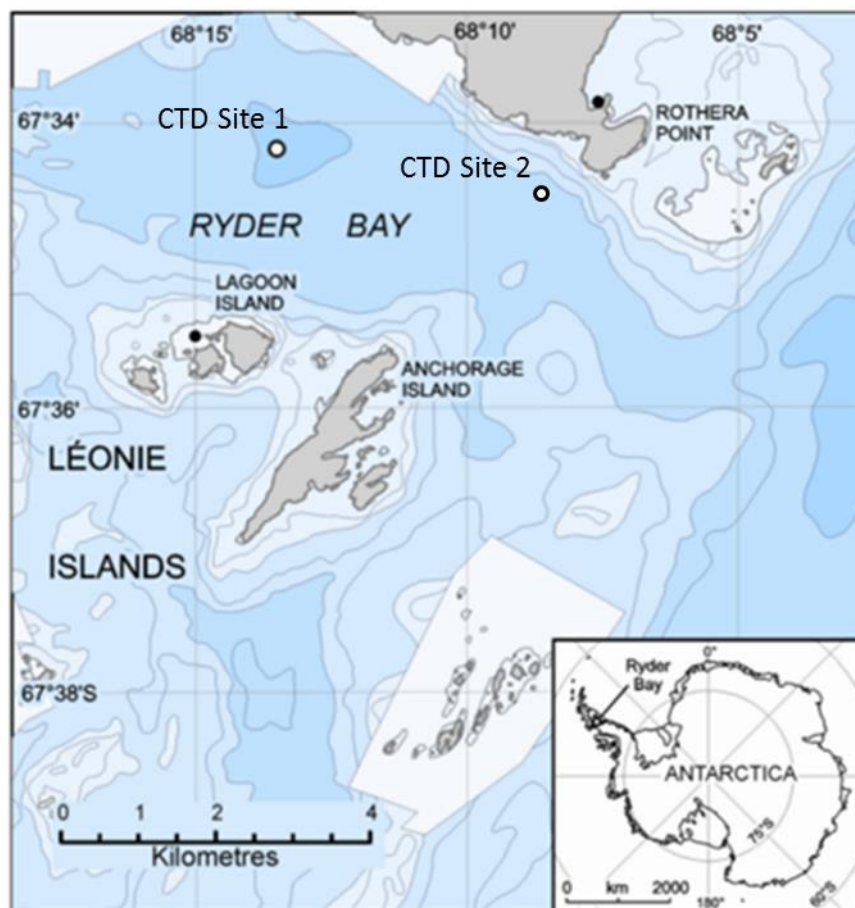


Figure 5-1: Map view of Ryder Bay and the location of Rothera Research Station on Rothera Point, and the location of RaTS CTD Sites 1 and 2. Inset shows the location of Ryder Bay in relation to the rest of the Antarctic continent.

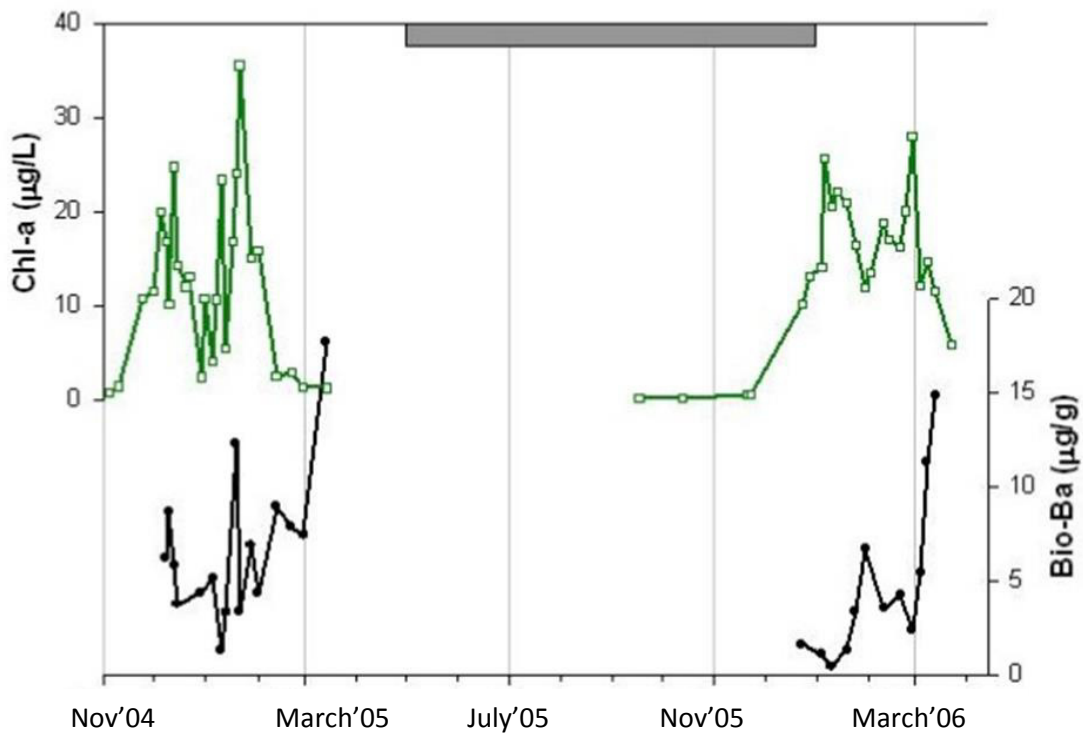


Figure 5-2: A preliminary time series of biogenic barium (particulate) and Chl-a concentrations measured at RaTS by Carson (2008)

oceanographic and biological measurements taken from a fixed site. The oceanographic setting of Ryder Bay is largely controlled by the circulation and characteristics of Marguerite Bay and the larger context of the WAP. Proximity to glacial ice on land plays an important role, with glacial meltwater from the retreating Sheldon Glacier flowing directly into Ryder Bay (Peck et al. 2012). The Bay is also seasonally covered by sea ice, the extent and thickness of which varies interannually, as do the timings of sea ice advance and retreat (Perovich et al. 2004; Clarke et al. 2008). The timings and duration of sea ice extent have been linked to variations in vertical mixing and heat loss to the atmosphere, with positive feedback effects that can persist for multiple years (Venables et al. 2013; Venables & Meredith 2014).

The oceanographic setting of the WAP has been previously described in Chapter 4, with relatively warm, saline UCDW flowing onto the continental shelf from the midlayers of the ACC (Sievers & Nowlin 1984). As it does so it is modified by cross-shelf and vertical diffusion of heat and salt, mixing with overlying Antarctic Surface Waters (AASW) (Smith et al. 1999) (Klinck 1998). Intrusions of this modified UCDW (cooler and fresher than the offshore variety) flow into Marguerite Bay through deep channels such as the Marguerite Trough (Klinck 1998; Venables et al. 2016), making this the water mass present below 200 m in Ryder Bay.

Overlying the modified UCDW is AASW, which experiences large levels of air-sea interaction during sea ice-free months, becoming warmer and fresher in summer due to increased insolation and the addition of ice melt (Smith et al. 1999). This creates strong water column stratification in the summer, isolating deeper waters from the surface. In the winter months however, the water column is well mixed, with colder, more saline waters dominating the upper water column (upper 100 – 150 m). A deep (approximately 100 m) remnant of this winter mixed layer persists through the summer and is referred to as Winter Water (WW), marked by a subsurface temperature minimum (Meredith et al. 2004; Klinck et al. 2004).

The biomass in Ryder Bay is typically dominated by microplankton (mainly large solitary or chain-forming diatoms, as well as colonial phytoplankton) that bloom in summer (November-January) with chlorophyll *a* levels typically 20 to 25 mg m⁻³ at depths between 20 m and 60 m, followed by low chlorophyll *a* levels (0.2 to 0.6 mg m⁻³) throughout the winter (Clarke et al. 2008). However, there are large levels of inter-annual variability in the composition and duration of the blooms, with which will be discussed further in Section 3.2.

2. Materials and Methods

RaTS sampling events were conducted periodically with a full CTD cast, and a Niskin bottle closed at 15 m to collect discrete seawater samples for the measurement of dissolved inorganic nutrients and $\delta^{18}\text{O}$. The CTD was deployed from a rigid inflatable boat at CTD Site 1 in Ryder Bay (67.570°S, 68.225°W) twice a week throughout spring and summer months, with more sporadic, opportune sampling throughout autumn and winter due to ice cover of the bay. On occasions when CTD Site 1 was not accessible, seawater samples and a cast were taken from CTD Site 2 (67.581°S, 68.156°W), which is slightly shallower but oceanographically very similar (Figure 5-1).

Seawater samples specifically for Ba_d analysis were collected by station personnel at Rothera from the Niskin bottle sampling once a week throughout spring and summer months, and whenever was convenient during the autumn and winter months. For further detail of the sites and sampling protocols see Chapter 2 Section 2.2.

2.1. Physical oceanography

During every RaTS sampling event a CTD cast is conducted throughout the whole water column (520 m deep at CTD site 1; 300 m deep at CTD Site 2) using a SeaBird 19+ CTD, containing temperature, conductivity, and pressure sensors. Conductivity measurements are calibrated post-season using discrete measurements made on an Autosal 8400B salinometer, and by comparison with the SeaBird 911+ instrument carried on the *Laurence M. Gould* during

annual joint casts. Salinity is determined from conductivity and temperature, and density is determined from salinity and temperature.

The stratification of the water column is examined by calculating the mixed layer depth (the depth at which the potential density anomaly of the water column exceeds 0.05 kg m^{-3} of the surface value (Clarke et al. 2008), in addition to calculating the density differences between several different depth ranges (Hendry et al. 2010; Venables et al. 2013). These two sets of measurements are used together to elucidate the active depth of mixing, and the strength of the stratification of the water column.

Direct observations of the concentration and type of sea ice present in the bays around the Rothera Station are recorded weekly by station personnel. Ice type is characterised as “brash” ice (floating ice fragments), “pack ice” (drifting blocks of ice), “grease ice” (thin surface layer of frazil ice), “pancake ice” (discs of ice with raised edges), or “fast ice” (ice layers affixed to the shore) (Petrich and Eicken 2010). Each category is scored and weighted based on its contribution to the freshwater dynamics of the region: brash and pack ice are considered less important as they tend to be transported in and out of the bay rather than forming or melting *in situ*; grease and pancake ice are weighted more heavily because although they are thin, they do form and melt *in situ*; fast ice is considered to have the largest impact (Meredith et al. 2008, 2010). From these observations the sea ice coverage is quantified, with an overall score calculated from 0 (ice free conditions) to 1 (full fast ice cover of the bay). As these observations are made by a series of station personnel, this overall score is somewhat subjective, but seasonal and interannual changes in sea ice coverage have been found to be much greater than the differences in assessment between investigators (Venables et al. 2013). In this chapter, I have used the sea ice types described above to characterise the condition of sea ice coverage at the RaTS site throughout the year.

2.2. Biological oceanography

Multiple seawater samples were collected from the 15 m Niskin to be analysed for concentrations of silicic acid, nitrate plus nitrite, phosphate, and ammonia, as well as determination of the size-fractionated chlorophyll *a* (Chl-*a*) content. These samples were kept in the dark below 4 °C and transferred to Rothera Research Station, where filtrations and chlorophyll extraction was carried out within 60 minutes. Pigments were extracted into methanol/chloroform (Wood 1985) and the concentration was determined by fluorescence. This was performed on triplicate samples, which were separated into size fractions via a sequence of filters (20, 5, 2, and 0.2 microns) (Table 5-1) (Clarke et al. 2008).

<i>Size of filter</i>	<i>Type of filter</i>	<i>Fraction collected</i>
20 μm	Nylon mesh filter	Micro-plankton
5 μm	Membrane filter	Large nano-plankton
2 μm	Membrane filter	Ultra-plankton (small nano-plankton)
0.2 μm	Membrane filter	Pico-plankton

Table 5-1: Sequential filters used to size-fractionate chlorophyll measurements from RaTS

Samples for macronutrient analysis were filtered and stored in dark polyethylene bottles before being transported to the UK (refrigerated and kept in the dark), where they were analysed using standard autoanalyser protocols (Strickland & Parsons 1970). Detection limits were 0.3 μM for nitrate, 0.1 μM for nitrite, 0.2 μM for phosphate, and 1.2 μM for silicic acid (Clarke et al. 2008). Concentrations of ammonium were analysed at Rothera with ortho-phthaldialdehyde (OPA) and fluorometry (Holmes et al. 1999), with a detection limit of 0.01 μM (Clarke et al. 2008).

2.3. Dissolved barium

The unfiltered seawater samples collected at 15 m were refrigerated, kept in the dark, and transported to the UK, where they were analysed for dissolved barium concentrations using isotope dilution inductively coupled plasma mass spectrometry (ID ICP-MS) as outlined in Chapter 2 Section 4. Sample preparation and measurements for this RaTS data set were carried out solely in the Bristol Isotope Group, Earth Sciences Department, at Bristol University, using a Thermo-Finnigan Element-2 (SEM detector only) for the ICP-MS analysis. Samples were measured in two batches (as they arrived in two different shipments from RaTS), either on the 29th to 30th April 2015, or the 10th to 11th September 2015.

A mass bias correction coefficient (K) was calculated each time samples were analysed by measuring the ratio of $^{138}\text{Ba}/^{135}\text{Ba}$ in a 1ppb Ba natural standard solution prepared in 5 % (v/v) seawater (NASS-6 seawater standard of 5 ppb \pm 0.15 Ba), and comparing this to the average natural ratio reported in the literature (10.88). The isotope ratio determined in this solution varied between 10.7 and 11.4, with measured uncertainty across each sample run usually around 0.4 % and never exceeding 1.3 % (2*RSD). Within each run, this uncertainty was always less than the mass bias determined for each sample run, which was on average a 1.2 % deviation from the literature value (minimum deviation 0.47 %; maximum deviation 4.8 %).

Blank solutions of 3 % (v/v of concentrated reagent) HNO₃ in 18.2 MΩ·cm water were analysed to correct for background barium signal from the introduction system of the ICP-MS (During the analytical runs of RaTS samples: ¹³⁵Ba blank counts < 0.15 % of seawater sample counts; ¹³⁸Ba blank counts < 0.5 % of seawater sample counts), and a set of consistency standards were measured at regular intervals (see Table 2-5 and Table 5-3). A correction for any seawater matrix effects was applied to the blank measurements by monitoring the sensitivity of a natural standard solution in 3 % HNO₃ vs. a natural standard solution in 5 % seawater, before the blanks were subtracted from sample counts.

Seawater standards of comparable barium concentration to the samples show a long term external reproducibility of ± 1.7 % or better across all analytical runs from March to November 2015 (Table 2-5). Within each two day set of analytical runs, reproducibility of these seawater standards was ± 0.5 % or better (April 2015) and ± 2 % or better (September 2015) (Table 5-3) Although none of these seawater standards have a certified barium concentration, accuracy was checked consistently against the average measurements of the same standards, measured using a Thermo-Finnigan Element-XR at the School of Earth and Ocean Sciences, Cardiff University (Chapter 2 Section 5). High precision analyses were necessary for discerning relatively subtle Ba_d changes throughout the time series, particularly to distinguish seasonal variation and any significant differences between the years studied. The full range of Ba concentrations observed at the RaTS site from 23/03/2013 to 13/01/2015 was 76 nM to 94 nM.

	Standard:	In-house Standard 1	NASS-5	NASS-6
Bristol	<i>2*RSD</i>	1.34 %	3.26 %	1.73 %
	<i>n</i>	72	33	70
	<i>Average [Ba](nM)</i>	73.5 ± 1.0	37.4 ± 1.2	49.3 ± 0.9
Cardiff	<i>2*RSD</i>	1.29 %	1.53 %	1.22 %
	<i>n</i>	23	22	23
	<i>Average [Ba] (nM)</i>	73.7 ± 1.0	37.0 ± 0.6	49.5 ± 0.6

*Table 5-2: Reproducibility of standards measured in Bristol from March to November 2016. Data from Cardiff (measured in 2014) provided for comparison. Values given are 2*relative standard deviation (2*RSD). Errors from In-house Standard 1 (from the Scotia Sea, 100 m depth) are considered most applicable to the samples reported in this chapter.*

	Standard:	In-house Standard 1	NASS-6
29th-30th April 2015	<i>2*RSD</i>	0.5 %	0.4 %
	<i>n</i>	7	7
	<i>Average [Ba] (nM)</i>	74.1 ± 0.4	49.1 ± 0.2
10th-11th September 2015	<i>2*RSD</i>	2.09 %	1.36 %
	<i>n</i>	7	7
	<i>Average [Ba] (nM)</i>	72.9 ± 1.5	49.9 ± 0.7

Table 5-3: Reproducibility of standards measured in Bristol during the running of RaTS samples (29th-30th April 2015 and 10th-11th September 2015). Values given are 2*relative standard deviation (2*RSD).

2.4. Oxygen isotopes and water mass fractions

Seawater samples for oxygen isotope analysis were also collected routinely from the Niskin bottle closed during CTD casts. These samples were transported to the UK and analysed for the ratio of stable oxygen isotopes at the Natural Environment Research Council Isotope Geosciences Laboratory (NIGL) at the British Geological Survey. Samples were equilibrated with CO₂ (Epstein & Mayeda 1953) using a VG Isoprep 18, with ¹⁸O/¹⁶O ratios then measured on a SIRA 10 mass spectrometer. Results were reported in standard δ¹⁸O notation, with reference to VSMOW. Regular duplicate analyses were used to establish data precision, which is typically ± 0.02 ‰ (Meredith et al. 2010).

From the δ¹⁸O and salinity measurements from 15 m water depth, a three-end-member mass balance was used to derive the relative contributions of sea ice melt, meteoric water, and Circumpolar Deep Water (CDW) to the sample, using the same method as discussed in Chapter 4 section 3.3.

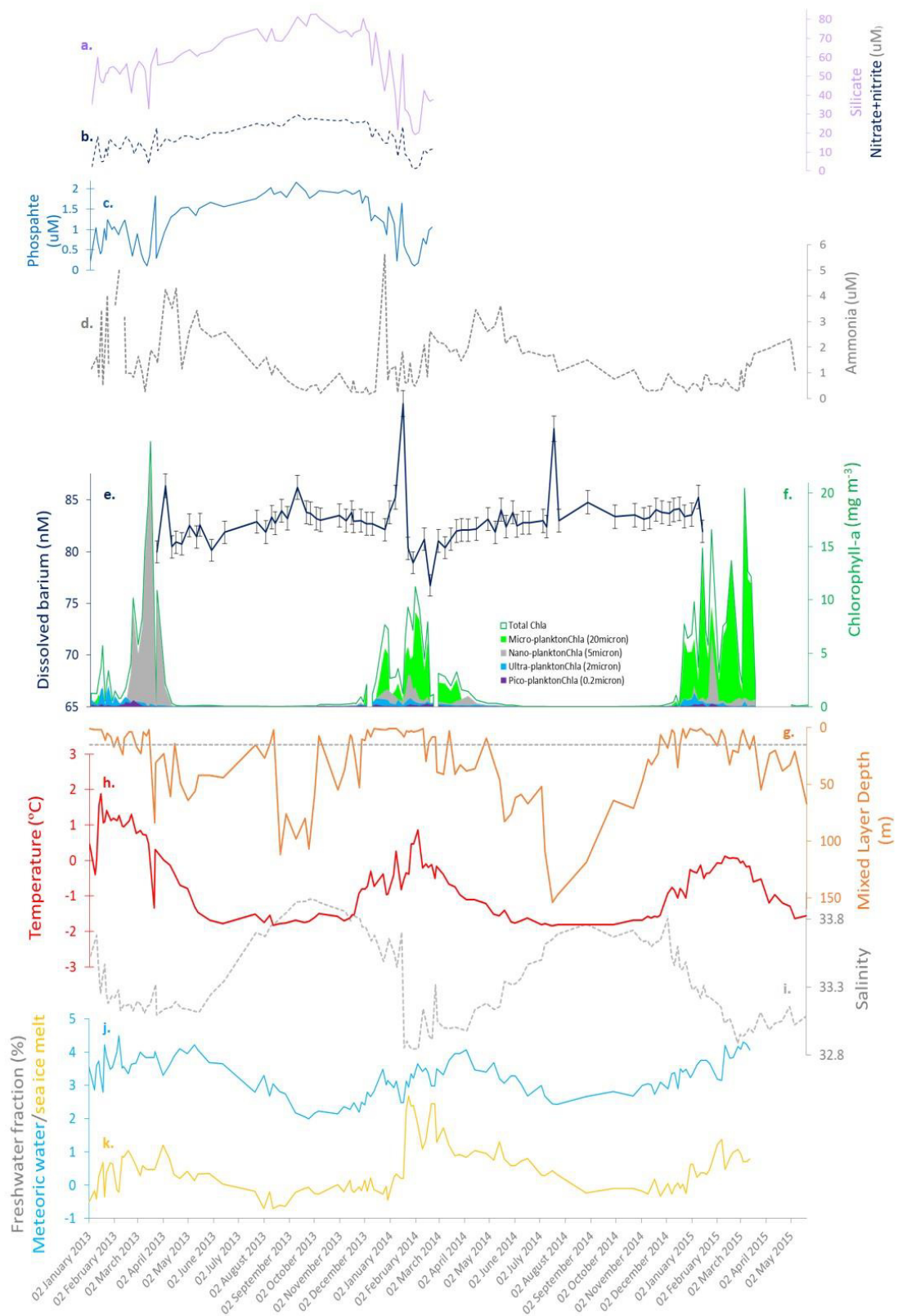
3. Results

The record of water properties from the sample site presented here covers a two and a half year period from late Summer 2013 to Autumn 2015, with Ba_d measurements covering from early Autumn 2013 to mid-Summer 2015 (Figure 5-3 and Figure 5-4). Throughout the two years sampled for Ba_d, concentrations show seasonal variation greater than the uncertainty on the measurements; this variability can be linked to seasonal changes in the structure of the water column. There is little inter-annual variation in the broad behaviour of Ba_d between 2013 and 2014, despite notable inter-annual variation in other parameters. There are also several Ba_d events (highs/lows of Ba_d concentration) that occur at different points throughout the sampling period that will be described in detail.

3.1. Seasonal variation

Seasonal variation at the RaTS site is observed in the structure of the 500 m water column (Figure 5-5), the onset and changing nature of sea ice cover, the input of freshwater, the cycling of nutrients, and the response of primary productivity to changing temperatures, light, and nutrient availability. Seasonal plots of potential temperature vs. salinity can be used to identify the different water masses present, and the changing influence of each throughout the year (Figure 5-6). Modified UCDW is the most saline endmember (salinity 34.5; 1°C) in all seasons, with the coldest waters occurring in the winter mixed layer (-1.5°C to -2°C; salinity 33.5 to 34) (Winter and Spring) and the WW remnant layer (-1°C to -1.5°C; salinity 33.5 to 34) (Summer and Autumn). AASW is present in summer and autumn (>0°C; salinity <33.5), with the temperatures of surface waters decreasing through the latter half of the autumn. The specific seasonal characteristics observed at the site are described in the following sections.

Figure 5-3: (next page): Time series plots of water properties at sample site at 15 m depth from January 2013 (RaTS Event #1427) to May 2015 (RaTS Event #1687). From top to bottom, a. Silicic acid (μM); b. Nitrate plus nitrite (μM); c. Phosphate (μM); d. Ammonia (μM); e. Ba_d (nM); f. Size fractionated Chl-a (mg/m^3) (green outline - total Chl-a; filled bright green – micro-plankton [$> 20 \mu\text{m}$]; filled grey – large nano-plankton [5 to $20 \mu\text{m}$]; filled blue – ultra-plankton (small nano-plankton) [2 to $5 \mu\text{m}$]; filled purple – pico-plankton [0.2 to $2 \mu\text{m}$]); g. MLD (m); h. Temperature ($^{\circ}\text{C}$); i. Salinity; j. Fraction of freshwater attributed to meteoric water (%); k. Fraction of freshwater attributed to sea ice melt (%).



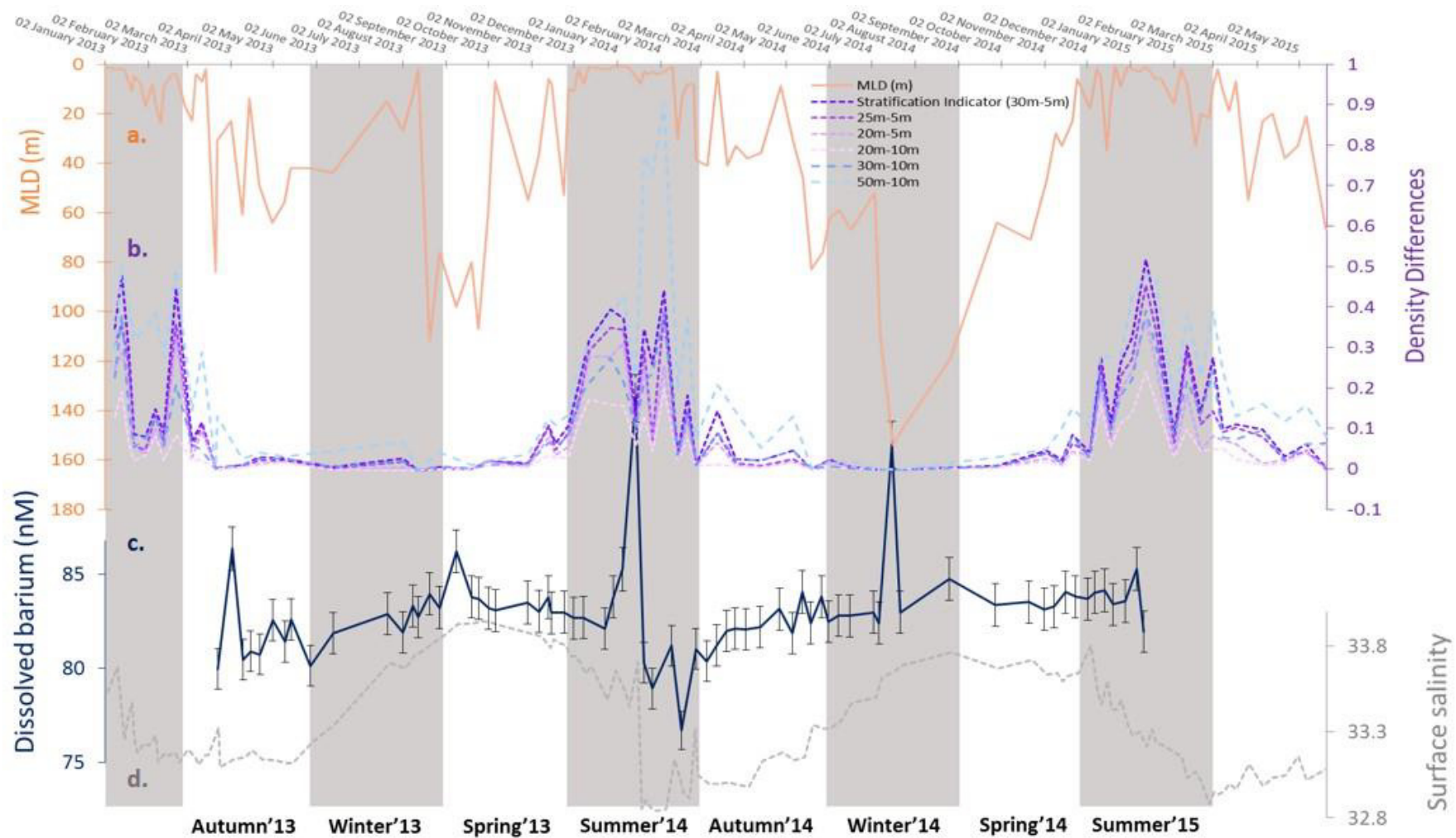


Figure 5-4: Time series at RaTS, from top to bottom, a. MLD (m); b. Density differences (kg/m³); c. Ba_d (nM) at 15 m, with error bars representing external reproducibility of 1.34 % (Table 5 3); d. Salinity at 15 m

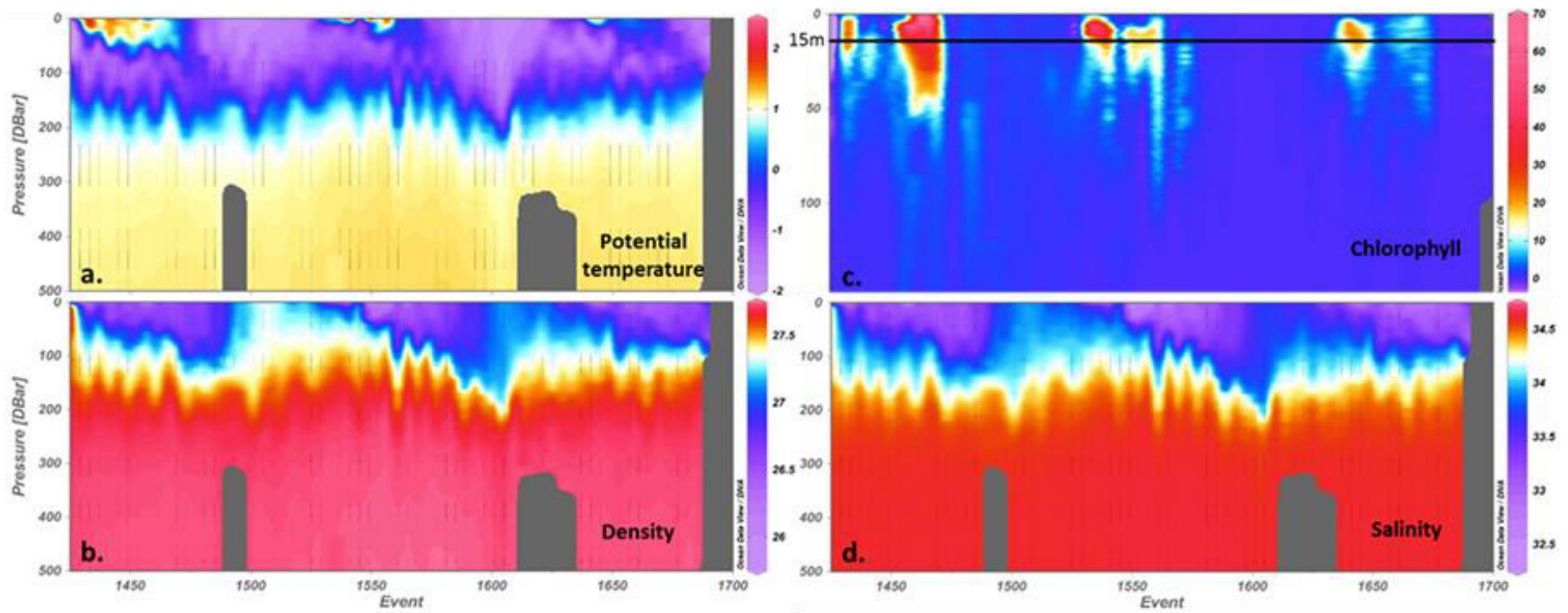
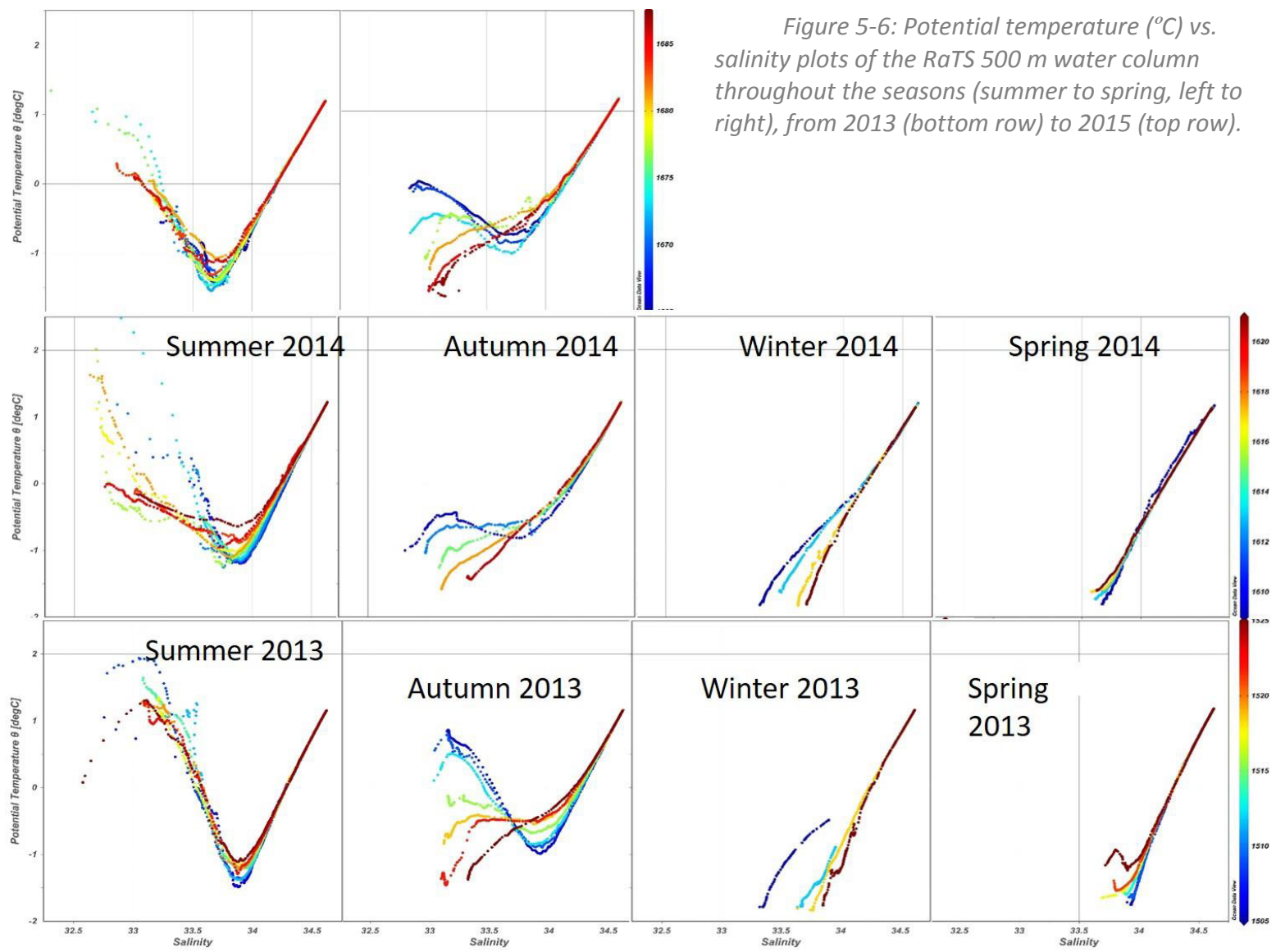


Figure 5-5: Time series plots of the 500 m water column at the RaTS site, from January 2013 (RaTS Event #1427) to May 2015 (RaTS Event #1687) a. Potential temperature ($^{\circ}\text{C}$); b. Density (kg/m^3); c. Chlorophyll (mg/m^3) in the top 150 m only, with a solid black line indicating the 15 m sampling depth; d. Salinity.



3.1.i Austral Autumn-Winter (March to end of August, 2013-2014)

In both of the Autumn/Winter periods recorded, the water column is characterised by a relatively deep mixed layer (typically 20 to 60 m in 2013; 10 to 160 m in 2014) (Figure 5-4). In autumn, particularly early in the season, the presence of warm surface waters and water column stratification persist from the previous summer (Figure 5-6). However, by the winter months the traces of this warmer, fresher surface water are no longer observed (Figure 5-6), and there is very little difference in the density of the top 50 m, indicating that this upper part of the water column has become fairly well mixed (Figure 5-4). The depth of the mixed layer ensures that the 15 m RaTS sampling is consistently sampling within the mixed layer during autumn and winter.

A peak in nanoplankton Chl-*a* early in autumn 2013 (March 2013) is accompanied by negative fluctuations in macronutrients, followed by a lagged peak in ammonia. The Ba_d record begins here with what is potentially a corresponding peak, although the positioning of the record makes this inconclusive. A relatively small microplankton bloom is recorded in early autumn 2014 (27th February to 21st March; no macronutrient data currently available for this period), with a similar lagged peak in ammonia in the following month, but no corresponding significant Ba_d peak (Figure 5-3 a-e).

The temperature of the water at 15 m is relatively invariant throughout the winter months (-1.5°C to -1°C), but salinity progressively increases, accompanied by decreases in both freshwater fractions, and therefore an increase in the influence of UCDW (Figure 5-3 h-k). A similar steady increase is observed in Ba_d and in the available macronutrient data (Winter 2013 only) (Figure 5-3 a-e). These Ba_d increases of approximately 4 to 6 nM through the autumn and winter months show a deviation around the yearly average concentration (83.0 nM) that is greater than the bounds of uncertainty ($\pm 1.34\%$, the long term reproducibility of In-house Standard 1 see Table 2-5). Throughout much of this period (June - August 2013) the surface of the bay was covered by fast ice (Figure 5-7). In July 2014 there is a significant (greater than 2*SD above the yearly average) peak in Ba_d concentration, coincident with a sudden increase in the MLD to approximately 150 m (Figure 5-4 a and c) but no notable changes in any other parameters.

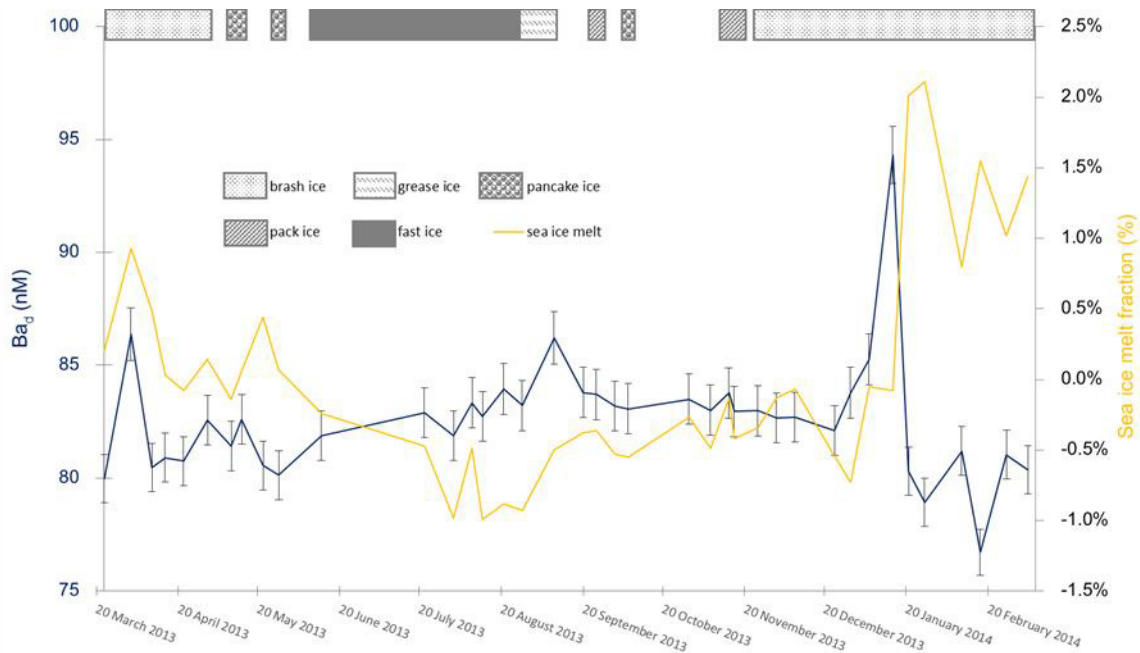


Figure 5-7: Times series showing Ba_d (nM) at 15 m (blue line), with error bars representing external reproducibility of 1.34 % (Table 5-3), and the fraction of sea ice melt (%) at 15 m (yellow line). Characterisation of sea ice throughout the year is represented along the top of the figure: brash ice (stippled), grease ice (dashed lines), pancake ice (polka-dot), pack ice (hatched) and fast ice (solid).

3.1.ii Austral Spring (September to end of November, 2013-2014)

During the spring months of both the years studied, all parameters measured at 15 m are predominantly invariant (Figure 5-4), though the mixed layer begins to shoal as re-stratification of the water column commences (Figure 5-4). Biological activity is negligible (Figure 5-4 f).

3.1.iii Austral Summer (December to end of February, 2013-2015)

In the summer months, temperatures at 15 m rise to maximum levels, and salinity decreases precipitously as fractions of meteoric water and sea ice melt rise (Figure 5-3 h-k). The mixed layer shoals to very shallow depths (< 10 m) and the changes in density between different layers of the upper 50 m of the water column show large increases (Figure 5-4), indicating a well-stratified water column. Because of this, the 15 m RaTS site is regularly sampling below the mixed layer (Figure 5-3 g).

With the exception of Summer 2012/13, the summer blooms are dominated by microplankton with smaller components of small and large nanoplankton (Figure 5-3 g), accompanied (where data are available) by decreases in the macronutrients. Unfortunately, Summer 2013/14 is the only year which fully captures the Ba_d behaviour across the whole of the bloom period, with the bloom itself relatively small at 15 m in this year (greater concentrations of Chl-a are observed at < 15 m depth – see Figure 5-5 c). However, during the beginning of the

microplankton bloom in 2013/14 and 2014/15 Ba_d appears to stay fairly constant (Figure 5-3 f and g). Several interesting features then present themselves in Summer 2013/14: the initial peak in total Chl- a and microplankton Chl- a , coincident with a large spike in ammonia concentrations (24th to 30th December 2013), suddenly decreases and remains low for several weeks, before increasing again in the latter half of January. This trough in the Chl- a record corresponds with a large positive Ba_d peak in early-mid January (Figure 5-3 f and g) and a negative spike in the density differences in the upper 50 m of the water column (Figure 5-4 b and c).

3.2. Interannual variation

Despite the seasonal variations in Ba_d concentration discussed in the previous section, there is no significant inter-annual variability between the two years studied. The increased concentration observed from March to September (austral autumn/winter) is of a similar magnitude in both 2013 and 2014, as is the steady state observed from September to December (austral spring), with concentrations all within range of the yearly average. Spring 2013 exhibits higher maximum salinity values than spring 2014, with corresponding lower fractions of meteoric water. There are also notable yearly differences in the profile of the mixed layer depth, with winter 2014 exhibiting a very deep mixed layer (150 m - Figure 5-4 a) comparable to the Deep Winter Mixing Years discussed by Venables et al. (2013).

It is unfortunate that barium sampling only fully covered one summer season, as a significant peak and trough in Ba_d concentration occurs from December to March 2013/14 that cannot be compared to behaviour in any other years. The timing, size, and composition of the summer chlorophyll bloom is very different over the three years investigated: in January to February 2013 the total Chl- a concentrations are relatively very low, followed by a peak in large nanoplankton (5 μm) in March/April (later summer/early autumn). The two subsequent blooms take place within the summer months, and are dominated by microplankton (20 μm), with much smaller contributions from nanoplankton that peak at approximately 3 to 5 mg/m^3 in February. The 2013/14 summer bloom appears to occur higher in the water column (<15 m) (Figure 5-5 c) with concentrations of Chl- a at 15 m low relative to other years (average total Chl- a : 4.5 mg/m^3), and divided into three separate peaks (the third, much smaller peak occurring in early Autumn), whilst the 2014/15 summer bloom exhibits consistently higher Chl- a concentrations at 15 m (average total Chl- a : 8.1 mg/m^3) throughout the summer months and into early Autumn (Figure 5-3 f).

Summer 2013/14 is also notable for exhibiting a sharp increase in the proportion of sea ice melt observed in mid-January (up to 2 %), accompanied by a sharp drop in salinity (Figure 5-3

l and k). In other years the increase in sea ice melt fraction increases steadily through the summer months, rarely exceeding 1 %.

4. Discussion

4.1. Behaviour of Ba_d in relation to biology

Significant inverse relationships have been observed between Ba_d and biological activity in isolated instances in other regions, with Ba_d decreases corresponding with phytoplankton blooms in a manner suggestive of biological uptake or association (Canadian Arctic (Thomas et al. 2011); North Pacific (Esser & Volpe 2002)). However, as discussed in previous chapters, Ba_d is not generally strongly correlated with NO_x or PO_4 , indicating that it is not taken up into or associated with organic matter in surface waters (Griffith & Paytan 2012), and surface Ba_d concentrations at the WAP do not show any significant positive relationship with indicators of primary productivity (Chapter 4 Section 4.4).

This finding in the wider WAP is supported by the record produced for the RaTS site, with no obvious negative relationship observed between bloom activity and Ba_d (Figure 5-3). Whilst there is a significant decrease in Ba_d in summer 2013/14, coincident with the second peak in the microplankton bloom, there is no similar decrease during Summer 2014/15, despite the presence of a Chl-*a* peak of similar intensity. It must be considered that the 2013/14 Summer bloom was in fact much larger than the 15 m Chl-*a* measurements suggest, as greater biological activity was taking place within the mixed layer, shallower than 15 m (Figure 5-5 c). However, whilst it is possible that this bloom activity could have been depleting Ba_d concentrations higher in the water column, the stable, well-stratified nature of the water column during this period would have prevented this Ba_d -depleted water being subsequently mixed down to the 15 m sampling depth (Figure 5-4).

There is some indication of more slight decreases in Ba_d concentrations associated with the Chl-*a* blooms, perhaps showing some lag behind the onset of intense phytoplankton activity (23/03/2013, 24/12/2013, and 13/01/2015). However, only one of these decreases is greater than the uncertainty on the measurements (80 nM on 23/03/2013), and this occurs at the very beginning of the record whilst the others appear at the termination of the record (82 nM on 13/01/2015) or potentially masked by a subsequent peak in Ba_d concentrations (discussed in Section 4.2; 82.1 nM on 24/12/2013), thus it is only possible to speculate that the biological activity in Ryder Bay may be exert a minor control on surface Ba_d concentrations.

Given the coincidence of the timings, it is impossible to categorically refute a connection between the Summer 2013/14 Ba_d minimum and the activity of the diatom bloom. However, the lack of a Ba_d response of comparable magnitude associated with either the end of the 2012/13

nanoplankton bloom or the onset of the diatom bloom in 2014/15 suggests that the behaviour of Ba_d during the 2013/14 diatom bloom may be the result of simultaneous mixing/dilution events (discussed in further detail in Sections 4.2 and 4.3) that have overprinted any slight biological control.

4.2. Vertical mixing and the enrichment of Ba_d in the water column below 15m

Throughout the autumn and winter months a steady increase of 4 to 6 ± 1 nM is observed in Ba_d concentrations at 15 m as stratification decreases and the upper water column homogenises (Figure 5-4). During this period, air-sea interactions are modulated by the development and expansion of sea ice (Figure 5-7), and the deepening of the mixed layer ensures that the 15 m sampling depth is almost always within this layer. The increase in Ba_d as the winter mixed layer develops is commensurate with increases in the macronutrients (Figure 5-3 a-c), and suggests an input from deeper waters below the mixed layer. This could be attributed to two main sources: remnant WW enriched in Ba_d from brine rejection during sea ice formation; or waters below the mixed layer enriched in Ba_d due to recycling of biogenic particulates, either in the water column itself or as fluxes from shelf sediments. Conversely, the increase in Ba_d could be result of decreased air-sea interactions, resulting in a lower input of atmospheric particulates for barium to adsorb onto, thus increasing the standing pool of Ba_d in the near surface throughout the season.

Addressing the first possibility, Antarctic sea ice is known to contain lower concentrations of Ba_d than the surface seawater in this region (sea ice Ba_d : 10 to 40 nM (Lannuzel et al. 2011)), although it is not known how much of this decrease difference is due to rejection during sea ice formation, and how much the Ba_d pool within sea ice may be depleted by biogenic or abiotic barite precipitation post-formation (discussed in Chapter 4 and investigated further in Chapter 6). Although the degree of enrichment is difficult to quantify, it is likely that brines expelled during sea ice formation will contain higher levels of Ba_d than the ambient seawater. These dense brines sink through the water column until they reach a level of neutral buoyancy within the WW, and could therefore enrich these waters with higher levels of Ba_d in a similar fashion to that proposed for WW enrichment of dissolved Al at this site (Hendry et al. 2010).

Progressive enrichment of Ba_d with depth is seen throughout the global ocean, and has been observed in WAP waters, with concentrations increasing by 3 to 6 nM over the upper 100 m of the water column (see Figure 4-3). This increase is thought to be due to recycling of particulate barium phases, possibly in conjunction with the remineralisation of biogenic silica (Lea & Boyle 1993; Jeandel et al. 1996; Jacquet et al. 2005; Horner et al. 2015). Depth profiles from the WAP continental shelf also displayed an approximately 5 nM higher concentration of

Ba_d throughout the water column in comparison to nearby stations in the open ACC (Chapter 4 Section 5.2 and Figure 4-3), indicating a potential enrichment of shelf bottom waters due to fluxes from the sediment. Such epibenthic Ba_d fluxes have been observed in pore water profiles from the Arabian Sea and the Equatorial Pacific (Schenau et al. 2001; Paytan & Kastner 1996), and benthic incubation experiments that have directly measured barium fluxes from California continental margin sediments (McManus et al. 1998; McManus et al. 1994).

Without the benefit of Ba_d profiles throughout the whole water column (in particular, measurements close to the sediment-water interface) it is difficult to discern which of these potential contributors is most likely to be the source of the Ba_d enrichment below the mixed layer. It is notable that the level of Ba_d enrichment that accompanies mixing is not significantly different between the two years studied, despite inter-annual variation in the depth of the winter mixed layer (Figure 5-4 a) and the extent of sea ice formation (Figure 5-3 k). However, there are peak Ba_d events in April 2013 (86.4 nM), September 2013 (86.2 nM), January 2014 (94.3 nM), and July 2014 (91.9 nM) that are all associated with deepening of the mixed layer (or decreased stratification below the mixed layer in the case of January 2014), with the magnitude of the Ba_d increases greater during the deeper mixing events (Figure 5-4). Due to the one-dimensional nature of the time series, it is possible that variable advection and horizontal gradients in water masses could be the cause of these sudden Ba_d fluctuations. However, for these peaks in Ba_d to be vertical mixing signals, the deeper waters concerned would have to be enriched by up to 10 nM compared to surface waters. Although this magnitude of concentration increase is consistent with our knowledge of the distribution of Ba_d with depth on the WAP shelf (a 13 nM increase was observed over the 500 m water column at PaLLTER Station 200.100 (Figure 4-3)), achieving this magnitude would require mixing with shelf bottom waters (below 400 m), and it is unlikely that this deep mixing would result in such transitory Ba_d peaks. However, it is possible that the water column above 400 m in Ryder Bay is more enriched in Ba_d than equivalent depths further out on the shelf (such as PaLLTER Station 200.100, Figure 4-3). Recent data from high resolution deep sea gliders have shown that as CDW flows through the Marguerite Trough, interaction with bottom topography (overspilling sills separating consecutive sub-basins) causes progressive between shelf bottom waters and the overlying water column (Venables et al. 2016; personal comm. from M.P. Meredith and H. Venables). In this way, CDW may become progressively enriched in Ba_d through interaction with bottom waters as it flows through the Marguerite Trough, bringing higher Ba_d concentrations to the depth just below the mixed layer in Ryder Bay, which could be mixed up into the surface layer and result in the large magnitude peaks observed.

This enrichment of the relatively shallow waters just below the mixed layer with high concentrations of Ba_d could also be a more temporary phenomenon, caused periodically by brine rejection from sea ice formation or intense periods of biogenic matter regeneration. For peaks during the winter months (September 2013 and July 2014), set against rising background concentrations, Ba_d -enriched brines from sea ice formation are a credible candidate. These dense waters, sinking and settling at the base of the winter mixed layer, may be sporadically entrained up to the 15 m sampling depth by deeper mixing events.

The peaks observed in summer/autumn (April 2013 and January 2014) both occur in proximity to phytoplankton bloom activity. In particular, the largest Ba_d peak in January 2014 occurs in conjunction with a sharp drop in the density contrasts over the upper 50 m of the water column, indicating a sudden mixing event that may be responsible for the interruption of the microplankton bloom also observed at this point (Figure 5-3 e and f; Figure 5-4 b and c). As previously discussed, the main bloom at this point is concentrated higher in the water column (Figure 5-5 c) and the effects of the sinking and decaying of organic matter are reflected in the spike in ammonia concentrations observed at 15 m (Figure 5-3 d). The release of Ba_d from decaying phytoplankton has been observed in laboratory cultures (Ganeshram et al. 2003) and regularly invoked in discussions of barite formation within bioaggregates (Dehairs et al. 1980, 1990). During the sinking and decay of phytoplankton from both of these bloom events (Autumn 2013 and Summer 2013/14), Ba_d may be released from adsorbed particulate phases such as manganese or iron oxyhydroxides (Schenau et al. 2001; Balakrishnan Nair et al. 2005) that associated with the biogenic material in surface waters, thus enriching the waters below the mixed layer with relatively high Ba_d concentrations. The mixing events that immediately follow such bloom activity will therefore stir these higher Ba_d concentrations up to the 15 m sampling depth.

Another important detail of this proposed mechanism of Ba_d enrichment via phytoplankton decay is the difference in magnitude observed between the Ba_d peak following the nanoflagellate-dominated Autumn 2013 bloom (86.4 nM), and that following the microplankton-dominated Summer 2013/14 bloom (91.9 nM) (Figure 5-3 e and f). The association of a larger Ba_d peak with the microplankton-dominated bloom, despite its lower intensity total Chl-*a* (Figure 5-5 c), suggests that more Ba_d is released by the breakdown of microplankton (diatoms) than of nanoplankton. This ties in with our previous finding at the WAP, and the Scotia Sea more broadly (discussed in Chapter 4 and 3 respectively), that the barium-carrying particulate phases which release Ba_d at depth appear to either preferentially associate with microplankton (rather than nanoplankton) in surface waters, or to release Ba_d more readily

during microplankton decay. There is evidence to support either of these hypotheses, as particulates such as iron and manganese oxyhydroxides that are known to adsorb Ba_d (Schenau et al. 2001; Balakrishnan Nair et al. 2005) are also known to associate with diatom cell surfaces (Sternberg et al. 2005), whilst larger, denser skeletal material (such as diatom frustules or colonial aggregates) can act as ballasting material and increase the downward flux of biogenic material from the mixed layer (Wilson et al. 2012).

4.3. Dilution of surface Ba_d by high levels of sea ice melt

Sea ice melt is a significant secondary control on surface Ba_d concentrations along the WAP, with input of these melt waters diluting Ba_d to a greater extent than silicic acid, potentially due to barite precipitation within the sea ice itself (see Chapter 4 Section 5.3). As silicic acid measurements are not available for the entirety of the temporal record presented here, it is not possible to ascertain if a similar pattern of behaviour is exhibited seasonally at the RaTS site.

There is a statistically significant negative linear relationship between Ba_d and the fraction of sea ice melt (%SI) ($R^2 = 0.13$; $p = 0.002$; $n = 69$). However, it is difficult to draw conclusions from the %SI in this record due to the large control exerted on Ba_d by vertical mixing (discussed above in Section 4.2), which manifests itself in the %CDW term in the calculation of the freshwater fractions (see Section 2.4). Therefore the apparent general negative correlation between %SI and Ba_d may be a non-causal manifestation of the positive relationship between Ba_d and mixing with a larger component of deeper waters.

One event does occur in the record that supports our previous conclusions about sea ice as a secondary control on Ba_d distributions: the sharp Ba_d minima in late January 2014 is coincident with a sharp rise in %SI and persists through to March, with %SI also remaining at peak values of 1.5 to 2 % for this period (Figure 5-7). The effect of the sea ice dilution may appear exaggerated because of the transition from a Ba_d peak immediately prior to the sea ice melt event. However, the Ba_d values during this period of high sea ice melt fluxes are consistently lower than the yearly Ba_d average. This supports the conclusions drawn in Chapter 4 that sea ice melt exerts a negative control on Ba_d concentration only when fluxes of sea ice melt are high. In coastal polar regions where the sea ice regime is seasonally and annually variable, this sea-ice controlled re-distribution of barium between dissolved and particulate phases may reduce the reliability of Ba_{excess} in underlying sediment as a proxy for export productivity. The potential implications of this will be discussed further in Chapter 6.

5. Conclusions

During the two year period studied at the RaTS site there is a steady increase in Ba_d of approximately 5 nM throughout the autumn and winter months as the winter mixed layer develops and air-sea interaction is modulated by sea ice formation. This increase is a result of vertical mixing with Ba_d -enriched waters from below the mixed layer. Whilst shelf bottom waters may be enriched in Ba_d via dissolution of particulate barium phases within the sediment, local vertical mixing between these deeper waters and the 15 m sampling depth studied here is likely to be low over the timescales considered. Rather, waters just below the mixed layer (100 to 150 m) may become enriched in Ba_d throughout the year by three different processes: in the autumn and winter months the rejection of Ba_d -rich brines from sea ice formation; in the summer and autumn months, release of Ba_d from particulates associated with sinking and decaying matter from phytoplankton blooms; or mixing of near-surface layers with CDW that becomes progressively enriched in Ba_d upstream through bathymetric interaction with shelf bottom waters.

The association between particulate barium phases and the phytoplankton blooms is not obvious in the Ba_d record, with no clear inverse relationship between biological activity and Ba_d concentrations. However, significant Ba_d peaks are observed when mixing events coincide with bloom activity, indicating that there is an increase in Ba_d concentrations simultaneous with phytoplankton decay. This effect is strongest during the diatom bloom observed in summer 2014 (rather than the nanoplankton bloom in autumn 2013), indicating there is a greater Ba_d release associated with the recycling of diatoms. This may be because particulate phases such as Mn and Fe oxyhydroxides scavenge Ba_d in surface waters and are then themselves adsorbed onto diatom cell surfaces.

There is no significant inter-annual variation in the extent of seasonal Ba_d enrichment, despite the deeper mixed layer exhibited in 2014 relative to 2013. This lack of variation could be an artefact of two simultaneous processes, with deeper mixing bringing more Ba_d to surface waters, whilst the related reduced sea ice (Venables & Meredith 2014) may have increased the input of atmospheric particles that scavenge Ba_d from the mixed layer. Sea ice melt itself is shown to have a significant dilution effect on Ba_d , resulting in minimum Ba_d concentrations that can overprint the effects of other controls, though only when sea ice melt fluxes are high.

The subtle variations in Ba_d concentration discerned by this high-precision record have revealed that the decay of biogenic material, particularly microplankton, does release Ba_d to the water column, which may then be associated with the precipitation of barite. This supports previous observations by Carson (2008) that particulate barium fluxes peak following periods of

high biological productivity (see Figure 5-2). However the Ba_d record also shows that a similar level of Ba_d enrichment below the mixed layer is observed independently of intense biological degradation, suggesting that other processes such as sea ice brine rejection or progressive mixing with enriched shelf bottom waters may play an equally important role in local Ba_d distributions. In addition, the interactions observed between sea ice melting and surface Ba_d concentrations indicate that as well as the potential Ba_d enrichment of waters below the mixed layer through brine rejection during sea ice formation, barium may be redistributed within sea ice between dissolved and particulate phases in a way that could impact on the use of barium as a proxy for freshwater parameters or of export productivity in sea ice dominated regions.



Chapter 6

The behaviour of Ba_d in Arctic and Antarctic sea ice

1. Introduction

From previous chapters, it is evident that high fluxes of sea ice melt exert a secondary control on the concentration of Ba_d in surface seawater in coastal Antarctica, with observations showing that high levels of sea ice melt (derived from $\delta^{18}O$ and salinity measurements) are associated with anomalously low Ba_d relative to $Si(OH)_4$. This could be the result of non-conservative processes acting within sea ice to remove barium from solution, leaving sea ice melt depleted in Ba_d relative to other dissolved cations. Additionally, such sea ice melt would be expected to be high in particulate barium, and may thus impact the interpretation of particulate barium as a proxy for productivity in polar waters (Carson 2008; McManus et al. 2002).

An ideal location to investigate this further is in the northern polar waters of the Arctic Ocean, where the persistence of sea ice cover is thought to be the cause of the broadly conservative observed behaviour of oceanic Ba_d (Taylor et al., 2003) (see Chapter 1, Section 2.4.i). The main control on oceanic Ba_d distribution in this region is considered to be the distinct Ba_d concentrations input to the Arctic Ocean from different rivers of the Eurasian and North American continents, with fluvial discharge from the North American continent generally more enriched in Ba (Guay and Falkner 1998). In the Eurasian Basin of the Arctic Ocean, where the

samples studied in this chapter were collected (see Figure 6-1), Ba_d concentrations are relatively low, with surface and intermediate waters influenced mainly by Eurasian river run-off and Atlantic Water entering the Arctic through the Fram Strait (40 – 45 nM), and some deep water enrichment observed at the base of the water column (up to 50 nM) (Taylor et al. 2003; Sirevaag and Fer 2009; Seidov et al., 2015).

In this chapter I will investigate the behaviour of Ba_d in sea ice directly by measuring Ba_d concentrations in a number of sea ice cores collected to the north of Svalbard in the Arctic Ocean, as well as in a set of sea ice brine samples collected at Rothera Point at the WAP. The interstitial brine samples from Rothera are used to assess the applicability of the seawater barium ID-ICP-MS method to sea ice samples, and to broadly characterise the relationship between Ba_d and salinity at the WAP. The sea ice core samples from the Arctic offer a more detailed insight into the distribution of Ba_d throughout the sea ice system, and how the relationship between Ba_d and salinity may vary as the sea ice grows and melts.

The work in this chapter has been made possible by the provision of samples and ancillary data from the Norwegian Polar Institute as part of the Norwegian Young sea ICE cruise (N-ICE 2015) project. The Ba_d concentration of these samples was measured by Barney Butler (MSci University of Bristol).

1.1. Introduction to sea ice

Sea ice forms a distinct environment in high latitude ocean waters, playing an important role in the biological productivity, water mass circulation, and ocean-atmosphere exchange of heat and gases in polar regions (Walsh and Johnson 1979; Kushnir et al. 2002), that have impacts on the global climate system (McBean et al. 2005; Liu and Alexander 2007).

During the formation of sea ice from seawater, sea salt ions are excluded from the crystal lattice structure of the developing ice, in a process known as ‘brine rejection’ (Petrich and Eiken 2010). Approximately two thirds of salt ions present in seawater are rejected during initial ice formation (Maykut 1985), with small pockets of brine solution remaining in a network of branching, interconnected pockets and channels within the ice. These channels form microhabitats for sea ice algae (Brearley and Thomas 2002) which are adapted to survive in the extreme conditions of low light levels, variable nutrient levels and very low temperatures (Nelson Treguer 1992; Mitchell and Beardall 1996; Mogan Kiss 2006).

As well as hosting sea ice microbial communities (SIMCO), the release of nutrients, micronutrients, and particulates from melting sea ice is associated with ice edge phytoplankton blooms. In total, biological activity associated with Antarctic sea ice is thought to contribute 10

to 28% of Southern Ocean biological production (Ablemann and Gersonde 1991; Arrigo and Thomas 2004), playing a significant role in the export of carbon.

2. Materials and Methods

As mentioned above, the Arctic sea ice core samples were collected as part of the N-ICE cruise from 7th January to 23rd June 2015, with additional cores from the test cruise undertaken the preceding year (February 2014). The objectives of this project were to understand the effects of the young Arctic sea ice regime on energy fluxes, ice dynamics, and the associated ecosystem by sampling the sea ice and underlying sea water continually through the year as the sea ice formed and melted. In order to achieve this, the *R.V. Lance* was allowed to freeze into sea ice north of Svalbard in the Arctic Ocean in late December 2014, and to drift passively with the ice until the floe began to break up in Jun 2015 (see Figure 2-5 for full cruise track). During this time sea ice cores were collected, accompanied by sampling of the water column via a CTD rosette deployed through holes in the ice (Figure 6-1). Sea ice cores were divided into sample depth sections and allowed to melt, with unfiltered sub-samples for Ba_d measurement stored in parafilm HDPE bottles in the dark and transported to Bristol University for analysis.

Interstitial waters were sampled from Antarctic sea ice by K. Hendry from various locations around Rothera Point (Figure 6-2) by sackhole drilling between the 13th October 2005

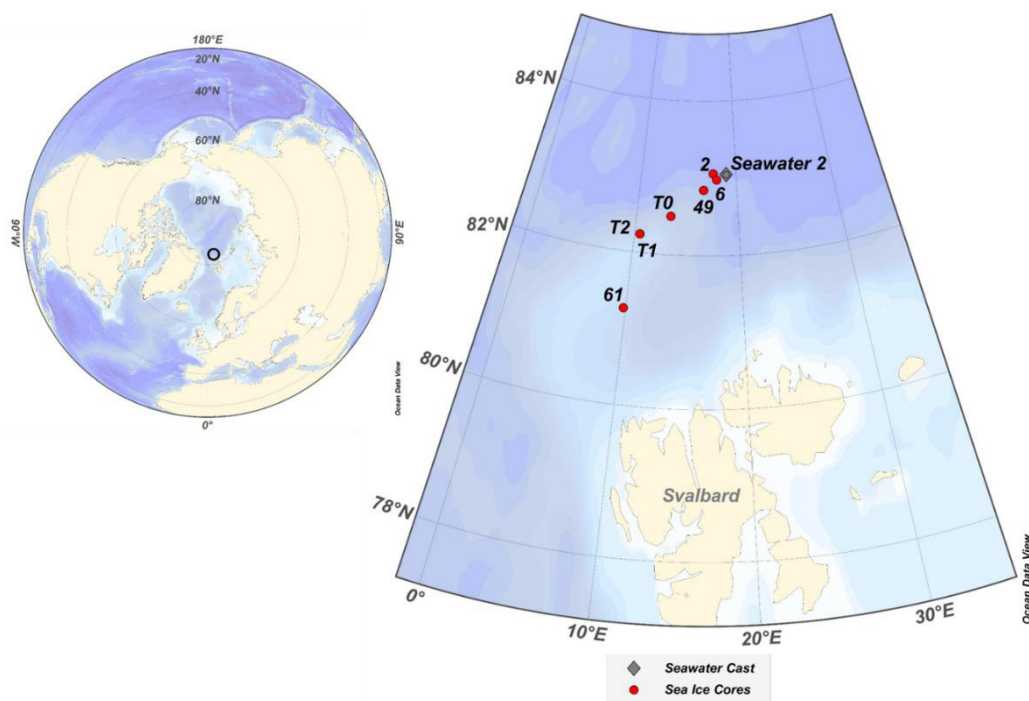


Figure 6-1: N-ICE sample locations in main figure, sea ice cores (red circles) labelled numerically, T denotes cores from the test cruise in 2014. Smaller inset shows black circle indicating location of sampling area in the context of the northern hemisphere.

and 21st November 2006. The sack hole drilling involved removing snow from the sea ice surface using a plastic edge, and drilling a hole into the sea ice, which was then cleaned of brash ice and contaminants, and covered for five minutes to one hour. The brine drained into the hole and was collected into clean HDPE containers. Samples were filtered at Rothera Station using 0.2 micrometer polycarbonate membranes (Whatman), the filtrate was then acidified using 1 ml HNO₃ per litre of brine before being transported to the UK and stored in the dark. Before being analysed for Ba_d, these samples had been previously used to measure cadmium (Cd) and aluminium (Al) (Hendry et al. 2009, 2010).

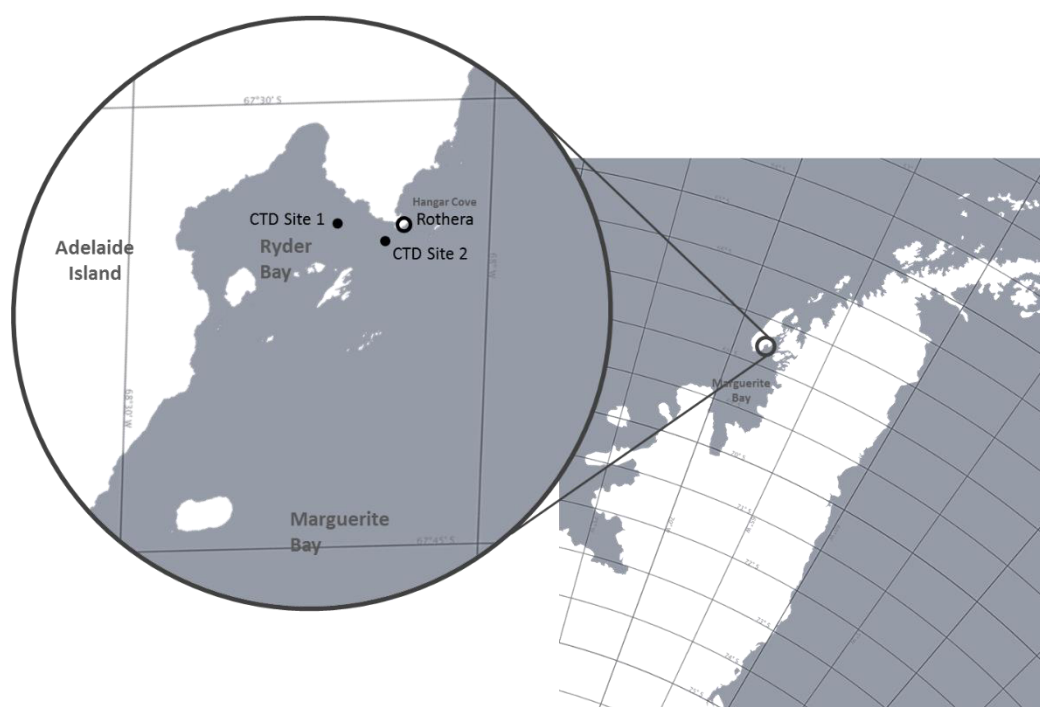


Figure 6-2: Map view of Ryder Bay, an inlet in Adelaide Island along the West Antarctic Peninsula. Interstitial sea ice brine samples were collected from location around Rothera Point in 2005/6 – CTD Site 1, CTD Site 2, Hanger Cove, the wharf of Rothera Station (within black circle marking Rothera Station).

2.1 Dissolved barium

The unfiltered sea ice samples from the N-ICE cruises (2014 test cruise and 2015 main project cruise) were analysed using isotope dilution inductively coupled plasma mass spectrometry (ID ICP-MS) as outlined in Chapter 2 Section 4. Sample preparation and measurements for this data set were carried out by B. Butler (MSci) in the Bristol Isotope Group, Earth Sciences Department, at Bristol University, using a Thermo-Finnigan Element-2 (SEM detector only) for the ICP-MS analysis.

The filtered, acidified sea ice brine samples collected at Rothera were analysed by K. Pyle using isotope dilution inductively coupled plasma mass spectrometry (ID ICP-MS) as outlined in Chapter 2 Section 4. Initial sample preparation and analysis took place in Cardiff University using a Thermo-Finnigan Element XR, with subsequent repeat sample preparation and analysis taking place at Bristol University using an Element-2.

2.1.i Ba_d estimates and isotope dilution spiking

It was expected that the range of Ba_d concentrations in the sea ice samples may be wider and less predictably distributed than in the seawater samples that had been measured previously. In particular, the large range in salinity of the interstitial brine samples (salinity 3 to 87) indicated that Ba_d ranges would exceed the minimum and maximum concentrations measured in Antarctic seawater (Chapters 3 to 5).

In order to achieve a spike to sample ratio of between 0.7 and 1 (see Chapter 2 Section 4.1.iii), the approximate Ba_d concentration of the sample must be known, as this is used to determine the volumes of sample and ¹³⁵Ba-enriched spike solution to be used (see Table 2-1). Ba_d concentrations of Rothera brine samples were initially estimated using Cd concentrations previously measured in the same samples (Hendry et al. 2009), which have been found to have a conservative relationship with regard to salinity (Equation 6-1). Using the average salinity and average Ba_d concentration of WAP seawater (salinity 33.6; Ba_d 80 nM; from PaALTER samples – Chapter 4), an estimated ratio of Cd/Ba was calculated for WAP seawater of 0.011. This ratio was applied to Rothera brine sample [Cd] to estimate the [Ba_d] for each sample.

$$[Cd] = 33.1 * S + 4.2$$

Equation 6-1: Relationship between cadmium (Cd) and salinity (S) in Antarctic seawater.

However, when samples were initially prepared using these estimated concentrations, and analysed at Cardiff University, the measured Ba_d concentrations varied significantly from the estimates (Figure 6-3). As a result of these inaccurate concentration estimates, the spike to sample ratios were significantly out of range, casting doubt on the reliability of the data.

The concentrations derived from this unsuccessful first attempt were used to re-calculate the volumes of sample and spike solution for each sample, and a second analysis was undertaken at Bristol University (Figure 6-3). The sample to spike ratios for this second analysis were all satisfactory (between 0.7 and 1).

For the subsequent analysis of the N-ICE sea ice core samples, salinity measurements were used to provide a rough initial estimate of Ba_d concentrations. In most cases these estimates were not accurate, and the sample to spike ratios were out of the acceptable range. The secondary preparation and analysis of samples, with sample and spike solution volumes refined by the Ba_d concentration measured in the first analysis, were therefore undertaken as general practice. The sample to spike ratios from secondary analyses were all satisfactory. The discrepancy in Ba_d concentration between analyses was generally ± 1 to 2 nM and was not systematic.

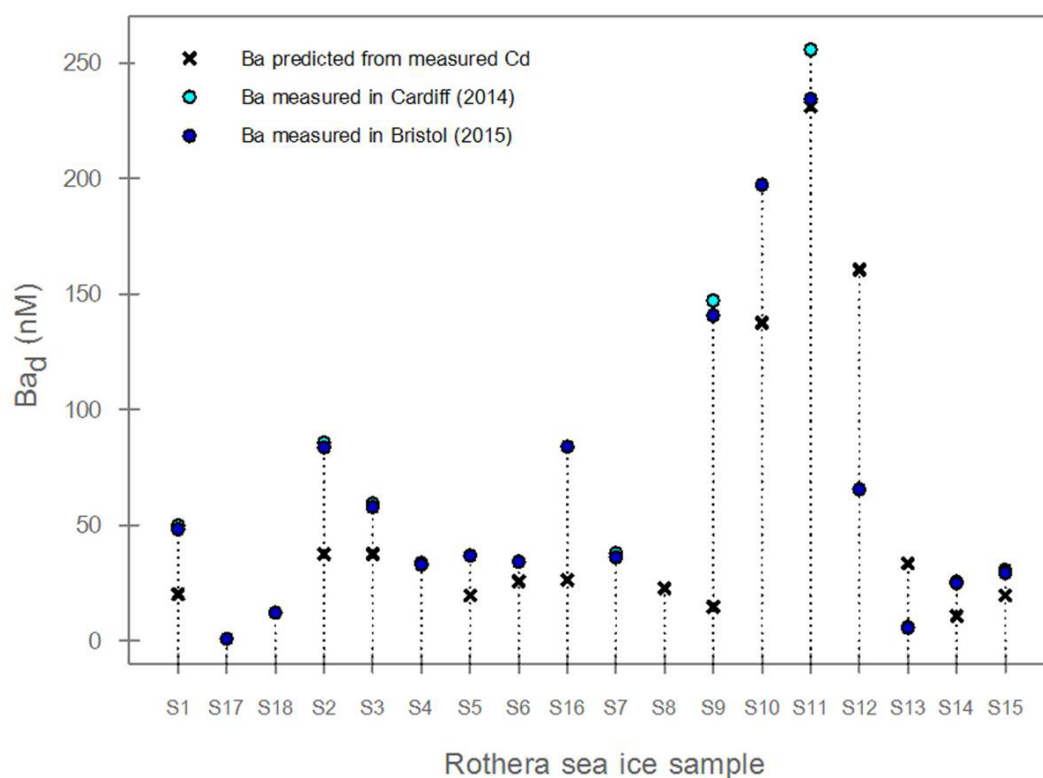


Figure 6-3: Ba_d concentrations in interstitial sea ice brines from Rothera Point. Ba_d concentration predicted from measured Cd concentration (Hendry et al. 2010) (black crosses); Ba_d concentration measured in Cardiff in 2014 using the sample and spike volumes calculated from predicted concentrations (cyan filled circles); Ba_d concentration measured in Bristol in 2015 using the sample and spike volumes calculated from concentrations measured in Cardiff (blue filled circles).

2.1.ii Correcting for matrix effects and assessing uncertainty

A mass bias correction coefficient (K) was calculated each time samples were analysed by measuring the ratio of $^{138}\text{Ba}/^{135}\text{Ba}$ in a 1 ppb Ba natural standard solution prepared in 5% (v/v) seawater (NASS-6 seawater standard of 5 ppb \pm 0.15 Ba), and comparing this to the average natural ratio reported in the literature (10.88). The isotope ratio determined in this solution varied between 10.7 and 11.5, with measured uncertainty across each sample run usually around 0.6 % and never exceeding 2.2 % (2*RSD). Within each run, this uncertainty was always

less than the mass bias determined for each sample run, which was on average a 1.1 % deviation from the literature value (minimum deviation 0.78%; maximum deviation 5.9%).

Blank solutions of 3 % (v/v of concentrated reagent) HNO₃ in 18.2 MΩ·cm water were analysed to correct for background barium signal from the introduction system of the ICP-MS (During the analytical runs of RaTS samples: ¹³⁵Ba blank counts < 0.16 % of seawater sample counts; ¹³⁸Ba blank counts < 0.15 % of seawater sample counts), and a set of consistency standards were measured at regular intervals (see Table 6-1 and Table 6-2). A correction for matrix effects was applied to the blank measurements by monitoring the sensitivity of a natural standard solution in 3 % HNO₃ vs. a natural standard solution in 5 % seawater, before the blanks were subtracted from sample counts. It is possible that the matrix effects for sea ice may be different to those for seawater, particularly at the salinity extremes. However, as time constraints prevented the testing of matrix effects in a range of media, the seawater matrix correction was applied to all sea ice samples.

Seawater standards show a long term external reproducibility of ± 1.7 % or better across all analytical runs from March to November 2015 (dates inclusive of Rothera brine analyses) and a reproducibility of ± 2.5 % across all analytical runs from February to March 2016 (period of analysis of N-ICE sea ice core samples) (Table 6-1 and Table 6-2). Although none of these seawater standards have a certified barium concentration, accuracy was checked consistently against the average measurements of the same standards, measured using a Thermo-Finnigan Element XR at the School of Earth and Ocean Sciences, Cardiff University (Chapter 2 Section 5). The NASS-5 and NASS-6 standards are most comparable to the Ba_d concentrations measured in sea ice samples. Unfortunately, none of the standards measured are comparable to the low Ba_d concentrations measured in some of the samples.

	Standard:	In-house Standard 1	NASS-5	NASS-6
Bristol	<i>2*RSD</i>	1.34%	3.26%	1.73%
	<i>n</i>	72	33	70
	<i>Average [Ba] (nM)</i>	73.5 ± 1.0	37.4 ± 1.2	49.3 ± 0.9
Cardiff	<i>2*RSD</i>	1.29%	1.53%	1.22%
	<i>n</i>	23	22	23
	<i>Average [Ba] (nM)</i>	73.7 ± 1.0	37.0 ± 0.6	49.5 ± 0.6

Table 6-1: Reproducibility of standards measured in Bristol from March to November 2016. Data from Cardiff (measured in 2014) provided for comparison. Values given are 2*relative standard deviation (2*RSD).

	Standard:	In-house Standard 1.1	In-house Standard 1.2	NASS-6
Bristol	<i>2*RSD</i>	1.19%	1.43%	2.52%
	<i>n</i>	14	28	23
	<i>Average [Ba] (nM)</i>	73.7 ± 0.9	72.6 ± 1.0	49.2 ± 1.2

Table 6-2: (previous page) Reproducibility of standards measured in Bristol from February to March 2016.

3. Results

3.1. Rothera sea ice brines (Antarctic)

As expected from the wide range of salinities observed, a wide range of Ba_d concentrations were measured in the fifteen interstitial brine solutions collected from Rothera (5 to 235 nM). The highest concentrations were seen in three samples from late winter/early spring of 2006 (140 to 235 nM), with the remainder of the samples not exceeding 100 nM. The lowest concentrations were recorded in November 2005 and 2006 (5 to 12 nM) (Figure 6-4).

Despite the significant variation between Ba_d concentrations predicted by [Cd] and the accurate Ba_d concentrations finally measured, the Ba_d in the brine solutions show a positive correlation with salinity (Figure 6-5). Positive correlations are also observed between Ba_d and inorganic dissolved nutrients (silicic acid, nitrate, and phosphate), although the clustering of the data make it challenging to determine the nature of the relationships (Figure 6-7 a).

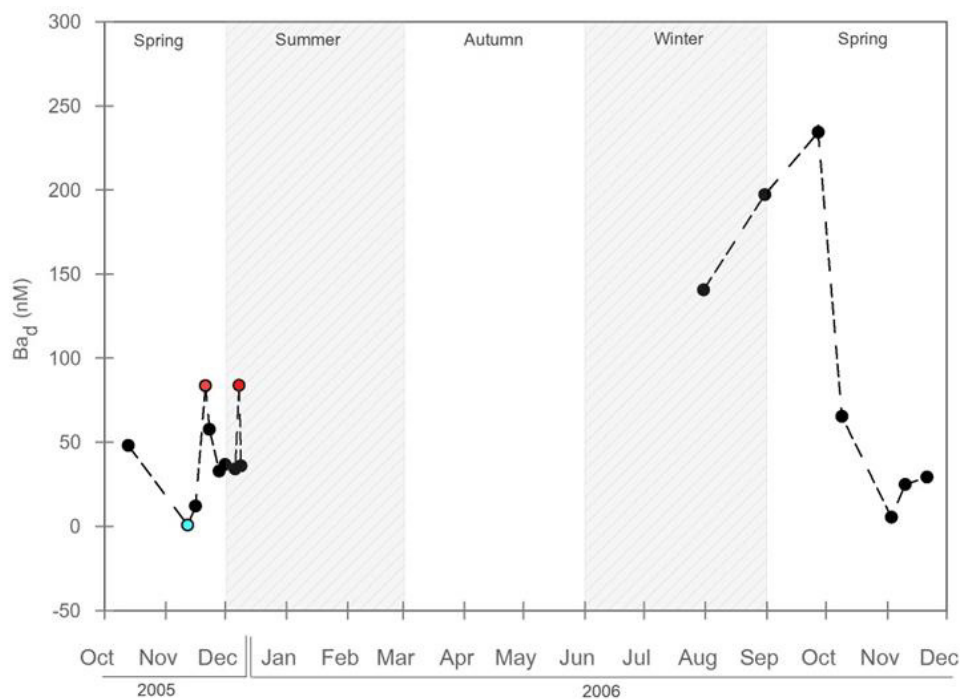


Figure 6-4: Time series of interstitial brines sampled at Rothera from October 2005 to December 2006, (black circles). Ba_d concentrations reported from the accurate second measurements, made in Bristol University. Seasons labelled, with summer and winter highlighted by grey hatched bands. Sample from the 12th November 2005 [Ba_d 0.7 nM] was a sample of melted snow, rather than interstitial sea ice brine (cyan filled circle); Samples from 21st November and 8th December 2005 [Ba_d 83.5 and 83.8 nM respectively] are samples of local seawater from Hangar Cove (orange filled circles).

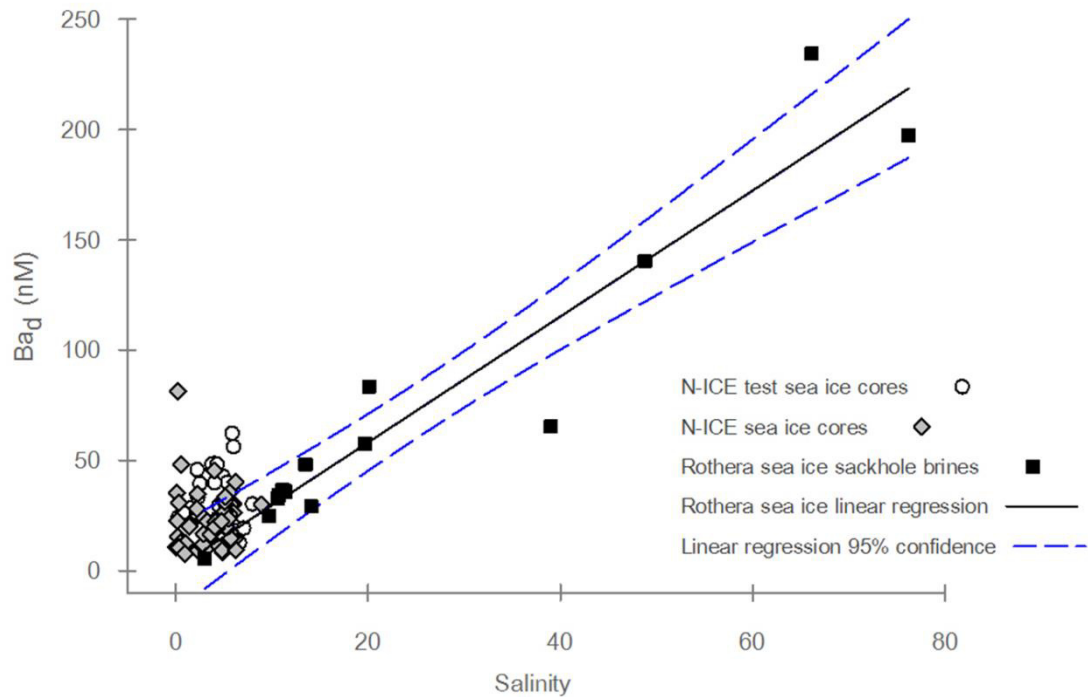


Figure 6-5: Ba_d concentrations (nM) vs. salinity in sea ice samples, with interstitial brine solutions from Rothera 2005/6 represented by filled black squares; whole sea ice cores from the Arctic N-ICE 2015 cruise represented by grey filled diamonds, whole sea ice cores from the N-ICE test cruise represented by light grey filled circles. The solid black represents the linear regression model (least squares) fitted to the Rothera sea ice samples, with blue dashed lines indicating the 95 % confidence boundary.

3.2. N-ICE seawater (Arctic)

Thirteen seawater depth profiles were analysed (97 samples in total) from CTD casts through the ice during the N-ICE cruise. A typical profile is shown in Figure 6-6. The range of Ba_d measured over the whole water column (surface to 4000 m) was 39 to 53 nM, a much smaller range than that observed in the seawater of the WAP or the Scotia Sea. From these samples Arctic seawater was characterised for comparison to sea ice as having an average Ba_d concentration of 44.0 nM, and an average salinity of 34.6.

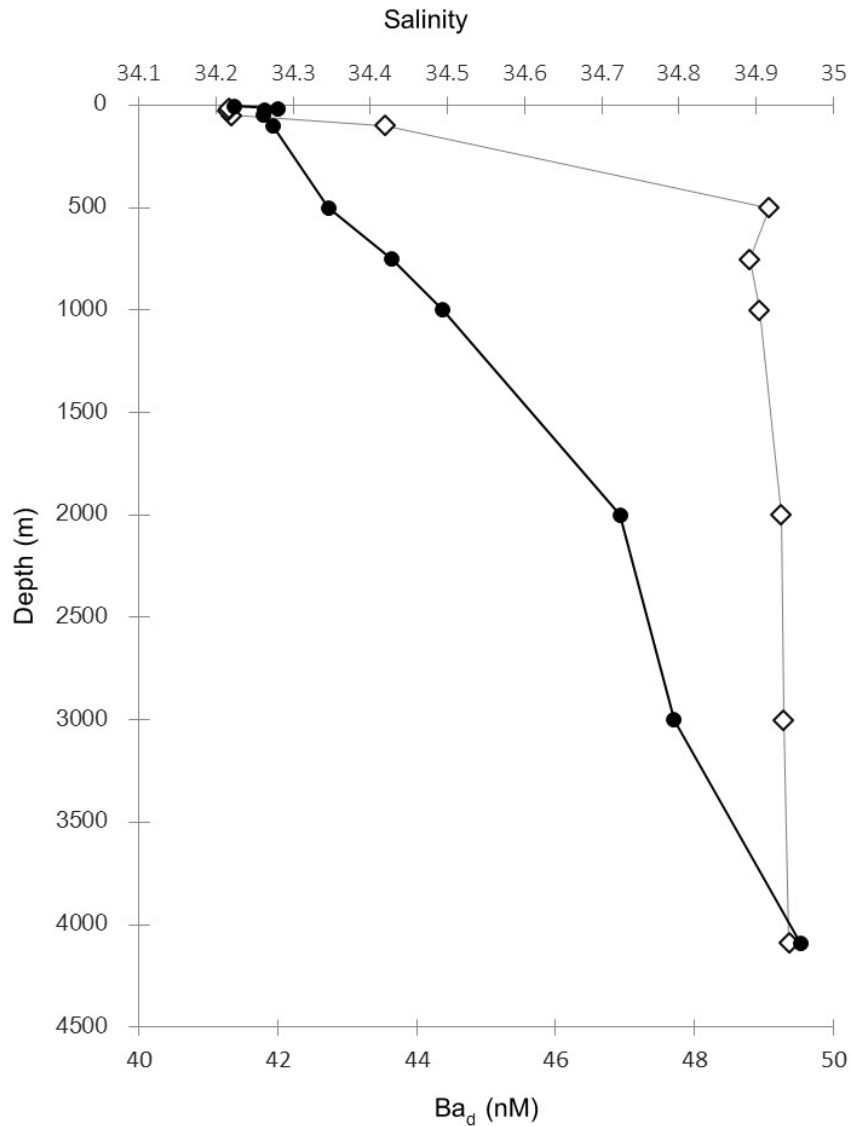


Figure 6-6: Ba_d (nM, filled black circles) and salinity (open diamonds) profiles with depth at Station 2, which can be regarded as representative of the water column throughout the study area.

3.3. N-ICE sea ice cores (Arctic)

78 sea ice core samples were analysed (from both the test cruise in 2014 and the official N-ICE cruise in 2015), displaying a larger total range of Ba_d (7 to 81 nM) than exhibited by Arctic seawater, with Ba_d concentrations varying within single cores by up to 50 nM (Figure 6-10). However, as these were whole-ice measurements, there were no samples with concentrations exceeding 100 nM, as found in the interstitial brine solutions from Rothera.

The salinity of the sea ice cores ranged from 0 to 9, and profiles of salinity down core do not show the typical 'C' shape of first year sea ice (Petrich and Eiken 2010), but show undulating

characteristics that suggest two- or multi-year ice (Figure 6-8). Two cores collected in the spring, Core 49 and Core 61, exhibit very low salinities (0 to 2) at the top of the core.

There is no obvious relationship between Ba_d and salinity in the Arctic sea ice core samples, although the bulk of the samples do fall within the error bounds of a curve describing the positive linear relationship seen in the Rothera sea ice brine samples (Figure 6-9). However, a proportion of the Arctic sea ice core samples collected in winter fall above this trend line.

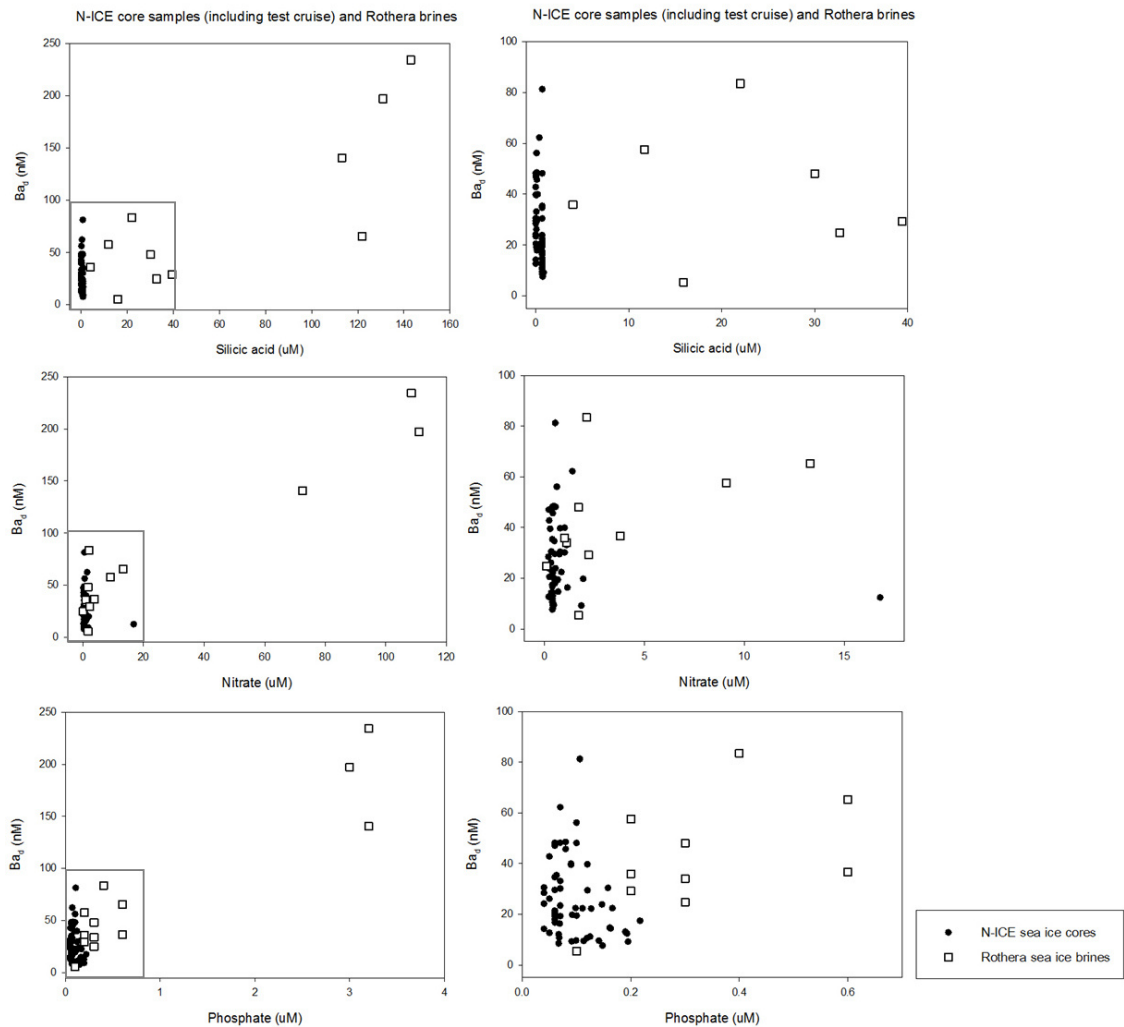


Figure 6-6: Relationship of Ba_d concentrations (nM) and macronutrient concentrations (μM) in sea ice samples. N-ICE whole sea ice cores represented by filled black circles; interstitial brine solutions from Rothera sea ice represented by unfilled black squares. Left column plots shows the full range of concentrations measured, with a grey square outline indicating the smaller range of concentrations displayed for clarity in the right hand plots. Top row plots show Ba_d vs. silicic acid; second row plots show Ba_d vs. nitrate; bottom row plots show Ba_d vs. phosphate.

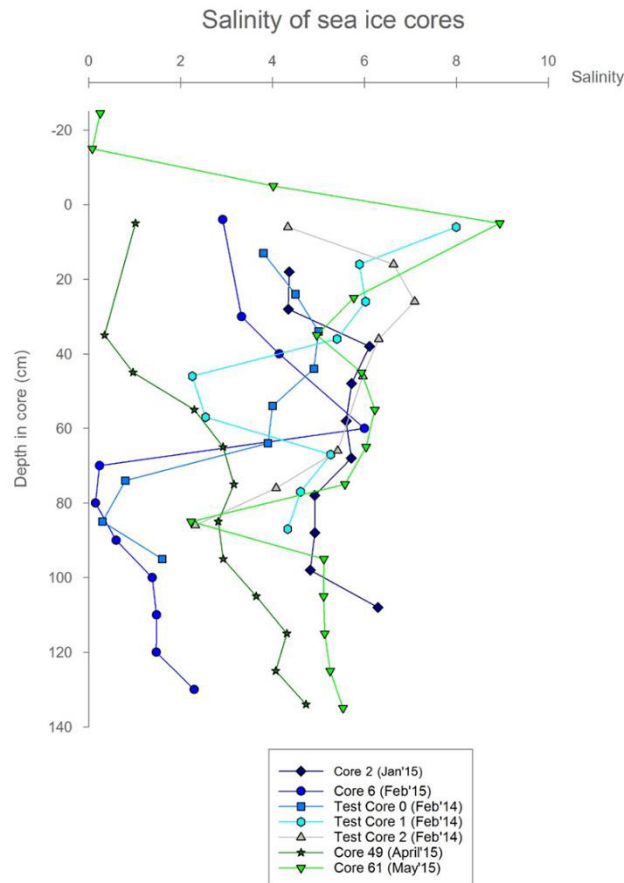


Figure 6-8: Salinity profiles with depth (cm) in whole sea ice core samples from the Arctic N-ICE cruise and test cruise; Core 2 (dark blue filled diamonds), Core 6 (blue filled circles), Test Core 0 (light blue filled squares), Test Core 1 (cyan filled circles), Test Core 2 (light grey filled triangles), Core 49 (dark green filled stars), and Core 61 (light green filled upside down triangles).

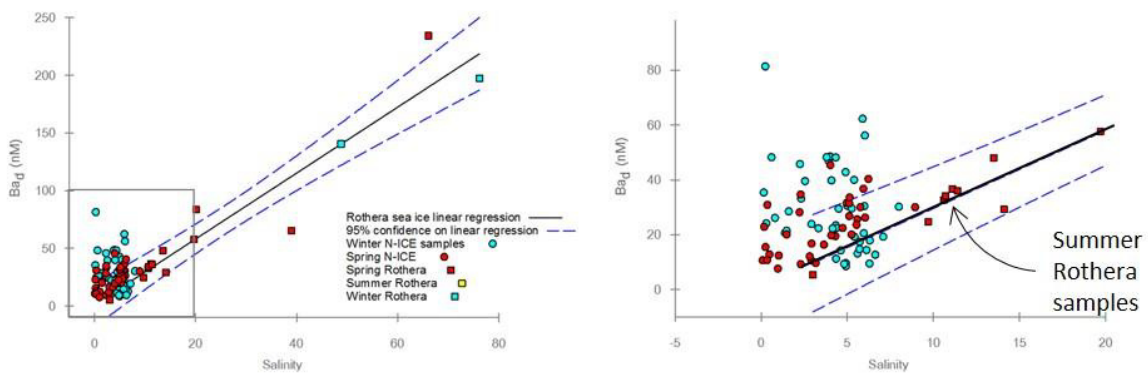


Figure 6-9: Relationship between Ba_d concentrations (nM) and salinity in sea ice samples. Filled circles represent N-ICE whole sea ice core samples from the Arctic (cyan – winter samples; red – spring samples), and filled squares represent interstitial brine solution from Rothera sea ice (cyan – winter samples; red – spring samples; yellow – summer samples (hidden behind spring samples in plot, but indicated by arrow in right-hand plot)). Solid black line represents linear regression model (least squares) fitted to Rothera sea ice brine samples, with blue dashed lines indicating the 95% confidence level of the model. Right-hand plot shows a smaller scale of concentrations (indicated by the grey rectangle outline in the left-hand figure) for clarity.

When cores are considered individually, some show a positive correlation between Ba_d and salinity (Test Cruise Core 0, Core 61, and Core 49), and two show negative correlations (Test Cruise Core 2, and Core 6, whilst two show no relationship. None of the cores show any correlation between Ba_d and any of the inorganic dissolved nutrients measured (nitrate, phosphate, and silicic acid), except for Test Core 2. The distributions of Ba_d and salinity observed in the cores are briefly described below (Figure 6-10):

3.3.i Core 2 (29th January 2015)

Relatively constant salinity throughout the core, with the lowest salinities recorded at the top of the core (4.4) and the highest at the base (6.3). Ba_d concentrations are relatively low, with minimum values of 8 to 10 nM at the base and a high of 22 nM at the top of the core. There is no correlation throughout the core between Ba_d and salinity.

3.3.ii Core 6 (6th February 2015)

Very low salinities (0 to 2.2) recorded in the lower 60 cm of the core, showing an increase with depth. At 60 cm depth in the core there is a sharp salinity discontinuity, with salinity values increasing upwards from 0 to 6, decreasing again to 2.9 at the top of the core. Ba_d concentrations are relatively constant throughout the top 60 cm and the lower 30 cm of the core (20 to 34 nM), but show a positive excursion to concentrations of 40 to 80 nM between 70 and 90 cm. this positive Ba_d excursion accompanies a decrease in salinity, and the subsequent decrease in Ba_d above 70 cm accompanies the salinity increase. This appearance of anti-correlation is reflected in a weak negative relationship ($R^2 = 0.2$) between Ba_d and salinity in the core as a whole.

3.3.iii Test Core 0 (23rd February 2014)

Very low salinities (0 to 1.6) recorded at the base of the core (75 to 95 cm), coupled with minimum Ba_d concentrations of 26 to 28 nM. At 65 cm a sharp discontinuity occurs in both Ba_d and salinity, with concentrations increasing to Ba_d 50 nM and salinity 4. In the top 50 cm of the core however, Ba_d and salinity appear anti-correlated, with Ba_d concentrations decreasing to 30 nM before increasing to 48 nM at the top of the core, whilst salinity increases to 5 before decreasing to 3.8 at the top of the core. Despite this behaviour in the top 50 cm, the whole core shows a positive correlation between Ba_d and salinity ($R^2 = 0.4$).

3.3.iv Test Core 1 (25th February 2014)

The highest salinity is recorded at the top of the core (8), decreasing to 4.3 at the base. Between 45 and 60 cm there is a negative excursion to minimum salinity values (2.4 to 2.5). Ba_d

fluctuates throughout the core over a large range of concentrations: the concentration at the top of the core is relatively low (30 nM), increasing sharply to maximum concentrations of 62 nM at 15 cm, which steadily decrease to minimum values of 14 nM at 77 cm; a relatively high concentration of 48 nM is observed at the base of the core. No relationship is observed between Ba_d and salinity.

3.3.v Test Core 2 (25th February 2014)

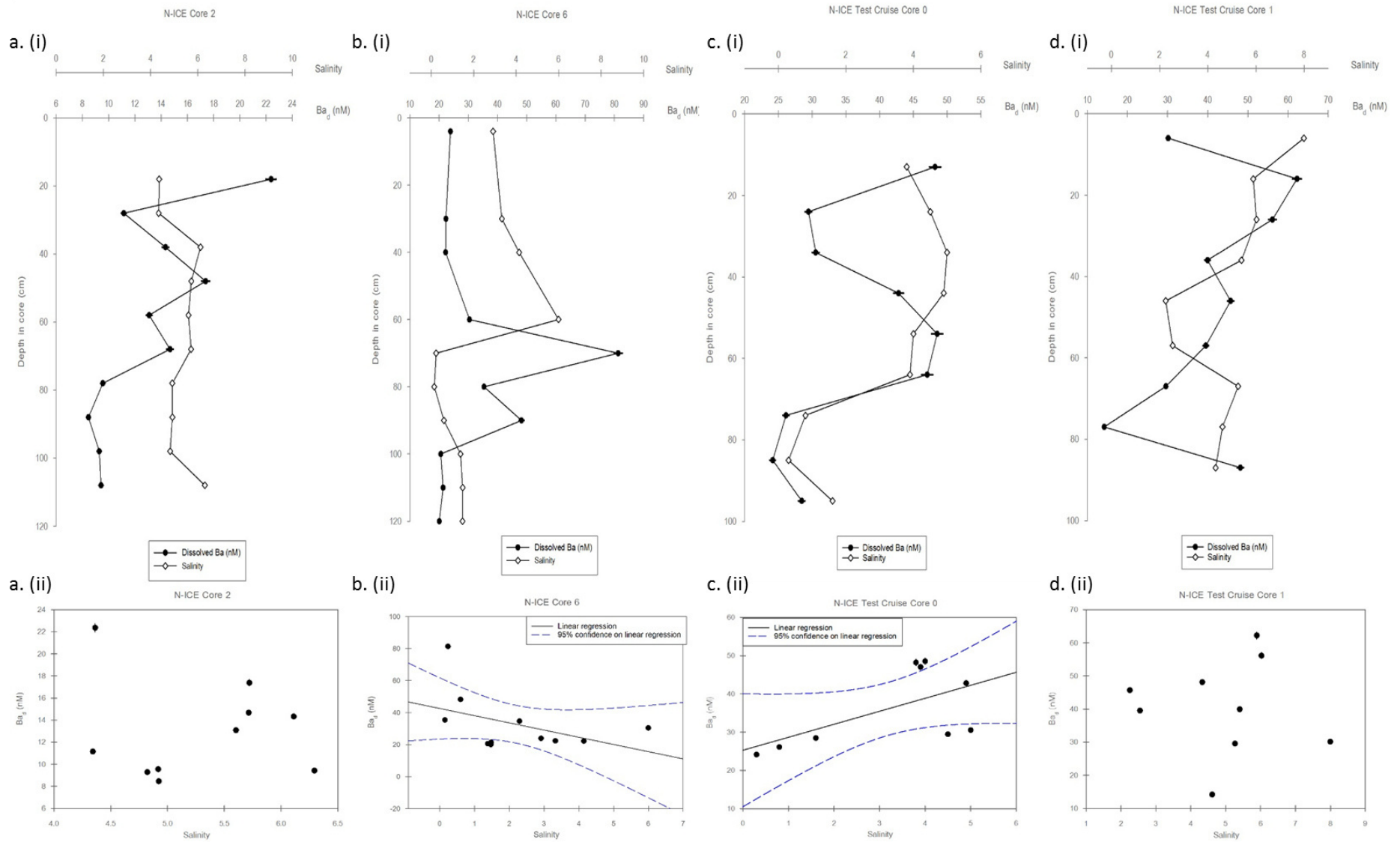
Salinity and Ba_d are significantly anti-correlated throughout this core; salinity at the top of the core is 4, increasing over the top 30 cm to maximum values of 7, before decreasing to low values of 2 at the base. Ba_d is 23 nM at the top of the core, decreasing to minimum concentrations of 12 nM over the top 15 cm, before increasing to maximum values of 40 nM within 10 cm of the base. At the very base of the core Ba_d concentration drops slightly to 33 nM. A significant negative correlation is exhibited between Ba_d and salinity ($R^2 = 0.63$), this is also the only core in which Ba_d shows a relationship with the macronutrients nitrate and phosphate, in the form of significant positive correlations ($R^2 = 0.54$ and 0.76 respectively). No correlation is observed between Ba_d and silicic acid.

3.3.vi Core 49 (22nd April 2015)

In the top 50 cm of the core salinity values are very low (0 to 1), increasing with depth, with several small undulations, to maximum values of 4.7 at the base. Ba_d values throughout the core are also very low, ranging from a minimum of 7.6 nM at 45 cm to a maximum concentration of 22 nM at the base. The general pattern of increasing values with depth in the core is displayed by both Ba_d and salinity, resulting in a positive correlation between the two variables ($R^2 = 0.6$). However, within this general trend the undulations between 45 and 80 cm in the core show decreases in Ba_d accompanied by increases in salinity.

3.3.vii Core 61 (21st May 2015)

At the top of the core, above the zero reference line, very low salinity values are recorded (0 to 0.3) along with relatively low Ba_d concentrations (10 to 15 nM). Between -15 cm and 5 cm in the core, salinity increases to maximum levels of 9, whilst Ba_d increases sharply to maximum values of 45 nM at -5 cm. In the rest of the core, salinity exhibits small undulations around 5, with one sharp negative excursion at 85 cm to values of 2. Ba_d concentrations vary between 20 and 40 nM, characterised by sharp transitions from relatively high concentrations to low concentrations, followed by steady increases, creating a saw-tooth pattern with depth. There is an overall positive correlation between Ba_d and salinity ($R^2 = 0.3$).



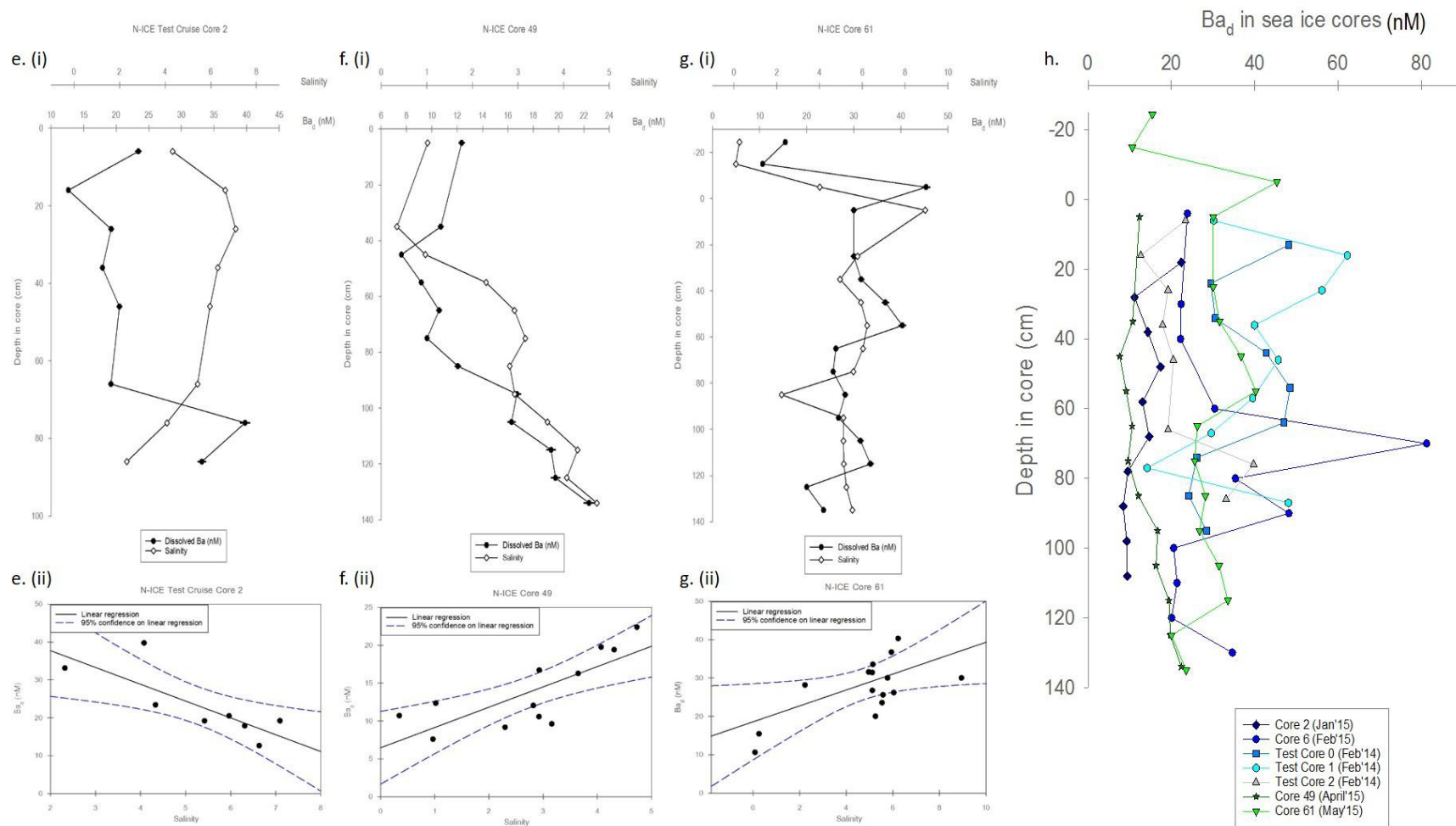


Figure 6-7: (previous two pages) a.(i) to g.(i) - Ba_d concentrations (nM) (black filled diamonds) and salinity (unfilled diamonds) profiles with depth (cm) in N-ICE whole sea ice cores. a. (ii) to g.(ii) – Relationship between Ba_d (nM) and salinity in each core:

a. Core 2 (no correlation)

b. Core 6 (scattered negative correlation – slope -4.5, intercept 42.5, R^2 0.20)

c. Test Core 0 (scattered positive correlation – slope 9.9, intercept 32.5, R^2 0.03)

d. Test Core 1 (no correlation)

e. Test Core 2 (negative correlation – slope -4.4, intercept 46.6, R^2 0.63)

f. Core 49 (positive correlation – slope 2.7, intercept 6.5, R^2 0.60)

g. Core 61 (scattered positive correlation – slope 2.1, intercept 18.6, R^2 0.28)

h. Ba_d concentrations in all cores shown in one plot for inter-core comparisons; Core 2 (dark blue filled diamonds), Core 6 (blue filled circles), Test Core 0 (light blue filled squares), Test Core 1 (cyan filled circles), Test Core 2 (light grey filled triangles), Core 49 (dark green filled stars), and Core 61 (light green filled upside down triangles).

4. Discussion

A crucial question in understanding the role of sea ice in Ba cycling is whether or not barium behaves conservatively throughout the formation and melting of sea ice; whether the Ba_d distribution in sea ice is controlled by the overall dilution and concentration of ions reflected in salinity measurements.

As discussed in Chapters 4 and 5, the relationship between the proportion of sea ice melt present in surface seawater (derived from $\delta^{18}O$ and salinity measurements) and the distribution of Ba_d in WAP seawater indicate that Ba_d may not behave conservatively in sea ice. When the proportion of sea ice melt in surface seawater is relatively high (as in coastal areas and Marguerite Bay in 2012), Ba_d appears to be disproportionately diluted relative to silicic acid. This suggests that WAP sea ice contains lower levels of Ba_d than would be expected from brine rejection processes alone (as this would be expected to affect Ba_d and silicic acid equally). By measuring that Ba_d and salinity in sea ice directly, this idea can be tested.

4.1. Conservative versus non-conservative behaviour of Ba_d in brine and sea ice

In the interstitial brine solutions collected from sea ice at Rothera (WAP), Ba_d concentrations were found to range widely, with particularly high concentrations observed in late winter and early spring (Figure 6-4). However, as can be seen in Figure 6-5, Ba_d appears to behave conservatively with respect to salinity, and the high Ba_d concentrations (>100 nM) of the late winter months do not exceed what would be expected from the high salinities recorded, nor are the low Ba_d concentrations (5 to 12 nM) in mid-spring lower than expected for the freshness of the samples. Moreover, representative seawater samples from Rothera and the wider WAP (average surface seawater Ba_d concentration of 79 nM and salinity of 33.6 taken

from PalTER samples discussed in Chapter 4) fall along this dilution line (Figure 6-11), indicating that the Ba_d of the WAP interstitial sea ice brines samples can be explained by a simple dilution model.

However, the Ba_d distribution within the Arctic sea ice cores does not follow the same simple trajectory. Although it is difficult to compare the much smaller salinity range of the whole ice cores to the large range of the brines solution, the Ba_d measured in the Arctic sea ice cores exhibit variable relationships with salinity (Figure 6-11). In some cores (Test Core 2 and Core 6) significant negative correlations between Ba_d and salinity are observed, and even in those cores which exhibit overall positive correlations between Ba_d and salinity (Test Core 0, Core 49, and Core 61), there are anti-correlative features (between 45 and 85 cm in Core 49; the upper 60 cm of Test Core 0; between -5 and 10 cm in Core 61). It is also notable that the positive linear regression models that can be fitted to these positive Ba_d /salinity relationships in Arctic sea ice cores do not define a linear dilution relationship between Arctic sea ice and Arctic seawater (average value of Arctic seawater represented by pink diamond in Figure 6-11). This suggests that whilst Ba_d behaves conservatively in the total brine solution represented by the Rothera brine samples, the Ba_d distribution throughout the sea ice itself (represented by the Arctic sea ice cores) may be governed by non-conservative processes. When considered in conjunction with the results from Chapter 4, which indicated that sea ice melt was a significant secondary control on the distribution of Ba_d relative to $Si(OH)_4$ in surface WAP waters, it seems that the non-conservative behaviour observed in the Arctic samples is also taking place in sea ice at the WAP. As the Arctic core meltwater was not filtered at the time of collection, both the dissolved and particulate barium phases within the sea ice will have been sampled. Some proportion of these particulate barium phases will have dissolved during the subsequent transport, storage, and preparation of the samples, meaning that the Ba_d measured is representative of the total barium content of the ice, rather than only the original dissolved phases. It is likely that whole sea ice cores from Rothera, sampled in the same way, would therefore display a similar non-conservative relationship between Ba_d and salinity, offset from the dilution line expressed by the brine solutions and average seawater. In the same way, if filtered interstitial brine samples were collected from the Arctic sea ice, they would be expected to fall on a dilution line with Arctic seawater, offset from the whole ice core values.

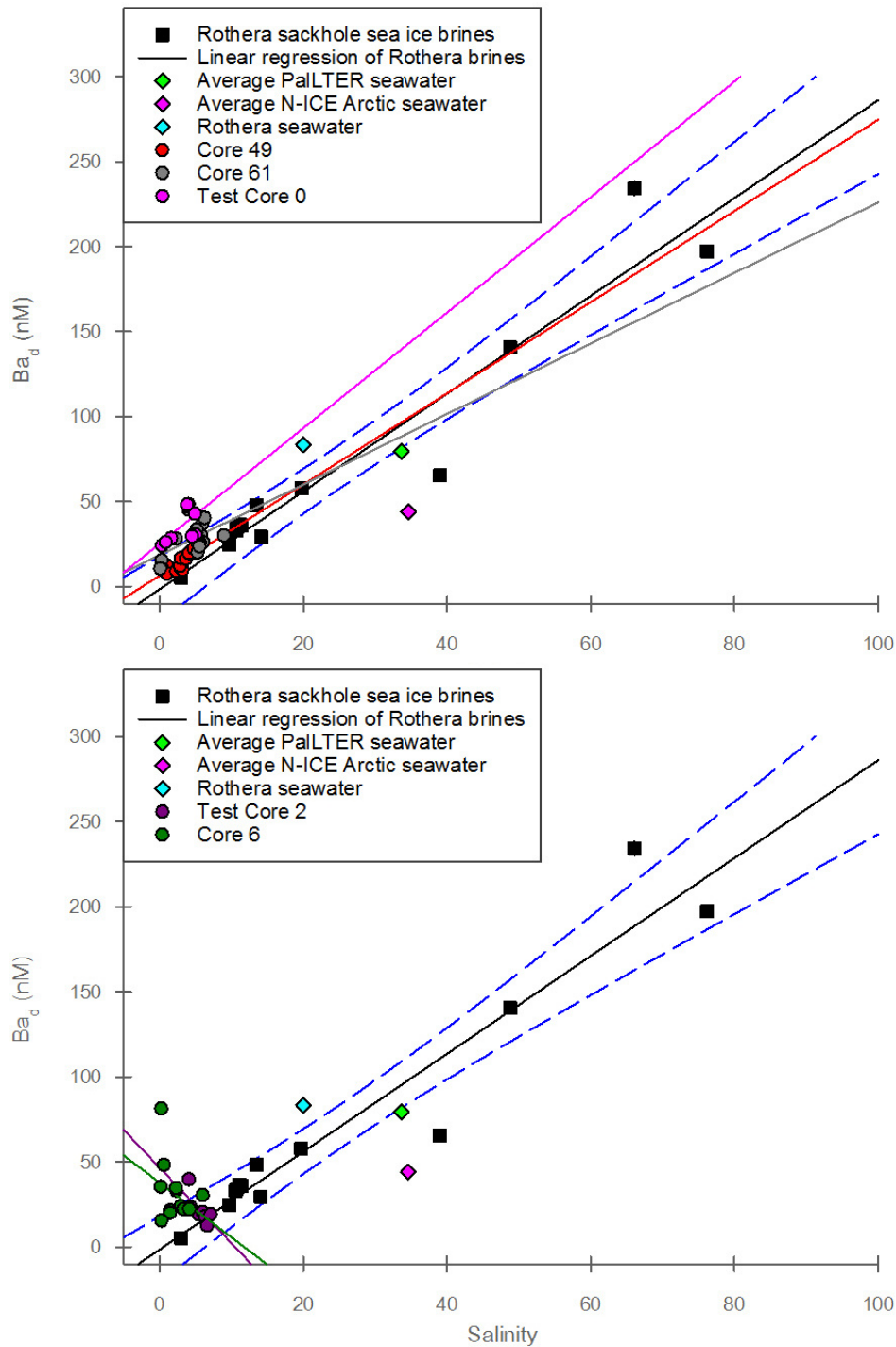


Figure 6-8: Relationship between Ba_d concentrations (nM) and salinity in sea ice samples. Filled black squares represent interstitial brine solutions from Rothera sea ice. Solid black line represents linear regression model (least squares) fitted to Rothera sea ice brine samples, with blue dashed lines indicating the 95% confidence level of the model. Filled diamonds show representative values for seawater samples (light green – PaLTER; pink – Arctic; cyan – Rothera).

Top: Filled circles represent N-ICE whole sea ice cores that exhibit positive correlations between Ba_d and salinity, with solid lines in corresponding colours showing the linear correlation (red – Core 49; grey – Core 61; pink – Test Core 49).

Bottom: Filled circles represent N-ICE whole sea ice cores that exhibit negative correlations between Ba_d and salinity, with solid lines in corresponding colours showing the linear correlation (purple – Test Core 2; dark green – Core 6).

4.2. Potential non-conservative processes acting within sea ice

For Ba_d to behave non-conservatively within sea ice, barium must be removed from or added to solution independently of salinity changes. As discussed above, sea salt ions are rejected from the ice crystal lattice as sea ice forms, forming pockets of brine that become trapped in a network within the ice (Weeks 2010). Over time, this trapped dense brine drains downwards through brine channels under the influence of gravity, typically leaving upper layers of ice fresher (Malmgren 1927; Cox et al. 1973; Weeks and Ackley 1986). The extent of this desalination is determined by the permeability of the sea ice, which in turn is controlled by the structure of the ice itself and its thermodynamic properties, with freezing in brine pockets decreasing porosity (Golden et al. 1998; Backstrom and Eicken 2006).

Within these brine pockets and channels, barium could be removed from solution and transferred to solid phases either by adsorption onto particulates, or through the precipitation of barium sulphate (barite). Indeed, particulate barium has been found to be high in Antarctic sea ice (Lannuzel et al. 2011; Carson 2008; Stroobants et al. 1991). As discussed in previous chapters, barite is thought to precipitate in the ocean in microenvironments associated with decaying organic matter (Dehairs et al. 1980; Collier & Edmond 1984; Bishop 1988). Sea ice contains a distinct and dynamic microbial community (Sea Ice Microbial Community – SIMCO) that is dominated by diatoms, but can also contain flagellates and other algal species, as well as protozoa, fungi, and invertebrates (Horner et al. 1992; Palmisana and Garrison 1993). It is possible that the microbial breakdown of phytoplankton within sea ice could concentrate Ba_d and sulphate (SO_4^{2-}) within brine channels and mediate the precipitation of barite micro-crystals. Provided that such barite crystals did not re-dissolve, this mechanism would remove barium from solution independently of salinity fluctuations. However, if this were the primary mechanism driving the dissociation between Ba_d and salinity that is observed in the Arctic sea ice core samples, a correlation could be expected between Ba_d and concentrations of dissolved inorganic nutrients (as indicators of productivity), which is not typically observed in these samples.

Alternatively, barite precipitation may be able to occur within sea ice without the aid of microbial microenvironments. Sulphate ions make up approximately 8% of the mass of salt ions in sea water (Petrich and Eiken 2010), and it is possible that brine pockets may reach high enough concentrations of barium and sulphate to cause abiotic precipitation of barite (Carson 2008). The results from the analysis of interstitial brine solutions from Rothera has shown that brine solutions can reach Ba_d concentrations 2- to 3.5-times those routinely measured in seawater. If barite were to form in this way from supersaturated brines solutions during brine

migration through the sea ice, these solid barium phases may remain behind in the sea ice matrix after the brine fluid has moved on. This would leave low salinity layers of sea ice enriched in these solid phases (Weeks and Ackley 1986), whilst the higher salinity layers would contain Ba_d -depleted brines. As the sea ice core samples analysed here are unfiltered whole-ice samples, it is probable that any particulate barium has been re-dissolved into the ice-melt during transport and storage, therefore the high Ba_d concentration/low salinity layers observed in the Arctic ice core records may represent localised areas of high particulate barium precipitated from migrating brines.

These layers displaying inverse Ba_d /salinity relationships are more prevalent in the top/middle of the sea ice cores, suggesting that this separation of stationary solid phase barium from migrating brines may become more pronounced as the sea ice ages, or be associated only with certain periods of sea ice growth.

4.3. Meltwater flushing

The sea ice cores collected during the spring months (Core 49 and Core 61) both exhibit very low salinities (0 to 2) at the tops of the cores. Such low salinities in sea ice are usually associated with meltwater flushing, as melt pools on the surface of the sea ice drain down through the sea ice (Petrich and Eiken 2010). In both of these cases the very low salinity values are accompanied by low Ba_d concentrations ($Ba_d < 15$ nM), suggesting that this initial meltwater flushing process (a precursor to summer melting) decreases the overall barium concentration of the affected sea ice. The relationship between Ba_d and salinity in these two springtime cores is a positive correlation, following linear regression models similar to that defined by the Rothera brine solutions (Figure 6-11), which suggests that the strong dilution effects of the meltwater flushing overwhelm the previously established non-conservative Ba_d signal.

5. Conclusions

A wide range of Ba_d concentrations are found in interstitial brine solutions from Rothera, with particularly high concentrations in winter of up to 3.5 times those in surrounding seawater. Nevertheless, at the extremes of high and low concentrations, Ba_d in these brine solutions appears to behave conservatively with respect to salinity, and forms a dilution line that incorporates local seawater.

In contrast, the distribution of Ba_d in whole-ice Arctic sea ice cores is found to be only partially conservative, sometimes displaying an anti-correlation between Ba_d and salinity. Distinct layers of apparently non-conservative Ba_d behaviour are observed, particularly in the middle and upper regions of winter cores, indicating that the processing controlling this

behaviour are only active during certain periods of ice growth/maturation. The most likely source of non-conservative behaviour of barium in sea ice is the precipitation of barite, which in oceanic conditions is considered to be biologically mediated. However, a lack of correlation between Ba_d and nitrate, phosphate, or silicic acid, means that the non-conservative behaviour of Ba_d observed here cannot be linked to sea ice microbial activity. An alternative mechanism is the abiotic precipitation of barite in supersaturated brine channels, followed by the migration of Ba_d -depleted brines away from the Ba solid phase. This would result in concentrated regions of particulate barium (measured in these unfiltered samples as Ba_d) associated with low salinities, and brine-rich, higher salinity layers depleted in Ba_d . The onset of meltwater flushing in the spring appears to dilute Ba_d throughout the sea ice, over-printing the non-conservative Ba_d signal.

These results are of interest as they indicate that Ba_d does not always behave conservatively in sea ice, and that particulate barium in sea ice may not be evenly distributed. This could be an important factor when considering the impact of sea ice melt on the dissolved and particulate distributions of barium in polar waters, as sea ice melting occurs in stages rather than all at once, and from this data it appears that different stages of melting will involve the input of different proportions of the dissolved and particulate barium pools from sea ice to seawater.

Chapter 7

Synthesis

As proxies for organic and inorganic carbon storage, various phases of barium have the potential to provide important insights into the role of the Southern Ocean in climate regulation over a range of timescales. However, the distribution of particulate and dissolved barium in this region is not solely controlled large scale water mass circulation and predictable biological associations, but by an additional combination of spatially and temporally variable local and coastal processes. In this thesis I have investigated the distribution of dissolved barium (Ba_d) in this region, producing high-resolution datasets across transects of the Scotia Sea and the surface waters of the West Antarctic Peninsula, alongside a study of the seasonal variation of Ba_d in Ryder Bay, and an investigation of Ba_d behaviour within sea ice. Due to the precision of these datasets, produced using ID-ICP MS, it has been possible to analyse subtle variations in Ba_d over different spatial and temporal scales, and discern the relationships between these variations and a number of oceanic and coastal processes.

In this concluding chapter, I will briefly summarise the major findings of each of my data chapters, followed by a synthesis of how these results have improved our knowledge of the barium cycle in Antarctic waters, and suggestions of further work that could be carried out to solidify these new perspectives.

1. Summary of major findings

1.1. Chapter 3 – Ba_d cycling in the Scotia and Weddell Seas

In this chapter I investigated the controls on the broader oceanic distribution of Ba_d observed in the Scotia and Weddell Seas. With reference to the distributions of Ba_d in different ocean basins (the GEOSECS dataset), the global correlation between Ba_d and silicic acid in ocean waters was confirmed for the Southern Ocean, although the linear correlation displayed in the Southern Ocean was generally found to have a shallower slope and higher intercept, as reported by previous studies (Jeandel et al., 1996; Jacquet et al., 2007), indicating that compared to the global ocean, Ba_d varies less with regard to silicic acid in this region.

Ba_d does not generally show a linear relationship with nitrate or phosphate, indicating that the link between Ba_d and biological activity is not dominated by a direct association with organic matter. However, a correlation between these parameters was observed in the surface waters north of the Polar Front, which was attributed to barite precipitation associated with nanoflagellate phytodetritus in surface waters, which was rapidly re-dissolved below the surface layer.

Decoupling between the Ba_d and silicic acid cycles was investigated by analysing $Ba_d^{Si\text{ residual}}$ values. Changing ratios of Ba_d /silicic acid were mainly found to be a function of large scale ocean circulation, with distinctive signatures in discrete water masses. Overprinting these predictable depth distributions were negative $Ba_d^{Si\text{ residual}}$ signatures coincident with the oxygen minimum zone, most likely representing the precipitation of barite, which is thought to be precipitated in supersaturated microenvironments associated with decaying organic matter (Dehairs et al., 1980; Bishop, 1988; Dymond and Collier, 1996). Higher levels of barite precipitation were inferred south of the Polar Front, in waters overlain by diatom-dominated primary productivity, as opposed to the nanoflagellate-dominated waters north of the Polar Front, which agrees with the previously postulated theory that diatom tests may catalyse barite precipitation (Bishop, 1988; Stroobants et al., 1991; Dehairs et al., 1991; Cardinal et al., 2005).

1.2. Chapter 4 – Spatial variations in Ba_d at the WAP

This high resolution dataset of the distribution of dissolved barium across waters adjacent to the WAP showed a robust relationship between Ba_d and silicic acid that was not only present in depth samples, but persisted in surface water samples. This positive association between Ba_d and surface silicic acid concentrations across the region was in contrast to previous some previous Southern Ocean studies, which have observed a complete breakdown of the Ba_d / $Si(OH)_4$ relationship in surface waters (Jeandel et al., 1996; Jacquet et al., 2007). The persistence of the relationship in this productive, diatom-dominated area suggests that diatoms may

passively concentrate Ba_d and remove it from the surface layer. Two possible mechanisms for this have been suggested:

- i.) Adsorption of Ba_d onto inorganic particulates such as iron- or manganese-oxyhydroxides, which themselves become 'stuck' to diatom cell surfaces;
- ii.) Precipitation of barite within diatom-dominated phytodetritus in the euphotic zone, which is not re-dissolved but exported out of the surface layer.

The overall Ba_d distribution along the WAP indicated that a coastal source of barium enriches the shelf waters before they mix with barium-depleted ACC waters at the shelf break. Freshwater fractions calculated from salinity and $\delta^{18}O$ measurements revealed that this coastal flux of barium cannot be attributed to glacial meltwater input, which appears to have no consistent impact on the coastal Ba_d distribution. The enrichment of shelf waters may be due to an epibenthic flux of barium from shelf sediments, but this could not be confirmed.

Sea ice was found to exert a secondary control on the surface water Ba_d distribution, with high levels of sea ice melt diluting Ba_d to a greater extent than silicic acid was diluted. This is indicative of some non-conservative process, such as barite formation, acting to remove barium from solution within sea ice, in agreement with previous observations of high concentrations of particulate barium within sea ice (Stroobants et al., 1991; Carson, 2008; Lannuzel et al., 2011).

1.3. Chapter 5 – Seasonal variations in Ba_d at the WAP

A year long time series of Ba_d was analysed from the RaTS site in Ryder Bay, which found seasonal variations in surface layer Ba_d concentrations that were broadly controlled by vertical mixing. A gradual increase in Ba_d was observed throughout the autumn/winter, followed by unchanging levels throughout the spring, and decreases in the summer that were associated with a high influx of sea ice melt. Sporadic peaks in Ba_d occurred throughout the year, associated with destabilisation of the water column that suggested Ba_d -enriched waters were being mixed up from below the surface layer (100 to 150 m). Three mechanisms were proposed to explain this near-surface Ba_d -enrichment:

- i.) In the autumn and winter months, the rejection of Ba_d -rich brines from sea ice formation;
- ii.) In the summer and autumn months, release of Ba_d from particulates associated with sinking and decaying matter from phytoplankton blooms;
- iii.) Mixing of near-surface layers with CDW that becomes progressively enriched over time in Ba_d upstream through bathymetric interaction with shelf bottom waters.

There was no clear inverse relationship between biological activity and Ba_d concentrations that would indicate a removal of Ba_d from the surface layer by phytoplankton, as has been observed during intense phytoplankton blooms in other regions (Nozaki et al., 2001);

Esser and Volpe, 2002). However, significant Ba_d peaks were observed when mixing events coincided with bloom activity, indicating that Ba_d concentrations in near surface waters increased during periods of intense phytoplankton decay. This effect was strongest during the diatom bloom observed in summer 2014 (rather than the nanoplankton bloom in autumn 2013), indicating a greater Ba_d release associated with the recycling of diatoms than with the recycling of nanoflagellates.

There was no significant inter-annual variation in the seasonal Ba_d enrichment, despite annual variation in the extent of mixing. It was postulated that this lack of expected could be an artefact of two related processes: deeper mixing observed in 2014 (relative to 2013) may have been accompanied by reduced sea ice cover, so that whilst the deeper mixing brought more Ba_d to the surface, greater air-sea interaction increased the input of atmospheric particles (such as iron- and manganese- oxyhydroxides) that could scavenge Ba_d from the mixed layer.

1.4. Chapter 6 – Behaviour of Ba_d in sea ice

In this chapter, the findings from Chapters 4 and 5 that non-conservative processes may act to remove barium from solution in sea ice were tested by analysing the Ba_d concentrations in whole sea ice cores from the Arctic, and in interstitial brine solutions collected from Antarctic sea ice. Ba_d concentrations of up to 3.5 times surrounding seawater were measured in Antarctic sea ice brine solutions, with a wide range of 5 to 240 nM. However, the Ba_d in these brine solutions behaved conservatively with respect to salinity, forming a dilution line that incorporated local seawater.

In contrast, the distribution of Ba_d in whole-ice Arctic sea ice cores was found to be only partially conservative, sometimes displaying an anti-correlation between Ba_d and salinity. This suggested that at under certain conditions non-conservative processes were altering the Ba_d content of the ice, as predicted from previous chapters. These alterations in Ba_d content did not exhibit any correlation with concentrations of macronutrients within the ice, indicating that the processes involved were not biologically mediated. It instead appears that abiotic barite precipitation may occur in supersaturated brine channels, followed by the migration of Ba_d -depleted brines away from the Ba solid phase. This mechanism would explain the concentrated regions of Ba_d (particulate barite converted back to Ba_d in these unfiltered samples) associated with low salinities, and brine-rich, higher salinity layers depleted in Ba_d .

In regions of cores that had experienced meltwater flushing, Ba_d concentrations were considerably diluted and behaved conservatively, indicating that this process over-writes the non-conservative process suggested above.

This direct analysis of Ba_d in sea ice cores and interstitial brine solutions builds upon previous work that has invoked barite precipitation within sea ice as a possible mechanism for surface Ba_d depletions in the Southern Ocean (Carson, 2008; Hoppema et al., 2010), and also offers evidence that this precipitation is abiotic, rather than biologically mediated by sea ice algae.

2. Refining the picture of the Southern Ocean Ba_d cycle

2.1. Interactions with biological cycling

Throughout the global ocean, barium is observed to have a broadly nutrient-like distribution, with minimum concentrations in surface waters that increase with depth to a sub-surface maximum, following the profile of a skeletal component such as silicic acid. This distribution, and its global positive linear correlation with silicic acid, is attributed to the biologically mediated cycle of barite, thought to precipitate in organic microenvironments at mesopelagic depths (see Figure 1-3).

Whilst this general representation is largely applicable to the Southern Ocean, my findings in this thesis allow a more detailed picture to be drawn, particularly for the coastal area adjacent to the WAP. In comparison to the global ocean, Ba_d concentrations measured in Antarctic waters are relatively high, and experience a greater level of surface drawdown (Figure 7-1).

The stronger near-surface gradient in Ba_d found in this study suggests that Ba_d is concentrated and removed from surface waters more strongly in this region than elsewhere in the global ocean. When viewed in context with the positive linear correlation observed between Ba_d and silicic acid in WAP surface waters (discussed in Chapter 4), it seems likely that this association is related to biological production, specifically diatoms. Given that there is no evidence of any direct uptake of Ba_d by phytoplankton, there are two alternative theories of passive biological association (discussed above) that could be responsible for the observed relationships:

- i.) Adsorption of Ba_d onto inorganic particulates such as iron- or manganese-oxyhydroxides, which are themselves associated with phytoplankton cell surfaces and exported from the surface layer;
- ii.) Precipitation of barite within phytodetrital microenvironments (that are supersaturated with respect to barite) in the euphotic zone, which is subsequently either re-dissolved within surface waters (e.g. in nanoflagellate dominated waters north of the Polar Front), or exported out of the surface layer within the phytodetritus, to be released and re-dissolved at depth (e.g. in the diatom-dominated waters south of the Polar Front).

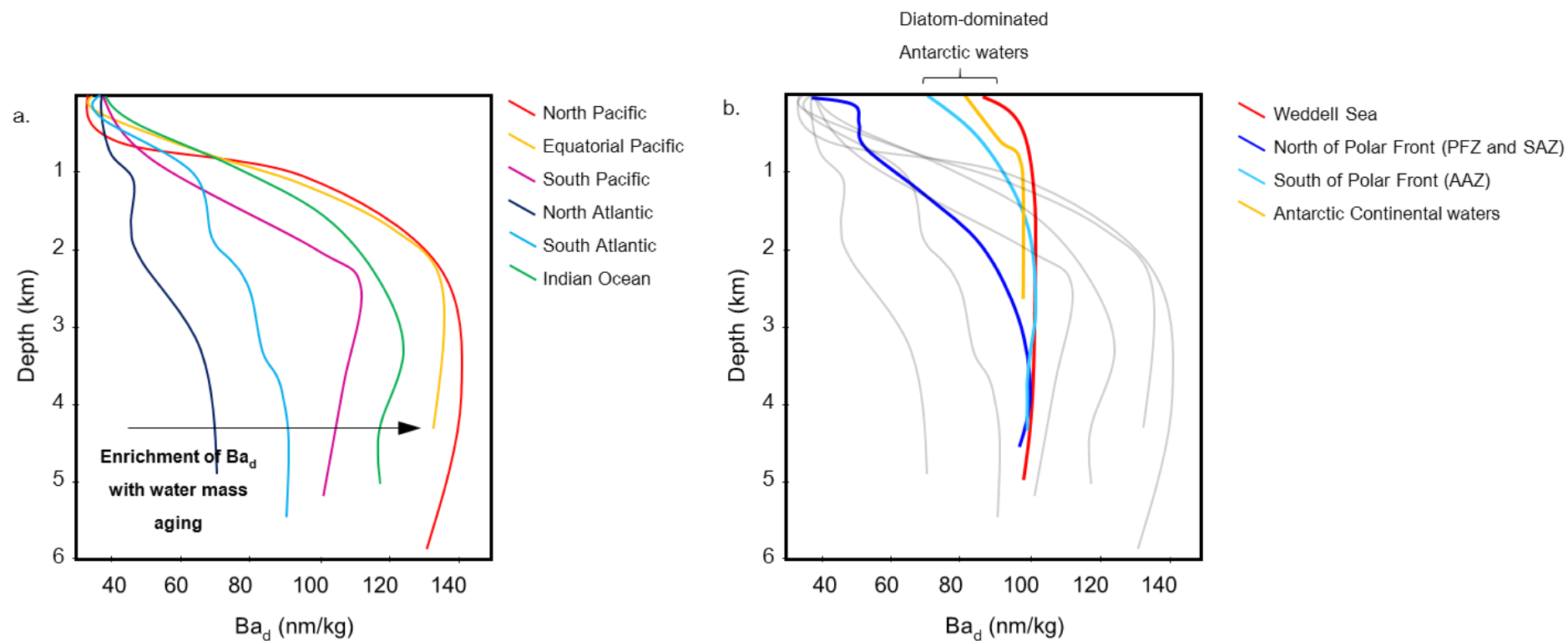


Figure 7-1: a. Schematic summary of the depth profiles of Ba_d concentrations (nM) recorded in different ocean basins by GEOSECS Expeditions (Ostlund et al. 1987): North Pacific (red line), Equatorial Pacific (yellow line), South Pacific (pink line), North Atlantic (dark blue line), South Atlantic (light blue line), Indian Ocean (green line). b. Schematic summary of Ba_d concentrations (nM) recorded in this study, with GEOSECS summaries greyed out: Weddell Sea (red line), PFZ and SAZ (dark blue line), AAZ (light blue line), Antarctic Continental waters (yellow line). Note that the all waters sampled south of the Polar Front have distinctly elevated Ba_d concentrations.

This latter theory explains the observation that in Scotia Sea samples north of the Polar Front, an anomalously strong co-variance is displayed between Ba_d and NO_x / PO_4 , suggesting that Ba_d is removed from surface waters and rapidly re-mineralised along with non-siliceous organic matter. In this nanoflagellate-dominated region, barite microcrystals would be associated with these smaller, less dense, less aggregated phytoplankton, and may therefore undergo re dissolution at the near surface, rather than being rapidly exported. In diatom-dominated regions, barite microcrystals precipitated in surface waters will be associated with denser diatom frustules that are more likely to form bio-aggregates and sink rapidly, exporting the barite to deeper water before the phytodetritus is fully broken down and the barite crystal can re-dissolved and/or continue to sink to the sediment.

Either theory could be invoked to explain the behaviour observed in near-surface waters in Ryder Bay, which appear to become enriched in Ba_d during the decay of phytoplankton blooms, with a greater enrichment inferred (from the greater magnitude of subsequent Ba_d peaks during mixing events) during the breakdown of diatom-dominated blooms (discussed in Chapter 5). It is plausible that both of these mechanisms could be occurring - the applicability of each in certain regions could be quantified by sampling the particulate barium in surface waters, and using microscopy and / or leaching processes to establish the proportions of barium solid phases present.

The idea that greater Ba_d export from the surface layer may occur when Ba_d is associated with diatom-dominated detritus ties in with another phenomenon observed in the Scotia Sea: increased mesopelagic barite formation (inferred from non-water-mass-derived excursions of $Ba_d^{Si\ residual}$ values coincident with the oxygen minimum zone) underlying the diatom-dominated waters south of the Polar Front, compared with the nanoflagellate-dominated waters north of the Polar Front (Chapter 3). The denser bio-aggregates formed by detrital diatom frustules are thought to provide a more suitable microenvironment for bacterially-mediated barite formation than the smaller nanoflagellate detritus. An investigation into the vertical distribution of particulate barium phases across this biogeochemical boundary, with simultaneous surveys of size-fractionated Chl-*a*, would help to ascertain whether barite formation is indeed more extensive below diatom-dominated regions, and how these differences impact on the quantification of export productivity estimates from the Ba_{excess} proxy. Another potential solution would be the measurement barium isotopes in the vertical seawater profiles. Coupled with the $Ba_d^{Si\ residual}$ values already calculated, barium isotopes would highlight whether the $Ba_d^{Si\ residual}$ excursion were caused by a process that affected only the barium, such as barite cycling, or a process that was affecting the cycling of silicic acid.

2.2. *The role of sea ice*

During this investigation, the role of sea ice in the barium cycle has been found to be more complex than a simple idea of conservative dilution/concentration during sea ice formation and melting. When sea ice forms, Ba_d will be rejected with other salt ions, which may lead to a Ba_d -enrichment of near-surface waters. Results from the analysis of Arctic sea ice (Chapter 6) then showed that Ba_d does not consistently behave conservatively with regard to salinity within the sea ice, but instead exhibits layers of Ba_d depletion and enrichment that anti-correlate with salinity. This implies that non-conservative processes such as barite formation occur extensively within the sea ice, removing barium from solution. When this sea ice melts the barium particulates will be released and sink through the water column, whilst the meltwater will be depleted in Ba_d relative to other components such as silicic acid. This over-dilution of Ba_d by high fluxes of meltwater was observed in WAP surface samples (Chapter 4 and Chapter 5).

The mechanism could be verified by measuring Ba_d from whole sea ice cores collected from the WAP, to confirm that sea-ice controls on barium cycling act in a similar manner in the Arctic and Antarctic. Additionally, microscopic analysis of barium particulate phases within the sea ice could help to establish the mechanism of formation, as abiotically precipitated barite is reported to have a very different habit to barite that is biologically-mediated.

2.3. *Benthic sediment fluxes*

Whilst benthic sediments fluxes have not been directly analysed in this thesis, it is apparent from the vertical and horizontal distributions of Ba_d around the WAP that fluxes from shelf sediments have a role to play in enriching shelf bottom waters with Ba_d and acting as a source of Ba_d to the near-shore Antarctic waters. The formation and sinking of particulate barium phases through the water column, particularly if accentuated by the presence of diatoms as discussed above, will be accumulated in shelf sediments. The dissolution of these particles within the sediment will then enrich pore water concentrations, providing a potential flux of Ba_d to enrich bottom waters on the shelf.

These fluxes could be quantified through benthic flux experiments at the WAP shelf, or direct measurement of pore waters and shelf bottom waters. The vertical mixing pathways of this enriched bottom water could also be further investigated, perhaps in conjunction with the characterisation of vertical mixing being undertaken at RaTS.

Reference List

- Abelmann, A., and Gersonde, R. (1991). Biosiliceous particle flux in the Southern Ocean. *Marine chemistry*, 35(1-4), 503-536.
- Allison N. and Finch A. A. (2007) High temporal resolution Mg/Ca and Ba/Ca records in modern *Porites lobata* corals. *Geochemistry, Geophys. Geosystems* **8**.
- von Allmen K., Böttcher M. E., Samankassou E. and Nägler T. F. (2010) Barium isotope fractionation in the global barium cycle: First evidence from barium minerals and precipitation experiments. *Chem. Geol.* **277**, 70–77. Available at: <http://www.sciencedirect.com/science/article/pii/S0009254110002615> [Accessed March 28, 2016].
- Anderson R. F., Ali S., Bradtmiller L. I., Nielsen S. H. H., Fleisher M. Q., Anderson B. E. and Burckle L. H. (2009) Wind-Driven upwelling in the Rise in Atmospheric CO₂. *Science* (80-.). **323**, 1443–1448.
- Aminot, A., Kérouel, R. and Coverly, S.C., 2009. Nutrients in seawater using segmented flow analysis. Practical guidelines for the analysis of seawater. CRC Press, Boca Raton, pp.143-178.
- Arrhenius, G., 1959. Sedimentation on the ocean floor. In *Researches in geochemistry* (Vol. 1, pp. 1-24). Wiley New York, NY.
- Arrigo, K. R., & Thomas, D. N. (2004). Large scale importance of sea ice biology in the Southern Ocean. *Antarctic Science*, 16(04), 471-486.
- de Baar H. J. W., de Jong J. T. M., Bakker D. C. E., Löscher B. M., Veth C., Bathmann U. and Smetacek V. (1995) Importance of iron for plankton blooms and carbon dioxide drawdown in the Southern Ocean. *Nature* **373**, 412–415.
- Bainbridge, A. E. 1981. GEOSECS Atlantic expedition. National Science Foundation
- Balakrishnan Nair T. M., Ittekkot V., Shankar R. and Guptha M. V. S. (2005) Settling barium fluxes in the Arabian Sea: Critical evaluation of relationship with export production. *Deep. Res. Part II Top. Stud. Oceanogr.* **52**, 1930–1946.
- Bates, S. L., Hendry, K. R., Pryer, H. V., Kinsley, C. W., Pyle, K. M., Woodward, E. M. S., & Horner, T. J. Barium isotopes reveal role of ocean circulation on barium cycling in the Atlantic, submitted to *Geochimica et Cosmochimica Acta*.
- van Beek P., François R., Conte M., Reyss J. L., Souhaut M. and Charette M. (2007) ²²⁸Ra/²²⁶Ra and ²²⁶Ra/Ba ratios to track barite formation and transport in the water column. *Geochim.*

- van Beek P., Reyss J. L., Bonte P. and Schmidt S. (2003) Sr/Ba in barite: A proxy of barite preservation in marine sediments? *Mar. Geol.* **199**, 205–220.
- van Beek P., Sternberg E., Reyss J. L., Souhaut M., Robin E. and Jeandel C. (2009) $^{228}\text{Ra}/^{226}\text{Ra}$ and $^{226}\text{Ra}/\text{Ba}$ ratios in the Western Mediterranean Sea: Barite formation and transport in the water column. *Geochim. Cosmochim. Acta* **73**, 4720–4737. Available at: <http://dx.doi.org/10.1016/j.gca.2009.05.063>.
- Belkin I. M. and Gordon A. L. (1996) Southern Ocean fronts from the Greenwich meridian to Tasmania. *J. Geophys. Res.* **101**, 3675.
- Bendschneider K. and Robinson R. J. (1952) A New Spectrophotometric Method for the Determination of Nitrite in Sea Water. *J. Mar. Res.* **11**, 87–96. Available at: <https://digital.lib.washington.edu/443/xmlui/handle/1773/15938>.
- Bernstein R. E. and Byrne R. H. (2004) Acantharians and marine barite. *Mar. Chem.* **86**, 45–50. Available at: <http://linkinghub.elsevier.com/retrieve/pii/S0304420303002214> [Accessed November 28, 2014].
- Bernstein R. E., Byrne R. H., Betzer P. R. and Greco A. M. (1992) Morphologies and transformations of celestite in seawater: The role of acantharians in strontium and barium geochemistry. *Geochim. Cosmochim. Acta* **56**, 3273–3279.
- Bernstein R. E., Byrne R. H. and Schijf J. (1998) Acantharians: A missing link in the oceanic biogeochemistry of barium. *Deep. Res. Part I Oceanogr. Res. Pap.* **45**, 491–505.
- Bertram M. a. and Cowen J. P. (1997) Morphological and compositional evidence for biotic precipitation of marine barite. *J. Mar. Res.* **55**, 577–593.
- De Bièvre, P.J. and Debus, G.H., 1965. Precision mass spectrometric isotope dilution analysis. *Nuclear Instruments and Methods*, 32(2), pp.224-228.
- Bishop J. K. B. (1988) The barite-opal-organic carbon association in oceanic particulate matter. *Nature* **332**, 341–343.
- Boyd P. W. (2002) Environmental factors controlling phytoplankton processes in the Southern Ocean. *J. Phycol.* **38**, 844–861.
- Brearley A. J., Meredith M. P., Naveira-Garabato A. C., Venables H. J. and Inall M. E. (2016) Controls on turbulent mixing processes on the West Antarctic Peninsula Shelf. *Deep Sea Res. Top. Oceanogr.* (in press).
- Von Breyman M. T., Emeis K.-C. and Suess E. (1992) Water depth and diagenetic constraints on the use of barium as a palaeoproductivity indicator. *Geol. Soc. London, Spec. Publ.* **64**, 273–284.

-
- Cao Z., Siebert C., Hathorne E. C., Dai M. and Frank M. (2016) Constraining the oceanic barium cycle with stable barium isotopes. *Earth Planet. Sci. Lett.* **434**, 1–9. Available at: <http://www.sciencedirect.com/science/article/pii/S0012821X15007219> [Accessed January 21, 2016].
- Cardinal D., Savoye N., Trull T. W., André L., Kopczynska E. E. and Dehairs F. (2005) Variations of carbon remineralisation in the Southern Ocean illustrated by the Baxs proxy. *Deep. Res. Part I Oceanogr. Res. Pap.* **52**, 355–370.
- Carroll, J., Brown, E.T. and Moore, W.S., 1993. The role of the Ganges-Brahmaputra mixing zone in supplying barium and ²²⁶Ra to the Bay of Bengal. *Geochimica et Cosmochimica Acta*, **57(13)**, pp.2981-2990.
- Carson D. S. (2008) Biogeochemical Controls on Productivity and Particle Flux in the Coastal Antarctic Sea Ice Environment. .
- Chan L. H., Edmond J. M., Stallard R. F., Broecker W. S., Chung Y. C., Weiss R. F. and Ku T. L. (1976) Radium and barium at GEOSECS stations in the Atlantic and Pacific. *Earth Planet. Sci. Lett.* **32**, 258–267.
- Clarke A., Meredith M. P., Wallace M. I., Brandon M. A. and Thomas D. N. (2008) Seasonal and interannual variability in temperature, chlorophyll and macronutrients in northern Marguerite Bay, Antarctica. *Deep. Res. Part II Top. Stud. Oceanogr.* **55**, 1988–2006.
- Coffey M., Dehairs F., Collette O., Luther G., Church T. and Jickells T. (1997) The behaviour of dissolved barium in estuaries. *Estuar. Coast. Shelf Sci.* **45**, 113–121. Available at: <http://linkinghub.elsevier.com/retrieve/pii/S0272771496901572>.
- Collier R. and Edmond J. (1984) The trace element geochemistry of marine biogenic particulate matter. *Prog. Oceanogr.* **13**, 113–199.
- Cook a J., Fox A. J., Vaughan D. G. and Ferrigno J. G. (2005) Retreating glacier fronts on the Antarctic Peninsula over the past half-century. *Science* **308**, 541–544.
- Cunningham S. A., Alderson S. G., King B. A. and Brandon M. A. (2003) Transport and variability of the Antarctic Circumpolar Current in Drake Passage. *J. Geophys. Res.* **108**, 8084. Available at: <http://doi.wiley.com/10.1029/2001JC001147>.
- Von Damm K. L., Edmond J. M., Grant B. and Measures C. I. (1985) Chemistry of submarine hydrothermal solutions at 21°N, East Pacific Rise. *Geochim. Cosmochim. Acta* **49**, 2197–2220.
- Deacon G. E. R. (1982) Physical and biological zonation in the Southern Ocean. *Deep Sea Res. Part A, Oceanogr. Res. Pap.* **29**, 1–15.
- Dehairs F., Baeyens W. and Goeyens L. (1992) Accumulation of suspended barite at mesopelagic
-

-
- depths and export production in the southern ocean. *Science* **258**, 1332–1335.
- Dehairs F., Chesselet R. and Jedwab J. (1980) Discrete suspended particles of barite and the barium cycle in the open ocean. *Earth Planet. Sci. Lett.* **49**, 528–550.
- Dehairs F., Goeyens L., Stroobants N., Bernard P., Goyet C., Poisson A. and Chesselet R. (1990) On suspended barite and the oxygen minimum in the Southern Ocean. *Global Biogeochem. Cycles* **4**, 85–102.
- Dehairs F., Shopova D., Ober S., Veth C. and Goeyens L. (1997) Particulate barium stocks and oxygen consumption in the Southern Ocean mesopelagic water column during spring and early summer: Relationship with export production. *Deep. Res. Part II Top. Stud. Oceanogr.* **44**, 497–516.
- Dehairs F., Stroobants N. and Goeyens L. (1991) Suspended barite as a tracer of biological activity in the Southern Ocean. *Mar. Chem.* **35**, 399–410. Available at: <http://www.sciencedirect.com/science/article/pii/S0304420309900329> [Accessed May 9, 2016].
- Dierssen H. M., Smith R. C. and Vernet M. (2002) Glacial meltwater dynamics in coastal waters west of the Antarctic peninsula. *Proc. Natl. Acad. Sci. U. S. A.* **99**, 1790–1795. Available at: <Go to ISI>://WOS:000174031100010\nhttp://www.ncbi.nlm.nih.gov/pmc/articles/PMC122272/pdf/pq0402001790.pdf.
- Ducklow H. W., Baker K., Martinson D. G., Quetin L. B., Ross R. M., Smith R. C., Stammerjohn S. E., Vernet M. and Fraser W. (2007) Marine pelagic ecosystems: the West Antarctic Peninsula. *Philos. Trans. R. Soc. B Biol. Sci.* **362**, 67–94. Available at: <http://rstb.royalsocietypublishing.org/cgi/doi/10.1098/rstb.2006.1955> [Accessed October 15, 2014].
- Dymond J. and Collier R. (1996) Particulate barium fluxes and their relationships to biological productivity. *Deep Sea Res. Part II Top. Stud. Oceanogr.* **43**, 1283–1308.
- Dymond J., Seuss E. and Lyle M. (1992) Barium in deep-sea sediment: A geochemical proxy for paleoproductivity. *Paleoceanography* **7**, 163–181.
- Edmond J. M., Measures C., McDuff R. E., Chan L. H., Collier R., Grant B., Gordon L. I. and Corliss J. B. (1979) Ridge crest hydrothermal activity and the balances of the major and minor elements in the ocean: The Galapagos data. *Earth Planet. Sci. Lett.* **46**, 1–18.
- Epstein S. and Mayeda T. (1953) VARIATION OF O-18 CONTENT OF WATERS FROM NATURAL SOURCES. *Geochim. Cosmochim. Acta* **4**, 213–224. Available at: <Go to ISI>://WOS:A1953YH19700001.
-

-
- Esser B. K. and Volpe A. M. (2002) At-sea high-resolution chemical mapping: Extreme barium depletion in North Pacific surface water. *Mar. Chem.* **79**, 67–79.
- Fagel N., André L. and Dehairs F. (1999) Advective excess Ba transport as shown from sediment and trap geochemical signatures. *Geochim. Cosmochim. Acta* **63**, 2353–2367.
- Fagel N., Dehairs F., André L., Bareille G. and Monnin C. (2002) Ba distribution in surface Southern Ocean sediments and export production estimates. *Paleoceanography* **17**.
- Falkner K. K., Macdonald R. ., Carmack E. . and Weigarter T. (1994) The Potential of Barium as a Tracer of Arctic Water Masses. *Polar Ocean. Their Role Shap. Glob. Environ. Geophys. Monogr. 85* **85**, 63–76.
- Feely, R.A., Lewison, M., Massoth, G.J., Robert-Baldo, G., Lavelle, J.W., Byrne, R.H., Von Damm, K.L. and Curl, H.C., 1987. Composition and dissolution of black smoker particulates from active vents on the Juan de Fuca Ridge. *Journal of Geophysical Research: Solid Earth*, 92(B11), pp.11347-11363.
- Fresnel, J., Galle, P.T. and Gayral, P., 1979. Résultats de la microanalyse des cristaux vacuolaires chez deux Chromophytes unicellulaires marines: *Exanthemachrysis gayraliae*, *Pavlova* sp.(Prymnesiophycées, Pavlovacées). Comptes rendus hebdomadaires des seances. Serie D. Sciences naturelles.
- Finlay B. J., Hetherington N. B. and Da Vison W. (1983) Active biological participation in lacustrine barium chemistry. *Geochim. Cosmochim. Acta* **47**, 1325–1329.
- Fortner S. K., Lyons W. B., Fountain A. G., Welch K. A. and Kehrwald N. M. (2009) Trace element and major ion concentrations and dynamics in glacier snow and melt: Eliot Glacier, Oregon Cascades. *Hydrol. Process.* **23**, 2987–2996.
- Franck V. M., Brzezinski M. A., Coale K. H. and Nelson D. M. (2000) Iron and silicic acid concentrations regulate Si uptake north and south of the Polar Frontal Zone in the Pacific Sector of the Southern Ocean. *Deep. Res. Part II Top. Stud. Oceanogr.* **47**, 3315–3338.
- Francois R., Honjo S., Manganini J. and Ravizza E. (1995) Biogenic barium fluxes to the deep sea: Implications for palaeoproductivity reconstruction. **9**, 289–303.
- Froelich, P., Klinkhammer, G.P., Bender, M.A.A., Luedtke, N.A., Heath, G.R., Cullen, D., Dauphin, P., Hammond, D., Hartman, B. and Maynard, V., 1979. Early oxidation of organic matter in pelagic sediments of the eastern equatorial Atlantic: suboxic diagenesis. *Geochimica et Cosmochimica Acta*,43(7), pp.1075-1090.
- Ganeshram R. S., François R., Commeau J. and Brown-Leger S. L. (2003) An experimental investigation of barite formation in seawater. *Geochim. Cosmochim. Acta* **67**, 2599–2605.
- Garibotti I., Vernet M., Ferrario M., Smith R., Ross R. and Quetin L. (2003) Phytoplankton spatial
-

-
- distribution patterns along the western Antarctic Peninsula (Southern Ocean). *Mar. Ecol. Prog. Ser.* **261**, 21–39.
- Gille S. T. (1994) Mean sea surface height of the Antarctic Circumpolar Current from Geosat data: Method and application. *J. Geophys. Res.* **99**, 18255.
- Goldberg, E. D. and Arrhenius, G. O. S. 1958. Chemistry of Pacific pelagic sediments. *Geochimica et Cosmochimica Acta* **13(2)**, pp. 153-212.
- Gonneea M. E. and Paytan A. (2006) Phase associations of barium in marine sediments. *Mar. Chem.* **100**, 124–135.
- Gonzalez-Muñoz M. T., Fernandez-Luque B., Martinez-Ruiz F., Ben Chekroun K., Arias J. M., Rodriguez-Gallego M., Martinez-Canamero M., de Linares C. and Paytan A. (2003) Precipitation of barite by *Myxococcus xanthus*: possible implications for the biogeochemical cycle of barium. *Appl Env. Microbiol* **69**, 5722–5725. Available at: <http://www.ncbi.nlm.nih.gov/pubmed/12957970>.
- Gonzalez-Muñoz M. T., Martinez-Ruiz F., Morcillo F., Martin-Ramos J. D. and Paytan a. (2012) Precipitation of barite by marine bacteria: A possible mechanism for marine barite formation. *Geology* **40**, 675–678.
- Gooday a J. and Nott J. a (1982) Intracellular Barite Crystals in 2 Xenophyophores, *Aschemonella-Ramuliformis* and *Galatheammia* Sp (Protozoa, Rhizopoda) with Comments on the Taxonomy of *Aschemonella-Ramuliformis*. *J. Mar. Biol. Assoc. United Kingdom* **62**, 595–605. Available at: <Go to ISI>://A1982PB63200008.
- Graham R. M., De Boer A. M., Heywood K. J., Chapman M. R. and Stevens D. P. (2012) Southern Ocean fronts: Controlled by wind or topography? *J. Geophys. Res. Ocean.* **117**.
- Griffith E. M. and Paytan A. (2012) Barite in the ocean - occurrence, geochemistry and palaeoceanographic applications. *Sedimentology* **59**, 1817–1835.
- Gruber N. (2008) The Marine Nitrogen Cycle: Overview and Challenges. In *Nitrogen in the Marine Environment* Elsevier Inc. pp. 1–50.
- Guay, C. K. and Falkner, K. 1997. Barium as a tracer of Arctic halocline and river waters. *Deep Sea Research Part II: Topical Studies in Oceanography* **44(8)**, pp. 1543-1569
- Guay C. K. and Falkner K. K. (1998) A survey of dissolved barium in the estuaries of major Arctic rivers and adjacent seas. *Cont. Shelf Res.* **18**, 859–882.
- Hall J. M. and Chan L.-H. (2004) Ba/Ca in *Neogloboquadrina pachyderma* as an indicator of deglacial meltwater discharge into the western Arctic Ocean. *Paleoceanography* **19**, 1–9.
- Hanor J. S. and Chan L.-H. (1977) Non-conservative behavior of barium during mixing of Mississippi River and Gulf of Mexico waters. *Earth Planet. Sci. Lett.* **37**, 242–250.
-

-
- Hendry K. R., Meredith M. P., Measures C. I., Carson D. S. and Rickaby R. E. M. (2010) The role of sea ice formation in cycling of aluminium in northern Marguerite Bay, Antarctica. *Estuar. Coast. Shelf Sci.* **87**, 103–112. Available at: <http://linkinghub.elsevier.com/retrieve/pii/S0272771409006003> [Accessed November 18, 2014].
- Hendry K. R., Rickaby R. E. M., de Hoog J. C. M., Weston K. and Rehkemper M. (2009) The cadmium-phosphate relationship in brine: biological versus physical control over micronutrients in sea ice environments. *Antarct. Sci.* **22**, 11. Available at: http://www.journals.cambridge.org/abstract_S0954102009990381.
- Hendy I. L. (2010) Diagenetic behavior of barite in a coastal upwelling setting. *Paleoceanography* **25**, 1–9.
- Henkel S., Mogollón J. M., Nöthen K., Franke C., Bogus K., Robin E., Bahr A., Blumenberg M., Pape T., Seifert R., März C., de Lange G. J. and Kasten S. (2012) Diagenetic barium cycling in Black Sea sediments - A case study for anoxic marine environments. *Geochim. Cosmochim. Acta* **88**, 88–105.
- Hernandez-Sanchez M. T., Mills R. a., Planquette H., Pancost R. D., Hepburn L., Salter I. and Fitzgeorge-Balfour T. (2011) Quantifying export production in the Southern Ocean: Implications for the Ba xs proxy. *Paleoceanography* **26**.
- Hetzinger S., Halfar J., Zack T., Mecking J. V., Kunz B. E., Jacob D. E. and Adey W. H. (2013) Coralline algal barium as indicator for 20th century northwestern North Atlantic surface ocean freshwater variability. *Sci. Rep.* **3**, 1–8. Available at: <http://www.pubmedcentral.nih.gov/articlerender.fcgi?artid=3641520&tool=pmcentrez&ndertype=abstract>.
- Hinz D. J., Poulton A. J., Nielsd??ttir M. C., Steigenberger S., Korb R. E., Achterberg E. P. and Bibby T. S. (2012) Comparative seasonal biogeography of mineralising nannoplankton in the Scotia Sea: *Emiliana huxleyi*, *Fragilariopsis* spp. and *Tetraparma pelagica*. *Deep. Res. Part II Top. Stud. Oceanogr.* **59-60**, 57–66.
- Hoelzl, R., Hoelzl, C., Kotz, L. and Fabry, L., 1998. The optimal amount of isotopic spike solution for ultratrace analysis by isotope dilution mass spectrometry. *Accreditation and quality assurance*, **3**(5), pp.185-188.
- Holmes R. M., Aminot A., Kerouel R., Hooker B. A. and Peterson B. J. (1999) A simple and precise method for measuring ammonium in marine and freshwater ecosystems. *Can. J. Fish. Aquat. Sci.* **56**, 1801–1808. Available at: <Go to ISI>://WOS:000083494700010.
- Holm-Hansen O., Naganobu M., Kawaguchi S., Kameda T., Krasovski I., Tchernyshkov P., Priddle
-

-
- J., Korb R., Brandon M., Demer D., Hewitt R. P., Kahru M. and Hewes C. D. (2004) Factors influencing the distribution, biomass, and productivity of phytoplankton in the Scotia Sea and adjoining waters. *Deep Sea Res. Part II Top. Stud. Oceanogr.* **51**, 1333–1350.
- Hoppema M., Dehairs F., Navez J., Monnin C., Jeandel C., Fahrbach E. and de Baar H. J. W. (2010) Distribution of barium in the Weddell Gyre: Impact of circulation and biogeochemical processes. *Mar. Chem.* **122**, 118–129. Available at: <http://linkinghub.elsevier.com/retrieve/pii/S0304420310000885> [Accessed November 18, 2014].
- Horner T. J., Kinsley C. W. and Nielsen S. G. (2015) Barium-isotopic fractionation in seawater mediated by barite cycling and oceanic circulation. *Earth Planet. Sci. Lett.* **430**, 511–522.
- Huang K., Ducklow H., Vernet M., Cassar N. and Bender M. L. (2012) Export production and its regulating factors in the West Antarctica Peninsula region of the Southern Ocean. *Global Biogeochem. Cycles* **26**.
- Hutchins D. a and Bruland K. W. (1998) Iron-limited diatom growth and Si²⁺: N uptake ratios in a coastal upwelling regime. *Nature* **393**, 561–564. Available at: <Go to ISI>://000074150100047.
- Jacquet S. H. M., Dehairs F., Cardinal D., Navez J. and Delille B. (2005) Barium distribution across the Southern Ocean frontal system in the Crozet–Kerguelen Basin. *Mar. Chem.* **95**, 149–162. Available at: <http://linkinghub.elsevier.com/retrieve/pii/S0304420304002464> [Accessed November 16, 2014].
- Jacquet S. H. M., Dehairs F., Dumont I., Becquevort S., Cavagna a. J. and Cardinal D. (2011) Twilight zone organic carbon remineralization in the Polar Front Zone and Subantarctic Zone south of Tasmania. *Deep. Res. Part II Top. Stud. Oceanogr.* **58**, 2222–2234. Available at: <http://dx.doi.org/10.1016/j.dsr2.2011.05.029>.
- Jacquet S. H. M., Dehairs F., Elskens M., Savoye N. and Cardinal D. (2007) Barium cycling along WOCE SR3 line in the Southern Ocean. *Mar. Chem.* **106**, 33–45.
- Jacquet S. H. M., Dehairs F. and Rintoul S. (2004) A high resolution transect of dissolved barium in the Southern Ocean. *Geophys. Res. Lett.* **31**, 7–10.
- Jeandel C., Dupré B., Lebaron G., Monnin C. and Minster J.-F. (1996) Longitudinal distributions of dissolved barium, silica and alkalinity in the western and southern Indian Ocean. *Deep Sea Res. Part I Oceanogr. Res. Pap.* **43**, 1–31. Available at: <http://www.sciencedirect.com/science/article/pii/0967063795000984>.
- Kasten S., Haese R. R., Zabel M., Rühlemann C. and Schulz H. D. (2001) Barium peaks at glacial terminations in sediments of the equatorial Atlantic Ocean—relicts of deglacial productivity
-

-
- pulses? *Chem. Geol.* **175**, 635–651. Available at:
<http://linkinghub.elsevier.com/retrieve/pii/S0009254100003776>.
- Kim I., Kim G. and Choy E. J. (2015) The significant inputs of trace elements and rare earth elements from melting glaciers in Antarctic coastal waters. **1**, 1–13.
- King J. C., Turner J., Marshall G. J., Connolley W. M. and Lachlan-Cope T. A. (2003) Antarctic Peninsula climate variability and its causes as revealed by analysis of instrumental records. *Antarct. Res. Ser.* **79**, 17–30. Available at:
<http://www.agu.org/books/ar/v079/AR079p0017/AR079p0017.shtml>.
- Klinck, J.M., (1998) Heat and salt changes on the continental shelf west of the Antarctic Peninsula between January 1993 and January 1994. *Journal of Geophysical Research*, **103**(C4), pp.7617-7636.
- Klinck J. M., Hofmann E. E., Beardsley R. C., Salihoglu B. and Howard S. (2004) Water-mass properties and circulation on the west Antarctic Peninsula Continental Shelf in Austral Fall and Winter 2001. *Deep. Res. Part II Top. Stud. Oceanogr.* **51**, 1925–1946.
- Klinkhammer G. P. and Chan L. H. (1990) Determination of barium in marine waters by isotope dilution inductively coupled plasma mass spectrometry. *Anal. Chim. Acta* **232**, 323–329.
- Korb R. E., Whitehouse M. J., Thorpe S. E. and Gordon M. (2005) Primary production across the Scotia Sea in relation to the physico-chemical environment. *J. Mar. Syst.* **57**, 231–249.
- Kozlowski W. A., Deutschman D., Garibotti I., Trees C. and Vernet M. (2011) An evaluation of the application of CHEMTAX to Antarctic coastal pigment data. *Deep. Res. Part I Oceanogr. Res. Pap.* **58**, 350–364.
- Kushnir, Y., Robinson, W. A., Bladé, I., Hall, N. M. J., Peng, S., & Sutton, R. (2002). Atmospheric GCM response to extratropical SST anomalies: Synthesis and evaluation. *Journal of Climate*, **15**(16), 2233-2256.
- Landry M. R., Selph K. E., Brown S. L., Abbott M. R., Measures C. I., Vink S., Allen C. B., Calbet a, Christensen S. and Nolla H. (2002) Seasonal dynamics of phytoplankton in the Antarctic Polar Front region at 170 degrees W. *Deep. Res. Part II-topical Stud. Oceanogr.* **49**, 1843–1865.
- Lannuzel D., Bowie A. R., van der Merwe P. C., Townsend A. T. and Schoemann V. (2011) Distribution of dissolved and particulate metals in Antarctic sea ice. *Mar. Chem.* **124**, 134–146. Available at: <http://dx.doi.org/10.1016/j.marchem.2011.01.004>.
- LaVigne M., Grottoli A. G., Palardy J. E. and Sherrell R. M. (2016) Multi-colony calibrations of coral Ba/Ca with a contemporaneous in situ seawater barium record. *Geochim. Cosmochim. Acta*. Available at:
-

<http://www.sciencedirect.com/science/article/pii/S0016703716300060> [Accessed February 10, 2016].

- Lea D. and Boyle E. (1989) Barium content of benthic foraminifera controlled by bottom-water composition. *Nature* **338**, 751–753.
- Lea D. W. and Boyle E. a (1991) Barium in planktonic foraminifera. *Geochim. Cosmochim. Acta* **55**, 3321–3331.
- Lea D. W. and Boyle E. a. (1990) A 210,000-year record of barium variability in the deep northwest Atlantic Ocean. *Nature* **347**, 269–272.
- Lea D. W. and Boyle E. a. (1993) Determination of carbonate-bound barium in foraminifera and corals by isotope dilution plasma-mass spectrometry. *Chem. Geol.* **103**, 73–84. Available at: <http://linkinghub.elsevier.com/retrieve/pii/000925419390292Q>.
- Lea D. W. and Spero H. J. (1994) Assessing the reliability of paleochemical tracers: barium uptake in the shells of planktonic foraminifera. *Paleoceanography* **9**, 445–452.
- Lea D. W. and Spero H. J. (1992) Experimental determination of barium uptake in shells of the planktonic foraminifera *Orbulina universa* at 22°C. *Geochim. Cosmochim. Acta* **56**, 2673–2680.
- Levin L. A. (1994) Paleoecology and ecology of Xenophyophores. *Adv. Deep Sea Paleoecol.* **9**, 32–41.
- Li Y. H., Ku T. L., Mathieu G. . and Wolgemuth K. (1973) Ba in the antarctic ocean and its implications regarding the marine geochemistry of Ba and $^{226}\text{Ra}^*$. *Earth Planet.* **19**, 352–358.
- Li, Y. H. and Chan, L. H. 1979. Desorption of Ba and ^{226}Ra from river-borne sediments in the Hudson estuary. *Earth and Planetary Science Letters* 43(3), pp. 343-350.
- Lovenduski N. S. and Gruber N. (2005) Impact of the Southern Annular Mode on Southern Ocean circulation and biology. *Geophys. Res. Lett.* **32**, 1–4.
- Marinov I., Gnanadesikan a, Toggweiler J. R. and Sarmiento J. L. (2006) The Southern Ocean biogeochemical divide. *Nature* **441**, 964–967.
- Martin J. H. (1990) Glacial-Interglacial CO₂ changes: The Iron Hypothesis. *Paleoceanography* **5**, 1–13.
- Martin J.-M. and Meybeck M. (1979) Elemental mass-balance of material carried by major world rivers. *Mar. Chem.* **7**, 173–206.
- Martinson D. G. and McKee D. C. (2012) Transport of warm upper circumpolar deep water onto the Western Antarctic Peninsula Continental Shelf. *Ocean Sci.* **8**, 433–442.
- Martinson D. G., Stammerjohn S. E., Iannuzzi R. a., Smith R. C. and Vernet M. (2008) Western

-
- Antarctic Peninsula physical oceanography and spatio-temporal variability. *Deep Sea Res. Part II Top. Stud. Oceanogr.* **55**, 1964–1987.
- Maykut, G. A. (1985). The ice environment. Department of Atmospheric Sciences/Geophysics Program, University of Washington.
- McBean, G., Alekseev, G., Chen, D., Foerland, E., Fyfe, J., Groisman, P. Y., ... & Whitfield, P. H. (2005). Chapter 2: Arctic Climate: past and present. Arctic Climate Impact Assessment.[np].
- McManus J., Berelson W. M., Hammond D. E. and Klinkhammer G. P. (1999) Barium cycling in the North Pacific: Implications for the utility of Ba as a paleoproductivity and paleoalkalinity proxy. *Paleoceanography* **14**, 53–61.
- McManus J., Berelson W. M., Klinkhammer G. P., Johnson K. S., Coale K. H., Anderson R. F., Kumar N., Burdige D. J., Hammond D. E., Brumsack H. J., McCorkle D. C. and Rushdi A. (1998) Geochemistry of barium in marine sediments: implications for its use as a paleoproxy. *Geochim. Cosmochim. Acta* **62**, 3453–3473.
- McManus J., Berelson W. M., Klinkhammer G. P., Kilgore T. E. and Hammond D. E. (1994) Remobilization of barium in continental margin sediments. *Geochim. Cosmochim. Acta* **58**, 4899–4907.
- McManus J., Dymond J., Dunbar R. B. and Collier R. W. (2002) Particulate barium fluxes in the Ross Sea. *Mar. Geol.* **184**, 1–15.
- Meijers (2014) - Cruise report for BAS cruise JR299, details and report available at http://www.bodc.ac.uk/resources/inventories/cruise_inventory/report/13406/
- Mengelt C., Abbott M. R., Barth J. A., Letelier R. M., Measures C. I. and Vink S. (2001) Phytoplankton pigment distribution in relation to silicic acid, iron and the physical structure across the Antarctic Polar Front, 170°W, during austral summer. *Deep. Res. Part II Top. Stud. Oceanogr.* **48**, 4081–4100.
- Meredith M. P., Brandon M. A., Wallace M. I., Clarke A., Leng M. J., Renfrew I. A., van Lipzig N. P. M. and King J. C. (2008) Variability in the freshwater balance of northern Marguerite Bay, Antarctic Peninsula: Results from $\delta^{18}O$. *Deep. Res. Part II Top. Stud. Oceanogr.* **55**, 309–322.
- Meredith M. P., Brandon M. a., Wallace M. I., Clarke A., Leng M. J., Renfrew I. a., van Lipzig N. P. M. and King J. C. (2008) Variability in the freshwater balance of northern Marguerite Bay, Antarctic Peninsula: Results from $\delta^{18}O$. *Deep Sea Res. Part II Top. Stud. Oceanogr.* **55**, 309–322. Available at: <http://linkinghub.elsevier.com/retrieve/pii/S0967064507003049> [Accessed November 28, 2014].
- Meredith M. P., Locarnini R. A., Van Scoy K. A., Watson A. J., Heywood K. J. and King B. A. (2000)
-

-
- On the sources of Weddell Gyre Antarctic Bottom Water. *J. Geophys. Res.* **105**, 1093–1104.
Available at: <http://www.agu.org/pubs/crossref/2000/1999JC900263.shtml>.
- Meredith M. P., Renfrew I. A., Clarke A., King J. C. and Brandon M. A. (2004) Impact of the 1997/98 ENSO on upper ocean characteristics in Marguerite Bay, western Antarctic Peninsula. *J. Geophys. Res. C Ocean.* **109**, 1–19.
- Meredith M. P., Stammerjohn S. E., Venables H. J., Ducklow H. W., Martinson D. G., Iannuzzi R. A., Leng M. J., van Wesseem J. M., Reijmer C. H. and Barrand N. E. (2016) Changing distributions of sea ice melt and meteoric water west of the Antarctic Peninsula. *Deep Sea Res. Part II Top. Stud. Oceanogr.* Available at:
<http://www.sciencedirect.com/science/article/pii/S0967064516300947>.
- Meredith M. P., Venables H. J., Clarke A., Ducklow H. W., Erickson M., Leng M. J., Lenaerts J. T. M. and van den Broeke M. R. (2013) The Freshwater System West of the Antarctic Peninsula: Spatial and Temporal Changes. *J. Clim.* **26**, 1669–1684. Available at:
<http://journals.ametsoc.org/doi/abs/10.1175/JCLI-D-12-00246.1> [Accessed November 28, 2014].
- Meredith M. P., Wallace M. I., Stammerjohn S. E., Renfrew I. a., Clarke A., Venables H. J., Shoosmith D. R., Souster T. and Leng M. J. (2010) Changes in the freshwater composition of the upper ocean west of the Antarctic Peninsula during the first decade of the 21st century. *Prog. Oceanogr.* **87**, 127–143. Available at:
<http://linkinghub.elsevier.com/retrieve/pii/S007966111000131X> [Accessed November 28, 2014].
- Mitchell A., Brown G. H. and Fuge R. (2001) Minor and trace element export from a glacierized Alpine headwater catchment (Haut Glacier d’Arolla, Switzerland). *Hydrol. Process.* **15**, 3499–3524.
- Mitchell, C., & Beardall, J. (1996). Inorganic carbon uptake by an Antarctic sea-ice diatom, *Nitzschia frigida*. *Polar Biology*, *16*(2), 95-99.
- Moline M. A., Claustre H., Frazer T. K., Schofield O. and Vernet M. (2004) Alteration of the food web along the Antarctic Peninsula in response to a regional warming trend. *Glob. Chang. Biol.* **10**, 1973–1980.
- Monnin C. and Cividini D. (2006) The saturation state of the world’s ocean with respect to (Ba,Sr)SO₄ solid solutions. *Geochim. Cosmochim. Acta* **70**, 3290–3298.
- Monnin C., Jeandel C., Cattaldo T. and Dehairs F. (1999) The marine barite saturation state of the world’s oceans. *Mar. Chem.* **65**, 253–261.
- Moore J. K., Abbott M. R., Richman J. G., Smith W. O., Cowles T. J., Coale K. H., Gardner W. D.
-

-
- and Barber R. T. (1999) SeaWiFS satellite ocean color data from the Southern Ocean. *Geophys. Res. Lett.* **26**, 1465.
- Moore, W. S. 1997. High fluxes of radium and barium from the mouth of the Ganges-Brahmaputra River during low river discharge suggest a large groundwater source. *Earth and Planetary Science Letters* **150**(1), pp. 141-150.
- Moore W. S. and Dymond J. (1991) Fluxes of ²²⁶Ra and barium in the Pacific Ocean: The importance of boundary processes. *Earth Planet. Sci. Lett.* **107**, 55–68.
- Mora S. J. De, Whitehead R. F. and Gregory M. (1994) The chemical composition of glacial melt water ponds and streams on the McMurdo Ice Shelf, Antarctica. *Antarct. Sci.* **6**, 17–27.
- Morgan-Kiss, R. M., Priscu, J. C., Pockock, T., Gudynaite-Savitch, L., & Huner, N. P. (2006). Adaptation and acclimation of photosynthetic microorganisms to permanently cold environments. *Microbiology and Molecular Biology Reviews*, 70(1), 222-252.
- Murphy E. J., Watkins J. L., Trathan P. N., Reid K., Meredith M. P., Thorpe S. E., Johnston N. M., Clarke a, Tarling G. a, Collins M. a, Forcada J., Shreeve R. S., Atkinson a, Korb R., Whitehouse M. J., Ward P., Rodhouse P. G., Enderlein P., Hirst a G., Martin a R., Hill S. L., Staniland I. J., Pond D. W., Briggs D. R., Cunningham N. J. and Fleming a H. (2007) Spatial and temporal operation of the Scotia Sea ecosystem: a review of large-scale links in a krill centred food web. *Philos. Trans. R. Soc. Lond. B. Biol. Sci.* **362**, 113–148.
- Naveira Garabato A. C., McDonagh E. L., Stevens D. P., Heywood K. J. and Sanders R. J. (2002) On the export of Antarctic Bottom Water from the Weddell Sea. *Deep. Res. Part II Top. Stud. Oceanogr.* **49**, 4715–4742.
- Nelson, D. M., & Treguer, P. (1992). Role of silicon as a limiting nutrient to Antarctic diatoms: Evidence from kinetic studies in the Ross Sea ice-edge zone. *Marine ecology progress series*. Oldendorf, 80(2), 255-264.
- Nozaki Y., Yamamoto Y., Manaka T., Amakawa H. and Snidvongs A. (2001) Dissolved barium and radium isotopes in the Chao Phraya River estuarine mixing zone in Thailand. *Cont. Shelf Res.* **21**, 1435–1448.
- Nurnberg C. C., Bohrmann G., Schlüter M. and Frank M. (1997) Barium accumulation in the Atlantic sector of the Southern Ocean: Results from 190,000-year records. **12**, 594–603.
- Nürnberg D., Wollenburg I., Dethleff D., Eicken H., Kassens H., Letzig T., Reimnitz E. and Thiede J. (1994) Sediments in Arctic sea ice: Implications for entrainment, transport and release. *Mar. Geol.* **119**, 185–214. Available at: <http://linkinghub.elsevier.com/retrieve/pii/0025322794901813>.
- Ohshima K. I., Fukamachi Y., Williams G. D., Nihashi S., Roquet F., Kitade Y., Tamura T., Hirano D.,
-

-
- Herraiz-Borreguero L., Field I., Hindell M., Aoki S. and Wakatsuchi M. (2013) Antarctic Bottom Water production by intense sea-ice formation in the Cape Darnley polynya. *Nat. Geosci.* **6**, 235–240. Available at: <http://www.nature.com/doi/10.1038/ngeo1738>.
- Orsi A. H., Nowlin W. D. and Whitworth T. (1993) On the circulation and stratification of the Weddell Gyre. *Deep. Res. Part I* **40**, 169–203.
- Orsi A. H., Whitworth T. and Nowlin W. D. (1995) On the meridional extent and fronts of the Antarctic Circumpolar Current. *Deep. Res. Part I* **42**, 641–673.
- Östlund H. G. and Hut G. (1984) Arctic Ocean water mass balance from isotope data. *J. Geophys. Res. Ocean.* **89**, 6373–6381. Available at:
<http://dx.doi.org/10.1029/JC089iC04p06373> \n <http://onlinelibrary.wiley.com/doi/10.1029/JC089iC04p06373/abstract> \n <http://onlinelibrary.wiley.com/store/10.1029/JC089iC04p06373/asset/jgrc3326.pdf?v=1&t=hhtggirm&s=8fa8e62a74ce99500f08df02a9b2c9128be032b5>
- Ostlund, H.G., 1987. GEOSECS Atlantic, Pacific, and Indian Ocean Expeditions Vol 7.
- Paytan A., Averyt K., Faul K., Gray E. and Thomas E. (2007) Barite accumulation, ocean productivity, and Sr/Ba in barite across the Paleocene-Eocene Thermal Maximum. *Geology* **35**, 1139–1142.
- Paytan A. and Griffith E. M. (2007) Marine barite: Recorder of variations in ocean export productivity. *Deep Sea Res. Part II Top. Stud. Oceanogr.* **54**, 687–705. Available at: <http://linkinghub.elsevier.com/retrieve/pii/S0967064507000422> [Accessed November 28, 2014].
- Paytan A. and Kastner M. (1996) Benthic Ba fluxes in the central Equatorial Pacific, implications for the oceanic Ba cycle. *Earth Planet. Sci. Lett.* **142**, 439–450. Available at: <http://linkinghub.elsevier.com/retrieve/pii/0012821X96001203>.
- Paytan A., Kastner M., Martin E. E., Macdougall J. D. and Herbert T. (1993) Marine Barite as a monitor of seawater strontium isotope composition. *Nature*.
- Perovich D. K., Elder B. C., Claffey K. J., Stammerjohn S., Smith R., Ackley S. F., Krouse H. R. and Gow A. J. (2004) Winter sea-ice properties in Marguerite Bay, Antarctica. *Deep. Res. Part II Top. Stud. Oceanogr.* **51**, 2023–2039.
- Peterson R. G. and Whitworth T. (1989) The subantarctic and polar fronts in relation to deep water masses through the southwestern Atlantic. *J. Geophys. Res.* **94**, 10817.
- Petrich, C. and H. Eicken (2010). Growth, Structure and Properties of Sea Ice. In *Sea Ice*, 2nd ed, D. N. Thomas and G. S. Dieckmann (eds), Wiley–Blackwell, Oxford, UK, pp. 23–77. <http://dx.doi.org/10.1002/9781444317145.ch2>
- Pingitore Jr, N. E. 1986. Modes of coprecipitation of Ba²⁺ and Sr²⁺ with calcite. *Geochemical*
-

processes at mineral surfaces, pp. 574-586.

- Plewa K., Meggers H. and Kasten S. (2006) Barium in sediments off northwest Africa: A tracer for paleoproductivity or meltwater events? *Paleoceanography* **21**, PA2015. Available at: <http://doi.wiley.com/10.1029/2005PA001136> [Accessed November 28, 2014].
- Plewa K., Meggers H., Kuhlmann H., Freudenthal T., Zabel M. and Kasten S. (2012) Geochemical distribution patterns as indicators for productivity and terrigenous input off NW Africa. *Deep Sea Res. Part I Oceanogr. Res. Pap.* **66**, 51–66. Available at: <http://linkinghub.elsevier.com/retrieve/pii/S0967063712000866>.
- Pollard R. T., Lucas M. I. and Read J. F. (2002) Physical controls on biogeochemical zonation in the Southern Ocean. *Deep. Res. Part II Top. Stud. Oceanogr.* **49**, 3289–3305.
- Raiswell R., Benning L. G., Davidson L. and Tranter M. (2008) Nanoparticulate bioavailable iron minerals in icebergs and glaciers. *Mineral. Mag.* **72**, 345–348.
- Raiswell R., Benning L. G., Tranter M. and Tulaczyk S. (2008) Bioavailable iron in the Southern Ocean: the significance of the iceberg conveyor belt. *Geochem. Trans.* **9**, 7.
- Rintoul S. R., Hughes C. and Olbers D. (2001) The Antarctic Circumpolar Current System. In *Ocean Circulation and Climate* (eds. G. Siedler, J. Church, and J. Gould). Academic Press. pp. 271–301. Available at: <http://www.agu.org/pubs/crossref/2011/2011GL046898.shtml\npapers2://publication/doi/10.1029/2011GL046898>.
- Roeske T., Bauch D., Rutgers V.D. Loeff M. and Rabe B. (2012) Utility of dissolved barium in distinguishing North American from Eurasian runoff in the Arctic Ocean. *Mar. Chem.* **132-133**, 1–14. Available at: <http://linkinghub.elsevier.com/retrieve/pii/S0304420312000084>.
- Rushdi A. I., McManus J. and Collier R. W. (2000) Marine barite and celestite saturation in seawater. *Mar. Chem.* **69**, 19–31.
- Van Santvoort P. J. M., De Lange G. J., Thomson J., Cussen H., Wilson T. R. S., Krom M. D. and Ströhle K. (1996) Active post-depositional oxidation of the most recent sapropel (S1) in sediments of the eastern Mediterranean Sea. *Geochim. Cosmochim. Acta* **60**, 4007–4024.
- Sarmiento J. L., Gruber N., Brzezinski M. A. and Dunne J. P. (2004) High-latitude controls of thermocline nutrients and low latitude biological productivity. *Nature* **427**, 56–60.
- Savenko, V.S., 2006, March. Principal features of the chemical composition of suspended load in world rivers. In *Doklady earth sciences* (Vol. **407**, No. 2, pp. 450-454). MAIK Nauka/Interperiodica.
- Schenau S. J., Prins M. a., De Lange G. J. and Monnin C. (2001) Barium accumulation in the Arabian Sea: Controls on barite preservation in marine sediments. *Geochim. Cosmochim.*

- Schloss I. R., Ferreyra G. A. and Ruiz-Pino D. (2002) Phytoplankton biomass in Antarctic shelf zones: A conceptual model based on Potter Cove, King George Island. *J. Mar. Syst.* **36**, 129–143.
- Schmitz B. (1987) Barium, Equatorial high productivity and the northward wandering of the Indian continent. *Paleoceanography* **2**, 63–77.
- Schroeder J. O., Murray R. W., Leinen M., Pflaum R. C. and Janecek T. R. (1997) Barium in equatorial Pacific carbonate sediment: Terrigenous, oxide, and biogenic associations. *Paleoceanography* **12**, 125.
- Seidov, D., Antonov, J. I., Arzayus, K.M., Baranova, O.K., Biddle, M., BOyer, T.P., Johnson, D.R., Mishonov, A.V., Paver, C., Zweng, M.M. (2015) Oceanography north of 60°N from World Ocean Database *Progress in Oceanography* **132** (153-173)
- Shannon, R. D. 1976. Revised effective ionic radii and systematic studies of interatomic distances in halides and chalcogenides. *Acta Crystallographica Section A: Crystal Physics, Diffraction, Theoretical and General Crystallography* 32(5), pp. 751-767.
- Sherrell R. M., Lagerström M. E., Forsch K. O., Stammerjohn S. E. and Yager P. L. (2015) Dynamics of dissolved iron and other bioactive trace metals (Mn, Ni, Cu, Zn) in the Amundsen Sea Polynya, Antarctica. *Elem. Sci. Anthr.* **3**, 000071. Available at: <https://www.elementscience.org/articles/71> \nhttp://dx.doi.org/10.12952/journal.elementa.000071.
- Sievers H. a. and Nowlin W. D. (1984) The stratification and water masses at Drake Passage. *J. Geophys. Res.* **89**, 10489.
- Sinclair D. J. and McCulloch M. T. (2004) Corals record low mobile barium concentrations in the Burdekin River during the 1974 flood: Evidence for limited Ba supply to rivers? *Palaeogeogr. Palaeoclimatol. Palaeoecol.* **214**, 155–174.
- Sirevaag, A. and Fer, i. (2009) Early Spring Oceanic Heat Fluxes and Mixing Observed from Drift Stations North of Svalbard. *Journal of Physical Oceanography* **39** DOI: 10.1175/2009JPO4172.1
- Skinner L. C., Fallon S., Waelbroeck C., Michel E. and Barker S. (2010) Ventilation of the deep Southern Ocean and deglacial CO₂ rise. *Science* (80-.). **328**, 1147–1151.
- Smith D. A., Hofmann E. E., Klinck J. M. and Lascara C. M. (1999) Hydrography and circulation of the West Antarctic Peninsula Continental Shelf. *Deep. Res. Part I Oceanogr. Res. Pap.* **46**, 925–949.
- Smith I. J., Stevens D. P., Heywood K. J. and Meredith M. P. (2010) The flow of the Antarctic
-

-
- Circumpolar Current over the North Scotia Ridge. *Deep. Res. Part I Oceanogr. Res. Pap.* **57**, 14–28.
- Smith K. L., Robison B. H., Helly J. J., Kaufmann R. S., Ruhl H. a, Shaw T. J., Twining B. S. and Vernet M. (2007) Free-drifting icebergs: hot spots of chemical and biological enrichment in the Weddell Sea. *Science* **317**, 478–482.
- Smith R. C. and Stammerjohn S. E. (2001) Variations of surface air temperature and sea-ice extent in the western Antarctic Peninsula region. *Ann. Glaciol.* **33**, 493–500.
- Stammerjohn S. E., Martinson D. G., Smith R. C. and Iannuzzi R. A. (2008) Sea ice in the western Antarctic Peninsula region: Spatio-temporal variability from ecological and climate change perspectives. *Deep. Res. Part II Top. Stud. Oceanogr.* **55**, 2041–2058.
- Stecher H. a. and Kogut M. B. (1999) Rapid barium removal in the Delaware estuary. *Geochim. Cosmochim. Acta* **63**, 1003–1012.
- Sternberg E., Jeandel C., Robin E. and Souhaut M. (2008) Seasonal cycle of suspended barite in the mediterranean sea. *Geochim. Cosmochim. Acta* **72**, 4020–4034.
- Sternberg E., Tang D., Ho T. Y., Jeandel C. and Morel F. M. M. (2005) Barium uptake and adsorption in diatoms. *Geochim. Cosmochim. Acta* **69**, 2745–2752.
- Strickland J. D. and Parsons T. R. (1970) J. D. H. Strickland and T. R. Parsons: A Practical Handbook of Seawater Analysis. Ottawa: Fisheries Research Board of Canada, Bulletin 167, 1968. 293 pp. \$ 7.50. In *Internationale Revue der gesamten Hydrobiologie und Hydrographie* pp. 167–167. Available at: <http://doi.wiley.com/10.1002/iroh.19700550118>.
- Stroobants N., Dehairs F., Goeyens L., Vanderheijden N. and Van Grieken R. (1991) Barite formation in the Southern Ocean water column. *Mar. Chem.* **35**, 411–421. Available at: [http://dx.doi.org/10.1016/S0304-4203\(09\)90033-0](http://dx.doi.org/10.1016/S0304-4203(09)90033-0).
- Taylor J. R., Falkner K. K., Schauer U. and Meredith M. P. (2003) Quantitative considerations of dissolved barium as a tracer in the Arctic Ocean. *J. Geophys. Res.* **108**, 3374. Available at: <http://doi.wiley.com/10.1029/2002JC001635> [Accessed November 28, 2014].
- Thomas H., Shadwick E., Dehairs F., Lansard B., Mucci A., Navez J., Gratton Y., Prowe F., Chierici M., Fransson A., Papakyriakou T. N., Sternberg E., Miller L. a., Tremblay J.-É. and Monnin C. (2011) Barium and carbon fluxes in the Canadian Arctic Archipelago. *J. Geophys. Res.* **116**, C00G08. Available at: <http://doi.wiley.com/10.1029/2011JC007120> [Accessed November 25, 2014].
- Thompson E. I. and Schmitz B. (1997) Barium and the late Paleocene d¹³C maximum: Evidence of increased marine surface productivity synchronous with the evolution of the late Paleocene in conjunction maximum versus water support originating. *Paleoceanography*
-

- Timmermans K. R. and van der Wagt B. (2010) VARIability in cell size, nutrient depletion, and growth rates of the southern ocean diatom *fragilariopsis kerguelensis* (bacillariophyceae) after prolonged iron limitation. *J. Phycol.* **46**, 497–506.
- Torres M. E., Brumsack H. J., Bohrmann G. and Emeis K. C. (1996) Barite fronts in continental margin sediments: A new look at barium remobilization in the zone of sulfate reduction and formation of heavy barites in diagenetic fronts. *Chem. Geol.* **127**, 125–139.
- Tréguer P. J. and De La Rocha C. L. (2013) The world ocean silica cycle. *Ann. Rev. Mar. Sci.* **5**, 477–501. Available at: <http://www.ncbi.nlm.nih.gov/pubmed/22809182>.
- Tréguer P. and Jacques G. (1992) Dynamics of nutrients and phytoplankton, and fluxes of carbon, nitrogen and silicon in the Antarctic Ocean. *Polar Biol.* **12**, 149–162.
- Tribovillard N., Algeo T. J., Lyons T. and Riboulleau A. (2006) Trace metals as paleoredox and paleoproductivity proxies: An update. *Chem. Geol.* **232**, 12–32. Available at: <http://linkinghub.elsevier.com/retrieve/pii/S000925410600132X> [Accessed August 5, 2014].
- Twining B. S. and Baines S. B. (2013) The trace metal composition of marine phytoplankton. *Ann. Rev. Mar. Sci.* **5**, 191–215. Available at: <http://www.ncbi.nlm.nih.gov/pubmed/22809181>.
- Vaughan D. G., Marshall G. J., Connolley W. M., Parkinson C., Mulvaney R., Hodgson D. A., King J. C., Pudsey C. J. and Turner J. (2003) Recent rapid regional climate warming on the Antarctic Peninsula. *Clim. Change* **60**, 243–274.
- Venables H. J., Clarke A. and Meredith M. P. (2013) Wintertime controls on summer stratification and productivity at the western Antarctic Peninsula. *Limnol. Oceanogr.* **58**, 1035–1047. Available at: <http://doi.wiley.com/10.4319/lo.2013.58.3.1035> [Accessed February 2, 2016].
- Venables H. J., Meredith M. P. and Brearley A. J. (2016) Modification of deep waters in Marguerite Bay, western Antarctic Peninsula, caused by topographic overflows. *Deep Sea Res. Part II Top. Stud. Oceanogr.* **(in press)**.
- Venables H. and Meredith M. (2014) Feedbacks between ice cover, ocean stratification, and heat content in Ryder Bay, western Antarctic Peninsula. *J. Geophys. Res. Ocean.* **119**, 5323–5336.
- Viers J., Dupré B. and Gaillardet J. (2009) Chemical composition of suspended sediments in World Rivers: New insights from a new database. *Sci. Total Environ.* **407**, 853–868. Available at: <http://dx.doi.org/10.1016/j.scitotenv.2008.09.053>.
- Volpe A. M. and Esser B. K. (2002) Real-time ocean chemistry for improved biogeochemical observation in dynamic coastal environments. *J. Mar. Syst.* **36**, 51–74. Available at:

<http://www.ingentaconnect.com/content/els/09247963/2002/00000036/00000001/art00125>\n[http://dx.doi.org/10.1016/S0924-7963\(02\)00052-0](http://dx.doi.org/10.1016/S0924-7963(02)00052-0).

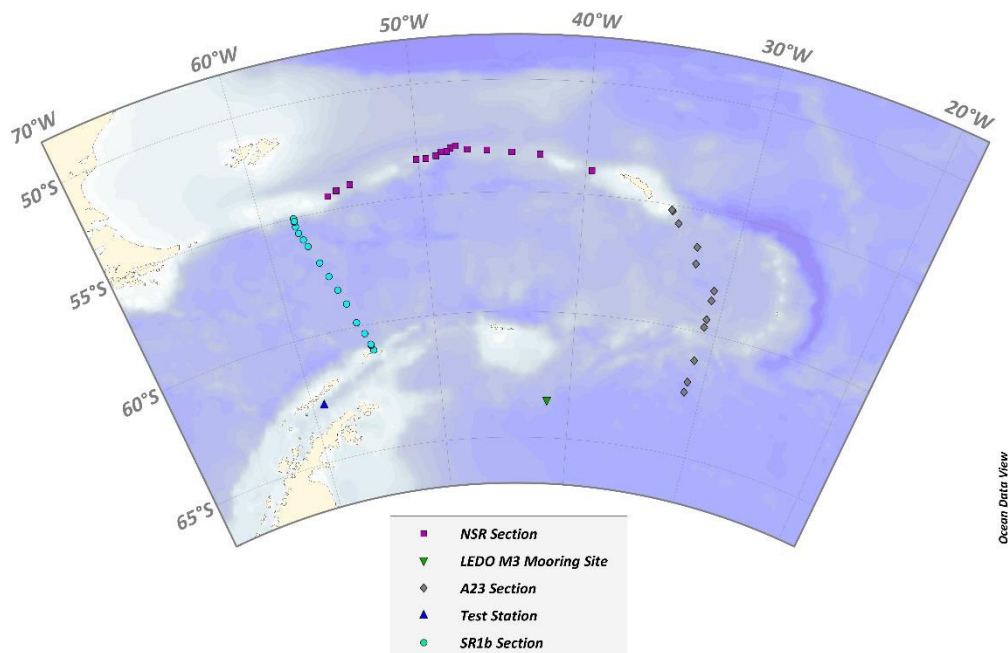
- Walsh, J. E., & Johnson, C. M. (1979). An analysis of Arctic sea ice fluctuations, 1953–77. *Journal of Physical Oceanography*, 9(3), 580–591.
- Waters K. J. and Smith R. C. (1992) Palmer LTER: A sampling grid for the Palmer LTER program. *Antarct. J. United States* **27**, 236–239.
- Watson A. J. and Naveira Garabato A. C. (2006) The role of Southern Ocean mixing and upwelling in glacial-interglacial atmospheric CO₂ change. *Tellus, Ser. B Chem. Phys. Meteorol.* **58**, 73–87.
- Weiss, R. F. 1983. GEOSECS Indian Ocean Expedition: Hydrographic Data 1977–1978. National Science Foundation.
- Whitehouse M. J., Atkinson A., Korb R. E., Venables H. J., Pond D. W. and Gordon M. (2012) Substantial primary production in the land-remote region of the central and northern Scotia Sea. *Deep. Res. Part II Top. Stud. Oceanogr.* **59–60**, 47–56.
- Wilcock J. R., Perry C. C., Williams R. J. P. and Brook a. J. (1989) Biological Minerals Formed from Strontium and Barium Sulphates. II. Crystallography and Control of Mineral Morphology in Desmids. *Proc. R. Soc. B Biol. Sci.* **238**, 203–221.
- Wilson J. D., Barker S. and Ridgwell A. (2012) Assessment of the spatial variability in particulate organic matter and mineral sinking fluxes in the ocean interior: Implications for the ballast hypothesis. *Global Biogeochem. Cycles* **26**.
- Wolgemuth K. and Broecker W. S. (1970) Barium in sea water. *Earth Planet. Sci. Lett.* **8**, 372–378.
- Wood L. W. (1985) Chloroform–Methanol Extraction of Chlorophyll a. *Can. J. Fish. Aquat. Sci.* **42**, 38–43.
- Yamamoto-Kawai M., Carmack E. C., McLaughlin F. a. and Falkner K. K. (2010) Oxygen isotope ratio, barium and salinity in waters around the North American coast from the Pacific to the Atlantic: Implications for freshwater sources to the Arctic throughflow. *J. Mar. Res.* **68**, 97–117.

TABLE OF CONTENTS

APPENDIX 1: REPORT OF BA_D SAMPLING ON CRUISE JR299, PLUS MEASURED BA_D DATA	II
APPENDIX 2: BA_D DATA FOR PALMER LTER GRID 2011 AND 2012.....	XIV
APPENDIX 3: BA_D DATA FOR RATS 2013 TO 2015	XIX
APPENDIX 4: BA_D DATA FOR ROTHERA SEA ICE BRINES 2005/6.....	XXI
APPENDIX 5: BA_D DATA FOR N-ICE CRUISE 2015.....	XXII
APPENDIX 6: BA_D DATA FOR N-ICE TEST CRUISE 2014.....	XXIV
APPENDIX 7: PLOTS OF GEOSECS BA_D AND ANCILLARY DATA.....	XXV
APPENDIX 8: PLOTS OF BA_D AND MACRONUTRIENTS NOX AND PO₄ IN THE SCOTIA SEA.....	XXXII

Appendix 1: Report of Ba_d sampling on cruise JR299, plus measured Ba_d data

Throughout BAS cruise JR299 water samples were collected and stored for future dissolved barium (Ba_d) concentration analysis. A total of 609 samples were collected across sections SR1b, and A23, along the North Scotia ridge, and from the LEDO M3 Mooring site in the Weddell Sea. These samples will be stored onboard the JCR until its return to the UK; they will then be analysed for dissolved barium concentrations at Bristol/Cardiff Universities using isotope dilution mass spectrometry (ID-ICP-MS).



Samples for Ba_d analysis were collected primarily from “CFC” designated stations, and were drawn from the 20L Niskin bottles attached to the CTD rosette only once samples sensitive to gas exchange (CFCs, carbon, or DIMES tracer) had already been taken. As Ba_d is present in seawater in only trace amounts, with a small dynamic range of approximately 70-100nM, care was taken with the sampling technique to reduce potential contamination between samples.

The water samples for Ba_d were drawn from the Niskin bottles using specified Tygon tubing into trace-metal clean 60mL or 125mL HDPE bottles. These HDPE bottles were cleaned at Cardiff University using 2N nitric acid and 18M Ω deionised water. The Tygon tubes were reserved for Ba_d sampling, and in between CTD stations were rinsed three times with, and stored

in, deionised water. Samplers were required to wear clean nitrile gloves when handling Ba_d bottles and Ba_d sampling equipment, and followed a sampling protocol summarised as follows:

- Attach Tygon tubing to Niskin spigot, and rinse water through tube for several seconds.
- Rinse HDPE bottle three times by filling with approximately 10mL, capping, shaking, and emptying over the tube and spigot.
- Fill to the neck of the bottle and screw cap on tightly. Throughout process, avoid touching the ends of the Tygon tubing, the neck of the bottle, or the thread of the screw caps, to avoid potential contamination from the outer surface of the gloves.

Once samples had been collected they were individually acidified with Optima for Ultra traces analysis 32-35% hydrochloric acid (HCl) by either Kimberley Pyle or Oliver Legge (60µL of HCl added to 60mL samples; 125µL added to 125mL samples) in order to prevent biological alteration of the sample during storage. If necessary, the necks of bottles were dried using Kimtech wipes to prevent salt crystal formation at the bottle rim. Bottles were then capped, sealed with Parafilm, and stored in the cool room at a constant temperature of 2-4°C to prevent evaporation.

This process was conducted in a fume hood in the Radiation Lab, which was cleaned thoroughly at the start of the cruise and kept as a 'barium clean' area as much as possible. In order to reduce air contamination, the length of time that samples were left uncapped was minimised, and 8 'blanks' of deionised water treated as samples were prepared throughout the cruise to quantify the level of air contamination.

In order to determine the level of uncertainty introduced by the sampling method, 16 duplicate samples were collected from various CTD casts throughout the cruise, whereby two samples were collected from the same Niskin. Five 'Niskin duplicates' were also collected, which entailed two samples being drawn from two different Niskins that were fired at the same depth. Comparison of the dissolved barium concentrations in each of these duplicates will allow a quantitative analysis of the uncertainty introduced by use of this CTD rosette and sampling method.

1. SR1b Section

15 samples were collected from Station 2 in Bransfield Strait, and 272 samples from 19 CTD casts along the SR1b section (Stations 3-41) crossing Drake Passage from the West Antarctic Peninsula to Punta Arenas, southern Chile.

Event Number	Station	CTD	Date	Barium bottles used	No. of Ba samples
2	2	2	12/03/2014	1-15	15
6	3	3	13/03/2014	16-24; 28; 32	11
9	5	5	13/03/2014	25-27; 29-31; 33-39	13
11	6	6	13/03/2014	40-46; 48, 49; 53	10
13	7	7	14/03/2014	50-52; 54-64; 67-69	17
17	9	9	14/03/2014	65, 66; 85-98	16
20	11	11	14/03/2014	71; 100-114	16
23	13	13	15/03/2014	70; 72-84; 99; 119	16
27	15	15	15/03/2014	115-118; 120-129; 140, 141; 143; 145	18
30	17	17	16/03/2014	130-132; 134; 142; 144; 146-155	16
33	19	19	17/03/2014	133; 135-139; 156-159; 161-167	17
40	26	23	17/03/2014	168-171; 174; 176-187	17
42	30	25	18/03/2014	172, 173; 175; 190; 192-194; 196, 197; 199-204	15
44	33	27	18/03/2014	189; 195; 205-208; 209-220	18
48	35	29	19/03/2014	188; 191; 198; 221-231; 234; 236	16
52	37	31	19/03/2014	232, 233; 235; 253-261; 263, 264; 267	15
55	39	33	01/04/2014	237-242; 244-247; 262; 265, 266; 268	14
56	40	34	01/04/2014	243; 248-252; 269; 271; 273-275	11
57	41	35	01/04/2014	270; 272; 276-289	16

2. A23 Section and the Weddell Sea

18 samples were collected from a CTD cast at Station 68 at the LEDO M3 mooring site in the Weddell Sea, and 167 samples from 13 CTD casts along the A23 section (Stations 45-67).

Event Number	Station	CTD	Date	Barium bottles used	No. of Ba samples
63	44	38	06/04/2014	290-304; 308; 311, 312	18
64	45	39	08/04/2014	305-307; 309, 310; 313-322; 324	16
65	46	40	08/04/2014	323; 325-338; 340	16
67	48	42	09/04/2014	339; 341-353	14
70	51	45	09/04/2014	354-367	14
71	52	46	09/04/2014	368-374; 376-383; 386	16
73	54	48	10/04/2014	387-400	14
74	55	49	10/04/2014	384, 385; 401-410	12
78	59	53	11/04/2014	411-422	12
80	61	55	12/04/2014	423-432; 434; 436, 437	13
83	64	58	13/04/2014	433; 435; 438-445; 447, 448	12
85	66	60	13/04/2014	446; 449-456	10
86	67	61	14/04/2014	457; 459, 460-468	12

3. North Scotia Ridge Section

143 samples collected from CTD casts along the North Scotia Ridge (NSR) section (Stations 68-128).

Event Number	Station	CTD	Date	Barium bottles used	No. of Ba samples
87	68	62	15/04/2014	469, 470; 489; 491-494	7
104	85	79	20/04/2014	473; 475; 478, 479; 486-488; 490	8
106	87	81	20/04/2014	472; 474; 476, 477; 480-485	10
118	95	83	21/04/2014	495-498; 500-507	12
120	97	85	21/04/2014	499; 508-515; 552	10
124	100	88	21/04/2014	2x 500mL bottles (labelled 16 and 17)	0
126	101	89	21/04/2014	553-564	12
129	103	91	22/04/2014	528-539	12
132	105	93	22/04/2014	516-527	12
136	107	95	22/04/2014	578-590	13
142	111	99	23/04/2014	540-551	12
144	113	101	23/04/2014	565-571; 573	8
156	123	107	24/04/2014	572; 575-577; 591-594	9
158	125	109	24/04/2014	595-605; 610	12
161	128	112	25/04/2014	606-609; 611; 616	6

Measured by K. Pyle at Bristol University in 2015

JR299 Event Number	Year	Month	Day	Station	Latitude	Longitude	Depth (m)	Ba (nM)	uncertainty on concentration
2	2014	3	12	2	-62.7652	-59.11	5	82.4	0.10%
2	2014	3	12	2	-62.7652	-59.11	20	83.0	0.10%
2	2014	3	12	2	-62.7652	-59.11	25	83.2	0.07%
2	2014	3	12	2	-62.7652	-59.11	50	82.7	0.14%
2	2014	3	12	2	-62.7652	-59.11	100	84.5	0.27%
2	2014	3	12	2	-62.7652	-59.11	150	84.7	0.15%
2	2014	3	12	2	-62.7652	-59.11	200	85.2	0.15%
2	2014	3	12	2	-62.7652	-59.11	500	86.0	0.16%
2	2014	3	12	2	-62.7652	-59.11	700	86.3	0.21%
2	2014	3	12	2	-62.7652	-59.11	900	85.8	0.12%
2	2014	3	12	2	-62.7652	-59.11	1100	85.4	0.14%
2	2014	3	12	2	-62.7652	-59.11	1200	85.4	0.12%
2	2014	3	12	2	-62.7652	-59.11	1300	85.0	0.24%
2	2014	3	12	2	-62.7652	-59.11	1350	85.2	0.06%
2	2014	3	12	2	-62.7652	-59.11	1420	85.5	0.18%
6	2014	3	13	3	-61.049	-54.589	5	81.6	0.19%
6	2014	3	13	3	-61.049	-54.589	15	81.8	0.10%
6	2014	3	13	3	-61.049	-54.589	50	82.3	0.05%
6	2014	3	13	3	-61.049	-54.589	75	82.3	0.09%
6	2014	3	13	3	-61.049	-54.589	100	82.5	0.18%
6	2014	3	13	3	-61.049	-54.589	200	84.7	0.11%

6	2014	3	13	3	-61.049	-54.589	300	86.6	0.11%
6	2014	3	13	3	-61.049	-54.589	358	88.4	0.06%
6	2014	3	13	3	-61.049	-54.589	358	88.0	0.10%
6	2014	3	13	3	-61.049	-54.589	358	88.2	0.13%
6	2014	3	13	3	-61.049	-54.589	358	88.5	0.09%
9	2014	3	13	5	-60.849	-54.713	5	78.9	0.06%
9	2014	3	13	5	-60.849	-54.713	50	82.9	0.05%
9	2014	3	13	5	-60.849	-54.713	100	83.6	0.13%
9	2014	3	13	5	-60.849	-54.713	200	86.1	0.05%
9	2014	3	13	5	-60.849	-54.713	300	84.9	0.09%
9	2014	3	13	5	-60.849	-54.713	400	87.1	0.08%
9	2014	3	13	5	-60.849	-54.713	600	94.7	0.10%
9	2014	3	13	5	-60.849	-54.713	700	95.2	0.06%
9	2014	3	13	5	-60.849	-54.713	800	94.8	0.12%
9	2014	3	13	5	-60.849	-54.713	900	95.3	0.09%
9	2014	3	13	5	-60.849	-54.713	950	95.1	0.05%
9	2014	3	13	5	-60.849	-54.713	1000	95.1	0.06%
9	2014	3	13	5	-60.849	-54.713	1030	95.0	0.10%
11	2014	3	13	6	-60.833	-54.722	5	82.1	0.13%
11	2014	3	13	6	-60.833	-54.722	50	82.2	0.18%
11	2014	3	13	6	-60.833	-54.722	200	84.6	0.09%
11	2014	3	13	6	-60.833	-54.722	700	94.4	0.06%
11	2014	3	13	6	-60.833	-54.722	800	95.9	0.12%
11	2014	3	13	6	-60.833	-54.722	1000	96.2	0.08%
11	2014	3	13	6	-60.833	-54.722	1200	95.4	0.09%
11	2014	3	13	6	-60.833	-54.722	1400	95.4	0.07%
11	2014	3	13	6	-60.833	-54.722	1600	95.5	0.08%
11	2014	3	13	6	-60.833	-54.722	1780	96.0	0.00%
13	2014	3	14	7	-60.801	-54.738	5	82.7	0.09%
13	2014	3	14	7	-60.801	-54.738	50	82.3	0.08%
13	2014	3	14	7	-60.801	-54.738	100	83.6	0.13%
13	2014	3	14	7	-60.801	-54.738	200	84.6	0.15%
13	2014	3	14	7	-60.801	-54.738	300	85.8	0.05%
13	2014	3	14	7	-60.801	-54.738	400	87.0	0.12%
13	2014	3	14	7	-60.801	-54.738	600	89.7	0.06%
13	2014	3	14	7	-60.801	-54.738	650	89.9	0.11%
13	2014	3	14	7	-60.801	-54.738	700	90.1	0.04%
13	2014	3	14	7	-60.801	-54.738	1000	97.2	0.17%
13	2014	3	14	7	-60.801	-54.738	1400	95.4	0.07%
13	2014	3	14	7	-60.801	-54.738	1800	96.3	0.06%
13	2014	3	14	7	-60.801	-54.738	2000	97.3	0.03%
13	2014	3	14	7	-60.801	-54.738	2200	96.3	0.10%
13	2014	3	14	7	-60.801	-54.738	2400	96.1	0.11%
13	2014	3	14	7	-60.801	-54.738	2585	96.0	0.10%

13	2014	3	14	7	-60.801	-54.738	2585	96.1	0.10%
17	2014	3	14	9	-60.333	-55.032	5	75.2	0.06%
17	2014	3	14	9	-60.333	-55.032	10	75.1	0.11%
17	2014	3	14	9	-60.333	-55.032	60	75.4	0.16%
17	2014	3	14	9	-60.333	-55.032	100	77.0	0.20%
17	2014	3	14	9	-60.333	-55.032	254	81.0	0.23%
17	2014	3	14	9	-60.333	-55.032	350	83.5	0.10%
17	2014	3	14	9	-60.333	-55.032	750	90.1	0.04%
17	2014	3	14	9	-60.333	-55.032	900	93.4	0.05%
17	2014	3	14	9	-60.333	-55.032	1000	94.4	0.06%
17	2014	3	14	9	-60.333	-55.032	1500	98.3	0.06%
17	2014	3	14	9	-60.333	-55.032	2000	99.7	0.04%
17	2014	3	14	9	-60.333	-55.032	2500	97.5	0.13%
17	2014	3	14	9	-60.333	-55.032	3000	96.4	0.16%
17	2014	3	14	9	-60.333	-55.032	3230	96.0	0.10%
17	2014	3	14	9	-60.333	-55.032	3330	96.2	0.13%
17	2014	3	14	9	-60.333	-55.032	3419	97.4	0.14%
20	2014	3	14	11	-59.834	-55.445	5	75.2	0.06%
20	2014	3	14	11	-59.834	-55.445	50	76.3	0.14%
20	2014	3	14	11	-59.834	-55.445	100	77.3	0.24%
20	2014	3	14	11	-59.834	-55.445	255	81.7	0.13%
20	2014	3	14	11	-59.834	-55.445	305	83.0	0.17%
20	2014	3	14	11	-59.834	-55.445	355	84.7	0.28%
20	2014	3	14	11	-59.834	-55.445	400	84.5	0.21%
20	2014	3	14	11	-59.834	-55.445	800	91.6	0.14%
20	2014	3	14	11	-59.834	-55.445	1000	93.6	0.09%
20	2014	3	14	11	-59.834	-55.445	1250	95.1	0.11%
20	2014	3	14	11	-59.834	-55.445	1500	97.2	0.17%
20	2014	3	14	11	-59.834	-55.445	2000	100.1	0.18%
20	2014	3	14	11	-59.834	-55.445	2500	98.2	0.15%
20	2014	3	14	11	-59.834	-55.445	3000	96.8	0.12%
20	2014	3	14	11	-59.834	-55.445	3500	96.9	0.16%
20	2014	3	14	11	-59.834	-55.445	3660	97.3	0.19%
23	2014	3	15	13	-59	-55.856	10	73.6	0.08%
23	2014	3	15	13	-59	-55.856	50	72.5	0.10%
23	2014	3	15	13	-59	-55.856	100	75.3	0.07%
23	2014	3	15	13	-59	-55.856	315	81.2	0.05%
23	2014	3	15	13	-59	-55.856	365	81.8	0.09%
23	2014	3	15	13	-59	-55.856	415	82.6	0.05%
23	2014	3	15	13	-59	-55.856	500	84.1	0.04%
23	2014	3	15	13	-59	-55.856	800	89.4	0.05%
23	2014	3	15	13	-59	-55.856	1000	92.0	0.06%
23	2014	3	15	13	-59	-55.856	1500	98.8	0.09%
23	2014	3	15	13	-59	-55.856	2000	99.9	0.16%

23	2014	3	15	13	-59	-55.856	2500	99.2	0.18%
23	2014	3	15	13	-59	-55.856	3000	97.3	0.10%
23	2014	3	15	13	-59	-55.856	3500	96.5	0.10%
23	2014	3	15	13	-59	-55.856	3760	96.4	0.10%
33	2014	3	17	19	-57.1002	-57.0357	5	67.4	0.22%
33	2014	3	17	19	-57.1002	-57.0357	50	66.5	0.19%
33	2014	3	17	19	-57.1002	-57.0357	90	70.3	0.15%
33	2014	3	17	19	-57.1002	-57.0357	125	70.3	0.15%
33	2014	3	17	19	-57.1002	-57.0357	300	76.6	0.13%
33	2014	3	17	19	-57.1002	-57.0357	400	79.6	0.23%
33	2014	3	17	19	-57.1002	-57.0357	685	82.5	0.16%
33	2014	3	17	19	-57.1002	-57.0357	1000	88.1	0.18%
33	2014	3	17	19	-57.1002	-57.0357	1500	96.0	0.12%
33	2014	3	17	19	-57.1002	-57.0357	2000	98.6	0.15%
33	2014	3	17	19	-57.1002	-57.0357	2500	99.3	0.14%
33	2014	3	17	19	-57.1002	-57.0357	3000	99.9	0.07%
33	2014	3	17	19	-57.1002	-57.0357	3500	99.1	0.13%
33	2014	3	17	19	-57.1002	-57.0357	3750	97.8	0.12%
33	2014	3	17	19	-57.1002	-57.0357	4210	97.3	0.10%
40	2014	3	17	26	-56.3082	-57.5243	5	67.8	0.36%
40	2014	3	17	26	-56.3082	-57.5243	50	68.1	0.19%
40	2014	3	17	26	-56.3082	-57.5243	100	69.2	0.21%
40	2014	3	17	26	-56.3082	-57.5243	200	68.7	0.16%
40	2014	3	17	26	-56.3082	-57.5243	300	69.0	0.16%
40	2014	3	17	26	-56.3082	-57.5243	400	71.9	0.13%
40	2014	3	17	26	-56.3082	-57.5243	500	74.8	0.19%
40	2014	3	17	26	-56.3082	-57.5243	700	78.9	0.19%
40	2014	3	17	26	-56.3082	-57.5243	900	80.8	0.15%
40	2014	3	17	26	-56.3082	-57.5243	1010	82.4	0.12%
40	2014	3	17	26	-56.3082	-57.5243	1250	87.5	0.15%
40	2014	3	17	26	-56.3082	-57.5243	1750	93.6	0.11%
40	2014	3	17	26	-56.3082	-57.5243	2250	97.1	0.15%
40	2014	3	17	26	-56.3082	-57.5243	2750	99.4	0.10%
40	2014	3	17	26	-56.3082	-57.5243	3000	99.3	0.11%
40	2014	3	17	26	-56.3082	-57.5243	3000	99.7	0.10%
40	2014	3	17	26	-56.3082	-57.5243	3265	98.7	0.10%
42	2014	3	18	30	-55.9938	-57.7187	10	52.2	0.18%
42	2014	3	18	30	-55.9938	-57.7187	60	55.5	0.32%
42	2014	3	18	30	-55.9938	-57.7187	200	56.8	0.28%
42	2014	3	18	30	-55.9938	-57.7187	400	59.1	0.25%
42	2014	3	18	30	-55.9938	-57.7187	800	72.8	0.20%
42	2014	3	18	30	-55.9938	-57.7187	1250	84.7	0.17%
42	2014	3	18	30	-55.9938	-57.7187	1550	86.8	0.12%
42	2014	3	18	30	-55.9938	-57.7187	2000	94.0	0.10%

42	2014	3	18	30	-55.9938	-57.7187	2500	97.3	0.08%
42	2014	3	18	30	-55.9938	-57.7187	3000		
42	2014	3	18	30	-55.9938	-57.7187	3500	100.3	0.12%
42	2014	3	18	30	-55.9938	-57.7187	3750	99.6	0.14%
42	2014	3	18	30	-55.9938	-57.7187	3950	99.9	0.11%
42	2014	3	18	30	-55.9938	-57.7187	4040	98.9	0.12%
42	2014	3	18	30	-55.9938	-57.7187	4270	97.7	0.07%
44	2014	3	18	33	-55.6768	-57.9125	10	43.5	0.39%
44	2014	3	18	33	-55.6768	-57.9125	50	43.4	0.72%
44	2014	3	18	33	-55.6768	-57.9125	100	44.7	0.35%
44	2014	3	18	33	-55.6768	-57.9125	200	55.0	0.22%
44	2014	3	18	33	-55.6768	-57.9125	300	56.4	0.29%
44	2014	3	18	33	-55.6768	-57.9125	500	56.7	0.20%
44	2014	3	18	33	-55.6768	-57.9125	1000	65.7	0.19%
44	2014	3	18	33	-55.6768	-57.9125	1000	65.8	0.21%
44	2014	3	18	33	-55.6768	-57.9125	1500	82.0	0.14%
44	2014	3	18	33	-55.6768	-57.9125	1750	87.6	0.10%
44	2014	3	18	33	-55.6768	-57.9125	1990	89.0	0.19%
44	2014	3	18	33	-55.6768	-57.9125	2500	98.1	0.16%
44	2014	3	18	33	-55.6768	-57.9125	3000	99.0	0.08%
44	2014	3	18	33	-55.6768	-57.9125	3500	100.7	0.10%
44	2014	3	18	33	-55.6768	-57.9125	4000	101.5	0.10%
44	2014	3	18	33	-55.6768	-57.9125	4150	100.5	0.07%
44	2014	3	18	33	-55.6768	-57.9125	4300	99.9	0.08%
44	2014	3	18	33	-55.6768	-57.9125	4387	98.2	0.08%
48	2014	3	19	35	-55.3683	-57.9993	5	44.8	0.54%
48	2014	3	19	35	-55.3683	-57.9993	50	45.5	
48	2014	3	19	35	-55.3683	-57.9993	100	47.5	
48	2014	3	19	35	-55.3683	-57.9993	300	56.9	0.39%
48	2014	3	19	35	-55.3683	-57.9993	500	57.1	0.39%
48	2014	3	19	35	-55.3683	-57.9993	700	58.7	0.41%
48	2014	3	19	35	-55.3683	-57.9993	1000	65.9	0.27%
48	2014	3	19	35	-55.3683	-57.9993	1500	81.0	0.12%
48	2014	3	19	35	-55.3683	-57.9993	1750	85.4	0.18%
48	2014	3	19	35	-55.3683	-57.9993	2020	91.1	0.08%
48	2014	3	19	35	-55.3683	-57.9993	2250	91.7	0.12%
48	2014	3	19	35	-55.3683	-57.9993	2750	97.2	0.11%
48	2014	3	19	35	-55.3683	-57.9993	3000	97.9	0.08%
48	2014	3	19	35	-55.3683	-57.9993	3500	101.0	0.24%
48	2014	3	19	35	-55.3683	-57.9993	4000	102.1	0.10%
48	2014	3	19	35	-55.3683	-57.9993	4240	100.1	0.07%
52	2014	3	19	37	-55.1717	-57.9972	10	48.5	0.37%
52	2014	3	19	37	-55.1717	-57.9972	50	52.3	0.33%
52	2014	3	19	37	-55.1717	-57.9972	100	51.5	0.38%

52	2014	3	19	37	-55.1717	-57.9972	200	55.5	0.34%
52	2014	3	19	37	-55.1717	-57.9972	300	55.9	0.26%
52	2014	3	19	37	-55.1717	-57.9972	500	57.0	0.23%
52	2014	3	19	37	-55.1717	-57.9972	700		
52	2014	3	19	37	-55.1717	-57.9972	1000	66.8	0.23%
52	2014	3	19	37	-55.1717	-57.9972	1250		
52	2014	3	19	37	-55.1717	-57.9972	1500	83.3	0.10%
52	2014	3	19	37	-55.1717	-57.9972	1750	86.5	0.08%
52	2014	3	19	37	-55.1717	-57.9972	2200	93.8	0.14%
52	2014	3	19	37	-55.1717	-57.9972	2600	96.3	0.09%
52	2014	3	19	37	-55.1717	-57.9972	2800	98.0	0.13%
52	2014	3	19	37	-55.1717	-57.9972	3095		
55	2014	4	1	39	-55.07491	-57.99907	10	53.7	0.21%
55	2014	4	1	39	-55.07491	-57.99907	50	53.2	0.26%
55	2014	4	1	39	-55.07491	-57.99907	100	54.2	0.30%
55	2014	4	1	39	-55.07491	-57.99907	200	55.5	0.26%
55	2014	4	1	39	-55.07491	-57.99907	300	56.7	0.22%
55	2014	4	1	39	-55.07491	-57.99907	400	57.4	0.28%
55	2014	4	1	39	-55.07491	-57.99907	450	58.0	0.40%
55	2014	4	1	39	-55.07491	-57.99907	495	59.1	0.31%
55	2014	4	1	39	-55.07491	-57.99907	495	58.8	0.33%
55	2014	4	1	39	-55.07491	-57.99907	495	62.0	0.21%
55	2014	4	1	39	-55.07491	-57.99907	495	58.6	0.15%
55	2014	4	1	39	-55.07491	-57.99907	495	58.8	0.26%
56	2014	4	1	40	-55.0102	-58.003	10	52.6	0.49%
56	2014	4	1	40	-55.0102	-58.003	50	53.3	0.47%
56	2014	4	1	40	-55.0102	-58.003	150	55.2	0.43%
56	2014	4	1	40	-55.0102	-58.003	250	55.1	0.42%
56	2014	4	1	40	-55.0102	-58.003	400	56.5	0.44%
56	2014	4	1	40	-55.0102	-58.003	600	58.4	0.47%
56	2014	4	1	40	-55.0102	-58.003	800	63.6	0.18%
56	2014	4	1	40	-55.0102	-58.003	1000	69.1	0.31%
56	2014	4	1	40	-55.0102	-58.003	1200	75.0	0.23%
56	2014	4	1	40	-55.0102	-58.003	1400	80.7	0.20%
56	2014	4	1	40	-55.0102	-58.003	1525	83.0	0.20%
57	2014	4	1	41	-55.125	-57.9992	10	52.7	0.48%
63	2014	4	6	44	-63.5463	-41.7513	5	84.0	0.22%
63	2014	4	6	44	-63.5463	-41.7513	20	85.0	0.14%
63	2014	4	6	44	-63.5463	-41.7513	20	84.2	0.12%
63	2014	4	6	44	-63.5463	-41.7513	90	87.5	0.15%
63	2014	4	6	44	-63.5463	-41.7513	150	88.3	0.24%
63	2014	4	6	44	-63.5463	-41.7513	250	91.9	0.18%
63	2014	4	6	44	-63.5463	-41.7513	400	94.3	0.11%
63	2014	4	6	44	-63.5463	-41.7513	900	96.6	0.15%

63	2014	4	6	44	-63.5463	-41.7513	1200	97.4	0.16%
63	2014	4	6	44	-63.5463	-41.7513	2000	97.1	0.19%
63	2014	4	6	44	-63.5463	-41.7513	2800	97.8	0.17%
63	2014	4	6	44	-63.5463	-41.7513	3500	99.3	0.18%
63	2014	4	6	44	-63.5463	-41.7513	3500	98.3	0.10%
63	2014	4	6	44	-63.5463	-41.7513	4100	99.4	0.17%
63	2014	4	6	44	-63.5463	-41.7513	4250	96.1	0.13%
63	2014	4	6	44	-63.5463	-41.7513	4400	93.6	0.12%
63	2014	4	6	44	-63.5463	-41.7513	4500	92.9	0.25%
63	2014	4	6	44	-63.5463	-41.7513	4580	93.1	0.18%
64	2014	4	8	45	-62.4887	-31.254	10	82.9	0.21%
64	2014	4	8	45	-62.4887	-31.254	20	83.8	0.15%
64	2014	4	8	45	-62.4887	-31.254	50	84.5	0.22%
64	2014	4	8	45	-62.4887	-31.254	100	86.0	0.14%
64	2014	4	8	45	-62.4887	-31.254	200	90.2	0.24%
64	2014	4	8	45	-62.4887	-31.254	300	91.8	0.12%
64	2014	4	8	45	-62.4887	-31.254	400	93.7	0.13%
64	2014	4	8	45	-62.4887	-31.254	1000	97.0	0.18%
64	2014	4	8	45	-62.4887	-31.254	2000	97.1	0.14%
64	2014	4	8	45	-62.4887	-31.254	3000	97.7	0.19%
64	2014	4	8	45	-62.4887	-31.254	3500	97.7	0.21%
64	2014	4	8	45	-62.4887	-31.254	4000	95.0	0.23%
64	2014	4	8	45	-62.4887	-31.254	4500	95.5	0.17%
64	2014	4	8	45	-62.4887	-31.254	4600	95.0	0.13%
64	2014	4	8	45	-62.4887	-31.254	4670	95.5	0.12%
64	2014	4	8	45	-62.4887	-31.254	4720	95.4	0.16%
118	2014	4	21	95	-53.175167	-45.9145	10	68.8	0.22%
118	2014	4	21	95	-53.175167	-45.9145	60	68.1	0.33%
118	2014	4	21	95	-53.175167	-45.9145	125	71.0	0.25%
118	2014	4	21	95	-53.175167	-45.9145	250	74.1	0.22%
118	2014	4	21	95	-53.175167	-45.9145	250	73.7	0.21%
118	2014	4	21	95	-53.175167	-45.9145	250	73.9	0.16%
118	2014	4	21	95	-53.175167	-45.9145	400	78.6	0.20%
118	2014	4	21	95	-53.175167	-45.9145	400	78.3	0.20%
118	2014	4	21	95	-53.175167	-45.9145	400	78.5	0.14%
118	2014	4	21	95	-53.175167	-45.9145	800	88.7	0.11%
118	2014	4	21	95	-53.175167	-45.9145	1000	91.2	0.13%
118	2014	4	21	95	-53.175167	-45.9145	1325	96.2	0.16%
118	2014	4	21	95	-53.175167	-45.9145	1475	98.8	0.02%
118	2014	4	21	95	-53.175167	-45.9145	1510	98.6	0.13%
120	2014	4	21	97	-53.107	-47.055333	10	63.2	0.29%
120	2014	4	21	97	-53.107	-47.055333	60	63.9	0.45%
120	2014	4	21	97	-53.107	-47.055333	150	68.1	0.18%
120	2014	4	21	97	-53.107	-47.055333	300	71.4	0.25%

120	2014	4	21	97	-53.107	-47.055333	400	75.0	0.13%
120	2014	4	21	97	-53.107	-47.055333	600	80.6	0.24%
120	2014	4	21	97	-53.107	-47.055333	800	86.0	0.21%
120	2014	4	21	97	-53.107	-47.055333	1000	89.0	0.18%
120	2014	4	21	97	-53.107	-47.055333	1100	90.6	0.12%
120	2014	4	21	97	-53.107	-47.055333	1225	95.1	0.23%
126	2014	4	21	101	-53.010333	-48.059	10	58.5	0.28%
126	2014	4	21	101	-53.010333	-48.059	125	58.6	0.34%
126	2014	4	21	101	-53.010333	-48.059	450	67.1	0.22%
126	2014	4	21	101	-53.010333	-48.059	600	71.8	0.17%
126	2014	4	21	101	-53.010333	-48.059	1000	81.1	0.17%
126	2014	4	21	101	-53.010333	-48.059	1200	85.5	0.20%
126	2014	4	21	101	-53.010333	-48.059	1600	89.7	0.17%
126	2014	4	21	101	-53.010333	-48.059	2300	97.0	0.17%
126	2014	4	21	101	-53.010333	-48.059	2700	99.1	0.13%
126	2014	4	21	101	-53.010333	-48.059	2850	98.9	0.10%
126	2014	4	21	101	-53.010333	-48.059	2950		
126	2014	4	21	101	-53.010333	-48.059	3051	100.8	0.13%
129	2014	4	22	103	-53.144833	-48.279167	10	59.7	0.33%
129	2014	4	22	103	-53.144833	-48.279167	100	59.6	0.25%
129	2014	4	22	103	-53.144833	-48.279167	150	60.7	0.25%
129	2014	4	22	103	-53.144833	-48.279167	400	65.9	0.24%
129	2014	4	22	103	-53.144833	-48.279167	800	72.8	0.16%
129	2014	4	22	103	-53.144833	-48.279167	1200	82.8	0.17%
129	2014	4	22	103	-53.144833	-48.279167	1400	89.9	0.17%
129	2014	4	22	103	-53.144833	-48.279167	2000	93.8	0.13%
129	2014	4	22	103	-53.144833	-48.279167	2300	97.4	0.11%
129	2014	4	22	103	-53.144833	-48.279167	2400	97.1	0.10%
129	2014	4	22	103	-53.144833	-48.279167	2500	97.2	0.12%
129	2014	4	22	103	-53.144833	-48.279167	2595	97.4	0.15%
136	2014	4	22	107	-53.299333	-48.925167	10	59.6	0.40%
136	2014	4	22	107	-53.299333	-48.925167	60	59.4	0.34%
136	2014	4	22	107	-53.299333	-48.925167	150	59.3	0.25%
136	2014	4	22	107	-53.299333	-48.925167	300	62.1	0.30%
136	2014	4	22	107	-53.299333	-48.925167	600	68.5	0.19%
136	2014	4	22	107	-53.299333	-48.925167	900	75.8	0.15%
136	2014	4	22	107	-53.299333	-48.925167	1350	83.7	0.14%
136	2014	4	22	107	-53.299333	-48.925167	2100	94.0	0.09%
136	2014	4	22	107	-53.299333	-48.925167	2600	96.6	0.12%
136	2014	4	22	107	-53.299333	-48.925167	3000	99.7	0.20%
136	2014	4	22	107	-53.299333	-48.925167	3100	99.3	0.13%
136	2014	4	22	107	-53.299333	-48.925167	3150	99.5	0.09%
136	2014	4	22	107	-53.299333	-48.925167	3170	99.1	0.08%
144	2014	4	23	113	-53.378333	-50.094667	10	63.8	0.28%

144	2014	4	23	113	-53.378333	-50.094667	100	59.4	0.29%
144	2014	4	23	113	-53.378333	-50.094667	160	60.5	0.29%
144	2014	4	23	113	-53.378333	-50.094667	350	64.4	0.25%
144	2014	4	23	113	-53.378333	-50.094667	550	68.8	0.15%
144	2014	4	23	113	-53.378333	-50.094667	750	72.1	0.17%
144	2014	4	23	113	-53.378333	-50.094667	900	76.6	0.15%
144	2014	4	23	113	-53.378333	-50.094667	950	86.7	0.12%
156	2014	4	24	123	-54.070167	-54.245	10	55.4	0.31%
156	2014	4	24	123	-54.070167	-54.245	10	56.7	0.25%
156	2014	4	24	123	-54.070167	-54.245	150	58.3	0.33%
156	2014	4	24	123	-54.070167	-54.245	250	58.3	0.29%
156	2014	4	24	123	-54.070167	-54.245	600	67.1	0.27%
156	2014	4	24	123	-54.070167	-54.245	760	72.1	0.29%
156	2014	4	24	123	-54.070167	-54.245	950	76.6	0.16%
156	2014	4	24	123	-54.070167	-54.245	1300	85.4	0.14%
156	2014	4	24	123	-54.070167	-54.245	1500	85.6	0.13%
158	2014	4	24	125	-54.229833	-55.095167	10	54.6	0.27%
158	2014	4	24	125	-54.229833	-55.095167	80	54.9	0.32%
158	2014	4	24	125	-54.229833	-55.095167	150	56.2	0.31%
158	2014	4	24	125	-54.229833	-55.095167	450	62.1	0.30%
158	2014	4	24	125	-54.229833	-55.095167	900	67.4	0.27%
158	2014	4	24	125	-54.229833	-55.095167	1100	70.7	0.22%
158	2014	4	24	125	-54.229833	-55.095167	1200	71.9	0.20%
158	2014	4	24	125	-54.229833	-55.095167	1450	80.8	0.23%
158	2014	4	24	125	-54.229833	-55.095167	1650	83.5	0.18%
158	2014	4	24	125	-54.229833	-55.095167	1750	84.8	0.13%
158	2014	4	24	125	-54.229833	-55.095167	1800	76.8	0.17%
158	2014	4	24	125	-54.229833	-55.095167	1920	85.6	0.13%
161	2014	4	25	128	-54.393833	-55.675333	10	53.8	0.29%
161	2014	4	25	128	-54.393833	-55.675333	100	55.1	0.25%
161	2014	4	25	128	-54.393833	-55.675333	180	55.5	0.32%
161	2014	4	25	128	-54.393833	-55.675333	450	57.8	0.24%
161	2014	4	25	128	-54.393833	-55.675333	850	60.6	0.24%
161	2014	4	25	128	-54.393833	-55.675333	1020	68.3	0.16%
	2014	4	26	132	-53.546	-55.300333	10	49.7	0.40%
	2014	4	26	132	-53.546	-55.300333	450	60.7	0.20%
	2014	4	26	132	-53.546	-55.300333	700	65.3	0.28%
	2014	4	26	132	-53.546	-55.300333	900		
	2014	4	26	132	-53.546	-55.300333	1235	79.9	0.12%
	2014	4	26	132	-53.546	-55.300333	1620	85.3	0.15%
	2014	4	26	132	-53.546	-55.300333	2065	92.8	0.12%
	2014	4	26	132	-53.546	-55.300333	2500	95.7	0.15%
	2014	4	26	132	-53.546	-55.300333	2980	97.2	0.17%

Appendix 2: Ba_d data for Palmer LTER Grid 2011 and 2012

- PalLTER dataset: PAL-LTER data system (dataset #266)
<http://oceaninformatics.ucsd.edu/datazoo/data/pallter/datasets>.

Pal LTER 2011 surface:

Measured by K. Pyle at Rutgers and Cardiff Universities in 2013 and 2014

LTER event #	Sample Name	Longitude	Latitude	Ba(nM)	Uncertainty on conc.	Run
559	-100.000	-75.514	-69.532	81.4	0.14%	16th April 2013 Rutgers
510	-100.020	-75.737	-69.432	80.8	0.41%	16th April 2013 Rutgers
508	-100.040	-76.127	-69.246	81.9	0.11%	21st Feb 2014 Cardiff
	-100.050	-76.305	-69.174	82.3	0.22%	21st Feb 2014 Cardiff
501	-100.060	-76.463	-69.096	85.9	0.18%	21st Feb 2014 Cardiff
	-100.070	-76.603	-69.033	82.8	0.25%	21st Feb 2014 Cardiff
496	-100.080	-76.757	-68.959	82.9	0.07%	21st Feb 2014 Cardiff
	-100.090	-76.897	-68.891	100.1	0.11%	21st Feb 2014 Cardiff
491	-100.100	-77.044	-68.786	81.6	0.13%	21st Feb 2014 Cardiff
	-100.110	-77.164	-68.761	81.1	0.19%	21st Feb 2014 Cardiff
489	-100.120	-77.333	-68.679	76.2	0.12%	21st Feb 2014 Cardiff
	-100.130	-77.457	-68.618	78.4	0.12%	21st Feb 2014 Cardiff
486	-100.140	-77.622	-68.536	75.3	0.20%	21st Feb 2014 Cardiff
	-100.150	-77.782	-68.458	77.8	0.14%	21st Feb 2014 Cardiff
482	-100.160	-77.941	-68.379	74.2	0.15%	21st Feb 2014 Cardiff
	-100.170	-78.081	-68.311	73.0	0.42%	16th April 2013 Rutgers
472	-100.180	-78.181	-68.247	70.7	0.69%	16th April 2013 Rutgers
	000.000 (1)	-76.299	-67.716	83.3	0.15%	21st Feb 2014 Cardiff
	000.000 (2)	-76.299	-67.716	84.9	0.17%	21st Feb 2014 Cardiff
464	000.180	-75.117	-68.275	85.3	0.13%	21st Feb 2014 Cardiff
	100.-030	-71.210	-68.579	83.0	0.27%	16th April 2013 Rutgers
416	100.-040	-71.082	-68.633	82.7	0.22%	16th April 2013 Rutgers
	100.090	-73.127	-67.772	81.4	0.42%	16th April 2013 Rutgers
458	100.100	-73.270	-67.711	81.5	0.24%	16th April 2013 Rutgers
280	200.-020	-69.617	-67.900	82.1	0.22%	16th April 2013 Rutgers
262	200.000	-69.971	-67.760	80.6	0.72%	15th April 2013 Rutgers
	200.010	-70.150	-67.695	81.4	0.32%	17th April 2013 Rutgers
309	200.020	-70.283	-67.634	82.3	0.29%	15th April 2013 Rutgers
	200.030	-70.433	-67.574	82.3	1.31%	15th April 2013 Rutgers
252	200.040	-70.636	-67.491	82.6	0.55%	15th April 2013 Rutgers
	200.050	-70.801	-67.422	81.3	1.18%	15th April 2013 Rutgers
304	200.060	-70.924	-67.369	81.2	1.71%	15th April 2013 Rutgers
	200.070	-71.074	-67.307	81.4	0.14%	17th April 2013 Rutgers
298	200.120	-71.857	-66.973	79.5	0.13%	16th April 2013 Rutgers
296	200.140	-72.208	-66.818	76.0	0.30%	16th April 2013 Rutgers
	300.050	-69.089	-66.823	82.0	0.35%	16th April 2013 Rutgers
223	300.060	-69.250	-66.756	82.1	0.22%	16th April 2013 Rutgers
	300.070	-69.415	-66.690	81.5	0.17%	21st Feb 2014 Cardiff
220	300.080	-69.569	-66.627	81.5	0.17%	22nd Feb 2014 Cardiff
	300.090	-69.736	-66.559	81.3	0.15%	23rd Feb 2014 Cardiff
215	300.100	-69.856	-66.505	81.2	0.24%	24th Feb 2014 Cardiff
	300.110	-70.043	-66.451	80.8	0.11%	25th Feb 2014 Cardiff
201	300.120	-70.184	-66.362	81.2	0.12%	26th Feb 2014 Cardiff
	300.130	-70.340	-66.303	80.9	0.18%	27th Feb 2014 Cardiff
198	300.140	-70.497	-66.241	79.7	0.18%	16th April 2013 Rutgers
	300.150	-70.637	-66.173	78.2	0.17%	16th April 2013 Rutgers
172	400.040	-67.364	-66.243	81.6	0.32%	16th April 2013 Rutgers
	400.050	-67.486	-66.195	82.0	0.26%	16th April 2013 Rutgers
	400.090	-68.116	-65.945	81.7	0.36%	16th April 2013 Rutgers

188	400.100	-68.283	-65.878	80.4	0.36%	16th April 2013 Rutgers
73	500.060	-66.195	-65.460	81.6	0.42%	16th April 2013 Rutgers
68	500.080	-66.481	-65.350	80.8	0.37%	16th April 2013 Rutgers
66	500.100	-66.781	-65.228	85.3	0.11%	21st Feb 2014 Cardiff
59	500.120	-67.110	-65.100	78.9	0.16%	22nd Feb 2014 Cardiff
54	500.140	-67.419	-64.976	75.3	0.24%	23rd Feb 2014 Cardiff
52	500.160	-67.697	-64.858	74.8	0.20%	24th Feb 2014 Cardiff
50	500.180	-67.995	-64.734	78.4	0.18%	16th April 2013 Rutgers
43	500.200	-68.244	-64.630	76.3	0.24%	16th April 2013 Rutgers
	600.040 (2)	-64.451	-64.913	79.9	0.86%	15th April 2013 Rutgers
	600.040(1)	-64.451	-64.913	80.9	1.02%	15th April 2013 Rutgers
	600.050	-64.598	-64.856	80.3	0.51%	15th April 2013 Rutgers
84	600.060	-64.738	-64.804	80.9	0.71%	15th April 2013 Rutgers
	600.070	-64.874	-64.755	80.6	0.56%	15th April 2013 Rutgers
83	600.080	-65.031	-64.692	80.6	0.17%	17th April 2013 Rutgers
12	600.100	-65.344	-64.582	81.5	0.58%	17th April 2013 Rutgers
21	600.120	-65.664	-64.448	81.0	0.43%	17th April 2013 Rutgers
23	600.140	-65.979	-64.329	80.7	1.27%	15th April 2013 Rutgers
	600.150	-66.110	-64.274	74.1	0.71%	15th April 2013 Rutgers
26	600.160	-66.271	-64.207	75.9	0.25%	17th April 2013 Rutgers
33	600.200	-66.855	-63.967	74.1	0.19%	17th April 2013 Rutgers

Pal LTER 2012 surface:

Measured by K. Pyle at Rutgers and Cardiff Universities in 2013 and 2014

LTER event #	Sample Name	Latitude	Longitude	Ba(nM)	Uncertainty on conc.	Run	Ba(nM)	Uncertainty on conc.	Run
496	PS 3.3	-69.179	-76.885				81.8	0.17%	27th Feb 2014 Cardiff
507	PS 3.4	-69.252	-76.711				81.7	0.13%	27th Feb 2014 Cardiff
308	PAPA_1	-67.752	-69.179				79.7	0.11%	27th Feb 2014 Cardiff
496	-100.100	-68.818	-77.049	81.5	0.4%	11th April 2013 Rutgers	82.2	0.14%	25th Feb 2014 Cardiff
449	-100.110	-68.746	-77.200	82.0	0.4%	11th April 2013 Rutgers			
448	-100.120	-68.673	-77.356	80.6	0.5%	15th April 2013 Rutgers	82.4	0.12%	25th Feb 2014 Cardiff
	-100.13						83.1	0.10%	21st Feb 2014 Cardiff
445	-100.140	-68.533	-77.640	81.6	0.3%	15th April 2013 Rutgers	81.5	0.17%	25th Feb 2014 Cardiff
441	-100.150	-68.463	-77.703	80.8	0.3%	11th April 2013 Rutgers			
439	-100.160	-68.389	-77.916	80.8	0.4%	11th April 2013 Rutgers	81.1	0.11%	25th Feb 2014 Cardiff
406	000.040	-68.658	-74.253	78.0	0.5%	11th April 2013 Rutgers	79.4	0.10%	25th Feb 2014 Cardiff
408	000.050	-68.623	-74.334	77.7	0.3%	11th April 2013 Rutgers			
417	000.100	-68.277	-75.119	79.1	0.6%	15th April 2013 Rutgers	80.2	0.11%	25th Feb 2014 Cardiff
420	000.110	-68.211	-75.259	78.5	0.6%	15th April 2013 Rutgers			
421	000.120	-68.137	-75.412	79.7	0.4%	15th April 2013 Rutgers	80.4	0.15%	21st Feb 2014 Cardiff
423	000.130	-68.067	-75.561	80.5	0.4%	15th April 2013 Rutgers			
424	000.140	-67.996	-75.712	80.5	1.0%	15th April 2013 Rutgers	80.8	0.09%	21st Feb 2014 Cardiff
426	000.150	-67.928	-75.854	79.7	0.7%	11th April 2013 Rutgers			

427	000.160	-67.858	-76.000	79.6	0.2%	11th April 2013 Rutgers	80.1	0.10%	25th Feb 2014 Cardiff
399	100.040	-68.063	-72.348				80.6	0.12%	25th Feb 2014 Cardiff
291	200.-040	-68.029	-69.282	77.8	0.3%	9th April 2013 Rutgers	77.1	0.14%	25th Feb 2014 Cardiff
288	200.-010	-67.831	-69.793	79.4	0.6%	11th April 2013 Rutgers			
281	200.000	-67.768	-69.954	79.6	0.2%	9th April 2013 Rutgers	79.1	0.10%	25th Feb 2014 Cardiff
280	200.010	-67.703	-70.112	79.6	0.4%	11th April 2013 Rutgers			
279	200.020	-67.636	-70.279	78.5	0.2%	11th April 2013 Rutgers	78.0	0.12%	25th Feb 2014 Cardiff
278	200.030	-67.571	-70.441	79.0	0.4%	11th April 2013 Rutgers			
277	200.040	-67.512	-70.583	78.8	0.2%	9th April 2013 Rutgers	77.5	0.10%	25th Feb 2014 Cardiff
359	200.050	-67.447	-70.744	79.5	0.5%	11th April 2013 Rutgers			
361	200.060	-67.379	-70.899	78.9	0.9%	11th April 2013 Rutgers	78.9	0.10%	25th Feb 2014 Cardiff
362	200.070	-67.313	-71.056	79.5	0.3%	11th April 2013 Rutgers			
363	200.080	-67.244	-71.213	79.5	0.2%	9th April 2013 Rutgers	78.7	0.14%	25th Feb 2014 Cardiff
365	200.090	-67.180	-71.360	79.0	0.9%	11th April 2013 Rutgers			
366	200.100	-67.114	-71.524	80.1	0.1%	9th April 2013 Rutgers	79.7	0.18%	25th Feb 2014 Cardiff
368	200.110	-67.067	-71.676	80.0	0.3%	11th April 2013 Rutgers			
369	200.120	-66.981	-71.825	79.9	0.2%	9th April 2013 Rutgers	78.8	0.11%	25th Feb 2014 Cardiff
371	200.130	-66.914	-71.974	79.6	0.3%	11th April 2013 Rutgers			
372	200.140	-66.848	-72.139	80.0	0.5%	11th April 2013 Rutgers	79.0	0.12%	25th Feb 2014 Cardiff
374	200.150	-66.784	-72.285	79.6	1.1%	11th April 2013 Rutgers			
375	200.160	-66.719	-72.433	75.9	0.2%	9th April 2013 Rutgers	76.6	0.22%	25th Feb 2014 Cardiff
265	300.040	-66.890	-69.931	79.3	0.6%	11th April 2013 Rutgers	78.5	0.09%	25th Feb 2014 Cardiff
264	300.050	-66.827	-69.077	78.9	0.5%	11th April 2013 Rutgers			
262	300.060	-66.757	-69.247	79.4	0.3%	15th April 2013 Rutgers	79.4	0.13%	25th Feb 2014 Cardiff
261	300.070	-66.692	-69.404	78.9	0.7%	15th April 2013 Rutgers			
259	300.080	-66.635	-69.557				79.5	0.11%	25th Feb 2014 Cardiff
257	300.090	-66.564	-69.723	79.0	0.5%	15th April 2013 Rutgers			
249	300.100	-66.501	-69.877				80.6	0.12%	25th Feb 2014 Cardiff
248	300.110	-66.435	-70.030	79.5	0.5%	15th April 2013 Rutgers			
245	300.120	-66.370	-70.181				93.3	0.11%	25th Feb 2014 Cardiff
244	300.130	-66.302	-70.338	78.0	0.5%	15th April 2013 Rutgers			
242	300.140	-66.240	-70.489				78.3	0.11%	25th Feb 2014 Cardiff
241	300.150	-66.175	-70.645	79.5	0.2%	15th April 2013 Rutgers			
236	300.160	-66.112	-70.808	79.1	0.2%	15th April 2013 Rutgers	79.1	0.11%	25th Feb 2014 Cardiff

235	300.170	-66.044	-70.936	76.5	0.5%	15th April 2013 Rutgers			
233	300.180	-65.980	-71.080	75.4	0.5%	11th April 2013 Rutgers	75.7	0.12%	25th Feb 2014 Cardiff
232	300.190	-65.911	-71.241	75.8	0.5%	15th April 2013 Rutgers			
230	300.200	-65.849	-71.380	74.0	0.3%	11th April 2013 Rutgers	73.5	0.13%	25th Feb 2014 Cardiff
186	400.040	-66.254	-67.337	78.6	1.0%	11th April 2013 Rutgers	78.6	0.11%	25th Feb 2014 Cardiff
188	400.050	-66.000	-67.000	79.4	0.2%	11th April 2013 Rutgers			
189	400.060	-66.132	-67.644	84.0	0.3%	15th April 2013 Rutgers	79.2	0.12%	25th Feb 2014 Cardiff
191	400.070	-66.044	-67.867	79.6	0.4%	15th April 2013 Rutgers			
192	400.080	-66.006	-67.962				80.7	0.10%	25th Feb 2014 Cardiff
194	400.090	-65.939	-68.130	79.9	0.5%	15th April 2013 Rutgers			
195	400.100	-65.876	-68.285				80.8	0.10%	25th Feb 2014 Cardiff
204	400.110	-65.815	-68.431	79.8	0.7%	15th April 2013 Rutgers			
205	400.120	-65.753	-68.582				80.2	0.10%	25th Feb 2014 Cardiff
207	400.130	-65.687	-68.739	79.7	0.2%	15th April 2013 Rutgers			
208	400.140	-65.624	-68.891				80.2	0.15%	25th Feb 2014 Cardiff
210	400.150	-65.559	-69.046	79.2	0.2%	17th April 2013 Rutgers			
211	400.160	-65.496	-69.190				79.2	0.13%	25th Feb 2014 Cardiff
213	400.170	-65.432	-69.342	77.6	1.4%	15th April 2013 Rutgers			
214	400.180	-65.369	-69.494				76.4	0.13%	25th Feb 2014 Cardiff
216	400.190	-65.301	-69.653	75.6	0.4%	11th April 2013 Rutgers			
217	400.200	-65.236	-69.800	76.5	0.5%	11th April 2013 Rutgers	76.6	0.10%	25th Feb 2014 Cardiff
168	500.060	-65.479	-66.149	79.9	0.3%	11th April 2013 Rutgers	82.2	0.25%	21st Feb 2014 Cardiff
167	500.070	-65.417	-66.306	79.7	0.4%	11th April 2013 Rutgers			
165	500.080	-65.354	-66.466				83.0	0.11%	21st Feb 2014 Cardiff
162	500.090	-65.292	-66.626	79.9	1.9%	15th April 2013 Rutgers			
154	500.100	-65.232	-66.777				81.9	0.10%	21st Feb 2014 Cardiff
152	500.110	-65.169	-66.931	79.9	0.2%	17th April 2013 Rutgers			
150	500.120	-65.108	-67.082				79.4	0.17%	27th Feb 2014 Cardiff
149	500.130	-65.044	-67.237	78.9	0.2%	17th April 2013 Rutgers			
147	500.140	-64.984	-67.385				79.8	0.11%	21st Feb 2014 Cardiff
146	500.150	-64.920	-67.540	79.2	0.4%	17th April 2013 Rutgers			
144	500.160	-64.859	-67.689				80.2	0.13%	21st Feb 2014 Cardiff
143	500.170	-64.798	-67.838	79.2	0.4%	17th April 2013 Rutgers			
141	500.180	-64.735	-67.987				81.0	0.14%	21st Feb 2014 Cardiff

139	500.190	-64.672	-68.142	78.5	0.4%	11th April 2013 Rutgers			
137	500.200	-64.611	-68.296	75.5	0.4%	11th April 2013 Rutgers	75.2	0.07%	27th Feb 2014 Cardiff
80	600.040	-64.926	-64.378	80.0	0.4%	11th April 2013 Rutgers	80.4	0.16%	27th Feb 2014 Cardiff
89	600.050	-64.875	-64.560	80.7	0.3%	11th April 2013 Rutgers			
90	600.060	-64.815	-64.718	81.8	0.4%	15th April 2013 Rutgers	81.3	0.13%	27th Feb 2014 Cardiff
96	600.080	-64.698	-65.025	79.8	0.6%	11th April 2013 Rutgers	80.2	0.11%	27th Feb 2014 Cardiff
97	600.090	-64.634	-65.191	80.5	1.2%	15th April 2013 Rutgers			
98	600.100	-64.579	-65.331	80.9	0.7%	11th April 2013 Rutgers	83.1	0.14%	27th Feb 2014 Cardiff
108	600.110	-64.515	-65.500	80.0	3.3%	17th April 2013 Rutgers			
110	600.120	-64.452	-65.658	78.1	0.8%	11th April 2013 Rutgers	78.6	0.12%	27th Feb 2014 Cardiff
111	600.130	-64.395	-65.799	78.8	1.4%	15th April 2013 Rutgers			
113	600.140	-64.333	-65.959	78.5	0.2%	11th April 2013 Rutgers	78.7	0.20%	27th Feb 2014 Cardiff
115	600.160	-64.210	-66.261	78.4	0.4%	11th April 2013 Rutgers	79.0	0.10%	27th Feb 2014 Cardiff
119	600.180	-64.087	-66.564	76.6	0.4%	11th April 2013 Rutgers	76.8	0.10%	27th Feb 2014 Cardiff
120	600.190	-64.029	-66.707	76.5	0.4%	11th April 2013 Rutgers			
121	600.200	-63.964	-66.854	77.0	0.7%	11th April 2013 Rutgers	78.7	0.07%	27th Feb 2014 Cardiff

Pal LTER 2012 depth profiles:

Measured by K. Pyle at Rutgers and Cardiff Universities in 2013 and 2014

Sample Name	Depth (m)	Latitude	Longitude	Ba(nM)	Uncertainty on conc.	Run
200.160-0	0	-66.719	-72.433	76.2	0.28%	9th April 2013 Rutgers
200.160-20	20	-66.719	-72.433	77.1	0.80%	11th April 2013 Rutgers
200.160-50	50	-66.719	-72.433	78.2	0.34%	9th April 2013 Rutgers
200.160-60	60	-66.719	-72.433	79.2	0.78%	11th April 2013 Rutgers
200.160-100	100	-66.719	-72.433	80.6	0.37%	9th April 2013 Rutgers
200.160-150	150	-66.719	-72.433	83.4	0.17%	11th April 2013 Rutgers
200.160-200	200	-66.719	-72.433	82.3	0.35%	9th April 2013 Rutgers
200.160-280	280	-66.719	-72.433	82.9	0.43%	11th April 2013 Rutgers
200.160-1000	1000	-66.719	-72.433	95.8	0.20%	9th April 2013 Rutgers
200.160-1500	1500	-66.719	-72.433	99.5	0.18%	9th April 2013 Rutgers
200.160-2000	2000	-66.719	-72.433	101.8	0.06%	9th April 2013 Rutgers
200.160-3100	3100	-66.719	-72.433	105.4	0.21%	9th April 2013 Rutgers
200.100-0	0	-67.114	-71.524	79.9	0.22%	9th April 2013 Rutgers
200.100-15	15	-67.114	-71.524	79.8	0.47%	11th April 2013 Rutgers
200.100-30	30	-67.114	-71.524	80.7	0.59%	11th April 2013 Rutgers
200.100-50	50	-67.114	-71.524	81.1	0.24%	9th April 2013 Rutgers
200.100-70	70	-67.114	-71.524	81.4	0.61%	11th April 2013 Rutgers
200.100-100	100	-67.114	-71.524	82.9	0.14%	9th April 2013 Rutgers
200.100-150	150	-67.114	-71.524	85.8	1.07%	11th April 2013 Rutgers
200.100-200	200	-67.114	-71.524	87.4	0.32%	9th April 2013 Rutgers
200.100-250	250	-67.114	-71.524	88.2	0.85%	11th April 2013 Rutgers
200.100-300	300	-67.114	-71.524	88.7	1.48%	11th April 2013 Rutgers
200.100-400	400	-67.114	-71.524	92.9	0.28%	11th April 2013 Rutgers
200.100-450	450	-67.114	-71.524	93.1	0.28%	9th April 2013 Rutgers

Appendix 3: Ba_d data for RaTS 2013 to 2015

Measured by K. Pyle at Bristol University in 2015

Date	RaTS event	Ba (nM)	Uncertainty on concentration
23 March 2013	1470 1	80.0	0.18%
02 April 2013	1472 1	86.4	0.14%
10 April 2013	1474 1	80.5	0.20%
15 April 2013	1476 1	80.9	0.17%
22 April 2013	1478 A1	80.8	0.08%
01 May 2013	1480 1	82.6	0.19%
10 May 2013	1482 1	81.4	0.19%
14 May 2013	1484 1	82.6	0.13%
22 May 2013	1486 1	80.6	0.12%
28 May 2013	1488 1	80.1	0.18%
13 June 2013	1490 1	81.9	0.14%
22 July 2013	1492 1	82.9	0.13%
02 August 2013	1494 1	81.9	0.16%
09 August 2013	1496 1	83.3	0.14%
13 August 2013	1498 1	82.7	0.13%
21 August 2013	1500 1	84.0	0.13%
28 August 2013	1502 1	83.2	0.19%
09 September 2013	1504 1	86.2	0.13%
20 September 2013	1506 1	83.8	0.20%
25 September 2013	1508 1	83.7	0.19%
02 October 2013	1510 1	83.2	0.17%
07 October 2013	1512 1	83.1	0.17%
30 October 2013	1514 1	83.5	0.15%
07 November 2013	1516 1	83.0	0.14%
14 November 2013	1518 1	83.8	0.12%
16 November 2013	1520 1	83.0	0.14%
25 November 2013	1524 1	83.0	0.20%
02 December 2013	1528 1	82.7	0.17%
09 December 2013	1532 1	82.7	0.16%
24 December 2013	1536 1	82.1	0.20%
30 December 2013	1540 1	83.8	0.16%
06 January 2014	1542 1	85.3	0.17%
15 January 2014	1546 1	94.3	0.09%
21 January 2014	1550 1	80.3	0.14%
27 January 2014	1554 1	78.9	0.20%

10 February 2014	1560 1	81.2	0.12%
17 February 2014	1564 1	76.7	0.13%
27 February 2014	1570 1	81.0	0.13%
07 March 2014	1572 1	80.4	0.20%
20 May 2014	1590 B 1	82.4	0.00
14 March 2014	1574 1	81.2	0.16%
21 March 2014	1576 1	82.0	0.17%
27 March 2014	1578 1	82.1	0.19%
04 April 2014	1580 1	82.1	0.13%
14 April 2014	1582 1	82.2	0.14%
28 April 2014	1584 A 1	83.2	0.27%
07 May 2014	1586 1	81.9	0.22%
14 May 2014	1588 1	84.1	0.17%
28 May 2014	1592 1	83.8	0.17%
02 June 2014	1594 1	82.5	0.20%
09 June 2014	1596 1	82.8	0.17%
17 June 2014	1598 1	82.8	0.15%
04 July 2014	1600 1	83.0	0.12%
08 July 2014	1602 1	82.4	0.17%
17 July 2014	1604 1	91.9	0.15%
23 July 2014	1606 1	83.0	0.18%
27 August 2014	1608 1	84.8	0.13%
29 September 2014	1610 1	83.4	0.17%
23 October 2014	1612 1	83.5	0.17%
03 November 2014	1614 1	83.1	0.23%
10 November 2014	1616 1	83.3	0.12%
18 November 2014	1620 1	84.1	0.12%
25 November 2014	1624 1	83.8	0.16%
04 December 2014	1626 AB	83.7	0.09%
09 December 2014	1628 1	84.0	0.14%
16 December 2014	163221 1	84.1	0.19%
22 December 2014	1636 1	83.4	0.14%
31 December 2014	1640 1	83.6	0.21%
08 January 2015	1644 1	85.3	0.19%
13 January 2015	164- 1	82.0	0.16%

Appendix 4: Ba_d data for Rothera sea ice brines 2005/6

Measured by K. Pyle at Bristol University in 2015

Reference	Site	Sample Code KRH	Date collected	Type	Ba _d (nM)	Uncertainty on concentration
S1	CTD Site 1	KRHAF14/02	13 October 2005	Brine	48.0	0.01%
S17	Rothera Point	KRH024	12 November 2005	Melted snow	0.7	238.79%
S18			16 November 2005	Sea ice block	12.0	0.10%
S2	Hangar	KRH026	21 November 2005	Seawater	83.5	0.01%
S3	Hangar	KRH027	23 November 2005	Brine	57.6	0.01%
S4	Hangar	KRH029	28 November 2005	Brine	32.7	0.04%
S5	Hangar	KRH030	01 December 2005	Brine	36.7	0.03%
S6	Hangar	KRH031	06 December 2005	Brine	34.0	0.03%
S16	Hangar	KRH032	08 December 2005	Seawater	83.8	0.01%
S7	Hangar	KRH033	09 December 2005	Brine	35.9	0.03%
S9	300m off wharf	KRH058	31 July 2006	Brine	140.6	0.00%
S10	CTD Site 1		31 August 2006	Brine	197.2	0.00%
S11	CTD Site 1		27 September 2006	Brine	234.3	0.00%
S12	CTD Site 1	KRH063	09 October 2006	Brine	65.3	0.00%
S13	South Cove	KRH065	03 November 2006	Brine	5.4	19.20%
S14	Biscoe 300m off wharf	KRH067	10 November 2006	Brine	24.8	0.08%
S15	South Cove	KRH069	21 November 2006	Brine	29.2	0.02%
S18		KRH027 for AI	23 November 2005	Brine	46.8	0.01%

Appendix 5: Ba_d data for N-ICE Cruise 2015

Measured by B. Butler (MSci) at Bristol University in 2015/6

Date	Average Ba (nM)	Core	Mid depth (cm)	Salinity
29/01/2015	22.37370408	2	18	4.362
29/01/2015	11.15539509	2	28	4.342
29/01/2015	14.33081342	2	38	6.111
29/01/2015	17.38599894	2	48	5.721
29/01/2015	13.08349947	2	58	5.603
29/01/2015	14.67450073	2	68	5.715
29/01/2015	9.554584755	2	78	4.918
06/02/2015	8.462496668	2	88	4.923
06/02/2015	9.28413634	2	98	4.822
06/02/2015	9.423906033	2	108	6.294
06/02/2015	23.86063812	6	4	2.9155
06/02/2015	22.3324776	6	30	3.3255
06/02/2015	22.20144798	6	40	4.1435
06/02/2015	30.39620982	6	60	5.9985
06/02/2015	81.29844586	6	70	0.23656
06/02/2015	35.35990793	6	80	0.149742
06/02/2015	48.20363333	6	90	0.598489
06/02/2015	20.55302854	6	100	1.3829
06/02/2015	21.36615823	6	110	1.478307
21/05/2015	20.04112898	6	120	1.471598
21/05/2015	34.64742672	6	130	2.2945
21/05/2015	15.45130205	61	-24.5	0.252209
21/05/2015	10.625358	61	-15	0.080794
21/05/2015	45.35086774	61	-5	4.0155
21/05/2015	30.00505642	61	5	8.9435
21/05/2015	30.02722814	61	25	5.7695
21/05/2015	31.56797629	61	35	4.9635
00/01/1900	36.72083935	61	45	5.9375
21/05/2015	40.31106827	61	55	6.2255
21/05/2015	26.19884185	61	65	6.0355
21/05/2015	25.603295	61	75	5.5765
21/05/2015	28.17974377	61	85	2.2275
21/05/2015	26.76601508	61	95	5.1175
21/05/2015	31.43654379	61	105	5.1125
21/05/2015	33.55164061	61	115	5.1375
28/05/2015	20.00323344	61	125	5.2545
28/05/2015	23.5819449	61	135	5.5355
28/05/2015	30.83339019	65	5	0.357244

28/05/2015	22.83405516	65	15	0.173141
28/05/2015	12.77223342	65	25	0.478904
22/04/2015	12.34832537	49	5	1.018228
22/04/2015	10.70223535	49	35	0.346467
22/04/2015	7.599273935	49	45	0.966378
22/04/2015	9.166531028	49	55	2.298
00/01/1900	10.57197273	49	65	2.923
22/04/2015	9.617617794	49	75	3.16
22/04/2015	12.04906786	49	85	2.819
22/04/2015	16.71166297	49	95	2.928
22/04/2015	16.28474568	49	105	3.645
22/04/2015	19.40836982	49	115	4.309
22/04/2015	19.75929944	49	125	4.07
22/04/2015	22.3976826	49	134	4.729

Appendix 6: Ba_d data for N-ICE Test Cruise 2014

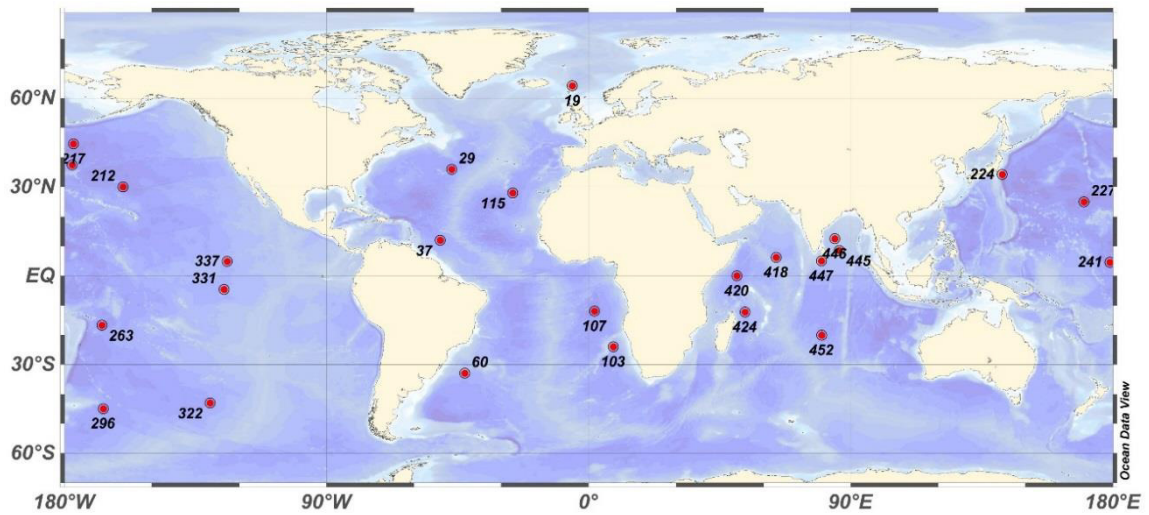
Measured by K. Pyle and B. Butler at Bristol University in 2015

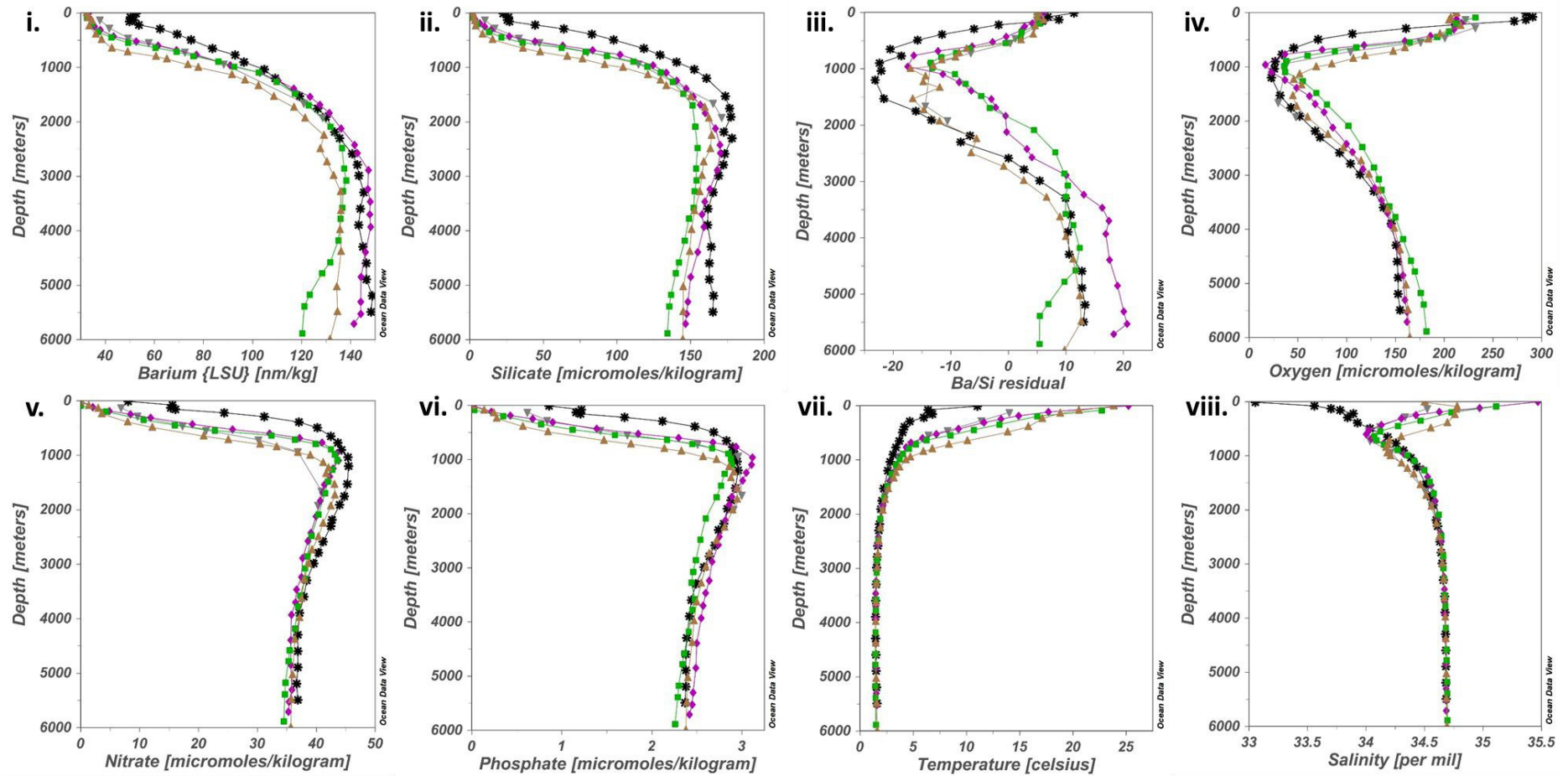
Core	Date	Lat	Long	Ba sample	Average Ba _d (nM)	Depth (cm)
0	23/02/2014	82.5	13.362	25	28.4	95
0	23/02/2014	82.5	13.362	26	24.1	85
0	23/02/2014	82.5	13.362	27	26.1	74
0	23/02/2014	82.5	13.362	28	47.0	64
0	23/02/2014	82.5	13.362	29	48.5	54
0	23/02/2014	82.5	13.362	30	42.8	44
0	23/02/2014	82.5	13.362	31	30.5	34
0	23/02/2014	82.5	13.362	32	29.5	24
0	23/02/2014	82.5	13.362	33	48.2	13
1	25/02/2014	82.24	10.523	44	48.1	87
1	25/02/2014	82.24	10.523	45	14.2	77
1	25/02/2014	82.24	10.523	46	29.6	67
1	25/02/2014	82.24	10.523	47	39.5	57
1	25/02/2014	82.24	10.523	48	45.7	46
1	25/02/2014	82.24	10.523	49	39.9	36
1	25/02/2014	82.24	10.523	50	56.1	26
1	25/02/2014	82.24	10.523	51	62.2	16
1	25/02/2014	82.24	10.523	52	30.2	6
2	25/02/2014	82.24	10.507	35	33.1	86
2	25/02/2014	82.24	10.507	36	39.8	76
2	25/02/2014	82.24	10.507	37	19.2	66
2	25/02/2014	82.24	10.507	39	20.5	46
2	25/02/2014	82.24	10.507	40	17.9	36
2	25/02/2014	82.24	10.507	41	19.2	26
2	25/02/2014	82.24	10.507	42	12.6	16
2	25/02/2014	82.24	10.507	43	23.4	6

Appendix 7: Plots of GEOSECS Ba_d and ancillary data

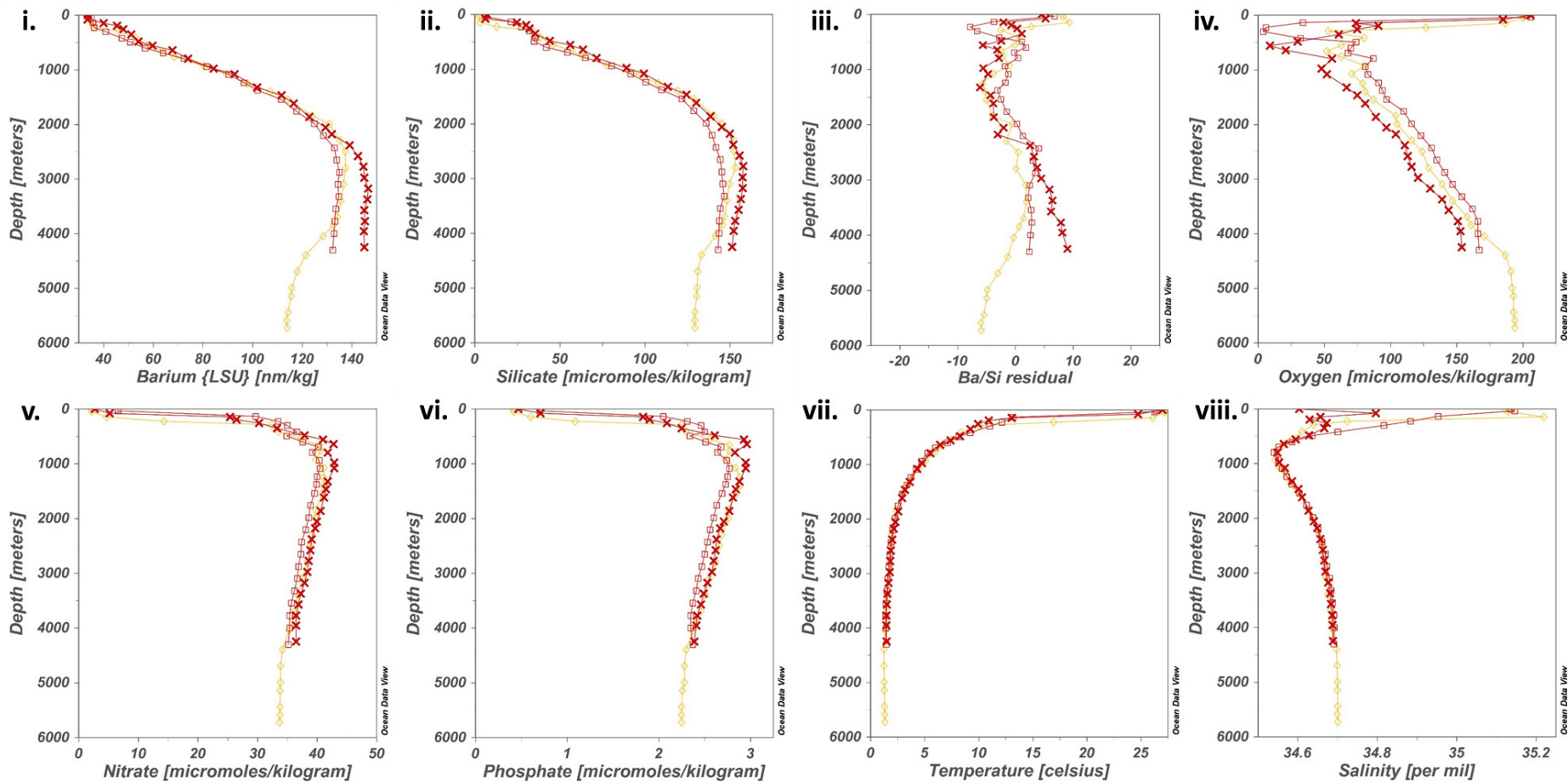
Locations of stations sampled for dissolved barium for the GEOSECS programme (KNORR and MELVILLE cruises from 1972-1978) (Ostlund et al. 1987).

Data available at <https://odv.awi.de/en/data/ocean/geosecs/>

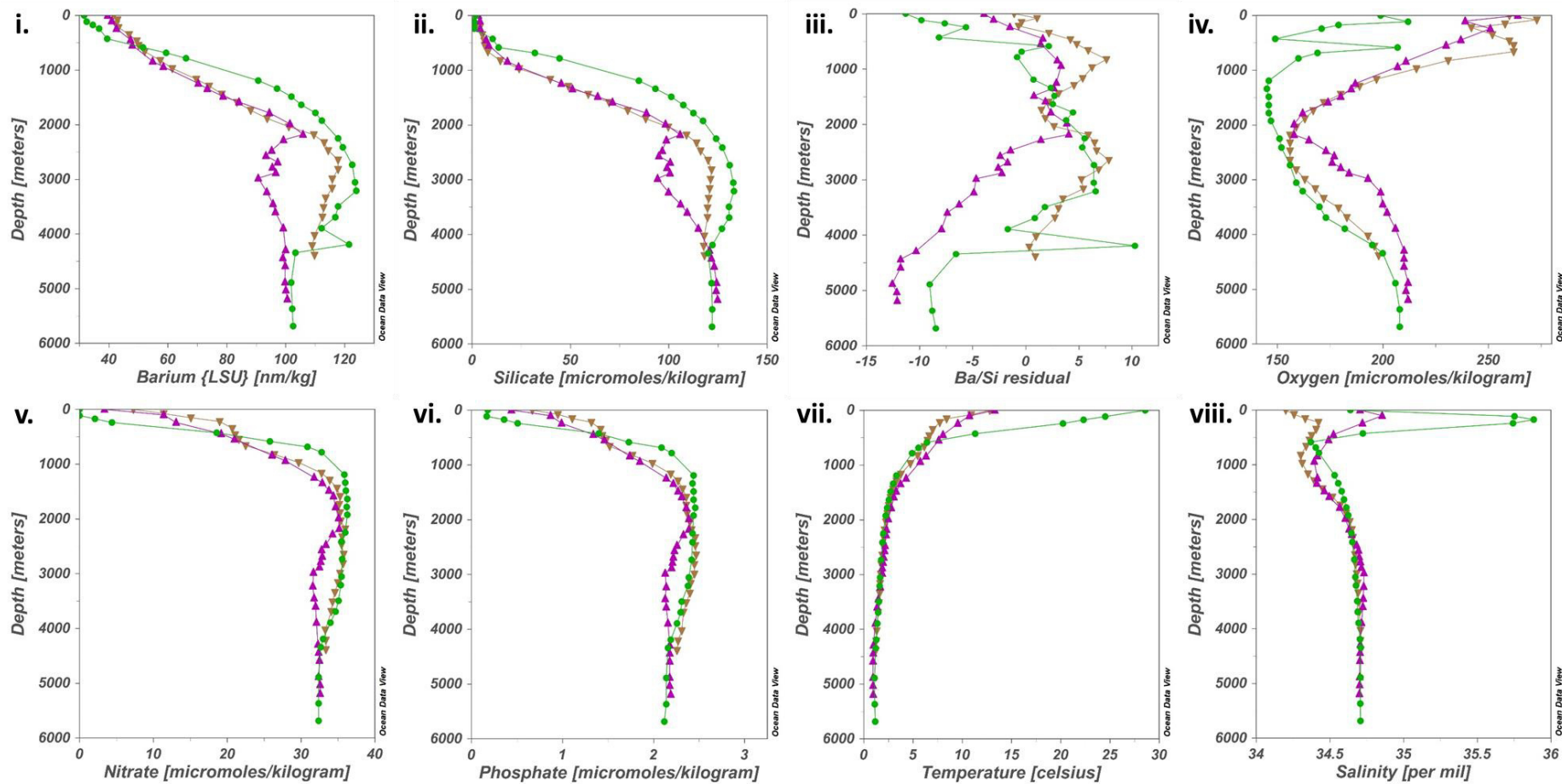




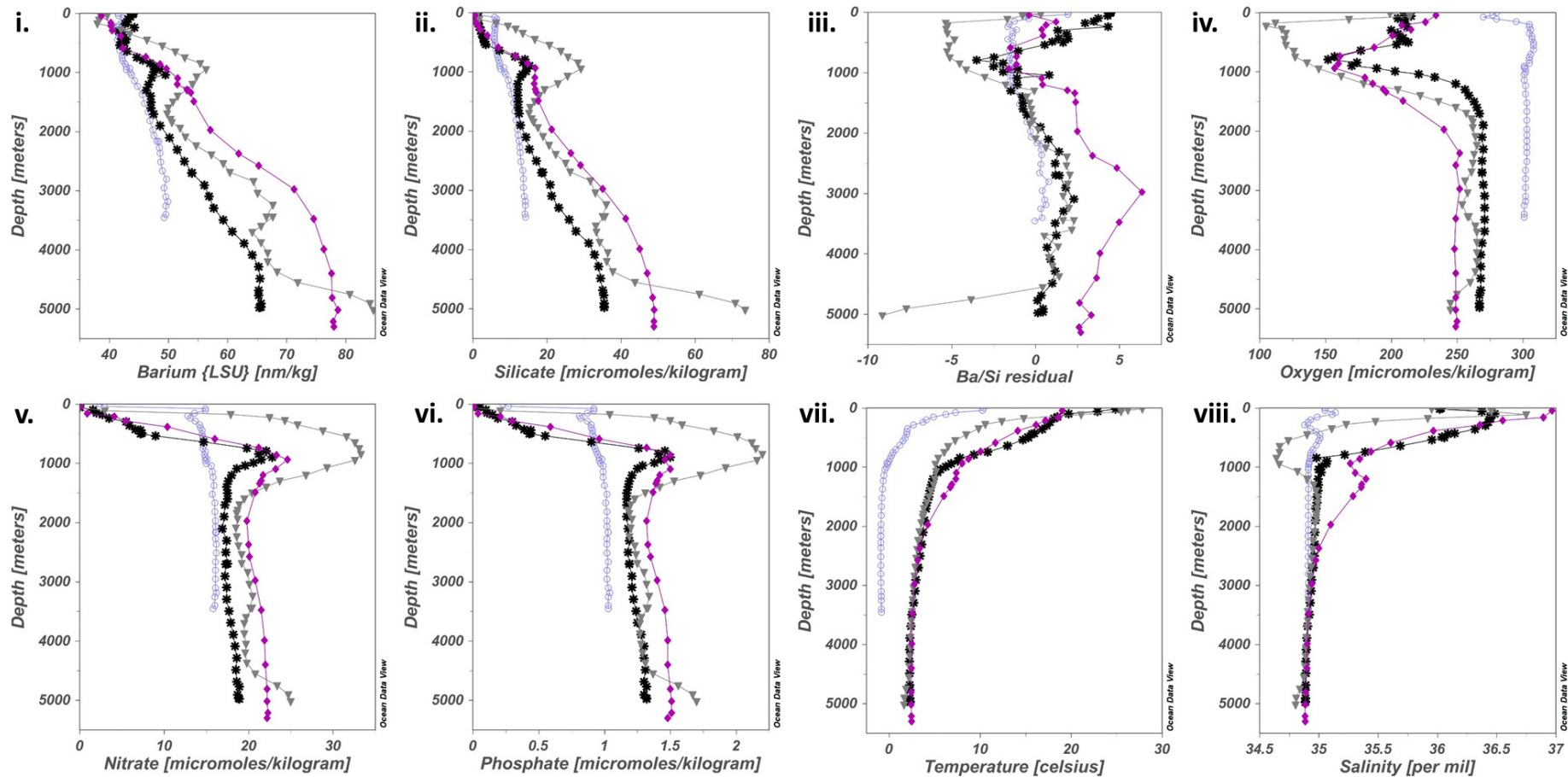
GEOSECS data for stations in the North Pacific: **i.** Dissolved barium concentrations (nm/kg); **ii.** Silicic acid concentrations (μM /kg); **iii.** $\text{Ba}_d^{\text{Si residual}}$ values; **iv.** Dissolved oxygen concentrations (μM /kg); **v.** Nitrate concentrations (μM /kg); **vi.** Phosphate concentrations (μM /kg); **vii.** Temperature ($^{\circ}\text{C}$); **viii.** Salinity.



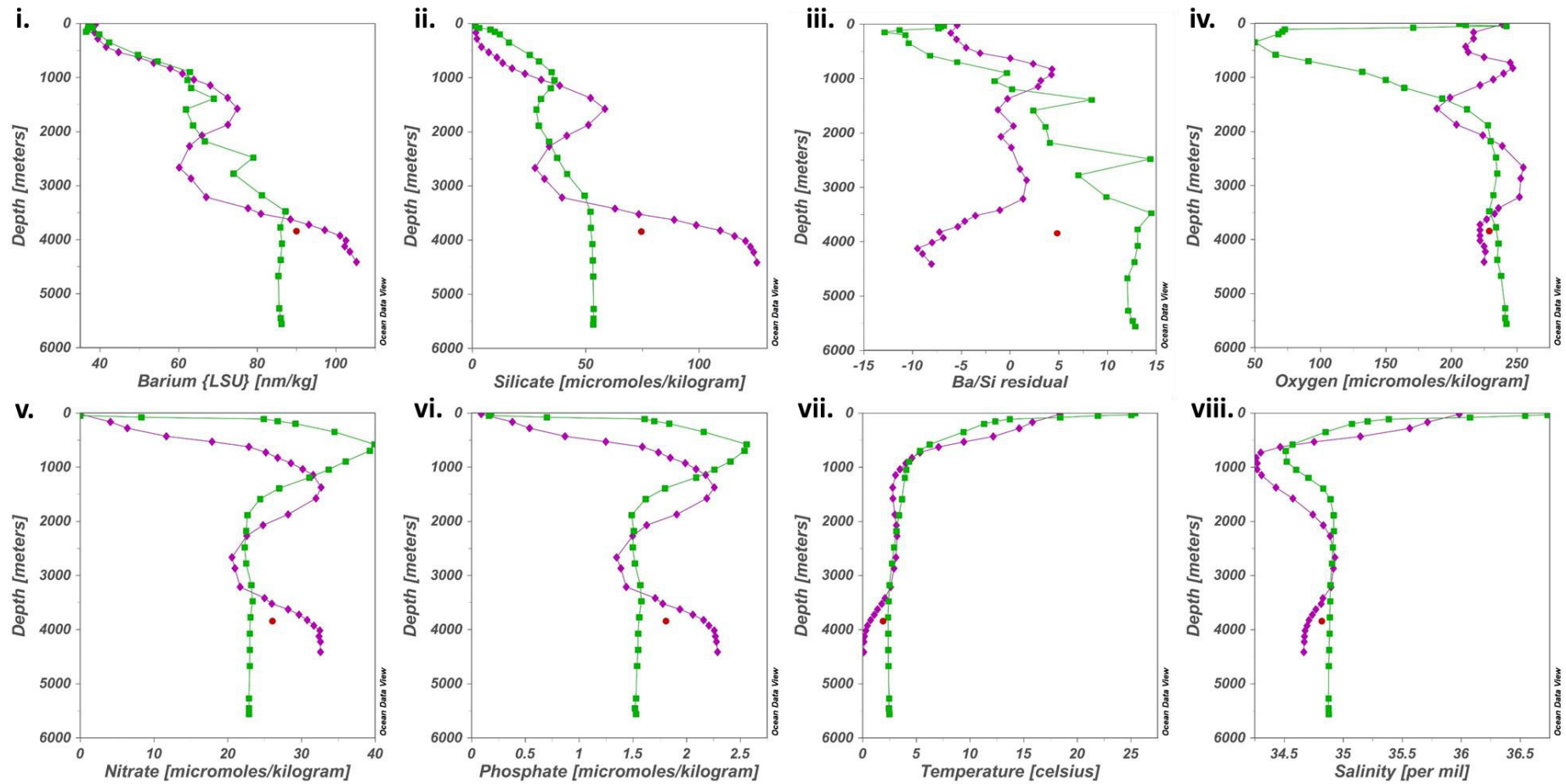
GEOSECS data for stations in the Equatorial Pacific: **i.** Dissolved barium concentrations (nm/kg); **ii.** Silicic acid concentrations ($\mu\text{m}/\text{kg}$); **iii.** $\text{Ba}_{\text{d}}^{\text{Si residual}}$ values; **iv.** Dissolved oxygen concentrations ($\mu\text{m}/\text{kg}$); **v.** Nitrate concentrations ($\mu\text{m}/\text{kg}$); **vi.** Phosphate concentrations ($\mu\text{m}/\text{kg}$); **vii.** Temperature ($^{\circ}\text{C}$); **viii.** Salinity.



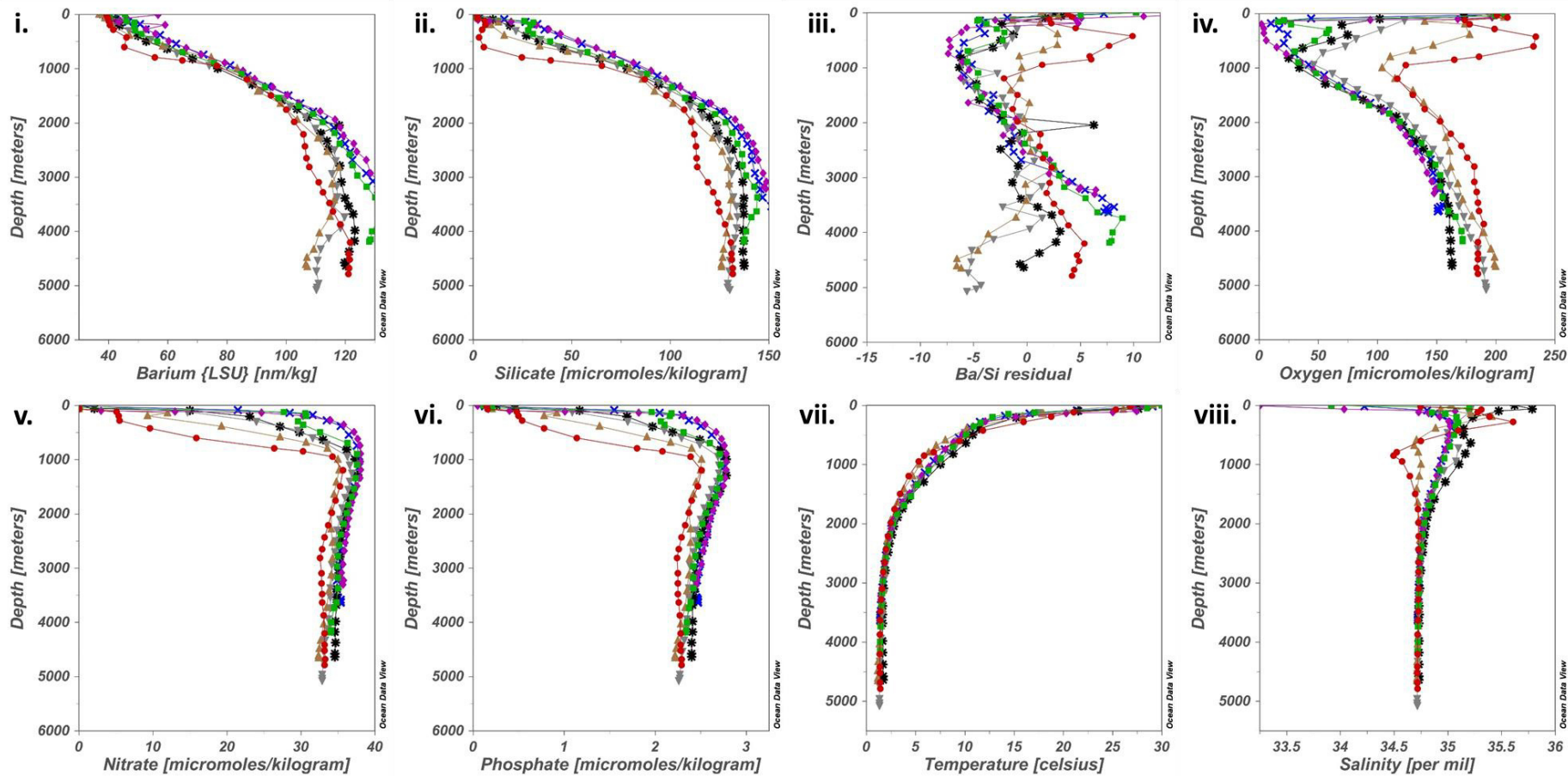
GEOSECS data for stations in the South Pacific: **i.** Dissolved barium concentrations (nm/kg); **ii.** Silicic acid concentrations ($\mu\text{m}/\text{kg}$); **iii.** $\text{Ba}_d^{\text{Si residual}}$ values; **iv.** Dissolved oxygen concentrations ($\mu\text{m}/\text{kg}$); **v.** Nitrate concentrations ($\mu\text{m}/\text{kg}$); **vi.** Phosphate concentrations ($\mu\text{m}/\text{kg}$); **vii.** Temperature ($^{\circ}\text{C}$); **viii.** Salinity.



GEOSECS data for stations in the North Atlantic: **i.** Dissolved barium concentrations (nm/kg); **ii.** Silicic acid concentrations ($\mu\text{m}/\text{kg}$); **iii.** $\text{Ba}_d^{\text{Si residual}}$ values; **iv.** Dissolved oxygen concentrations ($\mu\text{m}/\text{kg}$); **v.** Nitrate concentrations ($\mu\text{m}/\text{kg}$); **vi.** Phosphate concentrations ($\mu\text{m}/\text{kg}$); **vii.** Temperature ($^{\circ}\text{C}$); **viii.** Salinity.



GEOSECS data for stations in the South Atlantic: **i.** Dissolved barium concentrations (nm/kg); **ii.** Silicic acid concentrations ($\mu\text{mol/kg}$); **iii.** $\text{Ba}_d^{\text{Si residual}}$ values; **iv.** Dissolved oxygen concentrations ($\mu\text{mol/kg}$); **v.** Nitrate concentrations ($\mu\text{mol/kg}$); **vi.** Phosphate concentrations ($\mu\text{mol/kg}$); **vii.** Temperature ($^{\circ}\text{C}$); **viii.** Salinity.

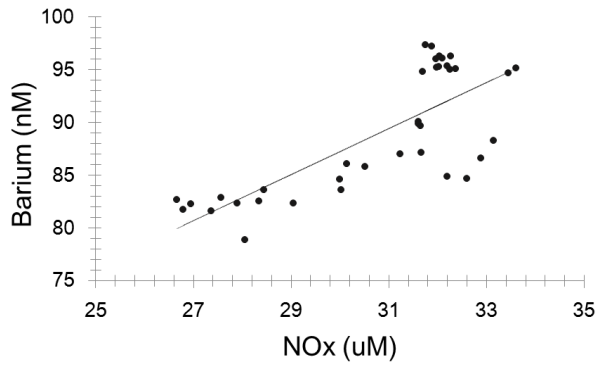


GEOSECS data for stations in the Indian Ocean: **i.** Dissolved barium concentrations (nm/kg); **ii.** Silicic acid concentrations ($\mu\text{m}/\text{kg}$); **iii.** $\text{Ba}_d^{\text{Si residual}}$ values; **iv.** Dissolved oxygen concentrations ($\mu\text{m}/\text{kg}$); **v.** Nitrate concentrations ($\mu\text{m}/\text{kg}$); **vi.** Phosphate concentrations ($\mu\text{m}/\text{kg}$); **vii.** Temperature ($^{\circ}\text{C}$); **viii.** Salinity.

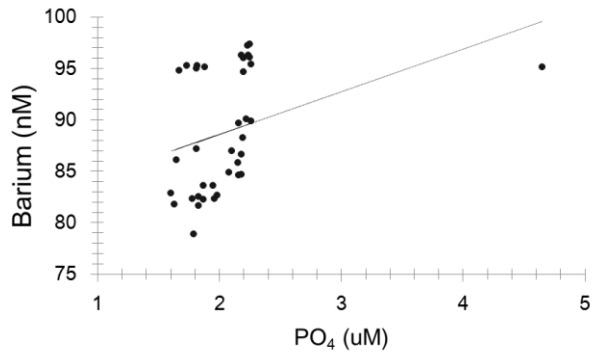
APPENDIX 8: Plots of Ba_d and macronutrients NO_x and PO_4 in the Scotia Sea

Antarctic Continental waters:

Ba_d / NO_x
 R Square 0.59
 P-value < 0.001
 Observations 37

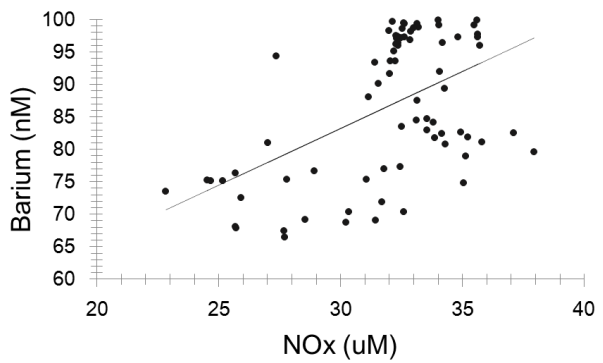


Ba / PO_4
 R Square 0.12
 P-value 0.04
 Observations 37

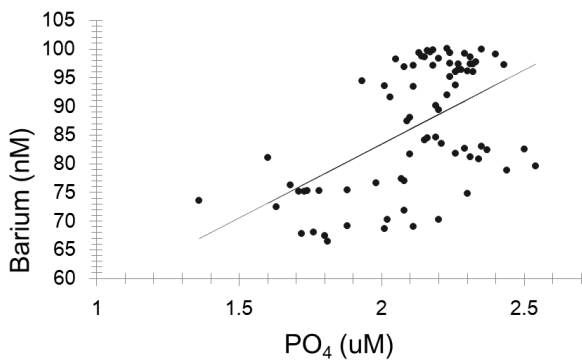


The Antarctic Zone (AZZ):

Ba / NO_x
 R Square 0.26
 P-value < 0.001
 Observations 76

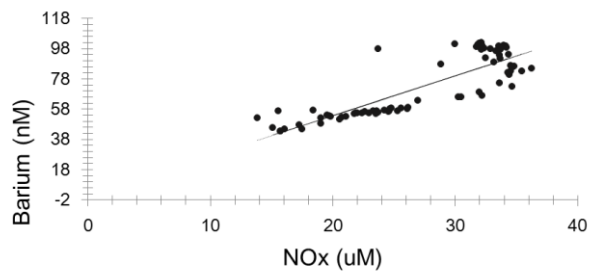


Ba / PO_4
 R Square 0.29
 P-value < 0.001
 Observations 76



North of the Polar Front (PFZ – SAZ)

Ba / NO_x
R Square 0.72
P-value < 0.001
Observations 78



Ba / PO₄
R Square 0.58
P-value < 0.001
Observations 78

